Universität Potsdam
Arbeitsgruppe Prof. Dr. A. Laschewsky

Amphiphilic BAB-Triblock Copolymers Bearing Fluorocarbon Groups: Synthesis and Self-organization in Aqueous Media

Dissertation

zur Erlangung des akademischen Grades
Doktor der Naturwissenschaften (Dr. rer. nat.)
in der Wissenschaftsdisziplin
Kolloid- und Polymerchemie

eingereicht an der Mathematisch-Naturwissenschaftlichen Fakultät
der Universität Potsdam

von

Juliane Ute Kristen

geboren am 22.03.1978 in Selb

Potsdam, im November 2011

Published online at the
Institutional Repository of the University of Potsdam:
URL http://opus.kobv.de/ubp/volltexte/2012/6178/
URN urn:nbn:de:kobv:517-opus-61782
http://nbn-resolving.de/urn:nbn:de:kobv:517-opus-61782

Für meine Familie und Freunde
in Dankbarkeit

Life is like a box of chocolates-
you never know what you`re
gonna get

Forrest Gump

Kraft kommt nicht aus
körperlichen Fähigkeiten.
Sie entspringt einem
unbeugsamen Willen.

Mahatma Ghandi (1869-1948)

Acknowledgements

First of all I want to thank my supervisor Prof. Dr. Andre Laschewsky (University of Potsdam (UP) and Fraunhofer Institute for Applied Polymer Research (IAP)) for giving me the opportunity to do my PhD thesis under his supervision on the interesting research topic of colloid and polymer science and learn a lot in this field of science. Numberless fruitful discussions and his tremendous stock of literature helped with many difficult questions.

Prof. Dr. Hans-Peter Fink and Prof. Dr. Ulrich Buller (Fraunhofer Institute of Applied Polymer Research (IAP)) are thanked for permitting me to work in the well equipped laboratories of the Fraunhofer Institute and the possibility to participate in many social activities at the IAP.

Prof. Dr. Helmuth Möhwald and PD. Dr. Hans Riegler should be thanked for the permit to work in the laboratories of the Max-Planck-Institute for Surfaces and Interfaces (MPI-MPG) and interesting discussions.

Furthermore I`d like to thank Dr. Eleonore Möller, Dr. Aleksandra Jelicic, Rebekka Siegmann and Sascha Prenzel from the group of Prof. Dr. Sabine Beuermann (UP) for measuring the GPC samples of my BAB-triblock copolymers.

I` m grateful to Dr. Stefano Bruzzano (Fraunhofer UMSICHT), Dr. Christoph Wieland, Sabrina Stiller, Anne Sänger, Kristina Blümel (all Fraunhofer IAP) and Carsten Canitz for helping me so much in measuring numberless GPC samples and the evaluation and interpretation of the elugramms.

Furthermore, I` m very thankful to Dr. Eckhard Görnitz (Fraunhofer IAP) for introducing me to the difficult field of rheology and the discussion of the results.

I would like to thank Dr. Hendrik Wetzel and his team (Fraunhofer IAP) for the elementary analysis measurements.

I further thank Dr. Andreas Ebert for measurement of polymer NMR-spectra and Dr. Andreas Büchtemann (both Fraunhofer IAP) for allowing me to measure at the FT-IR. Thank you very much Tonino Greco for helping with the evaluation of the measurements.

Big thanks to Dr. Hartmut Krüger and Dr. Jens Buchs (both Fraunhofer IAP) for allowing me to use their DSC- and TGA-apparatus.

I thank the late Prof. Dr. Jean-Louis Habib-Jiwan (Universite Catholique de Louvain (UCL)) and his technichian Raoul Rozenberg for their help in trying to record the mass spectra of the fluorinated CTAs as well as M. Winkler of Waters GmbH for trying to record the mass spectra using various technical equipment.

Big thanks to Stefan Karpitschka (MPI-MPG) for allowing me to use his tensiometer for determination of the surface tension measurements and helping me with the evaluation of the data.

PD Dr. Helmut Tauer and Irina Shekova (both MPI-MPG) should be tanked for measuring the T_g points of the BAB-triblock copolymers.

Thank you Olaf Niemeyer (MPI-MPG) for measuring the ^{19}F-NMR samples in really good quality.

Special thanks to the lab and office mates at the Fraunhofer IAP for the nice work atmosphere: Dr. Patrick Ott (also for funny jokes), Sophia Rehfeld, Steffi Reinhold, Verena Jentzen, Olivia Mauger, Richard Hoffmann, Thomas Brietzke, Dr. Joachim Storsberg, Dr. Jan Weiß, Dr. Erik Wischerhoff, Dr. Sebastian Pfeifer, Dr. Jean-Noel Marsat, Dr. Sebastien Garnier, Dr. Laurent Wattebled, Dr. Nezha Badi, Flavie Salles, Dr. Eleonore Möller, Dr. Özgür Akdemir, Dr. Achille Mayelle Bivigou-Koumba (jokes and discussion) and Dr. Zoya Zarafshani. The same to my office and my lab mates at the MPI Dr. Juan-Jose Giner-Cesares, Dr. Ingo Dönch, Dr. Dorothee Kohler, Dr. Dimitri Fix, Dr. Thorsten Sievers, Dr. Martin Hollamby, Stefan Karpitschka, Constans Weber, John Berg, Matthias Dittrich and Hidehiko Assuama.

I would like to thank Dr. Matthias Heydenreich and Angela Krititschka (UP) for measuring numerous NMR-spectra and finding solutions also for difficult cases.

I` m greatful to Prof. Dr. Veronika Strehmel (UP/Hochschule Niederrhein) for helping me with administrative work.

Furthermore, I thank Prof. Dr. Joachim Koetz for interesting discussions and giving me the permit to work in his laboratories at the University of Potsdam (UP).

Special thanks to Dr. Mabya Fechner (UP) for recording the partial phase diagrams of the microemulsions and her friendship.

I thank Dr. Sabine Kosmella (UP) for interesting discussions and suggestions for my work.

Big thanks to Sibylle Rüstig (UP) for recording the SEM-pictures and her tea supply.

Special thanks to Dr. Anja Köth, Oscar Rojas, Carina Lemke and Dr. Mabya Fechner (all UP) for the nice work atmosphere and both food and tea supplies.

Finally, I thank my parents and sister for their understanding and encouraging me to finish this thesis.

Thanks to Dr. Joachim Storsberg for his patience, numberless discussions and support in everyday life and being at my side whenever I need it.

Thanks to all, without you I could not have done it!

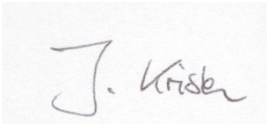

Abstract

In this work new fluorinated and non-fluorinated mono- and bifunctional trithiocarbonates of the structure Z-C(=S)-S-R and Z-C(=S)-S-R-S-C(=S)-Z were synthesized for the use as chain transfer agents (CTAs) in the RAFT-process. All newly synthesized CTAs were tested for their efficiency to moderate the free radical polymerization process by polymerizing styrene (**M3**). Besides characterization of the homopolymers by GPC measurements, end-group analysis of the synthesized block copolymers via ^{1}H-, ^{19}F-NMR, and in some cases also UV-vis spectroscopy, were performed attaching suitable fluorinated moieties to the Z- and/or R-groups of the CTAs.

Symmetric triblock copolymers of type BAB and non-symmetric fluorine end- capped polymers were accessible using the RAFT process in just two or one polymerization step. In particular, the RAFT-process enabled the controlled polymerization of hydrophilic monomers such as N-isopropylacrylamide (NIPAM) (**M1**) as well as N-acryloylpyrrolidine (NAP) (**M2**) for the A-blocks and of the hydrophobic monomers styrene (**M3**), 2-fluorostyrene (**M4**), 3-fluorostyrene (**M5**), 4-fluorostyrene (**M6**) and 2,3,4,5,6-pentafluorostyrene (**M7**) for the B-blocks.

The properties of the BAB-triblock copolymers were investigated in dilute, concentrated and highly concentrated aqueous solutions using DLS, turbidimetry, ^{1}H- and ^{19}F-NMR, rheology, determination of the CMC, foam height- and surface tension measurements and microscopy. Furthermore, their ability to stabilize emulsions and microemulsions and the wetting behaviour of their aqueous solutions on different substrates was investigated. The behaviour of the fluorine end-functionalized polymers to form micelles was studied applying DLS measurements in diluted organic solution.

All investigated BAB-triblock copolymers were able to form micelles and show surface activity at room temperature in dilute aqueous solution. The aqueous solutions displayed moderate foam formation. With different types and concentrations of oils, the formation of emulsions could be detected using a light microscope. A boosting effect in microemulsions could not be found adding BAB-triblock copolymers. At elevated polymer concentrations, the formation of hydrogels was proved applying rheology measurements.

Zusammenfassung

Im Rahmen dieser Arbeit wurden neue fluorierte und unfluorierte mono- und bifunktionelle Trithiocarbonate der Typen Z-C(=S)-S-R und Z-C(=S)-S-R-S-C(=S)-Z zur Anwendung als CTAs (chain- transfer agents) im RAFT-Polymerisationsverfahren hergestellt. Alle CTAs wurden erfolgreich auf ihre Effizienz zur Steuerung des radikalischen Polymerisationsverfahrens hin durch Polymerisation von Styrol (**M3**) getestet. Neben GPC-Messungen wurden Endgruppenanalysen der synthetisierten Blockcopolymere mittels ^{1}H-, ^{19}F-NMR und in manchen Fällen auch UV-Vis Spektroskopie durchgeführt. Dazu wurden die Z- und/oder R-Gruppen der CTAs mit geeigneten fluorierten Gruppen versehen.

Durch Anwendung des RAFT Verfahrens konnten symmetrische Triblockcopolymere vom Typ BAB bzw. mit einer Fluoralkylgruppe endgecappte unsymmetrische Polymere in nur zwei bzw. einem Polymerisationsschritt hergestellt werden. Das RAFT-Polymerisationsverfahren ermöglicht sowohl die Polymerisation hydrophiler Monomere wie N-Isopropylacrylamid (NIPAM) (**M1**) oder N-Acryloylpyrrolidin (NAP) (**M2**) für die A-Blöcke als auch der hydropoben Monomere Styrol (**M3**), 2-Fluorostyrol (**M4**), 3-Fluorostyrol (**M5**), 4- Fluorostyrol (**M6**) und 2,3,4,5,6- Pentafluorostyrol (**M7**) für die B-Blöcke.

Die Eigenschaften der Blockcopolymere in verdünnten, konzentrierten und hochkonzentrierten wässrigen Lösungen wurden mittels DLS, Trübungsphotometrie, ^{1}H- und ^{19}F-NMR, Rheologie, CMC- sowie Schaumhöhen- und Oberflächenspannungsmessungen und Lichtmikroskopie untersucht. Weiterhin wurden ihre Eigenschaften als Emulgatoren und in Mikroemulsion untersucht. Das Micellbildungsverhalten der hydrophob endfunktionalisierten Polymere wurde mittels DLS Messungen in verdünnter organischer Lösung untersucht.

Alle untersuchten BAB-Triblöcke bildeten Micellen und zeigten Oberflächenaktivität bei Raumtemperatur in verdünnter, wässriger Lösung. Weiterhin zeigen die wässrigen Lösungen der Polymere mäßige Schaumbildung. Mit verschiedenen Öltypen und Ölkonzentrationen wurden Emulsionen bzw. Mikroemulsionen gebildet. In Mikroemulsion wurde durch Zugabe von BAB-Triblockopolymeren kein Boosting-Effekt erzielt werden. Bei Untersuchung höherer Polymerkonzentrationen wurde die Bildung von Hydrogelen mittels rheologischer Messungen nachgewiesen. Verschiedene Substrate konnten benetzt werden. Die hydrophob endgecappten Polymere bilden in verdünnter organischer Lösung Micellen, die mittels DLS untersucht wurden, und zeigen somit Tensidverhalten in nichtwässriger Lösung.

Aim of this study

The goal of this work was the synthesis of new, thermoresponsive BAB-triblock copolymers consisting of a thermoresponsive, hydrophilic A-block and a permanently hydrophobic B-block. Furthermore, solvent sensitive fluorine end-capped polymers- copolymers consisting of a hydrophobic and lipophobic fluorinated moiety and a hydrophobic B-block had to be synthesized. The molar mass of the resulting end-capped polymers- and triblock copolymers should be characterized using the weight of the polymers, GPC-, NMR- and UV-measurements. As problems determining the molecular weight of the polymers were likely to occur due to missing standards for GPC and overlapping signals in ^{1}H-NMR, a new, simple method for determining the molar mass via NMR, independent of the applied polymers, should be developed. The aggregation properties of the block copolymers for the potential application as hydrogels and polymeric surfactants in aqueous and organic medium were investigated using DLS, turbidimetry, rheology, surface tension measurements, NMR-measurements and foaming tests. The BAB-polymers were studied in aqueous solutions from low to high polymer concentrations to get an overview and to draw conclusions about their self- assembly behaviour and validity for the desired use. The fluorine end-capped systems were investigated in organic solutions at low concentrations to find out about their self-assembly behaviour and validity of an application as low-foaming surfactants for organic solvents.

1) Among all polymerization methods, the RAFT process was chosen for polymer synthesis because of its applicability to a broad spectrum of monomers, insensitivity towards reaction conditions (except basic media) and availability of the desired fluorine end-capped and triblock copolymers in just one or two steps only providing a good polymer dispersity and control over the polymerization. For this purpose, new RAFT agents, so called trithiocarbonates of the symmetric type Z-C(=S)-S-R-S-C(=S)-Z and non-symmetric type Z-C(=S)-S-R were to be synthesized and the Z and/or R groups simultaneously equipped with specific markers for NMR detection. Fluorine containing groups were chosen as NMR-markers, because ^{19}F, a mononuclidic element, is a half- spin nucleus with good sensitivity, small line- width, non- complicated line pattern and the possibility to investigate the block copolymers without disturbing signal overlaps. The kinetics of the newly developed CTAs were studied by polymerizing the model monomer styrene.

2) Using the mono- and bifunctional fluorinated CTAs, different series of amphiphilic triblock copolymers of type BAB and fluorine end-capped polymers should be synthesized. Triblock copolymers of type BAB were synthesized using poly(NIPAM) as the thermosensitive, temporarily hydrophilic A-block and poly(styrene) (B) as a standard hydrophobic B-block. For the fluorine end-capped polymers, the fluorine moiety was introduced by the monofunctional CTA and an fluorine end-capped polymer is accessible in one step only just by polymerizing styrene. Poly(styrene) is a commonly used hydrophobic polymer while PNIPAM is characterized by good water solubility at ambient temperature, biocompatibility and a weak dependence of the volume phase transition on the concentration and molar mass in the range of 30-35 °C.

3) Furthermore, the PNIPAM used for the BAB-systems were replaced by PNAP, showing a transition temperature of about 50° C, in order to investigate and compare the behaviour of gels at room- and elevated temperatures and the influence of another hydrophilic block on the surfactant properties like foaming behaviour and surface activity or CMC. Furthermore, the

ability to stabilize emulsions and miniemulsions was studied using BAB-blocks composed of hydrophilic and hydrophobic blocks of variable length.

4) For investigating the influence of the hydrophobic blocks (type and length) on gel formation behaviour, surfactant properties and the stabilization of emulsions and miniemulsions as well as wetting investigations, poly(styrene) were replaced by its fluorinated derivatives 2,3,4,5-pentafluorostyrene, 4-fluorostyrene, 3-fluorostyrene and 2-fluorostyrene in order to vary the hydrophobicity and lipophobicity of the B-block in different steps. The length of these blocks was also varied.

Ziel dieser Arbeit

Ziel dieser Arbeit war die Synthese neuer, thermoresponsiver Triblockcopolymere vom Typ BAB bestehend aus einem thermoresponsiven, hydrophilen A-Block sowie einem permanent hydrophoben B-Block. Desweiteren sollten lösungsmittelsensitive Polymere bestehend aus einer hydrophoben and lipophoben, fluorierten Endgruppe und einem hydrophoben B-block hergestellt werden. Die Molmasse der hydrophob verkappten Polymere und Triblockcopolymere sollte mittels des Gewichtes der Polymere, GPC-, NMR- und UV-Messungen charakterisiert werden. Da bei der Bestimmung der Molmassen mittels GPC Schwierigkeiten aufgrund fehlender GPC-Standards und überlappender Signale im ^{1}H-NMR zu erwarten waren, sollte ein einfaches Verfahren zur Bestimmung der Molmassen mittels NMR, unabhängig von der Art der verwendeten Polymere, entwickelt werden. Desweiteren sollte das Aggregationsverhalten der Blockcopolymere für eine eventuelle Anwendung als Hydrogele und polymere Tenside mittels DLS, Trübungsphotometrie, Rheologie, Oberflächenspannungsmessungen, NMR-Messungen und Schaumtests untersucht werden. Dazu wurden die Polymere in wässriger Lösung von niedriger zu hoher Polymerkonzentration hin untersucht um einen Überblick und Rückschlüsse auf ihr Assoziationsverhalten und eine mögliche Anwendbarkeit zu erhalten. Die hydrophob endverkappten Polymere sollten in organischer Lösung bei niedriger Konzentration auf ihr Assoziationsverhalten als mögliche gering schäumende Tenside für organische Lösemittel untersucht werden.

1) Als Polymerisationsverfahren sollte das RAFT-Verfahren zur Polymersynthese herangezogen werden, da es auf ein breites Spektrum von Polymeren anwendbar ist, sich relativ unempfindlich gegenüber den Reaktionsbedingungen (außer basischen Medien) zeigt und die gewünschten hydrophob modifizierten Polymere und Triblockcopolymere in nur einem bzw. zwei Polymerisationsschritten bei guter Polydispersität und Kontrolle über den Polymerisationsprozess hergestellt werden können. Zu diesem Zweck sollen neue RAFT-agentien, sogenannte Trithiocarbonate, vom symmetrischen Z-C(=S)-S-R-S-C(=S)-Z und unsymmetrischen Typ Z-C(=S)-S-R hergestellt und die Z und/oder R- Gruppen gleichzeitig mit speziellen Markern für die NMR- Spektroskopie versehen werden. Fluorhaltige Gruppen wurden als NMR-Marker herangezogen, da es sich bei ^{19}F um ein Reinelement handelt, das einen Halbspin-Kern mit guter Empfindlichkeit, kleiner Linienbreite und unkompliziertem Aufspaltungsmuster sowie die Möglichkeit zur Untersuchung von Blockcopolymeren ohne störende Überlappung der Signale besitzt. Die Kinetik der neu entwickelten CTAs wurde durch Polymerisation von Styrol als Standardmonomer untersucht.

2) Unter Verwendung mono- und bifunktioneller fluorierter CTAs sollten verschiedene Reihen an amphiphilen Blockcopolymeren vom Typ BAB und mit einer Fluorgruppe hydrophob endverkappte Polymere hergestellt werden. Triblockcopolymere vom Typ BAB sollten mit PNIPAM als schaltbar hydrophilem, thermoresponsiven A-block und Polystyrol (B) als hydrophoben Standardblock hergestellt werden. Bei den endverkappten Systemen wurde die fluorierte Endgruppe durch Verwendung eines monofunktionellen, perfluorierten CTA eingeführt, sodaß das Polymer durch die Polymerisation von Styrol in nur einem Schritt zugänglich ist. Polystyrol ist ein häufig genutztes hydrophobes Standardmonomer, während sich das hydrophile PNIPAM durch gute Wasserlöslichkeit bei Raumtemperatur, Biokompatibilität und seine geringe Abhängigkeit der Phasenübergangstemperatur von der gewählten Konzentration und Molgewicht auszeichnet.

3) Desweiteren sollte PNIPAM in den BAB-Systemen durch PNAP mit einer Phasenübergangstemperatur von ungefähr 50 °C ersetzt werden, um das Verhalten von Gelen

bei Raum- und höheren Temperaturen zu untersuchen sowie den Einfluß eines anderen hydrophilen Blocks auf die Tensideigenschaften wie das Schaumvermögen und die Oberflächenaktivität zu vergleichen. Außerdem sollte die Fähigkeit der BAB-Blockcopolymere mit unterschiedlichen hydrophilen Blöcken variabler Länge zur Stabilisierung von Emulsionen und Miniemulsionen untersucht werden.

4) Um den Einfluß der hydrophoben Blöcke (Typ und Länge) auf das Gelbildungsverhalten, die Tensideigenschaften sowie die Stabilisierung von Emulsionen und Mikroemulsionen sowie das Benetzungsverhalten zu untersuchen, wurde Styrol als Baustein durch seine fluorierten Verbindungen 2,3,4,5-Pentafluorostyrol, 4-Fluorostyrol, 3-Fluorostyrol and 2-Fluorostyrol ersetzt, um die Hydrophobie sowie die Lipophobie des B-Blocks in verschiedenen Stufen zu variieren. Weiterhin sollte auch die Länge der Blöcke variiert werden.

Table of contents

List of symbols

A	amplitude
a_τ	shift factor
c	concentration
C_{tr}	chain transfer constant
C_{-tr}	reverse chain transfer constant
D_h	hydrodynamic diameter [nm]
DP_n	average degree of polymerization
E	extinction coefficient [L $mol^{-1}cm^{-1}$]
$E^{\#}$	activation energy for flowing
δ	chemical shift [ppm]
δ	phase difference angle [°]
G`	storage modulus [Pa]
G``	loss modulus [Pa]
I	initiator
K	absolute temperature [K]
k_{add}	addition rate constant
k_{frag}	fragmentation rate constant
k_d	dissociation constant
k_j	reverse transfer constant
k_{tr}	transfer rate constant
k_p	propagation rate constant
λ	absorbance
(m)	multiplet
M	monomer

M_n	number average molar mass
$M_{n,exp}$	experimental number average molar mass
$M_{n,th}$	theoretically expected number average molar mass
M_w	weight average molar mass
$[M]_0$	initial concentration of monomer
$M_{Wmonomer}$	molecular weight of monomer
$M_{W\ RAFT}$	molecular weight of RAFT agent
$P^{\cdot}$	propagating polymer radical
P_n	polymer chain with n-degree of polymerization
$P_n^{\cdot}$	propagating polymer radical with n-degree of polymerization
[P-X]	dormant polymer species
P-X	concentration of end capped polymer
R	leaving group of RAFT agent
$R^{\cdot}$	RAFT agent leaving group radical
$[RAFT]_0$	initial concentration of RAFT agent
R_{gas}	gas constant (= 8.31 J $mol^{-1}K^{-1}$)
R_g	radius of gyration [nm]
R_h	hydrodynamic radius [nm]
R_p	radical polymerization
R-X	alkyl halide
(s)	singlet
T	temperature [°C]
(t)	triplet
τ	shear stress [Pa]

τ_o	max. amplitude of shear stress
Y	deflection time
Z	stabilizing group of RAFT agent

List of abbreviations and acronyms

AFM	atomic force microscopy
AIBN	2,2`-azobis(isobutyronitrile)
ATRP	atom transfer radical polymerization
CTA	chain transfer agent
CAC	critical aggregation concentration
CMC	critical micellization concentration
^{13}C-NMR	carbon nuclear magnetic resonance
CP	cloud point
CR	count rate [kcps]
DLS	dynamic light scattering
DMAc	N, N-dimethyl acetamide
DSC	differential scanning calorimetry
EA	ethyl acrylate
EA	elementary analysis
^{19}F-NMR	fluorine nuclear magnetic resonance
4-FS	4-fluorostyrene
3-FS	3-fluorostyrene
2-FS	2-fluorostyrene
FS	fluorostyrene
GPC	gel permeation chromatography
HLB	hydrophilic-lipophilic balance
^{1}H-NMR	proton nuclear magnetic resonance
IR	infrared
LCST	lower critical solution temperature

MA	methacrylate
MADIX	macromolecular design by interchange of xanthates
MALDI-ToF	matrix assisted laser ionization time of flight
MMA	methyl methacrylate
m. p.	melting point [°C]
MWD	molecular weight distribution
NAP	N-acryloylpyrrolidine
NEt_3	triethylamine
NIPAM	N-isopropylacrylamide
NMP	nitroxide mediated polymerization
NMR	nuclear magnetic resonance
OEGMA	oligo(ethylene glycol)methacrylate
PDI	polydispersity index
PEG	poly(ethylene glycol)
PEGMA	poly(ethylene glycol)methacrylate
PEO	poly(ethylene oxide)
PFS	2, 3, 4, 5, 6-pentafluorostyrene
Ph	phenyl ring
PLA	poly(lactic acid)
PMDEGA	poly(methoxy ethylene glycol acrylate)
PPO	poly(propylene oxide)
PS	poly(styrene)
PTC	phase-transfer catalyst
PTFE	poly(tetrafluoro ethylene)
PVDF	poly(vinylidene fluoride)
RAFT	reversible addition fragmentation chain transfer

ROMP	ring-opening metathesis polymerization
SANS	small angle neutron scattering
SDS	sodium dodecyl sulphate
SEM	scanning electron microscopy
SLS	static light scattering
TEMPO	2,2,6,6-tetramethyl-1-piperidinyloxyl radical
TGA	thermogravimetric analysis
THF	tetrahydrofuran
TIM	tube inversion method
UV-Vis	ultraviolet/visible light spectroscopy
V-30	2-(carbamoylazo)-isobutyronitrile

Chapter I: Introduction

1.1 Polymers as modern materials

Polymers are a part of our everyday life. They can be found in countless kinds of goods such as inflatable rubber materials, household articles, plastic and biodegradable packages, automotive parts such as bumpers, aerospace applications, polymer based electronics [1-8], food structure improvement and conservation, e.g. cyclodextrines for microencapsulation [9-11], pharmaceutical and medical applications such as polymers with high binding capacity and biodegradable implants [12-15] and various other technical applications [16-18]. With further development of applications in techniques, production and medicine, the requirements polymers have to meet become more and more demanding. Therefore, the preparation of speciality polymers with distinct groups, functionalities and accurately controlled structures has become an important topic of research in modern polymer chemistry [19-21]. Properties and performances of polymers greatly depend on the kind and number of attached groups and functionalities as well as the development of synthetic strategies offering good control on the polymerization process in presence of these groups [21, 22].

1.2 Block copolymers

Many synthetical pathways exist to form block copolymers with defined structure and complex architectures. They are accessible using ionic polymerization methods like anionic- and cationic polymerization [23, 24], by coupling mono- or difunctional monoblocks (leading to AB- or ABA-blocks) using mechanistic transformations such as click-chemistry [25] or telechelic homopolymers endfunctionalized with hydrogen bonding or metal-coordination sites undergoing self-assembly with their complement homopolymer or small molecular analogue [27]. Another possibility is switching between different polymerization techniques, e. g. between ROMP and RAFT, ROMP and ATRP, RAFT and NMP just to mention a few possibilities [28-30]. Among the controlled radical polymerization techniques, NMP-, ATRP- and especially RAFT polymerization have turned out as convenient tools for the controlled synthesis of block copolymers with narrow polydispersities [31, 32]. Using the RAFT process, a prepolymer containing thiocarbonylthio groups can be synthesized and used as a macro-RAFT agent [33, 34]. Besides the stepwise addition of the blocks using the RAFT method, the obtained polymer can be analyzed after each polymerization step.

1.3 Amphiphilic polymers

Polymers can be seen as large molecules built up by repeatedly adding smaller chemical subunits, the so-called monomers [35]. Various architectures are possible and can be realized. They can be found in bulk applications as well as dissolved in different solvents serving several applications depending on their interaction properties with a specific solvent [36]. Especially water is an ecofriendly, interesting solving agent with easy handling properties.

Using water as a solvent, synthetic polymers can be characterized by their polarity [35, 37]:

- non-polar polymers, e.g. poly(styrene), poly(pentafluorostyrene)

- polar, but water insoluble polymers, e.g. poly(vinyl acetate), poly(methyl methacrylate)

- polar, water soluble polymers, e.g. poly(vinyl alcohol), poly(oxyethylene)

- polyelectrolytes, e.g. poly(acrylic acid), poly(ethyleneimine)

Combining polar and non-polar or conditionally polar (e.g. thermosensitive or pH-sensitive) and non-polar polymers in one molecule in form of block copolymers or statistical copolymers leads to so called amphiphilic polymers with special, tailorable properties [38, 39]. In order to manufacture hydrogels or surfactants, block copolymers showing amphiphilic behaviour are required. This means that the polymers forming the A- and B-blocks in the later BAB- and fluorine end-capped copolymers need to have an opposite chemical nature referring to the solubility in a given solvent- at least at room temperature (25 °C). In this work, poly(styrene) (**M3**) and its fluorinated derivatives based on 2-, 3-, 4-fluorostyrene (**M4, M5, M6**) and 2,3,4,5,6-pentafluorostyrene (**M7**) were chosen for the permanently hydrophobic block, whereas poly(N-isopropylacrylamide) (NIPAM) (**M1**) and poly(N-acryloylpyrrolidine) (NAP) (**M2**) were chosen for the conditionally hydrophilic block, leading to amphiphilic non-fluorinated and fluorinated block copolymers. Furthermore, polymers consisting of a hydrophobic poly(styrene)-block and a hydrophobic and lipophobic heptadecafluoro block for applications in non-aqueous systems such as organic solvents were synthesized.

Chapter II: Reversible deactivation ("controlled living") radical polymerization

2.1 Controlled radical polymerization techniques

Nitroxide **M**ediated radical **P**olymerization (**NMP**) [31, 40-48], **A**tom-**T**ransfer **R**adical **P**olymerization (**ATRP**) [31, 49-51] and **R**eversible **A**ddition-**F**ragmentation chain **T**ransfer polymerization (**RAFT**) [31, 32] are the most frequently used reversible deactivation radical polymerization methods. Especially the RAFT process is a valuable tool in controlled polymer syntheses revealing several advantages and is therefore explained in detail.

2.2 RAFT: Reversible Addition-Fragmentation-Chain-Transfer-Polymerization

Among degenerative chain transfer polymerizations, the RAFT process is the most versatile method. The reversible addition fragmentation chain transfer (RAFT) polymerization process is based on a degenerative transfer process [31]. In degenerative transfer (DT) conventional free radical initiators are used while control is established using chain transfer agent (RX)- in

the RAFT process exchanging a group or atom between all growing chains. The thermodynamically neutral (degenerative) transfer should be fast compared to the propagation ($k_{exch} > k_p$). The concentration of the dormant species P_n-X is much larger than that of the active species P_n^*. The ratio of concentrations of consumed monomer to the sum of concentrations of the consumed transfer agent and the decomposed initiator defines the degree of polymerization.

$$\overline{M_n} = \frac{[Monomer]_0 \times M_m \times conversion}{[CTA]_0} + M_{CTA} \qquad \text{equation } \mathbf{1} \text{ [31]}$$

Good control over the polymerization reaction can be obtained, if transfer is fast and the concentration of the decomposed initiator is by far lower compared to that of the transfer-agent. Polydispersities decrease initially with conversion and depend on the ratio of the rate constants of propagation to exchange. By initiation and termination processes, a steady-state concentration of radicals is generated as in the classical free radical polymerization process.

Though the radical-radical terminations cannot be eliminated entirely, it is possible to minimize their importance by limiting the number of growing chains reversibly trapping the growing polymeric radical as a dormant species. In practice, nearly all kinds of initiators like for example diazo compounds together with thermal initiation or gamma and UV-irradiation [52, 53, 54] can be used as a source for producing radicals. The concentration should be lower compared to that of the transfer agent (vide supra). Various dithioesters, dithiocarbamates, trithiocarbonates and xanthates (so called MADIX-reagents) (see figure 1) serve as chain transfer agents [32]-depending on the nature of the monomer to polymerize-mediating the active chain ends.

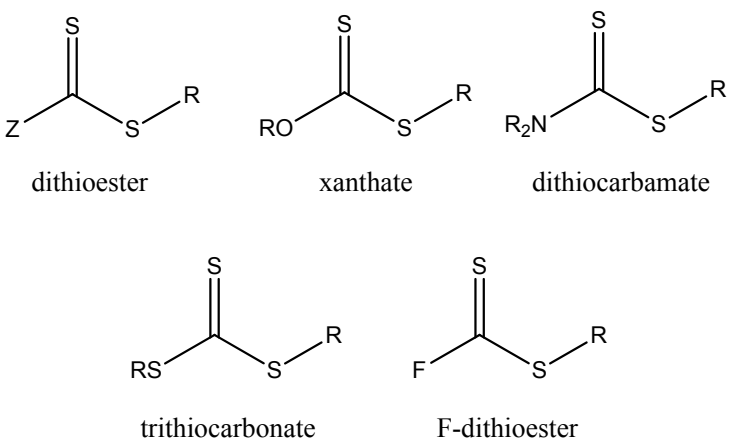

Figure 1: Generic structures of RAFT chain transfer agents [32]

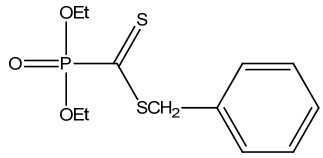

benzyl (diethoxyphosporyl)dithioformate I

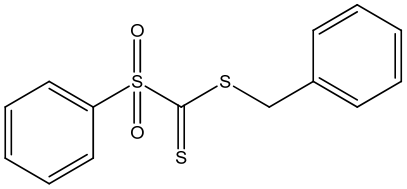

benzyl (phenylsulfonyl)dithioformate III a

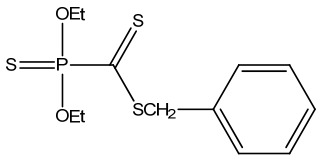

benzyl (diethoxythiophosporyl)dithioformate II

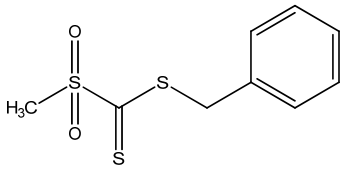

benzyl (methylsulfonyl)dithioformate III b

cyclic CTAs:

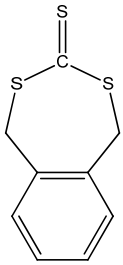

1,5-dihydrobenzo[e][1,3]dithiepine-3-thione IV

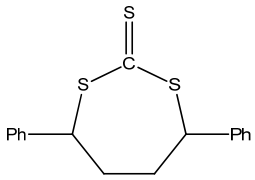

4,7-diphenyl-[1,3]dithiepane-2-thione V

Figure 2: Different classes of CTAs applied in the RAFT polymerization process [55-58].

Recently, phosphoryl dithioesters (I+II) [55] and lately the computer-designed benzyl phenylsulfonyldithioformate (III a) and benzyl methylsulfonyldithioformate (III b) [56] have been reported to successfully moderate the RAFT process (figure 2). Furthermore, cyclic trithiocarbonates have been reported by Hong et al. (IV, V) [57, 58] (figure 2).

Xanthates are applied in the so-called **MADIX** (= **M**acromolecular **D**esign via **I**nterchange of **X**anthates) process which is the best established controlled radical polymerization method enabling the controlled polymerization of vinyl acetate [59]. Despite the F-dithioester [32, 60], all mentioned CTAs can also be designed as multifunctional initiators enabling the synthesis of more complex geometries such as multiarm-stars or brushes [61-66].

2.3 Mechanism of RAFT polymerizations

Applying a thioester as a chain transfer agent, five steps can be distinguished in the RAFT polymerization process [31, 32, 67, 68, 69]:

Initiation: generation of propagating oligomeric radicals $P_1^{\cdot}$ (1)

Chain transfer: addition of the oligomeric radicals $P_1^{\cdot}$ (1) to the CTA (2) creating transient radicals (3). These radicals form a polymeric thiocarbonylthio- compound (4) and a radical(5)

originating from the R-group of the CTA (choice of R- and Z-groups is therefore crucial for the chain transfer process!)

***Reinitiation*:** The radical (5) formed from the R-group due to fragmentation of the CTA is then reinitiating the polymerization process representing a new propagating radical $P_1^{\cdot}$. Subsequent addition fragmentation steps enable the equilibration of chains establishing an equilibrium between the active propagating radicals (6) and the dithiocarbonylthio compound, which is dormant (7). This equilibrium is the crucial step for a controlled radicalic polymerization.

***Termination*:** As the RAFT process is a radical polymerization process (vide supra), dead polymers cannot be completely avoided. Polymers without any dithio function lead to irreversible termination of the polymerization process.Therefore, controlling the end-group functionality via end-group analysis can only be an approximation. Compared to propagation, termination is the minor process. Most of the synthesized chains therefore bear end groups if the polymerization is stopped at not too high conversions (up to 80 %). The whole process is depicted in figure 3:

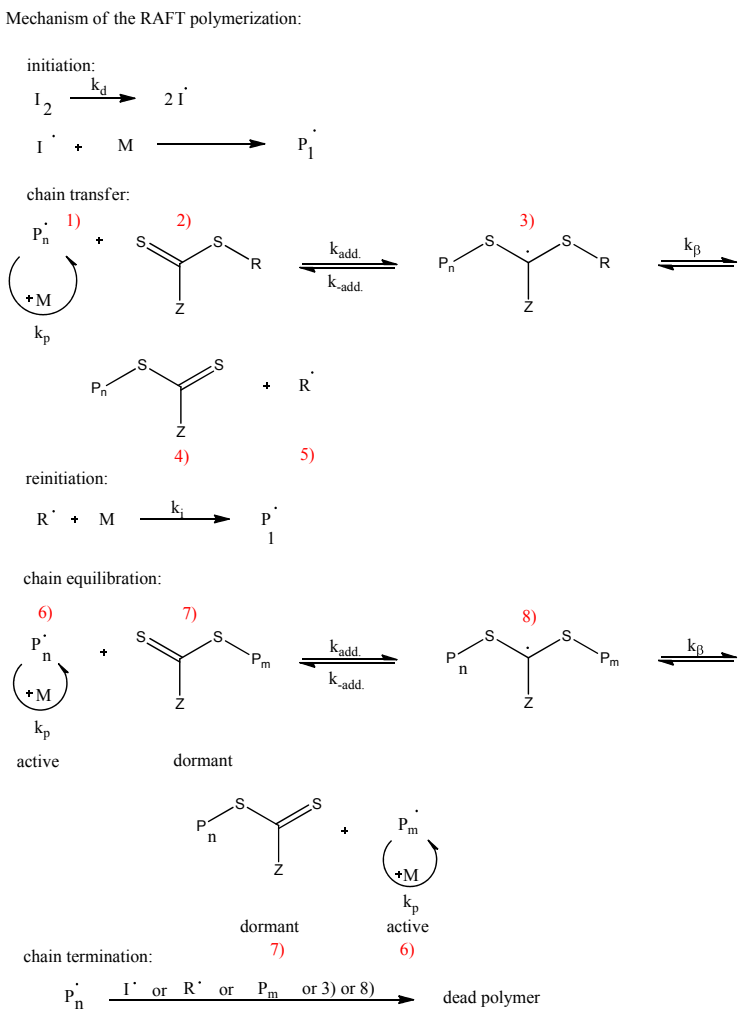

Figure 3: Polymerization mechanism of the RAFT polymerization technique. The polymerization is controlled, since the end-group in the polymeric dithio/trithioester is as labile as in the original dithio/trithioester CTA. The equilibrium between dormant and active chains allows a well-controlled radical polymerization process [31, 32, 67, 68, 69].

2.4 Z- and R-groups used for RAFT agents: Structure reactivity in practical RAFT systems

- In addition to the high reactivity of the C=S bond (k_{add} high) towards radical addition, the choice of the R- and Z-substituent is crucial to control the polymerization process applying the RAFT polymerization system [31, 32]. The degree of control achievable depends on a large extent on the propensity for addition of the propagating radical P_n to the C=S bond and the ability of P_n to be released from the RAFT-adduct radical (see also figure 3); the formed intermediate radical should fragmentate at a not too high rate (typically $k_{add}/k_\beta < 10^6$ L mol^{-1}) but partition in favour of products ($k_\beta > k_{-add}$) [44, 272]. Both abilities depend on both the steric and electronic properties of the R- and Z-group [31] (see figure 4).

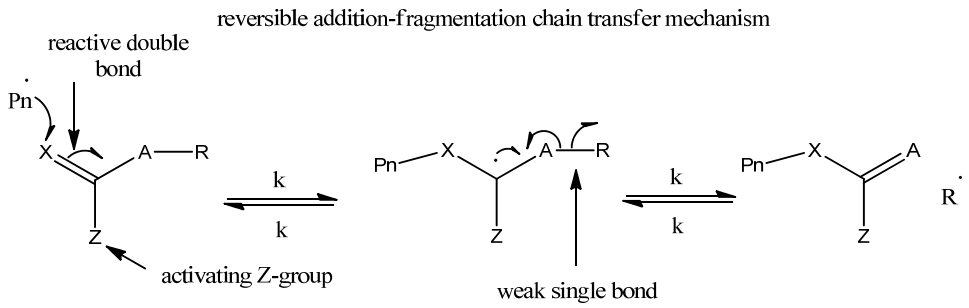

Figure 4: Crucial equilibrium in the RAFT process: the degree of control achievable depends on a large extent on both the propensity for addition of the propagating radical P_n to the C=S bond and the ability of P_n to be released from the RAFT-adduct radical (intermediate species in the middle). These abilities depend on both the steric- and electronic properties of the R- and Z-group [31].

The R-group should fragment from the intermediate radical in the preequilibrium but also be reactive enough to enable reinitiation of the polymerization [31, 32]. Side reactions should be avoided. R should be chosen such that it is a similar or better homolytic leaving group than the propagating radical derived from the monomer being polymerized. An ideal choice for R would be a propagating radical. In this case $k_\beta = k_{-add}$, k_{add} is the same for both initial and polymeric RAFT agents and $K_i = k_p$ [31, 32].

In order to guarantee both a high reactivity of the C=S bond of the initial and polymeric RAFT agents and an intermediate radical fragmentating at a not too high rate (vide supra), the Z-group should be carefully chosen. The choice of the Z-group is strongly dependent on the nature of the R-group and the selected monomer [31, 32].

Applying the RAFT method, monomers like styrene derivatives, many kinds of different (meth)acrylates (including hydroxyl-, amino-, amido-, ether-, ester-, siloxy-groups), (meth)acrylamides, vinyl pyridine and many others can be successfully polymerized depending on the nature of the chosen R- and Z-groups of the CTA [31, 32]. Figure 5 provides an overview, how the choice of the R- and Z-group influences the polymerization behaviour:

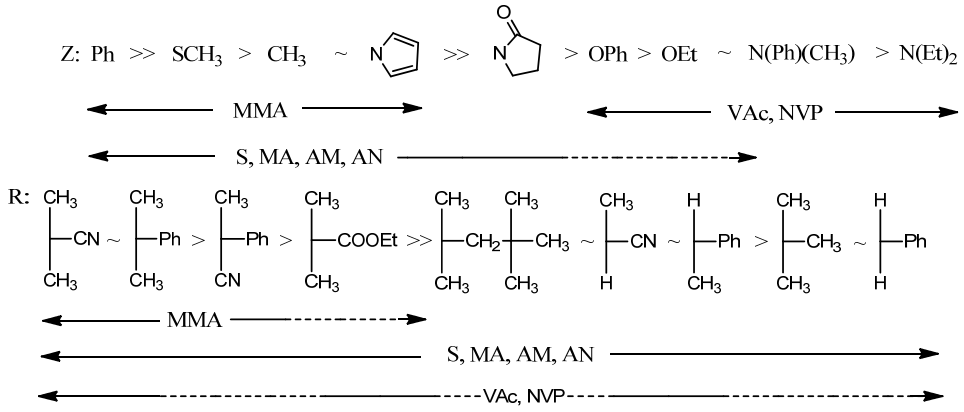

Figure 5: Usefulness of the R- and Z-groups for the polymerization of standard monomers [32].

According to **figure 5**

- Dithioester RAFT agents bearing alkyl- or aryl Z-groups can control the polymerization of styrene, acrylates and methacrylates but not the polymerization of vinyl acetate [32].

- Vinyl acetate can be polymerized applying xanthates (Z= OR) or dithiocarbamates (Z= NR_2). If R is a benzyl group, the RAFT agent is able to polymerize methyl acrylate but not methyl methacrylate; the latter one can be polymerized using R= $C(CH_3)_2Ph$ [32].

- Benzylic species (cumyl, 1-phenylethyl, benzyl) are not suitable for vinyl monomer polymerization (e.g. NVP) because rates of reinitiation are very low with respect to k_p. [32].

- Tert-butyl groups are an excellent choice for R with MA, AM, AN and styrene, but work poorly for MMA polymerization [32].

Nevertheless, some nitrogen containing monomers can lead to problems during polymerizations in water, since in the RAFT process the chain transfer agent is cleaved under basic conditions [32]. In this case, precise pH control is needed. RAFT polymerizations can be conducted in emulsion [70, 71] and miniemulsion [72, 73], microemulsion [74, 75] suspension [76, 77], bulk [78, 79], organic solvents such as toluene or solvent mixtures [80, 81], CO_2 [82, 83], and in aqueous systems [84-86]. Polymerization temperatures reported are in the range between RT and 140 °C [32].

In order to synthesize block copolymers enabling the determination of the molar mass or providing distinct functionalities such as fluorescent, bioactive, water soluble or reactive groups at their termini, tailor made CTAs have to be designed.

2.5 Functional end groups

In addition to their importance for the efficient polymerization control in the RAFT process, the R- and Z-groups can be used as an elegant method for the introduction of functional end groups to polymers, serving different purposes for either the CTA or the later polymer (figure 6).
Chen et al. describe the introduction of an anthracene-moiety for the investigation of the later polymer via fluorescence measurements VI [87]. Gondi et al. attach an azide group to the CTA that will enable click-chemistry at polymer terminus after polymerization VII [88]. The introduction of a vinyl group to the polymer terminus via a functionalized CTA by Patton et al. [89] VIII enables subsequent crosslinking, whereas the introduction of an norbornene-moiety IX enables Diels-Alder reactions either at the CTA or at the terminus of the polymer [90].

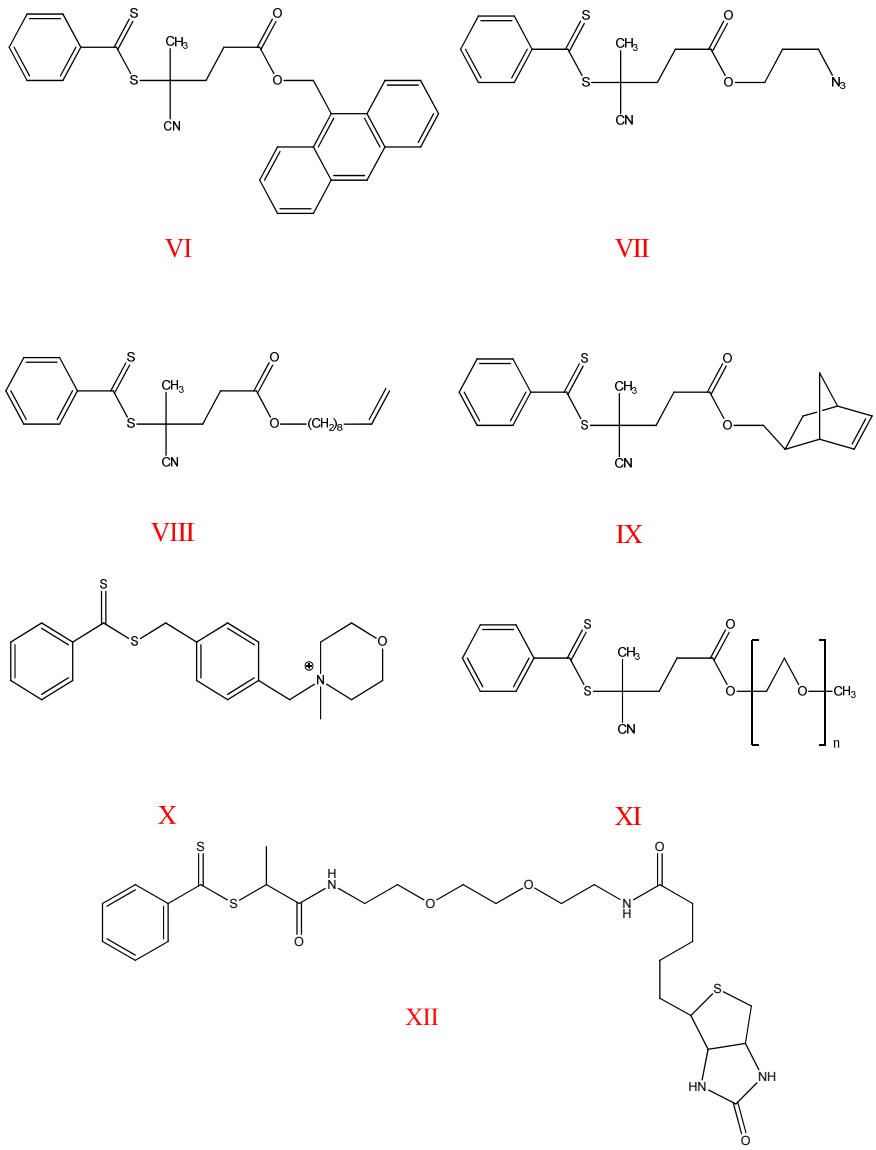

Figure 6: Introduction of functional end groups to chain-transfer agents (CTAs), leading to polymers enabling end-group analysis via VI) fluorescence spectroscopy [87], VII) addition of further blocks applying click-chemistry [88], VIII) crosslinking of polymer [89], IX) Diels-Alder-reactions of the polymer or CTA [90], X) water-solubility of the CTA [84, 91, 92], XI) addition of a polymer-chain to the CTA [93]) and application of a bioactive compound, such as a biotine derivative to a CTA XII [94].

Furthermore, the R-group can be chosen to enable water solubility of the CTA X in case the polymerization should be performed in aqueous environment as described by Mertoglu, Baussard and Lowe [84, 91, 92] or the addition of a polymer-chain to the CTA enabling the synthesis of multiblock-polymers or adding polymer segments that would cause problems in the synthesis of later block copolymers XI [93]. Also biological active compounds like biotine derivatives XII for medical applications can be added to the polymer terminus applying a CTA as reported by Bathfield et al. [94].

Besides these interesting possibilities, defined end groups supply a versatile method for molecular characterization via UV- and NMR- in cases where GPC measurements fail- which is in fact true for most homopolymers such as poly(pentafluorostyrene) (**M7**), poly(N-isopropylacrylamide) (**M1**) or poly(N-acryloylpyrrolidine) (**M2**) or block copolymers including the latter polymers as an appropriate calibration standard is not readily available. Mostly GPC calibration is made applying PS-standards, resulting in invalid numbers for M_n, M_w and M_z because the hydrodynamic values are not comparable [95]. The only reliable information from these elugrams is the distribution of the polymer being mono- or bimodal.

2.6 Fluorescent labels

As already reported, fluorescent labels (e.g. for FSC studies or investigating the diffusion behaviour of polymers in special solvents [96] or the hydrodynamic diameter of labelled particles [97]) have already been successfully synthesized by Zhou et al. XIII + XIV [98] and by Mertoglu et al. [84] for working in aqueous solutions XV. Mertoglu used them for determination of the Z/R-ratio or his block copolymers and molar mass determination. The CTAs are shown in figure 7:

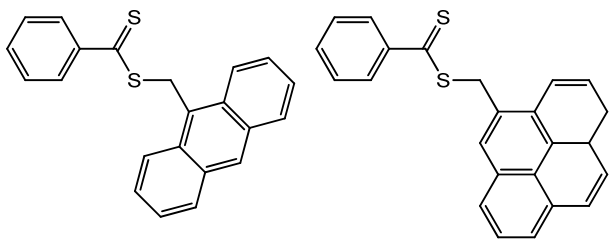

XIII XIV

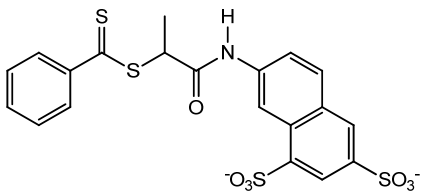

XV

Figure 7: Non-symmetric and symmetric RAFT agents bearing fluorescent labels for application in both organic [98] and aqueous media [84].

The problem with this kind of labels is that most of the fluorescent molecules are stiff and their solubility-and thus the solubility of the CTA- is limited. Consequently a common solvent for both CTA and monomer has to be found, or the polymerization has to be conducted in a

solvent mixture or a biphase system, which might lead to very broad molecular weight distributions due to a lack of control [99].

Furthermore, often problems occur due to fluorescence quenching, limiting the use of that method especially in combination with the RAFT process. Farinha et al. [100] report the quenching of coumarin 343 (C343) fluorescence by four different chain transfer agents (CTA) used in RAFT polymerizations: carboxymethyl dithiobenzoate (CMDB), tert-butyl dithiobenzoate (tBDB), menthonyl dithiobenzoate (MDB), and bis(3-methylbutyl)-2-(thiobenzoylthio)succinate (MBTS). They interpreted the results of stationary and time-resolved fluorescence measurements of C343 with the different CTA and macroCTA with a single kinetic model, which considers the reversible formation of a C343-CTA exciplex and static as well as dynamic quenching of C343. Additionally, the photophysical properties of tert-butyl mercaptane (tBM), resulting from the aminolysis of the tBDB dithioester, were additionally studied applying the same experimental conditions, confirming that the thiol group does not quench the C343 fluorescence. This was further tested by converting poly(DcA)-MBTS to the corresponding thiol-ended chain, eliminating the fluorescence quenching of coumarin previously observed. This might be the reason why York et al. [101] attached rhodamine as a fluorescent label after synthesizing the diblock copolymers via the RAFT technique and subsequent aminolysis of the Z-functionality. On the other hand, De et al. reported the synthesis of trithiocarbonate CTAs bearing a boronic acid group and diblock copolymers thereof, and confirmed the identity of the boronic acid end-groups by reaction with the dye alizarin. In the presence of boronic acids or boronates, the catechol of alizarin creates a boronic ester or boronate ester, respectively, which emits orange fluorescence upon excitation with long-wavelength UV irradiation [102]. Due to the described problems and controversal results, the design of a fluorescent label was postponed and focus shifted on other methods for reliable determination of the molar mass.

2.7 Features of mono- and bifunctional trithiocarbonate RAFT agents for reliable determination of the molar mass

The following 1) absolute, 2) relative and 3) equivalent methods are typically used for determination of the molar mass [103-106]:

1) ***Absolute methods**:* colligative properties (cryoscopy, ebullioscopy, osmometry), static light scattering, ultracentrifuge and MALDI-ToF

2) ***Relative methods**:* viscometry, GPC, field-flow-fractionation

3) ***Equivalent methods**:* end-group analysis (via NMR, IR, UV-Vis, elementary analysis)

Cryoscopy, ebullioscopy, viscosimetry, osmometry, static light scattering, field-flow-fractionation and ultracentrifuge are time consuming; especially the three latter ones need high mathematical effort and the interpretation is often ambiguous.
For GPC measurements a proper solvent has to be found and especially with NIPAM- and NAP-containing polymers aggregation and adsorption phenomena at the column cannot be avoided, leading to mistakes. Furthermore, no readily available standards for the calibration of these systems exist. For this reasons, the analysis of block copolymers is always challenging

using GPC. MALDI-ToF can be a useful tool for the determination of the molar mass also of block copolymers but a proper matrix must be found first and the molecular weight distribution has to be narrow (around 1.2). In case the chemical structure of the molecule/polymer is known, end-group analysis via NMR, IR or UV-vis can be a versatile tool and an absolute method. The methods require no huge apparative effort. Adsorption or aggregation phenomena do not show an influence on the result, which is a drawback when applying e.g. viscometry measurements.

Considering all the described problems, analysis of M_w applying end-group determination is coming into focus. Using the RAFT method, appropriate labels for UV- and NMR-spectroscopy can be attached to the polymers via functionalization of the R- and Z-groups of the trithiocarbonates. The only drawback of this method is that a loss of endgroup must be avoided otherwise leading to wrong results (= too high molar masses). Therefore, the conversion of the polymerization should not exceed 60 % [69].

2.8 Analysis of M_n of polymers using ^{19}F-NMR-spectroscopy

NMR-spectroscopy is a mighty tool for both the analysis of low molecular weight compounds and polymers. It can be used for controlling the purity and conformation of the synthesized compounds [107] as well as the tacticity [107], chain mobility [107] and molecular weight (M_n) of polymers by end-group analysis [35]. The significance of NMR-spectroscopy with heteronuclei can be seen from the numerous kinds of publications, monographs, review articles and tables existing. The most important non metallic nuclei in NMR-spectroscopy are-besides ^{1}H and ^{13}C- ^{15}N, ^{33}S, ^{31}P, ^{29}Si and ^{19}F [108]. The big advantage of ^{19}F-NMR spectroscopy is the F-nucleus being as easy to investigate as a simple H-nucleus and fluorine representing a half spin nucleus with a natural abundance of 100 % (pure isotope), almost as sensitive as a proton in ^{1}H-NMR spectroscopy [109]. Fluoro compounds are not so much widespread in nature compared to those containing only carbon and hydrogen, which enables the easy detection of such compounds in ^{19}F-NMR without other signals disturbing.

As a reference substance trichlorfluoromethane is used as an internal standard, although the chemical shift of ^{19}F is independent of solvent, concentration and temperature [109]. The organic compound is inert, volatile and can be mixed with different organic compounds. As the compounds` signal is located at lower strength of the field compared to those of most of the organic fluorocompounds, ^{19}F chemical shifts mostly show negative values.

2.9 ^{19}F-labelled dithiocarbonates and xanthates

Properly working CTAs belonging to the class of dithioesters bearing a fluorinated moiety either at the Z- or the R-group have been reported by few authors only. For example, Lebreton et al. [110] and Bengalia et al. [111] synthesized CTAs either fluorinated at the R- or the Z-moiety as shown in figure 8:

CTAs bearing a fluorinated R-moiety ***CTAs bearing a fluorinated Z-moiety***

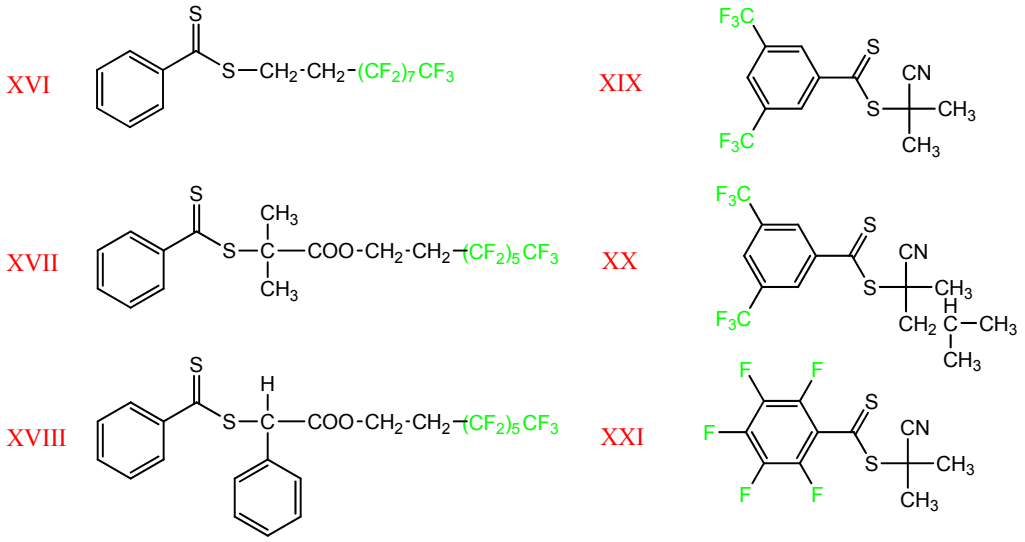

Figure 8: Dithioesters bearing a fluorinated chain connected to the R-group via a spacer successfully polymerized styrene, MMA, EA and 1,3-butadiene (XVI-XVIII); the species bearing fluorinated Z-groups (XIX-XXI) enabled the polymerization of MMA [110, 111].

Lebreton et al. [110] were able to successfully polymerize styrene, MMA, EA and 1,3-butadiene applying the RAFT agents bearing a fluorinated chain connected to the R-group (XVI-XVIII). This way, a short, fluorinated moiety can be introduced to the polymers terminus via the RAFT-agent avoiding an additional polymerization step. Thus, it can be seen as a smart way to achieve fluorine end-capped polymers in just one polymerization step. Bengalia [111] applied RAFT agents bearing fluorinated moieties at the Z-group for the polymerization of MMA (XIX-XXI). Obviously also in this case, the fluorinated moieties showed no disturbing influence on the RAFT process resulting in the well-controlled polymerization of MMA monomers leading to polymers showing a low molecular weight distribution and distinct molar masses.

Even more variations of Z-groups modified with F atoms were reported [111] (figure 9):

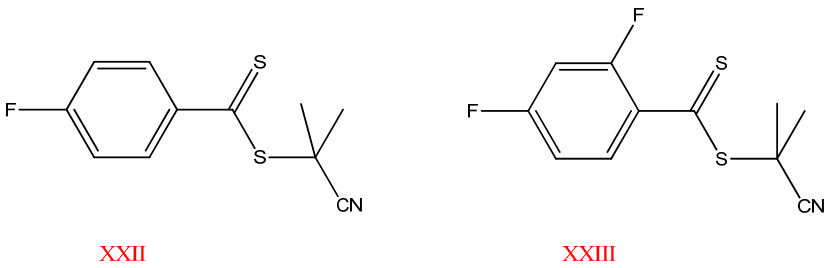

Figure 9: Further CTAs bearing a variable fluorinated Z-group presented by Benaglia (XXII, XXIII) [111].

Dithioesters bearing a differently fluorinated Z- or R-group successfully polymerizing different monomers were also reported by Takopuckdee et al. XXIV [112], Albertin et al. XXVI + XXVII [113] and Moad et al. XXV [114] (figure 10 a):

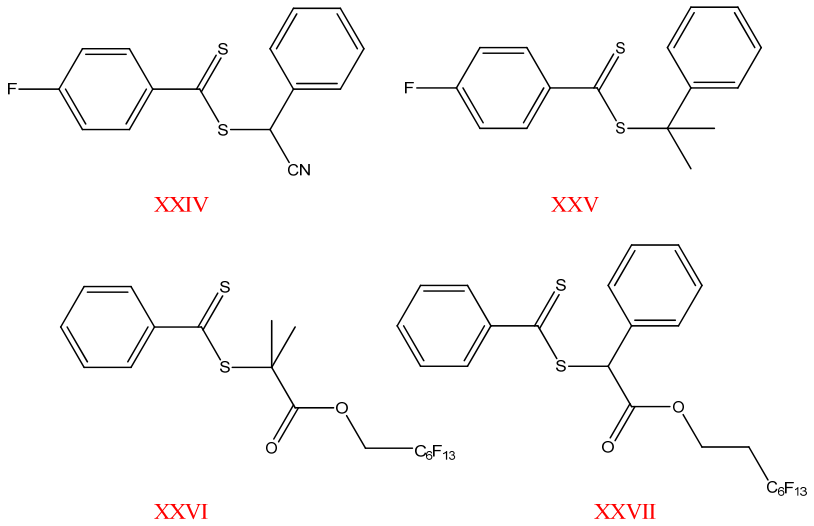

Figure 10a: Dithioesters bearing a differently fluorinated Z-group successfully polymerizing different monomers reported by Takopuckdee et al. XXIV [112], Albertin et al. XXVI and XXVII [113] and Moad XXV [114].

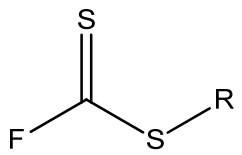

XXVIII

Figure 10b: F-dithioester XXVIII [60].

Also a RAFT-agent bearing a fluorine Z-group XXVIII -which can be seen as a Z-label at the same time- has been reportet by M. Coote et al. [60] (figure 10b). These first computationally designed class of RAFT agents, the fluorodithioformates or F-RAFTs were designed as multipurpose RAFT agents able to control both monomers with stable and unstable propagating radicals [60].

Despite the labelling aspect, the introduction of electron-withdrawing substituents such as fluorine to the dithiobenzoate ring (Z-group) leads to a higher activity of the chain-transfer agent resulting in a narrower molecular weight distribution especially in the first two hours of the polymerization process [32, 60]. The opposite effect was described for electron-donating substituents [32, 60]. Also substituents on the ring system reducing the conjugation of the phenyl with the C=S group reduce the effectiveness of the RAFT agent. Substitution of the R-group against a bulkier species was also reported to improve the MMA polymerization remarkably [32]. The effect of an electron attracting substituent on the stabilities of the radicals involved in RAFT-mechanism was partially studied by M. Coote (vide supra).

Therefore, it could also be interesting to study the effect on polymerization rates of zero, one or two CF_3 functions in the R-group.
Furthermore, also fluorinated MADIX agents or so called xanthates [31, 32] have been successfully applied in the polymerization process. Chiefari et al. and Destarac et al. introduced a fluorine bearing dithiocarbonate, PFPBX-MADIX XXIX [115] and PF-MADIX [116] agent XXX, as well as Postma et al. XXXI [117] and Wan et al. XXXII [118] (figure 11):

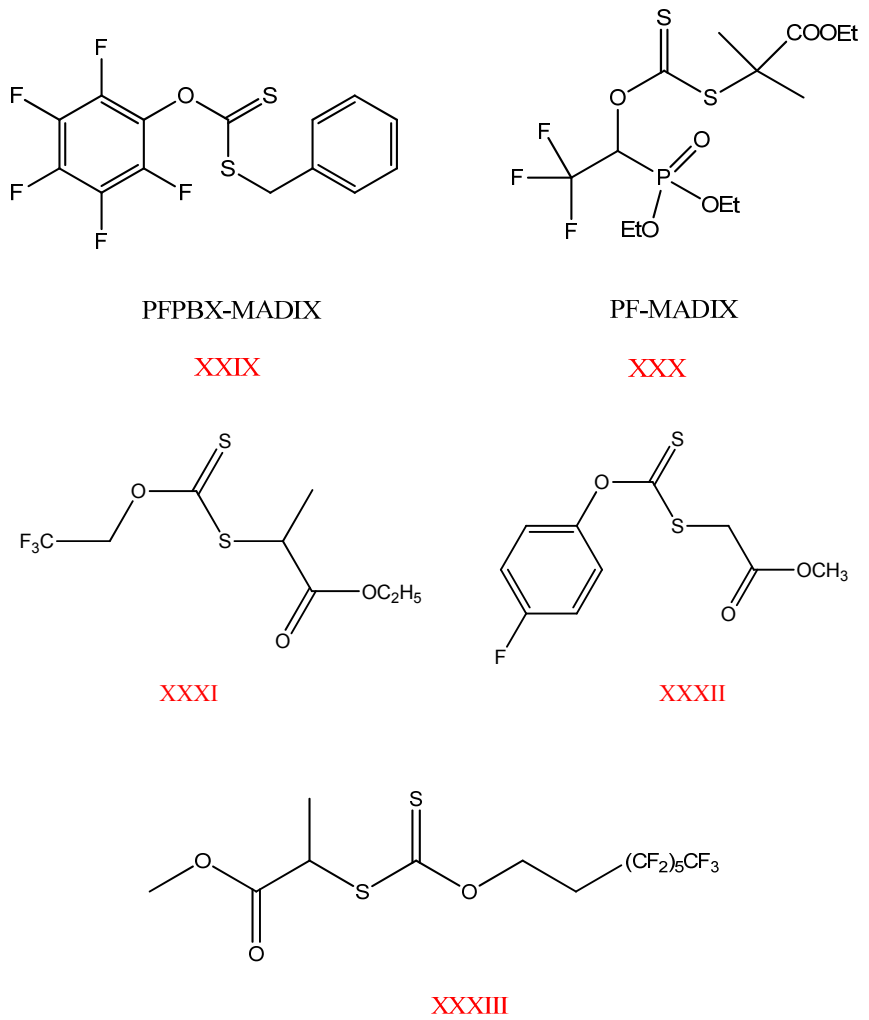

Figure 11: Fluorinated xanthates applied in RAFT polymerization process presented by Chiefari et al. XXIX [115], Destarac et al. XXX [116], Postma et al. XXXI [117], Wan et al. XXXII [118] and Girard et al. XXXIII [119].

Especially the xanthate recently presented by Girard et al. [119] XXXIII enables the synthesis of well defined polymers in supercritical CO_2 due to the fluorinated end groups providing good emulsification properties. Thus, introducing an F-label to the Z- or R-group led to RAFT agents enabling the synthesis of different polymers of low molecular weight distribution.

Chapter III: Behaviour of amphiphilic block copolymers in solution

3.1 Aggregation behaviour of amphiphilic polymers

Self-assembly of block copolymers leads to the formation of aggregates or micelles of various forms [120, 121, 122]. The micellization of the block copolymers is dependent on their composition [112, 213]. Polymers consisting of highly hydrophobic blocks such as e.g. styrene (**M3**) show different micellization behaviour than those composed of more hydrophilic ones. Styrene (**M3**) containing amphiphilic polymers display a lower CMC (= lower critical solution temperature) in water compared to polymers composed of less hydrophobic ones [123]. Garnier chose e. g. poly(butyl acrylate), a quite hydrophobic monomer, for the hydrophobic block of all diblock copolymers reporting that no CMC could be detected down to $1 \cdot 10^{-5}$ g·mol $^{-1}$ [69]. In case of the blocks -such as poly(styrene)- showing a high glass transition temperature, the dynamics of the micellar systems formed are slow [69, 124, 125] . Micelles with a glassy core are formed, referred to as frozen micelles, allowing almost no exchange of polymer between the micelles. Most studies however have focused on the micellization behaviour of commercially available PEO-PPO and PEO-PBO diblock copolymers [126-128]. For BAB-systems, almost no data except for Pluronic® or Poloxamer ® polymers are available.

In order to optimize the performance of formulations and technical processes, often different surfactants are combined [36]. So far, only few mixed systems of amphiphilic block copolymers have been studied [36, 96] and most studies deal with the mixing of Pluronics® [129, 139]. Mixing two different kinds of polymeric micelles is possible in case mixing is related to a gain in both enthalpy ΔH and entropy ΔG and no unfavourable interactions such as electrostatic repulsion and phase separation are present between the polymers [103]. Whereas mixing often enables a gain in entropy, the gain in enthalpy is often negative, especially when working with polymers. Consequently, the gain in entropy is the crucial factor for the formation of mixed aggregates.

3.2 Gels

Many natural compounds such as collagen and its derivative gelatine, hyaluronates, fibrin, alginates, agarose and chitosane form gels [35].

The word “gel” can be deduced from “gelatine” (lat. gelatum= frozen material), which represents a decomposition product of collagen. Gels [35] can be considered as two component systems, consisting of about only 5 % of polymer network and about 95 % of swelling agent. In the case of hydrogels, water is applied as a swelling agent. It enters the gel structure via diffusion making the gel subsequently swell. Hydrogels can show different structures such as linear-, block-, graft- or interpenetrating networks and polymer blends. They are either natural polymers or derivatives of natural polymers, synthetic polymers or a combination of both.

Hydrogels are achievable following different synthetic pathways [140]. For the preparation of hydrogels in this work, gel formation via physical crosslinking using amphiphilic BAB-

triblock copolymers was chosen. The amphiphilic polymers create physically crosslinked micelles forming due to self-assembly in aqueous environment.

3.3 Rheology

The term rheology was inspired by the quotation of Simplicius "panta rei", meaning everything flows. In general, rheology is concerned with the flow behaviour of material [132]. It plays an important role in the characterization of the mechanical properties of substances having a complex structure, e.g. foods [133, 134], non-plastic materials (e.g. creams [36], pharmaceuticals [36], suspensions [135], sludges [136]) as well as polymer melts and their solutions [137-140]. A crucial parameter in this context is the dynamic viscosity η representing the internal friction of the system.

3.3.1 Rheology investigations on gels

As adressed in the introduction, a gel can be seen as highly swollen, chemical or physical crosslinked polymer in which the taken up liquid is strongly bound. Rheologic investigations of hydrogels show viscoelastic properties lying between those measured for a solid and a liquid. The gels prepared from the BAB-triblock copolymer systems belong to the class of physical crosslinked gels achieving crosslinking via bridging of the micelles formed in concentrated aqueous solution. From a physical point of view, gels are only slightly deformed by hydrostatic pressure, whereas shear forces induce strong deformations on the material [35]. Applying rheology measurements, the elastic properties of micellar gels prepared from BAB-triblock copolymers can be studied and the concentrations necessary for gel formation from a distinct polymer or polymer type can be determined and accurately selected from the samples showing liquid behaviour. Investigations on thermosensitive BAB-systems applying rheology measurements have been described by Jeong et al. and Bivigou et al. [141, 142].

3.3.2 Rheology investigations on polymer solutions [35, 143]

A liquid arranged between two plane-parallel plates can be seen as an arrangement of thin layers lying upon each other (figure 11). In order to dislocate two proximate layers against each other, a force is required. The force relating to the area needed to keep the material flowing is defined as the so-called shear stress τ.

$$\tau = \frac{\text{force}}{\text{area}} \quad [\text{Pa}] \qquad \text{(equation } \mathbf{2}\text{)}$$

The shear stress is affecting the top layer of the fluid. The molecules within the layer transfer a part of this impulse on the following layer due to the internal friction resulting in a laminar flow of the liquid. For homogenous media the flow speed is declining linear with the distance x from the moving plate (figure 11). The difference in velocity Δv referring to the distance of the plates is denominated as the velocity gradient or shear rate γ .

$$\gamma = \frac{\text{velocity difference } \Delta v}{\text{plate distance x}} [s-1] \qquad \text{(equation } \mathbf{3}\text{)}$$

Following the law of Newton, the shear stress τ can be directly correlated to the shear rate γ. The constant of proportionality is the dynamic viscosity η, depending on pressure and temperature.

$$\eta = \frac{\text{shear stress } \tau}{\text{shear rate } \gamma} \qquad \text{(equation } \mathbf{4}\text{)}$$

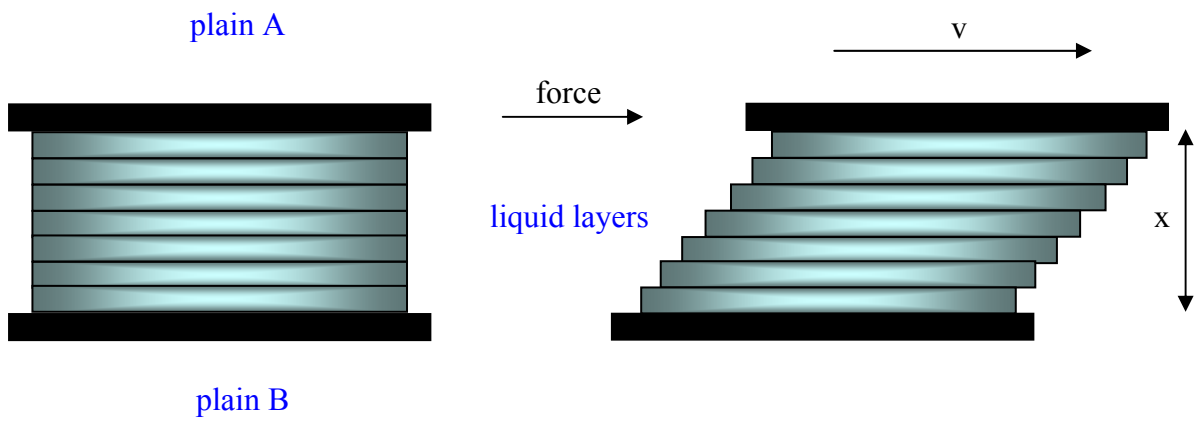

Figure 12: Dynamic viscosity in a liquid induced by applying a force to plain A and B.

-Demonstration of the dynamic viscosity

The energy needed to keep the material flowing will be irreversibly transformed into heat energy. For a quantitative measurement of this energy, which is a direct value for η, the liquid is exposed to a force τ and the speed of velocity γ is being determined.

-Flow characteristics of polymers and polymer solutions

Plotting the determined values for the shear stress τ against the shear rate γ in a graphic chart will result in the so-called flow-curve; plotting the dynamic viscosity against the shear rate will yield the viscosity function of the investigated material. If the viscosity is not changing with increasing shear velocity $\eta \neq f(\dot{\gamma}), \eta = \text{const.}$, the substance is referred to as an Newtonian fluid. Water and many other organic solvents show this ideal flow behaviour. Other substances have to overcome a certain modulus of force -the yield stress- as a barrier/limit before they are able to reach the ideal state of flowing. These substances are referred to as so-called Bingham-materials. The decrease of viscosity with increasing shear velocity towards a certain limit is denominated as shear thinning or pseudo-plastic behaviour.

With polymer solutions this behaviour can be found when intermolecular hydrogen bonds are formed between the polymer strains or –depending on the length of the polymers- entanglements are formed in a way that they get disconnected faster than being reformed at high shear rates. This phenomenon was described first by the theory of Grassley. In case the viscosity is increasing together with the shear velocity, the material is referred to as shear thickening or dilatant (Examples: ketchup or non-drippy wall-paint). For example, graft copolymers composed of a water soluble backbone and hydrophobic arms work as associative thickeners [332]. The described flow-behaviours are graphically displayed in figure 13 and figure 14:

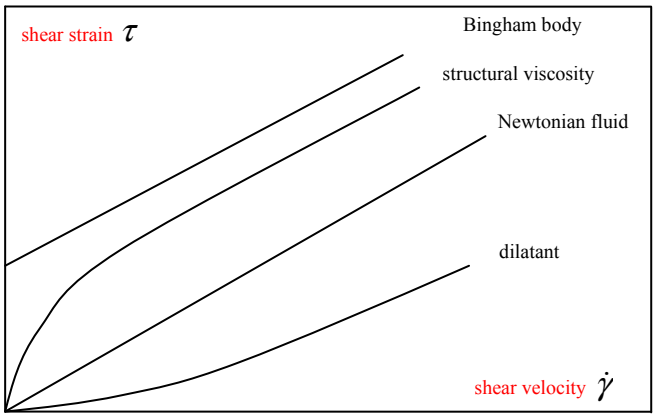

Figure 13: Schematic figures of flow anormalities in flow curves [35, 143].

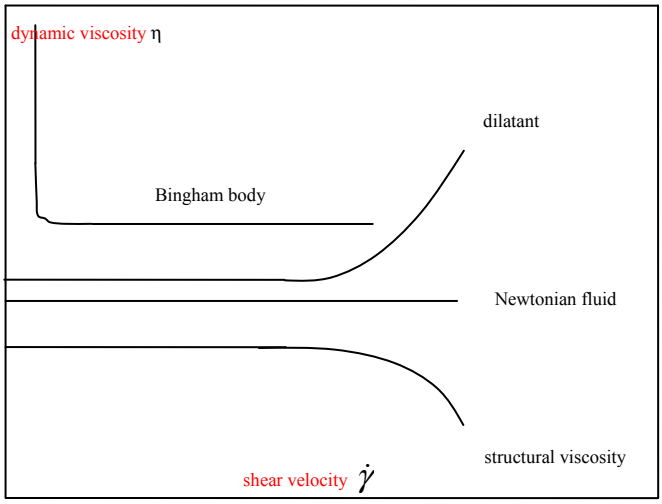

Figure 14: Schematic figures of flow anormalities in viscosity curves [35, 143].

Investigating ideal materials, the first- and backcycle are congruent when the shear velocity is first increased to a certain maximum limit and afterwards diminished. In case the graphs are not congruent the flowing behaviour is time dependent. In this context, two phenomena worth mentioning exist: thixothropic and rheoplectic behaviour.

Thixothropic materials show a decrease of the viscosity at a constant shear velocity to a certain limit, increasing temporally delayed with diminishing shear velocity. Thixothrophy can often be found with gels of linear polymers. The opposite case, the viscosity growing with constant shear rate and then diminishing with time is called rheoplexy. The described phenomenon is quite seldom and can be investigated when dissolving gypsum in water.

-Zero-shear viscosity [35, 143]

The dependence of the shear viscosity on the shear stress can be divided into three regions. With small shear velocities the material will behave like a Newtonian fluid (1.st Newton area). Within this interval the molecules are able to relax fast resulting in the viscosity being independent of the shear speed; therefore it is also referred to as zero-shear viscosity η_0.
Encountering a certain critical shear velocity, the logarithm of viscosity will drop with the shear gap with the material under investigation showing non-Newtonian behaviour in the so-called power-law-region.

-Temperature dependent behaviour of the viscosity [35, 143]

Besides molecular properties (e.g. molar mass, the polydispersity, type of repetition units) and other parameters such as pressure, concentration and type of solvent the viscosity of polymer solutions is strongly dependent on the temperature. The temperature dependence of the viscosity η can be described by the Arrhenius-equation in good approximation:

$$\eta = k \cdot e^{\frac{E^{\#}}{RT}} \qquad \text{(equation } \mathbf{5}\text{)}$$

K is a constant factor, $E^{\#}$ is the activation energy for flowing ([J mol^{-1}]; T is the absolute temperature [K] and R is the gas constant (8.31441 J $mol^{-1}K^{-1}$)

In rheology, k is often defined as viscosity at a defined temperature. This enables the introduction of the shift-factor a_T describing the viscosity behaviour of the material depending on the temperature normalized to a reference temperature (normally 20 °C).

$$a_T = \frac{\eta_{0,\,T}}{\eta_{0,\,T\,=\,20°C}} \qquad \text{(equation } \mathbf{6}\text{)}$$

Introducing the logarithm to equation is leading to a linear equation. From the slope of the equation the flow-activation energy $E^{\#}$, which is specific for a certain material, is accessible. Plotting η measured at different temperatures against the reciprocal temperature and analyzing the slope of the plot, yields $E^{\#}$. It becomes evident, that a high activation energy stands for a high dependence of the viscosity on temperature. Examining a polymer solution, the value for $E^{\#}$ is positive and higher compared to that of the solvent. In most cases negative values are not possible.

$$\ln \eta = \ln k + \frac{E^{\#}}{R} \cdot \frac{1}{T}$$ (equation **7**)

with η representing the viscosity, k as a constant factor, $E^{\#}$ representing the activation energy for flowing ([J mol^{-1}]; T is the absolute temperature [K] and R is the gas constant (8.31441 J $mol^{-1}K^{-1}$)

-3.3.3 Oscillation rheology [35, 143]

With oscillation rheology the sample under investigation is subjected to oscillating deformation at small amplitudes. The measurements provide access to the investigation of complex rheologic characteristics of the material. In contrast to rotation experiments, shear strain experiments are not influenced by the shear velocity. The values for shear strain are achieved from the frequency and amplitude of the oscillation the sample is subjected to. In a first investigation step, the linear-viscoelastic area of the sample has to be determined. After adapting the oscillation to sufficiently small values the assumption is valid, that the drawback force, pulling the molecules back into their rest position, is proportional to the distance from it. This fact offers the advantage to investigate viscous and elastic parts of the stored energy apart from each other. The time dependent oscillation can be described by the following equation:

$$y(t) = A \cdot \sin(\omega \cdot t)$$ (equation **8**)

y= deflection at time (t), A= amplitude, ω= angular frequency, $\nu = \frac{\omega}{2\pi}$, ν= frequency of oscillation

The derivative of the shear strain with respect to time results in the shear velocity γ:

$$\frac{dy(t)}{dt} = \dot{\gamma} = \omega A\cos(\omega t) = \omega A\sin\left[\omega t + \frac{\pi}{2}\right]$$ (equation **9**)

y= shear velocity , A= amplitude, ω= angular frequency

The response of the sample (τ(t)) -the resulting deformation- to the deflection y(t) is oscillating with the same frequency but phase delayed by a phase difference angle δ. The circumstance is depicted in figure 15:

The amplitude of the measured function is dependent on viscous, the phase delay on elastic parts of the sample.

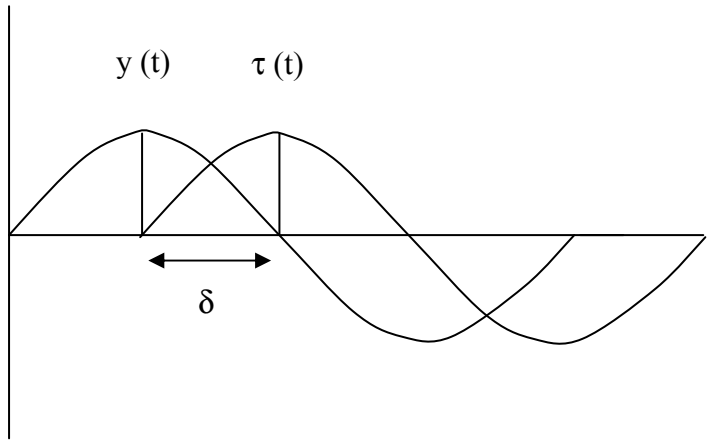

Figure 15: Excited oscillation and reaction of the probe (shear stress) are phase-shifted. δ is referred to as the so-called phase angle.

The sinusoidal shear stress τ in dependence on the time t can be described by the following equation:

$$\tau = \tau_0 \cdot \sin(\omega i + \delta) \qquad \text{(equation } \mathbf{10}\text{)}$$

τ= sinusoidal shear stress, ω= angular frequency, δ= phase angle

τ_0 is the maximum amplitude of the shear stress, diminishing with the distance of the oscillating probe.

The phase difference angle δ and the amplitude of the shear stress are the basic measurement categories in a rheology oscillation measurement. Depending on the value for the phase angle δ, the following material classification can be made by definition:

δ= 0° = > pure *elastic* material

δ= 90° = > pure *viscous* material

0° < δ < 90° = > *viscoelastic* material

Chapter IV: Surfactant properties of fluorinated and non-fluorinated block copolymers

4.1 Surface activity

Due to their amphiphilic structure, block copolymers are able to accumulate at the interface between air and water exposing their hydrophilic segments in direction of water and hiding their hydrophobic segments away from water by orientating them towards the gas phase. This process is referred to as adsorption [36, 144, 145]. This behaviour leads to a lowering of the free interfacial energy per unit area, which can be characterized by the surface tension γ. The surface tension of surfactants, especially the polymeric ones, is gradually decreasing with increasing concentration due to a slow, gradual accumulation of the polymeric surfactant in the monolayer. The Gibbs adsorption isotherm describes this behaviour:

$$\Gamma = -\frac{1}{RT} \cdot \frac{d\gamma}{d\ln C} \quad [146] \qquad \text{(equation } \mathbf{11}\text{)}$$

Γ= excess concentration of surfactant in the surface layer, γ= surface tension, C= concentration

The surfactant molecules in the layer are in equilibrium with the non-aggregated molecules in solution (unimers). Therefore, when the critical micellization concentration is reached, the value for the surface tension remains virtually constant from that point on due to a constant concentration of unimers in solution. Depicting the surface tension against the surfactant concentration, a break in the graph can be found representing the CMC of surfactants [36, 144, 145, 147].

4.2 Classification and properties of polymer surfactants

Depending on their molecular structure, two different types of polymer surfactants can be distinguished [148]:

- macro-surfactants
- polysoaps

Macro-surfactants are defined as amphiphilic block copolymers and graft copolymers with the complete macromolecule behaving like an amphiphile. Within this surfactant class, different architectures can be realized. An amphiphilic block copolymer consists of both a hydrophobic block insoluble in water and a water soluble hydrophilic block covalently bound to each other [36, 144, 145]. Polysoaps consist of amphiphilic repeat units which do not necessarily have to be covalently bound to each other [148].

Amphiphilic block copolymers like BAB-triblock copolymers or CF-end capped polymers belong to the class of macro-surfactants. They show different interesting features. In a selective solvent for one of the blocks, the reversible aggregation process is analogous to the micellization process of low molecular weight surfactants and occur by closed association processes [36, 144]. This self-assembly process occurs due to an unfavourable mixing enthalpy and small mixing entropy. The block segments try to separate, but the covalent bonds between them avoid a macroscopic phase separation of the blocks [36].

The majority of conventional surfactants is composed of a polar head group and a hydrocarbon chain as the surfactants tail [149]. The tail is either of aliphatic or alkylaryl nature. The minimum surface tension achievable using this type of surfactants is in the order of 26-28 mN/m [36, 145]. In case an even lower surface tension is required, e.g. for special applications like spreading water-based formulations on surfaces on polyolefines or spreading aqueous foams on top of burning oil [145], speciality surfactants are used.

Extreme reduction of the surface tension is possible applying silicone surfactants and fluorinated or perfluorinated surfactants, able to lower the surface tension down to 20 mN/m [36, 145]. Silicone surfactants are based on polydimethylsiloxane moieties for the non-polar group, whereas fluorinated surfactants contain a fluorocarbon or a combination of hydrocarbon and fluorocarbon moieties for the surfactants tail.
Fluorinated and perfluorinated surfactants show the following general structures [36]:

CF_3-$(CF_2)_n$-**X** perfluorinated surfactants

CF_3-$(CF_2)_n$-$(CH_2)_n$-**X** fluorinated surfactants

X represents a polar group, which can be charged or uncharged. The fluorocarbon chain is mostly short, with n showing a value of about 5-9 [150, 151]. The perfluorinated species is composed of CF-groups only, whereas the fluorinated samples contain also $–CH_2$-groups as a spacer [36]. The number and location of the F atoms determines the surfactants behaviour [36, 145]. Originating from the strong inductive effect of the fluorine atomes, fluorinated surfactants are often strong acids and relatively insensitive towards low pH-values or hard water [36, 145]. The commercially available products are mostly a mixture of homologues.

4.3 The outstanding properties of fluorinated surfactants

Fluorinated surfactants display outstanding properties making them prone for special applications (also valid for silicone systems) [36, 145]:

- tremendous lowering of the surface tension (down to about 20 mN/m)

- powerful antifoamers

- excellent wetting and spreading behaviour on low-energy surfaces

They are used for rendering surfaces, e.g of textiles or paper and as surfactants in paints or other non-aqueous formulations due to their surface activity in organic solvents [145]. Fluoro- and silicone surfactants are the only surfactants suitable for the use in non-aqueous systems [36, 145]. A disadvantage of perfluorinated surfactants is their high production costs and especially their poor biodegradability, leading to persistence in environment [152, 153].
The HLB (hydrophobic-lipophilic balance) of the polymers can be adapted by carefully playing with the length of the hydrophilic and hydrophobic blocks of the BAB- and ABA-systems as well as the hydrophobic and lipophobic blocks of the CF end-capped polymers.

4.4 The HLB-concept

For classifying the surfactants properties, Griffin developed the concept of the hydrophilic-lipophilic balance (HLB-concept) for non-ionic surfactants [36, 144, 145, 154]. The HLB-value attributes a characteristic number for a surfactant molecule. Applying this concept, the nature of the surfactant can be determined by simple calculations [36]. The concept was further developed by Davies, presenting a scheme giving the chemical groups present in a surfactant specific HLB group numbers [36]. By variation of the length of the hydrophobic block, the HLB of a surfactant can be tuned [36]. Due to the HLB-scheme, possible applications for surfactants can be deduced [36, 145], e.g:

-Emulsifiers for w/o emulsions should be hydrophobic showing and HLB number of 3-6

-Emulsifiers for o/w emulsions should be hydrophilic displaying an HLB number of 8-18

Unfortunately, only a restricted number of polymers can be classified using this system and the numbers are strictly valid only at room temperature for non-ionic surfactants.
As a general rule, the investigated BAB-systems become more hydrophobic with the length of the hydrophobic B-blocks (**M3**, **M7**) increasing, keeping the length of the hydrophilic PNIPAM (**M1**) block constant. Heating aqueous solutions of the BAB-systems above the cloud point will result in a completely hydrophobic polymer due to the hydrophilic PNIPAM-block (**M1**) collapsing changing the HLB of the system completely (HLB shifted to values below 8).

4.5 Foams

Foams appear in context with all kinds of cleaning activities such as shaving, showering, cleaning laundry and at the surface of beverages such as beer. All described foams have to fullfill different criteria: a foam used for shaving or beer foam should be stable and show good foaming activites [155], whereas a detergent for laundry cleaning using a washing machine or dishwasher should show defined foaming activities only [36]. Also for industrial applications the knowledge of the foaming activities of a liquid for example in a reactor or in case the liquid should be pumped, destilled or transported is crucial [36, 156, 157].
Foams can be described as dispersions of a gas in either a liquid or a solid [36, 158]. This work deals with the dispersions of gas in a liquid. Almost all liquid foams are not thermodynamically stable [36, 144]. Foams can only be gained from mixtures, pure liquids

never foam [36]. As a general rule, anionic-, cationic and amphoteric surfactants are often good foaming agents, whereas non-ionic surfactants, like the foams created from polymer surfactants such as BAB-triblock copolymers described in this thesis, tend to less foam formation [36]. Foam formation is a characteristic feature for low molecular weight and distinct polymer surfactants (also examples for non-foaming polymeric surfactants exist [36, 159]. The foaming ability and –stability is characteristic for a distinct surfactant.

4.5.1 Foam formation and stability

From a kinetic kind of view, two different kinds of foam categories can be distinguished: Metastable or permanent foams having a lifetime of hours or days and transient foams having a lifetime of seconds [36, 160]. In general, surfactants bearing a high value for the HLB (= hydrophilic-lipophilic balance) show a good formation of foams having a high stability whereas surfactants bearing a low value for the HLB do not show this behaviour and are often used as foam inhibitors [36, 144, 145]. The ratio of gas to liquid is responsible for the appearance of the foam and is referred to as the foam number [36]. Spherical gas bubbles with thick liquid lamellae can be observed with low foam numbers whereas at high foam numbers polyhedral gas bubbles with thin, planar lamellae are formed. Normally a foaming liquid shows both types of bubbles with the polyhedral gas bubbles located above the spherical ones [155, 158]. Effective foaming agents have to display a rapid movement to newly created interfaces and need a high concentration of free molecules not bound in micelles, similar to wetting agents [36].

Two conditions are crucial for the formation of a foam [36]:

- One component must show surface activity. Most organic substances show low surface tensions. Mixing organic compounds with water therefore leads to foam formation.

- The formed foam film must own surface elasticity; that means the film has to be pulled back after stretching to its former, original position. The surface elasticity E can be defined as:

$$E = A\frac{d\gamma}{dA} \qquad \text{(equation } \mathbf{12}\text{)}$$

with A, the surface area and γ, the surface tension

The mechanical properties of the surface layers and thus the foam stability are controlled by the adsorbed surfactant film. Nevertheless, the stability and drainage of liquid foams is not fully understood and affected by many factors such as mechanical disturbances or environmental stress. More experiments are necessary for understanding the activity at the interface of these complex systems.

4.6 The preparation of emulsions and their stabilization

Emulsions can be encountered in various types of industrial applications such as emulsion polymerization of styrene [161], acrylic paints for artists or buildings [162], pharmaceutical [163], cosmetical and personal care products [164-166], foods [167] and much more [168, 169]. In general, an emulsion can be described as a thermodynamically instable, heterogeneous system composed of two non-miscible liquids dispersed in each other in the form of small droplets with the diameter ranging between 0,1 µm and 200 µm [36, 144]. Depending on the composition of the mixture and the hydrophobic-lipophilic balance (HLB) of the applied surfactant, three different types of emulsions can be distinguished [36, 144]:

- the **oil-in-oil** systems (**O/O**),

- the **oil-in-water** systems (**O/W**) or

- the **water-in-oil** (**W/O**) systems

Factors like the electrolyte concentration in water, the polarity of the applied oil and the chosen water to oil ratio may also influence the type of emulsion formed [36]. The most important systems among them are the oil in water and water in oil systems [144].

For the successful preparation of emulsions the surfactant has to fulfil two crucial conditions [36, 144]:

- The surfactant must be able to reduce the interfacial tension between the oil and water to small values. The triblock copolymers could fulfil this requirement and especially the fluorinated species are known to drastically lowering the surface tension.

- The surfactant must be able to reach the newly developed surface quickly in order to stabilize it against coalescence. For achieving rapid diffusion, low to medium molar weight surfactants are preferred.

Macro surfactants of different architectures and compositions- also ABA- and BAB-systems [170-172] have proved to be efficient stabilizers in emulsion formation via steric stabilization [36, 173]. The stability of the emulsions can be varied by using polymeric thickeners. E.g, hydrophobically modified polymers can adsorb at the interface between two phases and simultaneously thicken the emulsion [174, 175]. The application of stimuli-responsive polymers, like pH- or thermo-responsive block copolymers [176, 177] can lead to smart emulsions sensitive to environmental changes. Especially supramolecular surfactants, among them block copolymers, have turned out to be good stabilizers for multiple emulsions, in which the droplets of the phase dispersed include even smaller dispersed droplet [178, 179].
In this study the ability of the fluorinated and non-fluorinated BAB-triblock copolymers to form emulsions was investigated. The study of these polymers as possible emulsifiers is interesting for their molar mass is still not too high and especially the fluorinated block copolymers could serve as emulsifiers for fluorinated oils.

In the emulsion process, an initial large droplet of the disperse phase with an area of A is spread in the continuous, immiscible phase in the shape of many smaller droplets creating the total area A` with $\Delta A = A` - A >> 0$. During the process, the free energy is changing due to the positive value for the surface energy term $\Delta A \cdot \gamma_{1,2}$; in which γ represents the tension of the interface between both phases, and the positive value for the entropy of dispersion $T \cdot \Delta S_{disp}$ [69, 144].

$$\Delta G_{emulsification} = \Delta A \cdot \gamma_{1,2} - T \cdot \Delta S_{disp} \quad \text{(equation 13)}$$

In most of the studied cases, the values for ΔG are positive, implying a non-spontaneous formation of the solution. The emulsification has to be forced by adding energy in form of sonication or stirring to the system.

The stability of emulsions is depending on different factors [36, 144]. The most important are the HLB of the used surfactant and its mechanical properties at the interface, the miscibility of the phases and the viscosity of the outer phase, the strength of the repulsive forces between the drops and the interfacial tension $\gamma_{1,2}$. The system is destabilized by van-der-Waals forces which are compensated by repulsive electrostatic forces in case an ionic surfactant is used or by repulsive forces in case a macro-surfactant is applied or both if using a polyelectrolyte as a surfactant.

Emulsions are known to change their properties with time on different time scales. The time interval for changes can vary from seconds to years. Different processes leading to the destruction of the emulsion are known, originating from the influence of differences in density or the distribution of the particles size [36, 180, 181]. Flocculation occurs due to attractive Van-der-Waals forces and can be compensated by means of steric or electrostatic stabilization. Different particle sizes lead to the so-called Ostwald ripening in which molecules of the dispersed phase diffuse from small to large droplets causing a continuous increase of the droplet size. Coalescence is occurring due to the growth of the droplet size induced by the thinning and disruption of the interfacial film if two drops come in contact to each other. Creaming and sedimentation are originating from the influence of gravity with time especially in case the density of the disperse phase is lower compared to that of the continuous one and the higher the differences in density. In microemulsions the latter effects can be avoided due to the smaller size and thus volume of the droplets ($d << 1\ \mu m$) diminishing the influence of gravity.

4.7 Microemulsions

Microemulsions were first observed by Schulman [182] and Winsor [183] in the 1950s.
Microemulsions can be described as slightly opaque or homogeneously transparent mixtures of water, surfactant and oil as the third component [36, 184]. The nature of the applied oil and surfactant can be varied on a large scale. Compared to emulsions they are thermodynamically stable and show very low interfacial tensions (< 1mN/m, for comparison pure water 73 mN/m [36, 144, 145]).

$$\Delta G_{emulsification} = \Delta A \cdot \gamma_{1,2} - T \cdot \Delta S_{disp} < 0 \quad \text{(equation 14)}$$

When preparing a microemulsion, co-surfactants like medium-chain alcohols are applied in defined relations to oil and water. The microstructure is dependent on the surfactants properties, especially the critical packing parameters [36, 144].

Depending on composition, three different types of microemulsions can be distinguished. If oil is used as the excess compound, it is referred to **Winsor I** type; if water is used in excess it belongs to the category of **Winsor II** type and in case the microemulsion is prepared using an excess of both water and oil it belongs to the **Winsor III** type [36, 185, 186]. Microemulsions of **Winsor IV** type require huge amounts of surfactants which can be seen as a disadvantage for their applications (> 20 weight percent) [187].

This drawback can be compensated by adding little amounts of amphiphilic block copolymers which can improve the solubilization capacity of the used surfactants referred to as "efficiency boosting" in the literature [188]. Generally, amphiphilic polymers can strongly influence phase behaviour because of their impact on the bending rigidity of the surfactant film [189]. Especially in droplet microemulsions, very low concentrations of amphiphilic polymers suffice to interconnect microemulsion domains leading to ordering phenomena changing the phase behaviour [144]. The strong influence of amphiphilic polymers on the phase behaviour of microemulsions can be exploited economically and for environmental protection due to lower surfactant concentrations needed. In this context, the use of efficient surfactants is a disadvantage due to the formation of liquid crystalline phases, which are often highly viscous and result in phase separation in case the liquid crystalline phase coexists together with a microemulsion phase. Amphiphilic polymers can help to overcome these difficulties [186].

How can the influence of polymer on the microemulsion behaviour be understood? [186]

The addition of block copolymer causes changes, which are closely connected to the increase in efficiency. The low interfacial tension between water and oil is reduced further after polymer addition in agreement with the behaviour of low molecular weight surfactants, where lower interfacial tensions were found for more efficient systems. Furthermore, the reduction of the total amphiphile content leads to the microemulsions becoming turbid; this means that the sizes of water and oil domains must get larger. A small angle neutron scattering study revealed that the characteristic length scale of the water and oil domains is inversely proportional to the volume fraction of surfactant. From this result the conclusion can be drawn that the block copolymer shows no influence on the overall interfacial area. This is given by the surfactant. However, the polymer allows stabilising larger structures that cannot exist without the polymeric additive. The theoretical explanation of this effect goes back on the Helfrich free energy.

Chapter V: Styrene and its derivatives suited for the permanently hydrophobic B-block

5.1 Styrene

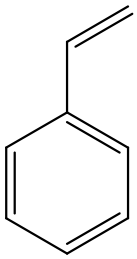

Figure 16: Structure of styrene (**M3**)

Styrene (**M3**) (figure 16) is among the most applied monomers in polymer chemistry. It can be polymerized using anionic and cationic polymerization technique [190, 191], tacticity controlled applying metallocene catalysts [192, 193], using controlled radical polymerization techniques like ATRP [31] and RAFT [31, 32] and, of course, free radical polymerization technique [31]. Furthermore, different reaction conditions like polymerization in solution [194, 195], emulsion- and miniemulsion [196, 197] and in bulk [198, 199] are possible.

Free radical polymerization of styrene is possible with and without addition of an initiator. Besides the initiation of the polymerization via different kinds of initiators [200-203], electroinitiation [31], plasma [204] and pure thermal initiation is also possible and was simulated by Hui and Pryor [205, 206]. Styrene and substituted styrenes have been shown to undergo self-initiated polymerization [207, 208]. It must be pointed out that the rate of self-initiated polymerization is much slower than the corresponding polymerization initiated by thermal homolysis of an initiator such as AIBN but far from negligible. The rate of self-initiated polymerization rate for neat styrene at 60 °C is $1.98 \cdot 10^{-6}$ [31, 209].

The two main theories for the thermal, self-initiated polymerization are those proposed by Flory and Mayo [31, 210, 211]. For the Mayo theory, in the initiation mechanism for styrene, first a Diels-Alder dimer is formed by a [4 + 2] addition between two styrene molecules [209, 211]. This gives the non-aromatized Mayo adduct, 1, which cannot undergo a thermal 1,3-sigmatropic shift due to symmetry considerations and therefore undergoes a molecular assisted homolysis reaction with another molecule of styrene to give the aromatized radical and the radical derived from styrene via the transfer of a hydrogen atom from the dimer to a styrene molecule. It is not completely clear, whether the formation of the Diels-Alder dimer or its reaction with styrene is the rate-determining step in the initiation of the pure thermal initiation (figure 17).

The dependence of R_i on [M] is closer to 3rd- order than 2nd-order, which indicated that this is the slow step. The hypothetical Diels-Alder dimer has so far never been isolated but ultraviolet spectroscopy of the reaction system points to its presence.

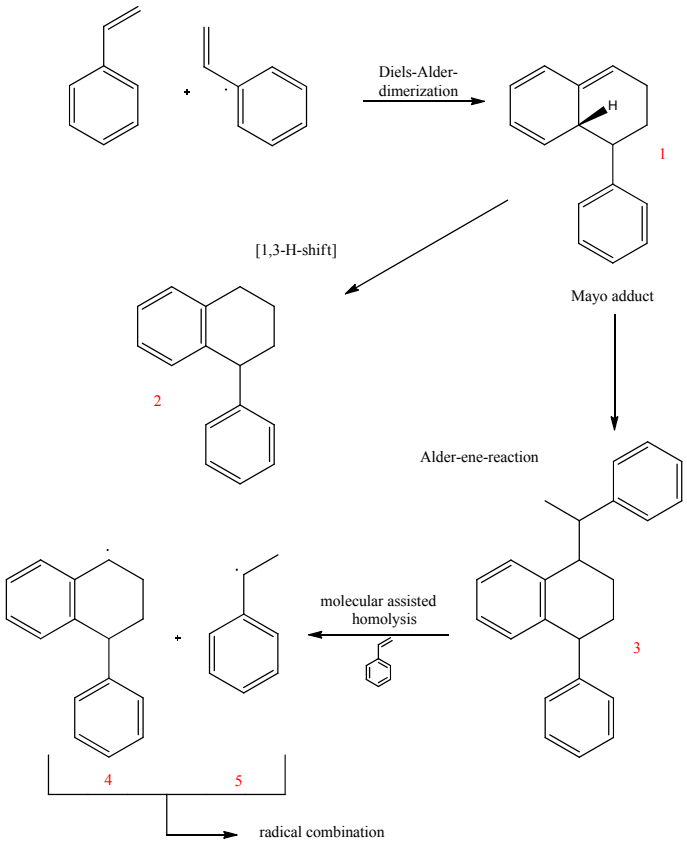

Figure 17: Self-initiation of the polymerization of styrene (**M3**) following the mechanism proposed by Mayo adapted from [31, 209]. The mechanism was confirmed by Chong et al. [212] and Buzanowski et al. [213].

For the fluorinated styrenes, especially 2,3,4,5,6-pentafluorostyrene (**M7**), problems are reported for the thermal initiation of the polymerization. Pentafluorostyrene was not observed to give significant amounts of polymer under prolonged heating at 125 °C in the presence of TEMPO (see also NMP-polymerization mechanism) [214]. This behavior is consistent with the low ability of pentafluorostyrene to undergo autopolymerization via a Mayo mechanism reported by Pryor et al. [215]. In contrast to these findings, Hvilsted et al. reported the thermally initiated polymerization of pentafluorostyrene up to high yields at 110 °C under ATRP conditions in a controlled manner [216]. The apparent polymerization rate was found to be first order with respect to the conversion of monomer with the molecular weight increasing linearly with monomer conversion. Also Hussain et al. [217] reported the polymerization of 2,3,4,5,6-pentafluorostyrene (**M7**) at 100 °C under ATRP conditions synthesizing poly[poly(ethyleneglycol)methyl ether methacrylate]-b-poly(pentafluorostyrene) amphiphilic diblock copolymers.

Several groups described the successful, controlled polymerization or copolymerization of pentafluorostyrene (**M7**) in presence of an initiator or inimer [218-221]. Due to the discussed controversy, V 30 was chosen for initiation in bulk at a polymerisation temperature of 120 °C [222].

5.2 The special behaviour of fluorocarbons [223]

Fluorine is the most electronegative element, with a very low polarizability and a high ionization potential [145, 223, 224]. Fluorine atoms are larger compared to hydrogen ones (van der Waals radius 1.47 Å of fluorine compared to 1.20 Å of hydrogen) [225]. Therefore, $(CF_2)_n$-chains are bulkier compared to $(CH_2)_n$-chains (cross sections 30 $Å^2$ compared to 20 $Å^2$) [223, 225]. Furthermore, F-chains show a greater stiffness due to the larger size of the fluorine atom; the stiffness goes along with a low of gauche/trans freedom [223]. Perfluorinated chains adopt a helical conformation in order to minimize steric hinderance. In organic chemistry, the C-F bond represents the most stable single bond due to effective overlapping of the orbitals (~ 485 kJ mol^{-1} for C-F- compared to ~ 425 kJ mol^{-1} for C-H-bonds) [223]. Therefore, fluorinated compounds show a high chemical and thermal stability. The dense electron cloud around the fluorine atoms provides a repellent sheath that effectively protects fluorinated chains against attacks of other reagents [226]. Fluorinated compounds are often used in medical and biological applications due to their inertness [227].
The low polarizability of fluorine leads to weak van der Waals interactions between the fluorinated chains and low cohesive energy densities in liquid fluorocarbons [226, 228]. The weak interactions are also responsible for excellent spreading properties, low surface tensions, low dielectric constants, high fluidity and vapour pressure (of liquid FCs), high compressibility of gas and also high gas solubilities [223, 226] of these compounds. The only weak van der Waals interactions are also responsible for the FCs not mixing with substances made from hydrocarbon chains having a higher cohesive energy density [223]. They show surface activity in liquids made from hydrocarbons at the interface between air and oil and the interface between water and oil [223]. The low polarizability of fluorine atoms together with the large surface of the fluorinated chains leads to increased hydrophobicity and a pronounced lipophilic character.

5.3 Fluoropolymers

Fluoropolymers can be divided into two subclasses [229]: First, the fluorocarbon polymers, which are polymers made from perfluoromonomers and second, all polymers that are made from monomers or comonomer systems that contain enough fluorine to contribute significantly to the performance and properties of the polymer. A commercially important fluorocarbon polymer is e.g. poly(tetrafluoroethylene) PTFE, better known under the brand TEFLON®. TEFLON® finds numerous applications like hydrophobic surface coatings [230], isolation material for wires [231], fibers for both technical applications and for cloth [232, 233] and many more due to its unique properties. Fluoropolymers or copolymers can be synthesized by various synthetic techniques depending on the type of monomer chosen. The majority is made by free radical polymerization.

Polymers bearing fluorinated groups, e.g. fluorinated chains can either be achieved by postderivatization, which means modification of an existing (co-)polymer by reacting different functional groups on the original material or by applying controlled polymerization methods like ATRP or RAFT directly polymerizing fluorinated monomers [31, 32, 234-237].
Many examples for successfully polymerizing fluorinated monomers gaining polymers for various applications applying controlled radikalic polymerization techniques can be found in the literature. A short overview:

A RAFT-mediated process was already successfully applied in the synthesis of PVDF, poly(vinylidene fluoride), with living PEGMA poly(ethylene glycol) methacrylate side chains through molecular graft copolymerization of the PEGMA macromonomer with an ozone-preactivated PVDF (poly(vinylidene fluoride)) backbone [238]. The microfiltration membranes manufactured from these polymers displayed resistance to γ-globuline fouling. Furthermore, the synthesis of PVDF-g-poly(methacrylic acid) (PVDF-g-PAA) polymers with well-defined PAA side chains for acrylic acid with ozone-pretreated PVDF applying the RAFT process was described [239]. The membranes prepared from these polymers were further functionalized using a surface-initiated block copolymerization with N-isopropylacrylamide (NIPAM). The gained PVDF-g-PAA-b-PNIPAAM membranes showed pH- and temperature-dependent permeability for aqueous solutions. Chen et al. carried out the thermally initiated graft polymerization of PEGMA with ozone-pretreated fluorinated polyimide (FPIDS) [240]. From this diblocks, two interesting materials were produced: nanoporous FPIDS films with ultra-low dielectric constants by solution casting of the graft copolymers and thermal decomposition of the labile PEGMA side chains in air. PTFE (poly(tetrafluorethylene)) films were surface modificated by Yu et al. applying block copolymer brushes [241]. A surface initiated RAFT process in the presence of a chain transfer agent using peroxide initiators on the film surface to polymerize PEGMA was applied. The epoxy groups were transformed into initiating groups for ATRP by reacting them with 2-bromo-2-methylpropionic acid. The macroinitiatior was used for ATRP of PEGMA and the sodium salt of poly(4-styrenesulfonic acid). Novel surface functionalities and molecular architectures were created in this way. Wooley et al. describe the synthesis of hyperbranched fluoropolymers (HBFPs) and linear poly(ethylene glycol) based amphiphilic crosslinked networks as efficient antifouling coatings [242]. The coatings of crosslinked HBFP–PEG networks are designed to exhibit varying wettability and hydrophobicity, the factors that have been shown to impart resistance towards biofouling.

5.4 2,3,4,5,6-pentafluorostyrene

Despite being even more hydrophobic compared to mere styrene, 2,3,4,5,6-pentafluorostyrene (**M7**) (figure 18) offers also lipophobic properties [223] which could enable the solubilization of lipophobic compounds in case the amphiphilic triblock copolymer is used as surfactant [145]. Furthermore, the introduction of perfluorinated chains [243] or semi-fluorinated polymers, such as poly(pentafluorostyrene) promises the occurrence of a rich phase behaviour in both solution and bulk [244-246].

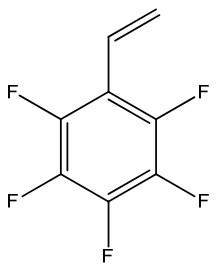

Figure 18: 2,3,4,5,6-pentafluorostyrene (**M7**)

Pentafluorostyrene (figure 18) is a reactive compound and pentafluorostyrene polymers promise less persistence in the environment compared to common perfluorinated surfactants

due to the possibility of chemical modification (vide infra). Another promising feature of the fluorinated styrenes is the possibility to replace selected F-positions by other chemical groups or moieties thus modifying the later polymer for various purposes.

A very interesting feature is the modification of PFS containing polymers attaching different kinds of sugar units via a thiol nucleophilic substitution. Glycosylation mimicking biological structures such as glycopolymers was reported by Voit and Schubert using this method [247-249] (figure 19):

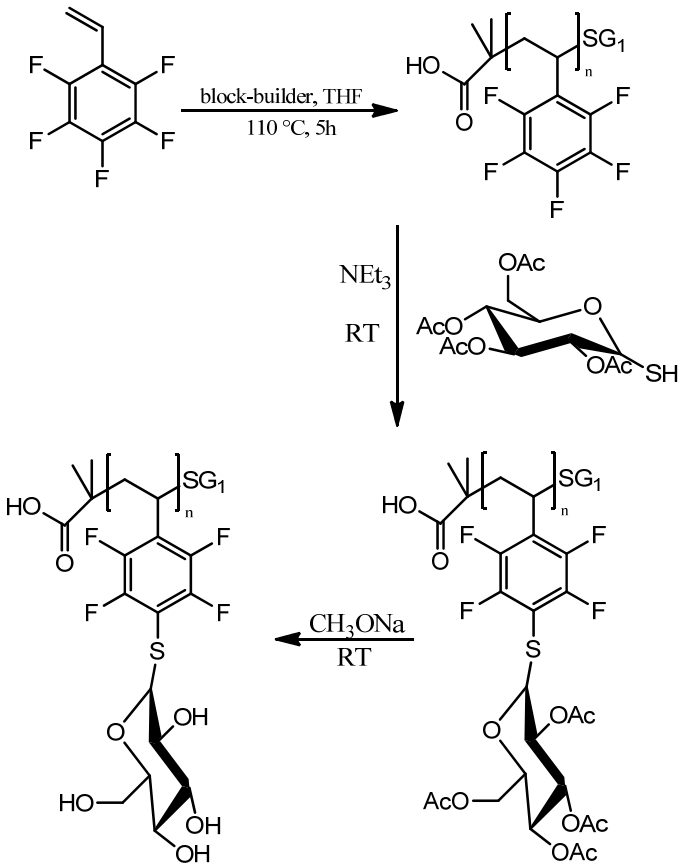

Figure 19: Schematic representation of the overall reaction scheme for the preparation of glycopolymers from a pentafluorostyrene precursor, from [248]. Graph adapted from [248].

Similary adjusting of the LCST by modifiying the pentafluorostyrene precursor block was reported, thus obtaining polymers with tailor-made cloud points.

Becer et al. [250] modified (PFS)-(OEGMA) comb-shaped polymers by applying a polymer-analogous nucleophilic substitution on PPFS (figure 20):

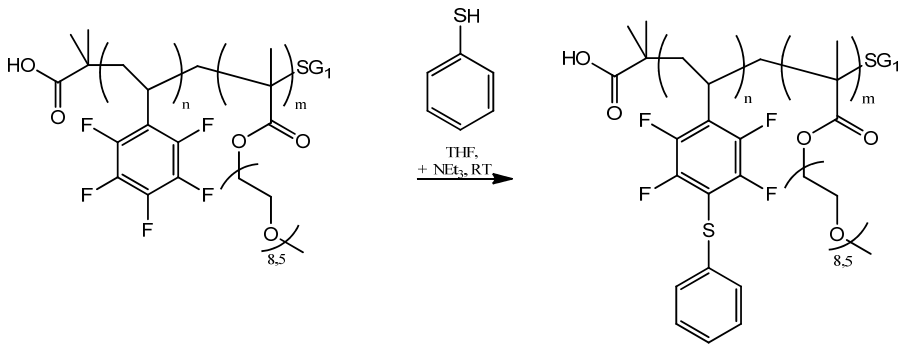

Figure 20: Nucleophilic substitution on PFS blocks (**M7**) by thiols [250], leading to thiophenol substituted PPFS. By controlled substitution of the thiophenol groups at different ratios, the cloud point can be tuned. Graph adapted from [250].

Another example for altering the LCST and simultaneously attaching groups actively influencing the polymers aggregation structure modifying the pentafluorostyrene-block was reported by Hussain et al. tuning PPFS-PEG polymers via amino-reaction on PFS blocks **(M7)** [251], leading to polyhedral oligomeric silsesquioxane (POSS) modified brush-like polymers with unique properties (figure 21):

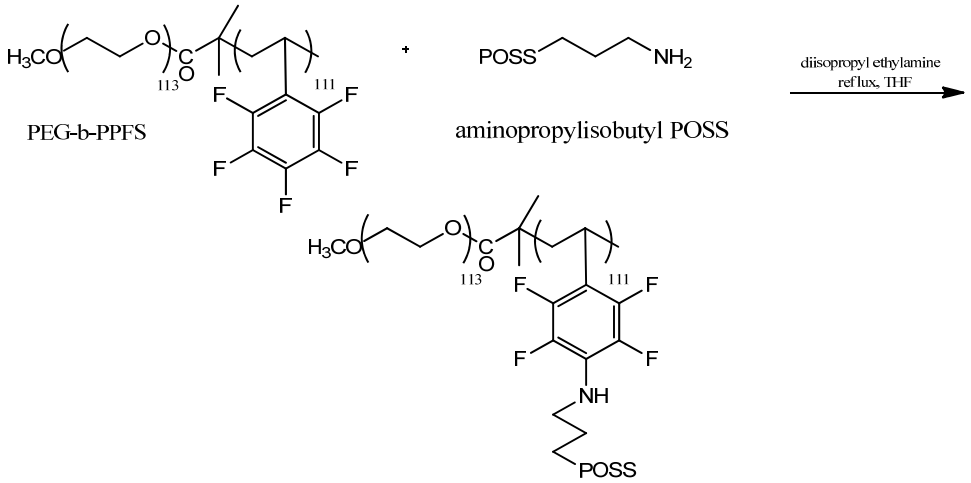

Figure 21: Modification of fluorinated styrenes (**M7**) via substitution of the para–F position at the aromatic ring providing access to brush-like polymers and polymers with a well tunable LCST by variation of the degree of substitution [251]. Graph adapted from [251].

The pentafluorostyrene-polymers are accessible via different polymerization techniques, among them ATRP- and RAFT polymerization [31, 32] and NMP [250].

5.5 2-, 3-, 4-fluorostyrene

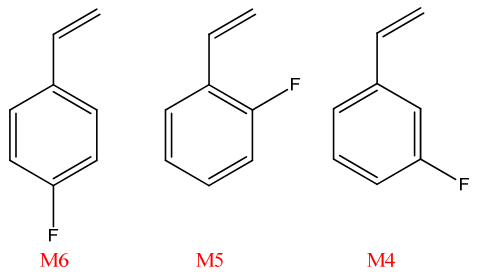

Figure 22: 4-, 2- and 3-fluorostyrene (**M6**, **M5**, **M4**)

The monofluorinated styrenes (**M4, M5, M6**) (figure 22) should provide a block showing a hydrophobicity and lipophobicity different from that of styrene (**M3**) and pentafluorostyrene (**M7**) and furthermore the effect of the position of the F-group on the polymerization behaviour and micellization behaviour should be studied. Also in this case, the polymers are accessible applying the controlled radical polymerization techniques ATRP and RAFT [31, 32]. The polymerization of 4-fluorostyrene (**M6**) might have been possible by pure thermal initiation due to formation of a Diels-Alder dimer according to the reported scheme (figure 15), but problems might have occurred with 2- and 3-fluorostyrene (**M4, M5**), therefore addition of an initiator (e.g. V 30) is recommended. Polymers composed of monofluorinated styrenes such as 4-fluorostyrene (**M6**) can be found in applications requiring ^{19}F stable isotopic labels located regioselectively within the core domain of block copolymers as reported by Becker et al. [252] or pyroelectric polymer films [253].

Chapter VI: Polymers suited for the hydrophilic block

6.1 Stimuli-responsive polymers for the hydrophilic block

Polymers or block copolymers showing sensitivity to a stimulus such as solvent, temperature or pH have come into focus as intelligent or "smart" materials. They are subject to relatively large and sharp physical transitions caused by small changes in their environment. Especially temperature sensitive systems are of interest for enabling easy control of parameters and low apparative cost. Furthermore, environmental influences on the system under investigation can be reduced due to working in a materially closed system.

6.2 Stimuli responsive block copolymers

The particulary complex behaviour of polymeric micelles- especially those of block copolymers and statistical copolymers- sensitive to different types of stimuli has been intensively studied. The stimulus forces the micelle to adopt a certain conformation on demand. Various stimuli have been described, for instance change of [254-263]:

- pH
- pressure
- solvent
- electric field
- magnetic field
- temperature
- UV- and visible light
- redox-potential
- ionic strength
- ion-ion interactions

By changing the stimulus, the micellar polymer can be switched from one conformation into another, due to an induced change in the polarity of one or more blocks depending on the polymers architecture and the length of the blocks (= M_w). This way core shell micelles and reverse micelles are accessible [264, 265]. In some cases the micelles cannot be switched due to kinetic reasons. Micelles bearing a glassy or frozen core due to high T_g values of their polymer segments, show a reduced dynamics of the polymer molecules forming the micelle leading to a reduced exchange of molecules between micelles and the surrounding solution [266-268]. Furthermore, the generation of micelles with a complex core becomes possible by combining blocks sensitive to different stimuli leading to the formation of multiresponsive polymers [269, 270].

6.3 Phase separation and thermodynamic properties of thermoresponsive polymers

The interest has focused on aqueous polymer solutions because the physical properties of water determine the conformation and reaction of biopolymers responsible for life on earth [271]. In fact, many non-ionic polymers or block copolymers are sensitive to a change of temperature in aqueous solution, and phase separate upon increasing temperature. Their transition from a water-soluble, hydrophilic to water insoluble, hydrophobic polymer occurs abruptly above the LCST (= **L**ower **C**ritical **S**olution **T**emperature) [272].

6.4 NIPAM and NAP: Acrylamide monomers for the temporarily hydrophilic A-block

Both NIPAM, N-isopropylacrylamide (**M1**) (figure 23), and NAP, N-acryloylpyrrolidine (**M2**) (figure 24), (A-block of BAB-polymers) belong to the class of acrylamide monomers. The synthetic strategies valid for the polymerization of acrylamide monomers leading to well-defined acrylamide polymers avoiding protective chemistry (anionic polymerization) and huge synthetic effort are limited. Besides ATRP needing special agents for complexing [31], the RAFT technique provides access to polymers of this class without huge synthetic effort and good control.

6.4.1 PNIPAM: poly(N-isopropylacrylamide)

PNIPAM first appeared in literature in 1956. The reports described the synthesis and polymerization of the monomer N-isopropylacrylamide, NIPAM (figure 24) [273-275].

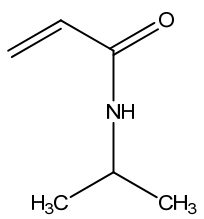

Figure 23: N-(isopropyl)acrylamide (**M1**), an acrylamide

Heskins et al. observed visually the macroscopic phase transition upon heating a PNIPAM solution [276]. Until now, PNIPAM has been studied for use in different applications.

The phase transition of PNIPAM can be used for various technical and biological applications. A useful property especially for medical and biomedical applications is the PNIPAM phase transition changing the surface properties from a low-fouling (cell and protein resistive) state to a collapsed and biologically adhesive surface [277-279]. Applications such as temperature responsive culture surfaces, controlled adsorption and release of proteins from surfaces, cell patterning using microheater-controlled thermoresponsive plasma films, gene expression control by temperature with thermo-responsive polymeric gene carriers and

temperature dependent gene expression induced by PNIPAM-based copolymers as well as enzyme and cell-immobilization has been described in the literature[280-286].

Furthermore, modified PNIPAM polymers have been investigated for applications such as wastewater treatment [287], oil recovery [288], photoresponse [289], flocculating agents [290], drug release [291], molecular recognition (sensors) by thermal stimulation [292, 293] as well as different types of functional gels [294], serving motile functions such as artificial muscles, micromachines [295] and mass transport [296, 297], information transmission and transformation such as the shape memory effect described by Osada et al. or polymerized crystalline colloidal arrays prepared by Holtz and Asher as a new sensor material [298, 299]. Additionally, gels of different structure like topological gels [300], nanocomposite gels [301], graft-gels [302], and porous gels [303] prepared from PNIPAM were reported.

PNIPAM shows good water solubility due to its hydrophilic amide group able to develop strong hydrogen bonds with sourrounding water molecules around room temperature (< 32 °C), while cage-like structures are formed at the hydrophobic isopropyl groups of the side chains [304]. The cage structures result in polymer-polymer interactions for entropic reasons. At the cloud point (32 °C [305, 306]), the hydrogen bonds get broken and the former linear polymer chains undergo a transformation from linear polymer chains to globules [307, 308] releasing water molecules grouped around the hydrophilic acrylamide moieties before. From a thermodynamic view, the polymer-polymer interactions are now favourable compared to the interactions between water and polymer. With the formation of globules, the former clear solution turnes dull. The point of switching can be investigated using a turbidimeter [36]. PNIPAM can be found among the most applied thermosensitive polymers due to its low sensitivity towards environmental conditions [309]. Variations of concentration, chemical environment or pH generally show a small effect on the transition temperature of PNIPAM by a few degrees only [307].

6.4.2 PNAP: poly(N-acryloylpyrrolidine)

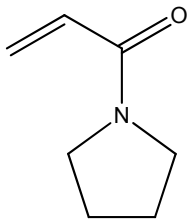

Figure 24: N-acryloylpyrrolidine (**M2**), an acrylamide

Compared to PNIPAM (**M1**), PNAP (**M2**) (figure 24) is rarely studied despite easy access to the monomer due to simple, but temperature controlled synthesis [310]. The compound has been originally patented in Japan [311, 312]. Kuramoto et al. [313] describe the synthesis of thermally responsive and electroactive poly(N-acryloylpyrrolidine-co-vinylferrocene) polymers (figure 25):

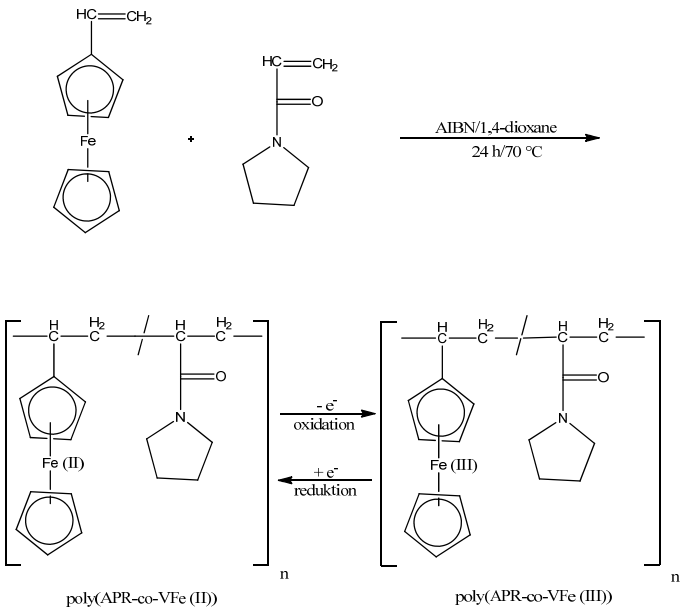

Figure 25: Poly(N-acryloylpyrrolidine-co-vinylferrocene) polymers synthesized by Kuramoto et al. [313]. Figure adapted from [313].

Furthermore, gels consisting of poly(N-acryloylpyrrolidine-co-styrene) polymers (figure 26) were synthesized and then investigated in water-ethanol mixtures displaying high swelling rates, whereas in pure water only low swelling rates are reported [312].

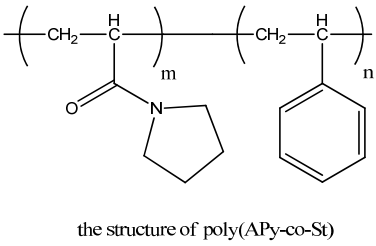

Figure 26: Poly(N-acryloylpyrrolidine-co-styrene) polymers for gel synthesis [312]. Figure adapted from [312].

Garnier et al. investigated the surfactant properties of PNAP containing diblock copolymers synthesized by the RAFT process [314, 315], whereas Mertoglu et al. [316] investigated the thermoresponsive behaviour of PNAP containing di- and triblock copolymers synthesized by the same polymerization technique. Further polymerization methods for NAP monomer such as anionic polymerization can be found [317].

Containing also a hydrophilic acrylamide group, PNAP polymers are well water soluble at room and elevated temperature (< ~ 50 °C) and show a LCST temperature around 50 °C [305, 306, 312]. The high transition temperature restricts its application to non-biological systems. As PNIPAM, PNAP is able to form hydrogen-bonds to the surrounding water molecules, but the structuring of the surrounding liquid is of course different compared to PNIPAM leading to different effects in LCST and turbidimetry measurements due to different destruction of the hydrogen bonds as presumed by Fujimoto et al. [318].

Chapter VII: The LCST (= Lower Critical Solution Temperature)

7.1 The LCST described from a thermodynamic point of view

As already mentioned, the amphiphilic BAB-triblock copolymers transform to hydrophobic polymers abruptly at a sharp transition temperature, also often referred to as the cloud point [36, 145].

Prigogine and De Fay [319, 272] defined the thermodynamic requirements for the LCST:

$$(\delta^2\Delta H/\delta X_2^2)_{T,P} > 0,\ T\,(\delta^2\Delta S/\delta X_2^2)_{T,P} > 0,\ \Delta G > 0 \qquad \text{(equation } \mathbf{15}\text{)}$$

with ΔG, ΔH, ΔS > the ideal free energy, enthalpy and entropy of the polymer mixed with water. X_2 describes the mole fraction of the polymer in water. Assuming the functions not to change sign, for the case of mixing

$$\Delta G > 0,\ \Delta H < 0,\ \Delta S << 0$$

can be deduced. For mixtures showing a positive deviation from Raoults law, exothermically and with a loss in the entropy on formation, a LCST may be found as proposed by Taylor and Cerankowsky [272, 320]. They offered a general rule for the LCST of aqueous polymer solutions:

"As a polymer which is soluble in water at all temperatures is made increasingly hydrophobic, before complete water insolubility is reached, a range of compositions will be found which will have temperature inverse solubility and the more hydrophobic the increment, the lower the LCST".

This means that by substituting a water soluble polymer with hydrophobic groups a polymer with a LCST may be obtained due to entropic reasons.

In aqueous solutions the LCST behaviour is based on the ordering of solutes resulting from specific orientations required to form hydrogen bonds with the arranged water molecules [321]. The initial driving force for the dissolution of polymers are the hydrogen bonds formed between the polar groups in the polymer and the water molecules. Water molecules not able to form hydrogen bonds with non polar domains of solutes have to reorientate themselves around those regions resulting in a decreased entropy upon mixing [273, 322, 323]. This effect is called the hydrophobic effect. With increasing temperature, the entropy term starts to dominate over the exothermic enthalpy of the hydrogen bond formation. As a consequence, the free energy change of mixing becomes a positive value and phase separation takes place.

In aqueous systems the LCST behaviour can be applied as a switch. Below the switching temperature -which is called the cloud point- water is a good solvent for the synthesized

polymers, dissolving the blocks completely. The polymers adopt random coil-like conformations [103]. Above the switching temperature, the thermosensitive blocks collapse (coil-to-globule transition, see following chapter) and are no longer able to form sufficient hydrogen bonds. The solutions under investigation show phase separation becoming optically cloudy.

7.2 The coil-to-globule transition of neutral polymers

The conformation of a polymer in solution is determined by the chemical structure of the polymer (rigid or flexible backbone or side chains of polymer) and the quality of the solvent used [35, 103]. Experimentally, the conformation of the polymer chain can be determined by measuring the ratio of the mean-square radius of gyration, R_g to the hydrodynamic radius R_h of the polymer using static light scattering (SLS) [272, 273, 324, 325]. The ratio of R_g/R_h shows values of about 0.78 for a uniform, hard sphere and around 1.5 for a monodisperse random coil [35, 272]. The value of the ratio R_g/R_h is increasing with growing rigidity of the chains.

In a good solvent, a polymer swells due to elastic forces and the excluded volume interactions [35, 103]. The elastic forces cause the contraction, the volume interactions the expansion of the chain. The interactions of the excluded volume are dominant and the second virial coefficient, A_2, which can be seen as a measure of the thermodynamic quality of the solvent for a polymer, is positive. The solvent quality can be lowered by an external stimulus, resulting in a state at which the polymer coil behaves like an ideal coil. This is the so called theta(θ)-point [35, 103]. At this point the the coil is in an unperturbed state and the second virial coefficient is becoming zero. If the quality of the solvent is decreased further, the attraction between the units of the polymer chain becomes dominant finally leading to the precipitation of the polymer. When the point of precipitation is reached, the second virial coefficient shows a negative value.

When heating an aqueous solution of thermosensitive polymers like PNIPAM **(M1)**, PNAP (**M2**) (vide supra) or PMDEGA, poly(methoxy diethylene glycol acrylate), the polymer chains undergo a coil-to-globule transition (figure 27) at an LCST of about 32 °C , 50 °C and 35-38 °C [305, 306, 142] . The LCST represents the theta (θ)-point.

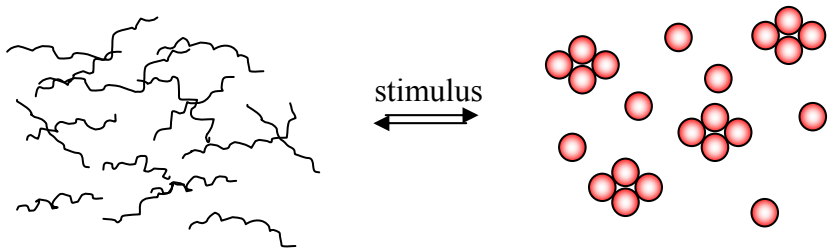

Figure 27: Coil-to-globule transition of polymers sensitive to an external stimulus, e.g. a change in temperature. Often aggregates or clusters can be found. Adapted from [142].

7.3 Definition of the cloud point and critical point [36]

Due to the increased turbidity of the polymer solution at the temperature at which phase separation occurs for a polymer solution this point is called cloud point. The critical temperature represents the highest or lowest temperature at which phase separation occurs. The polymer concentration at that point is referred to as the critical composition.
Difference between cloud point and critical point/critical composition: Cloud point is the temperature at which the polymer phase separates visually at a given concentration. The critical point/composition presents the minimum or maximum temperature or concentration at which phase separation behaviour occurs in the phase diagram.

7.4 Turbidimetry

At the cloud point, phase separation occurs (vide supra) and the former clear solution is scattering light. This point or interval can be detected besides the reversibility of the thermosensitive behaviour investigating heating and cooling cycles. Turbidimetry measurements can be conducted without great effort [36].

7.5 DLS (= Dynamic light scattering)

DLS measurements provide information about the size D_h of the particles diffusing in a solution [35].

- The aggregation of particles can be determined on different size levels and the size distribution can be detected. This way, a distinction between single molecules, small associates –such as micelles- and huge aggregates becomes possible

- DLS measurements can be performed temperature dependent providing interesting insights in the development of the particles size, size distributions and general aggregation behaviour with increasing or decreasing temperature.

- As micelles are dynamic systems [36, 144], DLS-measurements can also help to get an insight in the dynamics of surfactants forming the micelle [327, 328]. At concentrations above the CMC, the surfactants are molecularily dissolved (so-called unimers) forming a dynamic equilibrium with the molecules bound in the micelles [36]. Both micelles and unimers can be identified applying DLS measurements. In case micelles with glassy cores are formed from surfactants possessing a block with a high T_g-value, such as the styrene and pentafluorostyrene containing BAB-systems, the exchange of surfactant molecules between micelles and surrounding liquid is negligible. Furthermore the mobility of polymeric surfactants is inherently lower compared to the low- molecular weight species [36, 69].

7.6 Factors influencing the position of the cloud point

The experimental conditions at which cloud point measurements are performed play a crucial role. The cloud point of thermosensitive polymers can be influenced by attaching different end groups to the polymer [329, 330], variation of the polymers concentration [331, 332], architecture [333, 334] and mass (= chain length, also of side chains) [335, 336] in aqueous solution and also the polymers tacticity [337, 338]. Furthermore, co-monomers [339-342] and the choice of co-solvent [36, 343], additives (e.g. addition of salt [36, 344-346] or surfactants [347]) and pressure [348] show an influence.

In this study, the influence of various end groups, variable polymer mass referring to the mass of the hydrophilic- and hydrophobic block as well as the polymer concentration on the value of the cloud point was investigated in detail.

7.6.1 Effect of different end groups on the cloud point

Pure PNIPAM (**M1**) homopolymers are reported to show a LCST temperature of 32 °C [305, 306, 349].

Attaching specific end groups to PNIPAM polymers may lead to changes in the LCST of those polymers, especially when dealing with low molecular weight species. For example, Duan et al. reported a LCST of 21.7 °C for PNIPAM functionalized with 1-pyrenyl-2-chloropropionate [142, 250]. The pyrene group at the chain-terminus leads to the formation of large aggregates lowering the LCST. The investigations of Winnik et al. [142, 351] disprove this result by observing similar values (around 32 °C) for the cloud point of PNIPAM, unmodified and modified with octadecyl pyrene as a fluorescent label. A possible explanation could be that at the point of the LCST the modified polymers are likely to form micelles hiding the strongly hydrophobic label within the micellar core whereas the hydrophilic PNIPAM forms a hydrophilic corona. Also Baltes and Freitag et al. [352, 353] reported no significant changes in the LCST investigating carboxyl-terminated PNIPAM oligomers.

Nevertheless, shifting of the LCST via the end-group seems to be possible. Recently, Rauwald et al. were able to shift the LCST of PNIPAM by complexation of the endgroup applying a curburbit-[8]-uril-viologen complex by more than 5 °C [354]. Also Choi and Ritter report a markable shift of the LCST of PNIPAM investigating NIPAM based pseudopolyrotaxanes complexed with Cucurbituril [6] [355]. Studies on the effect of fluorinated endgroups on the LCST behaviour of pure PNIPAM polymers seem to be missing yet; the reported systems were blends [356]. For high molar mass polymers the effect of the endgroup on the cloud point is believed to be negligible as the influence of the end groups is diluted with increasing molar mass. Wether this effect is valid for other polymers than PNIPAM, too, is not clear as only a very restricted number of studies can be found in the literature, so that further studies for an understanding are necessary.

7.6.2 Effect of molar mass and concentration of polymer on the cloud point

The influence of the molar mass on the cloud point is controversially discussed in literature. As a general rule, water based solutions of linear PNIPAM homopolymers with high molar masses are reported to show a phase-transition temperature shifted to lower values compared to the lower mass ones [36]. Additionally, the transition temperature is shifted to lower values with increasing concentration of polymer and vice-versa [357] as reported by Schild et al..

Schild et al. [357] showed that the LCST of PNIPAM (**M1**) (molar masses from 5400-160000 g/mol) decreases with increasing molar mass. At elevated polymer concentrations, the polymer globules formed due to the collapse of the PNIPAM coils are able to aggregate and thus the molar mass is thought to show a huge influence on the LCST. An effect of the chain length/molar mass on the LCST was also reported by Tong et al. [142, 358], showing a monotone decrease of the cloud point with increasing polymer concentration in PNIPAM solutions. Contrary to these results, Ding [142, 359] and others described no remarkable changes in the cloud point investigating PNIPAM polymers of different molar masses [361]. Afroze [360] describes a change in the cloud point only when diluting the polymer solutions.

As a consequence of these controversial results, samples should be measured and results compared again following the same protocols for preparation and measurement.

Chapter VIII: Amphiphilic polymers sensitive to temperature as a stimulus

In many cases temperature is chosen as stimulus for smart polymers, because the experimental setup is straight-forward and experimental parameters can be changed without great effort. Furthermore, the gained data is easily reproducible. In fact, thermosensitive block copolymers of different architectures give rise to manifold types of polymeric micelles, with interesting core-shell architectures such as worm-like micelles and cylindrical micelles or vesicles and many more [362-364].

8.1 AB-diblock copolymers

In the simplest case, polymeric micelles can be formed by linear AB-amphiphilic diblock copolymers consisting of a hydrophilic A- and a hydrophobic B-block. Many combinations of different polymers for the hydrophobic and hydrophilic parts as well as block-lengths are possible and have for instance been synthesized in our group [69, 84, 365] leading to diblocks with a different HLB (hydrophobic-lipophilic balance) [366-369] and thus surfactant properties such as solubilization behaviour, phase inversion temperature of emulsion, CMC, spreading and interfacial tension [370-373]. The micellar structures gained from these diblock copolymers can be subdivided into an inner core and the swollen corona [36, 144, 374] (figure 28):

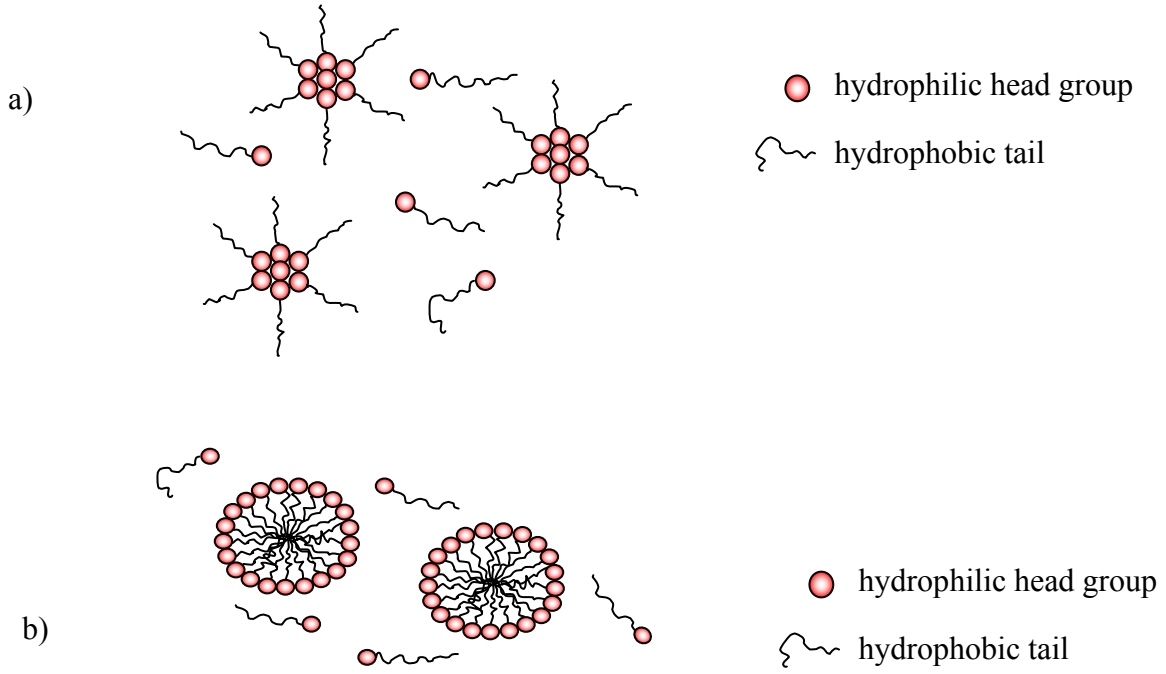

Figure 28: Aggregation behaviour of AB-diblock copoloymers in a) organic solution and b) aqueous solution. The aggregation process in a selective solvent for one of the blocks is similar to the micellization reported for the low molecular weight surfactants following a model similar to the closed association process [69, 375]. The hydrophobic head group is hiding away from the aqueous solution inside the micellar core due to the hydrophobic effect [376-378], whereas the hydrophilic tail is able to interact with the surrounding water molecules forming the micelles` corona.

The formation of micelles of AB-diblocks in aqueous environment is driven by the effort of the hydrophobic, unpolar block to minimize contact with water [376-378] (so-called hydrophobic effect). The inner core is formed by the hydrophobic part of the polymer, whereas the swollen corona is created from the hydrophilic segments of the polymer [36]. The introduction of polymers composed of blocks showing a lower critical solution temperature (LCST) gives the possibility to tune the swelling properties of these micelles [379]. In this context, diblock copolymers can be composed of two hydrophilic blocks, with on of the blocks being stimuli sensitive able to undergo switching to hydrophobic on demand or of a permanently hydrophobic block plus a temporarily hydrophilic one.

8.2 ABA-triblock copolymers

In order to achive more complex micellar structures, the focus has shifted from amphiphilic diblock copolymers of type AB to triblock copolymers of type ABA, BAB and ABC [380-383]. Even tetra- and pentablock copolymers are reported in the literature [384, 385]. ABC-triblocks, for example, consisting of three blocks varying in the chemical nature of the polymer and block length, have been successfully synthesized and applied in our group for manufacturing multicompartment micelles [270, 271] providing micelles with a distinct architecture.
Depending on the concentration of a selective solvent, ABA- and BAB-block copolymers are also able to form core-shell micelles of distinct structure as already described for the AB-systems at dilute concentrations, and show complex aggregation behaviour forming transient networks –hydrogels- at high concentrations [386, 387].

The micelles composed of ABA-triblock polymers show a similar aggregation behaviour in aqueous solution as observed for the corresponding AB-diblocks (vide supra) driven by the effort of the hydrophobic, unpolar block to minimize and avoid contact with water following an association process. ABA-block copolymers form globular, spherical loop-like micelles with the hydrophobic part of the copolymers hidden in the core of the micelle and the hydrophilic part forming the swollen corona in aqueous environment [388, 389].

With increasing concentration of polymer in solution, the formation of networks and thus gels becomes possible. The mechanism for gel-formation is not fully understood. It is assumed, that the micelles pack closely to fill the free volume and forming an immobile phase, which is often referred to as hard gel- or jamming phase [390, 391]. Another explanation could be a stronger entanglement of the blocks forming the corona between different micelles in a sample at elevated concentration.

ABA-systems have been studied for various reasons. Depending on the nature of the blocks, microphase separation occurs. Qiao et al. investigated the bulk morpholgie of poly(isoprene)-PS-poly(isoprene structures) [392] whereas A. Avgeropoulos et al. [393] studied ABA-systems containing poly(pentamethyldisilyl)styrene (P(PMDSS)) for the B-block and polyisoprene (PI) for A-block for the same reason. Furthermore, various systems display gel formation or can be used as drug-carriers useful for medical applications. Heller et al. patented ABA- and BAB-block copolymers as drug carriers [394]. Zhao et al. report the use of ABA- and BAB-systems composed of HEMA-NIPAM-HEMA (2-hydroxyethyl methacrylate-N-isopropylacrylamide-2-hydroxyethyl methacrylate) and vice versa for the formation of medical gels [395] as well as Packhaeuser et al. reporting the use of ABA- and BAB-triblock copolymers containing PLGA (poly(D,L-lactide-co-glycolide)) A-blocks and

PEG (polyethylene glycol) B-blocks as thermally induced gelling systems for parenteral application [396]. Also Pluronics® have been reported for thermoresponsive medical gels for drug delivery by Shim et al. [397]. In this context, the tuning of the gelation or transition behaviour is coming into focus. This can be realized applying thermoresponsive block copolymers sensitive to different temperature regions for the gel formation, e. g. polyethylene or butylene in poly(styrene)-b-poly(ethylene/butylene)-b-poly(styrene) triblock copolymers in n-octane as a non-aqueous system [398] or PEO in poly(ethylene oxide)-poly(lactic acid)-poly(ethylene oxide) (PLA-b-PEO-b-PLA) triblock copolymers [399] and ethylene glycol in poly(caprolactone-b-ethylene glycol-b-caprolactone) (PCL-PEG-PCL) triblock copolymer in aqueous solution (>15 wt%) [400].
The mechanism responsible for the gel formation at higher temperature is assumed to be the same as for the formation at ambient temperature described before [401]. Various examples for temperature controlled formation of gels ("thermogelling") can be found in the literature [402, 403]. At temperatures high above the switching point, the collapsed A- or B-blocks in ABA-, BAB- or AB-systems release the rest of the bound water further reducing the free volume. Eventually formed networks get broken and the polymers precipitate resulting in a macroscopic phase separation.

8.3 BAB-triblock copolymers

Most studies on the micellization behaviour of BAB-systems can be found employing commercially available Pluronic® triblock systems (BASF) or Synperonics® (ICI) [404] of different block lengths and additives (e.g. salts) [405-409]. Pluronics® or Poloxamers® are non-ionic triblock copolymers showing a block sequence of polyoxyethylene–polyoxypropylene–polyoxyethylene (PEO–PPO–PEO) or vice versa for the ABA-systems (PPO–PEO–PPO) [410]. Compared to the ABA-systems, few articles are reported investing the behaviour and synthesis of the BAB-systems.
Whereas the self-assembly of ABA-blocks in water is well understood and investigated, the assembly of BAB-blocks is still not fully clear. Zhou et al. [128, 411] assumed the micellization of most Pluronic® systems to follow a closed association process, which is also likely for other BAB-systems, leading to different morphologies. Different states of morphologies can be formed like bridging-structures, dangling-structures, linear free chains and structures displaying loops also referred to as flower-like structures [412-420] (figure 29):

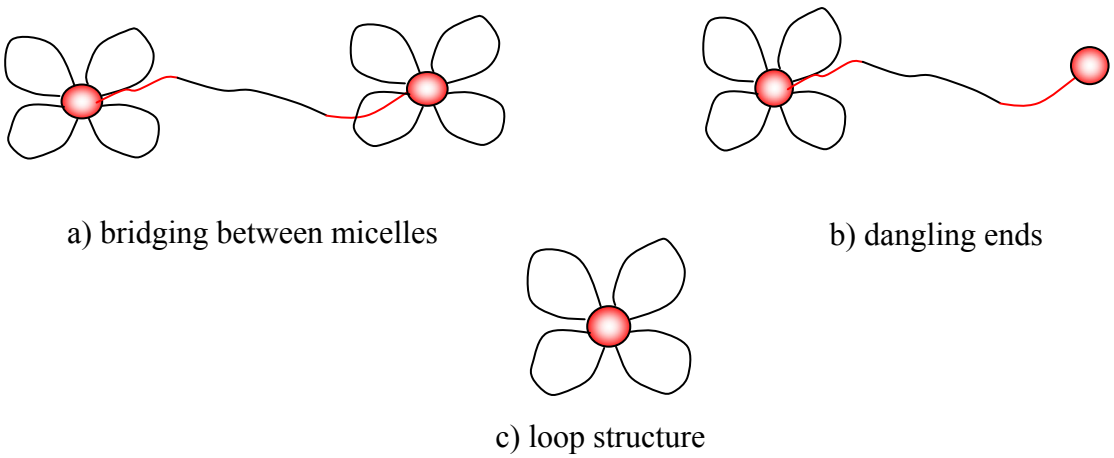

Figure 29: Micellar structures from left to right: a) bridging, b) dangling, c) loop structures ("flower-like micelles") of BAB-triblock copolymers in aqueous solution.

With regard to entropy, the flower-like geometry of BAB-blocks is more demanding. The formation of this type of micelles implies a loss of entropy (entropic penalty) needed for the loop-formation of the hydrophilic A-block and keeping the hydrophobic B-blocks apart from water inside the micellar core, as calculated by Kim et al. [312]. Furthermore, the middle block must be long enough to enable loop formation. In case the corona-forming block is much smaller than the core-forming block(s), the aggregates formed are referred to as ‘‘crew-cut’’ aggregates as described by Yuan et al. investigating poly(styrene)-poly(ethylene oxide)-poly(styrene) (PS-PEO-PS) triblocks [421] including short PEO-blocks or PS-PEO-systems reportet by Yu and Eisenberg [422].

The sol-gel transition of BAB-block copolymers is induced –like for ABA-systems- by denser packing of the micelles when the total volume fraction is larger than the maximum packing fraction and additionally by entanglements between the micelles. The so-called bridging (vide supra) in concentrated solutions is possible due to the ability of the linear block copolymer chains to leave the flower-like micelle structure and introduce their hydrophobic end-blocks into different micellar cores by diffusion phenomena leading to clusters of highly interconnected micelles [423, 424]. Bridging from dangling chains is described as possible as well (vide supra). In general, the bridging of the micelles formed by the BAB-triblocks leads to physical networks (figure 30):

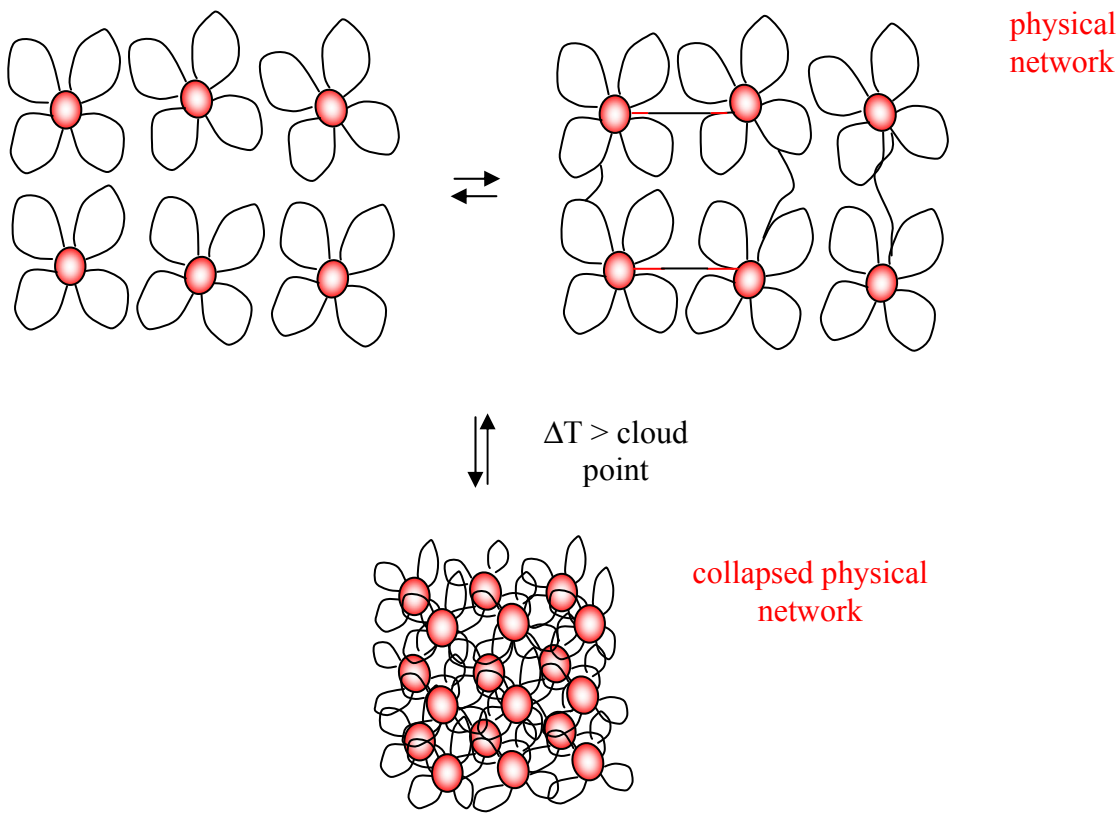

Figure 30: Formation of physical networks (gel formation) due to bridging between flower-like micelles in concentrated solutions by some BAB-polymers introducing their hydrophobic end-blocks away from water in two different micellar cores instead of becoming part of one micelle by themself. With increasing temperature first clusters are formed until at temperatures well above the cloud point the network is collapsing showing macroscopic phase separation.

With increasing temperature at a given concentration of the block copolymers, a transition from a flowing, aqueous solution to a non-flowing sample can be investigated for thermoresponsive BAB-triblocks, too [425]. A gel is formed of micelles packed together closely or by overlapping of micelles. With further rising the temperature, the dynamic equilibrium between the micelles and clusters is shifted in direction of the clusters as reported by Mortensen et al. [413, 414], suggesting, that the sol-gel formation can be seen as the hydrophobic aggregation between micelles. The formation of intermicellar bridges between BAB-block copolymers leads to the generation of clusters more easily compared to the ABA-type systems [426]; furthermore a lower transition temperature at the transition point from sol to gel was found with the BAB-blockcopolymer systems [427]. With increasing the temperature further, even more water will be squeezed out of the micelles, leading to a tremendous shrink of the micellar shell [428]. In case the micelles are loaded with a water soluble substance, the substance will be released at temperatures above the cloud point. Consequently, also the BAB-systems may be useful for medical applications for controlled release in shape of gels or micelles [429, 430]. At the same time the interaction between the micelles is decreasing and gradually a sol or mobile phase appears.

Chapter IX: Objectives

This thesis focuses on the use of mono (non-symmetric) and bifunctional (symmetric) trithiocarbonates as CTAs for the RAFT process because of their well known efficiency in the synthesis of block copolymers [431].

A closer look at the literature revealed, that CTAs bearing a fluorinated label either at the Z- or at the R-group have already been successfully applied in the RAFT polymerization process and only few examples of xanthates and dithiobenzoates, but no trithiocarbonates, have been reported so far [60, 110-114]. The fluorinated groups at the Z- and R-moiety should be introduced to enable a definite identification of the signals via ^{19}F-NMR-spectroscopy independent of the chosen monomers and thus smart access to molar mass determination of the fluorinated styrenes, especially pentafluorostyrene (**M7**) and determination of the Z/E-ratio for an insight in the degree of functionality, crucial for enlarging of the polymers to block copolymers.

So far, applying an F-label to both Z- and R-group of a CTA working additionally as a label in ^{19}F-NMR spectroscopy for end-group analysis giving access to the molar weight of polymers has not been tried and reported before. Drew et al. reportet using ^{19}F-NMR to quantify resin-bound chemistry independent of the molar mass in conjunction with a polymeric support bearing fluorine as an internal standard [432]. Amado et al. [433] characterized their α-, ω-perfluoroalkyl functionalized poly(ethylene oxides) by adding 1,4-difluorobenzene for ^{19}F-NMR analysis, but as an external standard. Gudipati et al. monitored the conversion of the reaction of crosslinking of mixtures of hyperbranched fluoropolymer (HBFP) and diamino-terminated poly(ethylene glycol) (PEG) applying ^{19}F-NMR for the preparation of antifouling coatings [242]. The fluorine atoms in para-position of the pentafluorophenyl end groups of the HBFP were reactive and addressable by ^{19}F-NMR

spectroscopy. They enable both intramolecular and intermolecular crosslinking of the HBFP percursor via nucleophilic aromatic substitution by the amine termini of the PEG. He et al. used ^{19}F-NMR for proving the synthesis of the fluorinated block in their newly synthesized triblock terpolymers of poly(n-butyl methacrylate)-b-poly(methyl methacrylate)-b-poly(2-fluoroethyl methacrylate) (PnBMA-PMMA-P2FEMA) using the RAFT process [434]. Furthermore, Miles et al. [435] used fluorine as a chemical label, for the detection of the reaction mechanism applying nucleophillically activated fluorine. The fluoride ions occurring during the reaction were identified by the zirconium-alizarine method.

Additionally, the influence of the labelled groups on the polymerization process should be investigated performing kinetic studies.

Applying monofunctional RAFT agents for block copolymer synthesis, the blocks can be added step by step. The CF end-capped systems should be synthesized using a monofunctional CTA introducing the fluorinated moiety in one step.

Bifunctional CTAs enable the preparation of triblocks in just two steps and give access to symmetric triblocks of types ABA and BAB. For the symmetric species, two types of CTAs can be generated:

- The first type contains the active group of the growing chain at the outer ends of the polymer chain Z-C(=S)-S-R-S-C(=S)-Z [32]

- The second CTA-type positions the active group in the center of the polymer chain R-S-C(=S)-Z-C(=S)-S-R [32]

All newly synthesized symmetric CTAs should be designed like the second type leading to the desired BAB-systems in two steps only. This species has the advantage that no decomposition of the triblocks to diblocks by hydrolysis of the thiocarbonyl group is possible. Avoiding oxidative conditions (which would disturb the polymerization process anyway), the risk of pentablock formation is negligible [436].

Styrene (**M3**) was chosen as a standard monomer, which can be polymerized under good control using the RAFT process, for the hydrophobic, B-block of the BAB and hydrophobic, lipophilic block of the CF end-capped systems. 2,3,4,5,6-pentafluorostyrene (**M7**) was chosen as a monomer for being even more hydrophobic compared to styrene (**M3**) and providing also lipophobic properties. Furthermore, the system could be varied by S_N-aryl substitutions. 2-, 3- and 4-fluorostyrene (**M4, M5, M6**) were chosen almost for the same reasons already expounded for the pentafluorinated species (**M7**).

For the hydrophilic A-block, NIPAM (**M1**) was chosen as a standard monomer due to the good water solubility of the PNIPAM polymers and its narrow interval for the LCST point (around 32 °C). The PNIPAM containing polymers at ambient temperature should be compared to PNAP (**M2**) containing ones.

The combination of the hydrophobic B- and hydrophilic A-block in BAB-triblock copolymers should lead to amphiphilic block copolymers, which enables to form physical hydrogels and polymer surfactants should be investigated applying different methods. The surfactant properties of the fluorine end-capped systems should be investigated in organic solvents.

Chapter X: Synthetic strategy towards CTAs bearing a fluorinated label and their kinetics in the polymerization of styrene

This chapter describes the synthetic attempts made for the synthesis of new mono- and bifunctional CTAs applied in RAFT polymerization.

Mono- and bifunctional fluorinated RAFT agents synthesized in this thesis are presented in figure 31 (XXXIV-XXXVIII) and figure 32 (XXXIX-XXXXIV):

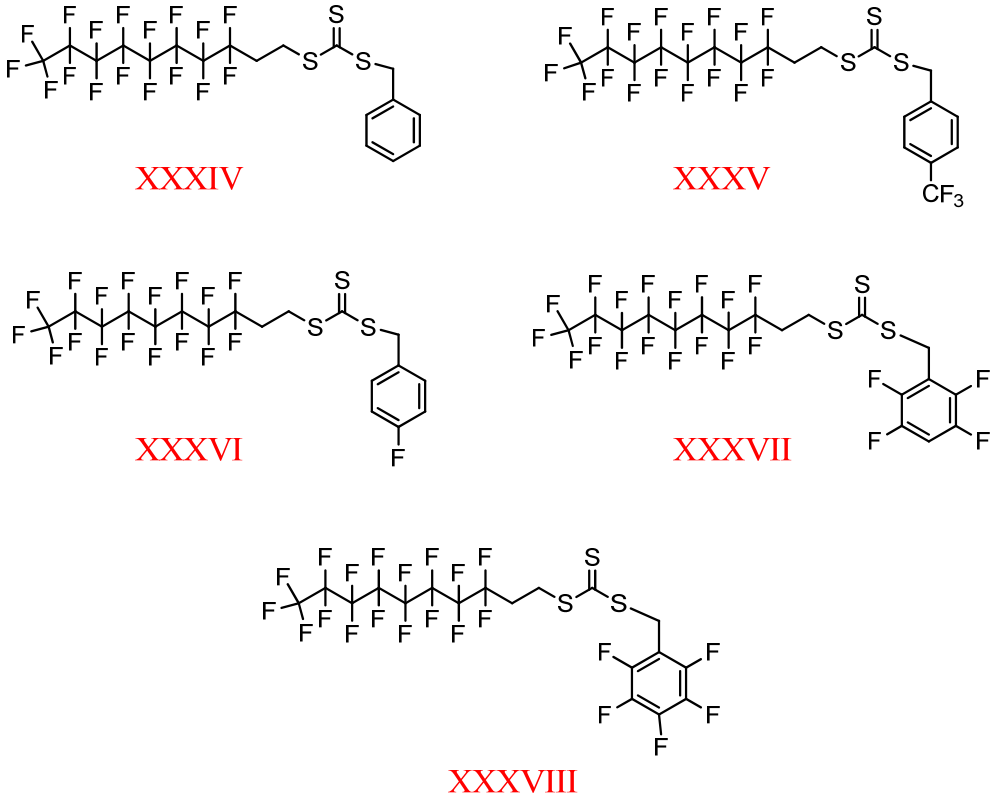

Figure 31: Synthesized monofunctional, non-symmetric CTAs (XXXIV-XXXVIII) bearing a fluorinated label at both Z- and R-group, except non-symmetric CTA XXXIV. The substitution pattern at the phenyl ring is varied. These CTAs are referred to as non-symmetric CTAs in the text.

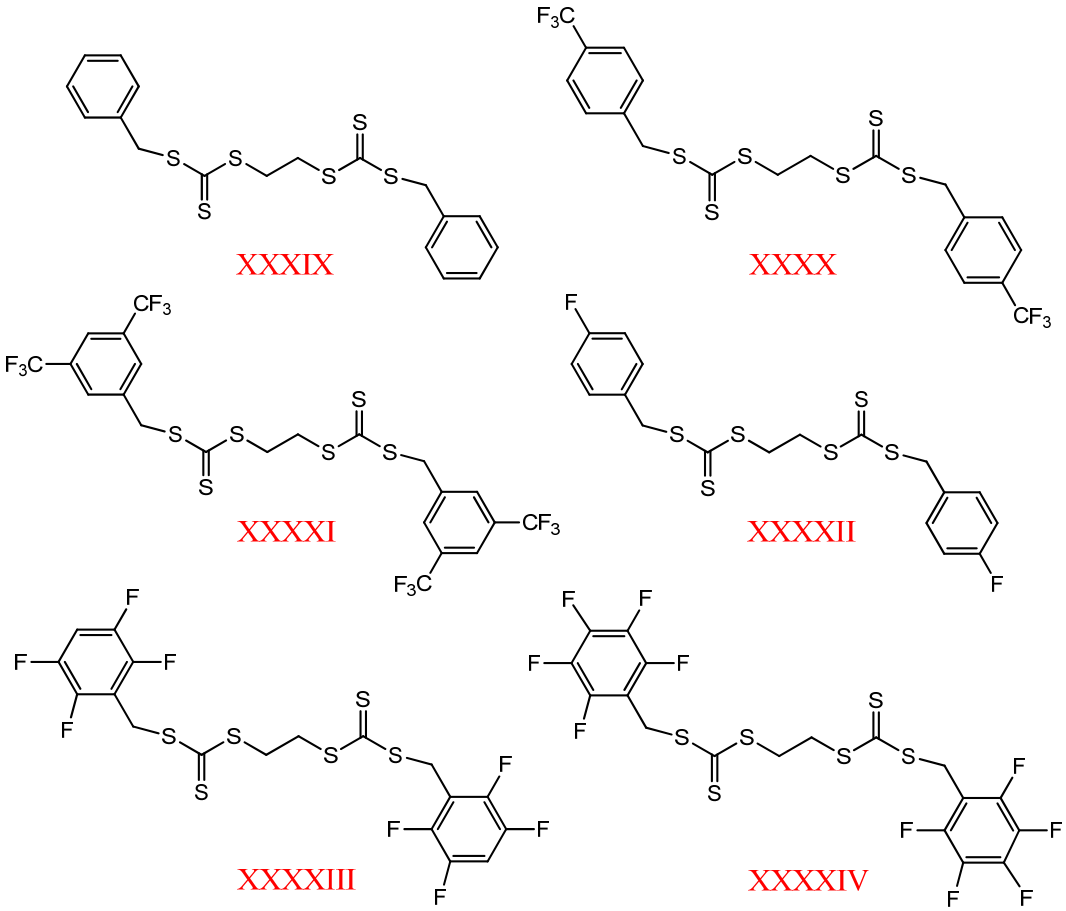

Figure 32: Symmetric, bifunctional fluorinated- and non-fluorinated RAFT agents synthesized (XXXIX-XXXXIV). These CTAs are referred to as symmetric CTAs in the text.

10.1 Functionalization using NMR-labels for ^{1}H- and ^{19}F-NMR: a universal label for polymers

In order to guarantee a good identification of the signals in the NMR spectrum, the labels have to fulfill certain criteria:

- No overlap with signals originating from the polymer or its backbone
- Small line width
- Not too high dispartment of lines
- Easy identification of the label
- No interference with the RAFT process

In order to guarantee good functionality of the RAFT agent, two basic CTA types were chosen for modification [142, 437] (figure 33):

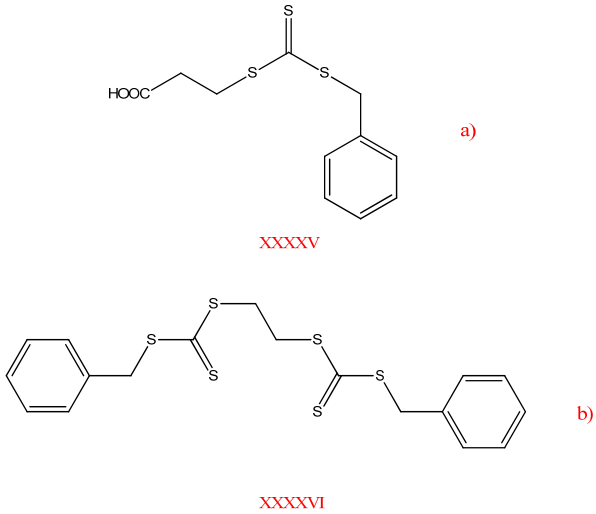

Figure 33: RAFT agents chosen for modification. a) A non-symmetric RAFT agent XXXXV of the described type has already been successfully applied by Wang et al. in polymer synthesis [437]. b) The symmetric CTA XXXXVI was reported to successfully polymerize poly(styrene) (**M3**) by Bivigou-Koumba [142].

Monofunctional **CTA XXXV** (figure 34) was chosen for a non-symmetric trithiocarbonate. The Z-group is an alkyl group showing signals between 1 and 2 ppm in ^{1}H-NMR. The R-group is an aromatic system showing signals typically around 7 ppm. The signals can easily be identified and meet almost all criteria except the possible overlap with signals originating from the polymer or its backbone.

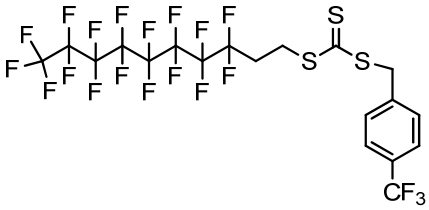

Figure 34: Non-symmetric **CTA XXXV** as a model compound

Bifunctional, symmetric **CTA XXXX** (figure 35) was chosen for a symmetric trithiocarbonate. The Z-group is also a hydrocarbon, showing signals between 1 and 3 ppm in ^{1}H-NMR, the R-groups are aromatic showing signals typically around 7 ppm. The signals can easily be identified, too, and meet almost all criteria except signal overlap.

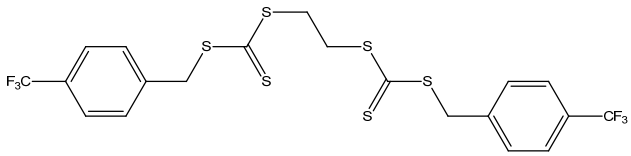

Figure 35: Symmetric **CTA S XXXX** as a model compound

The main problem in both cases is the overlap of signals originating from aromatic or aliphatic protons from the block copolymer and signals from the polymer backbone with those provided by the end groups in ^{1}H-NMR. Attaching electron-withdrawing substituents to the R- and Z-groups could help to solve this problem by shifting the aromatic and alkylic signals to lower field in NMR. Therefore, non-symmetric **CTA XXXV** (figure 31) was modified by introducing a fluorinated polymer chain CF_2-$(CF_2)_7$-$(CH_2)_2$- for the Z-group and a CF_3-group in p-position of the benzyl group. From the literature, no hinderance on the RAFT process is known from these groups.

The symmetric and non-symmetric RAFT agents were synthesized under consideration of six objectives:

- one-pot synthesis followed by an easy work up and good yields
- access to triblock copolymers of type BAB- and fluorine end-capped polymers in as few steps as possible
- polymerization of both styrene and acrylic monomers
- attachment of sensitive UV- and ^{19}F-label to the polymer terminus for end-group analysis (good intensity= high sensitivity) (criteria for NMR vide supra)
- avoiding difficult fluorine chemistry or postsynthetical fluorine modifications
- high effectivity

Trithiocarbonates are a class of CTAs successfully applied in the polymerization process and can be modified in a way to meet all requirements [32]:

Two basic CTA types were developed for this purpose (figure 36 and figure 37):

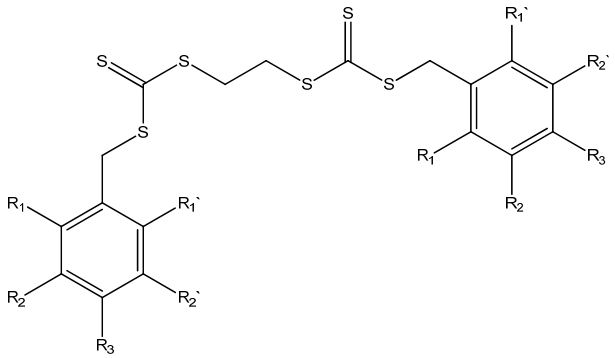

CTA XXXIX: $R_1 = R_{1'} = R_2 = R_{2'} = R_3 = H$
CTA XXXX: $R_1 = R_{1'} = H$ $R_2 = R_{2'} = H$ $R_3 = CF_3$
CTA XXXXI: $R_1 = R_{1'} = H$ $R_2 = R_{2'} = CF_3$ $R_3 = H$
CTA XXXXII: $R_1 = R_{1'} = H$ $R_2 = R_{2'} = H$ $R_3 = F$
CTA XXXXIII: $R_1 = R_{1'} = F$ $R_2 = R_{2'} = F$ $R_3 = H$
CTA XXXXIV: $R_1 = R_{1'} = R_2 = R_{2'} = R_3 = F$

Figure 36: Symmetric CTAs to be applied in the synthesis of BAB-triblock copolymers in two steps. The groups chosen for Z and R match the requirements for the polymerization of styrenics and acrylics, for the later polymerization of styrene (**M3**) and its fluorinated derivatives (**M4, M5, M6, M7**) as well as for NIPAM (**M1**) and NAP (**M2**) (see also [142, 32]).

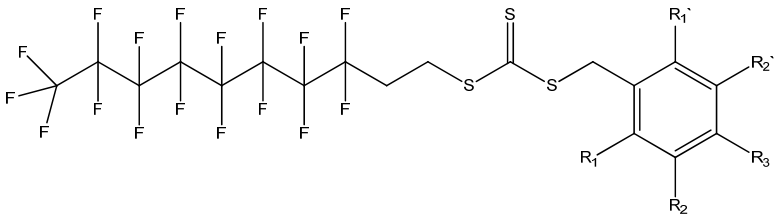

CTA XXXIV: $R_1 = R_{1'} = R_2 = R_{2'} = R_3 = H$
CTA XXXV: $R_1 = R_{1'} = H\ R_2 = R_{2'} = H\ R_3 = CF_3$
CTA XXXVI: $R_1 = R_{1'} = H\ R_2 = R_{2'} = H\ R_3 = F$
CTA XXXVII: $R_1 = R_{1'} = F\ R_2 = R_{2'} = F\ R_3 = H$
CTA XXXVIII: $R_1 = R_{1'} = R_2 = R_{2'} = R_3 = F$

Figure 37: Non-symmetric CTAs to be applied in the synthesis of fluorine end-capped polymers in two steps. The groups chosen for Z and R match the requirements for the polymerization of styrene (**M3**) (see also [32]).

10.2 Synthetic pathway towards trithiocarbonates

Trithiocarbonates have been reported to be effective chain-transfer agents in the RAFT process [32]. Three synthetic pathways are commonly used to synthesize trithiocarbonates:

- deprotonation of thiols applying strong bases followed by addition of CS_2 to give the carbodithioate salt, and subsequent alkylation [32, 438] (figure 38):

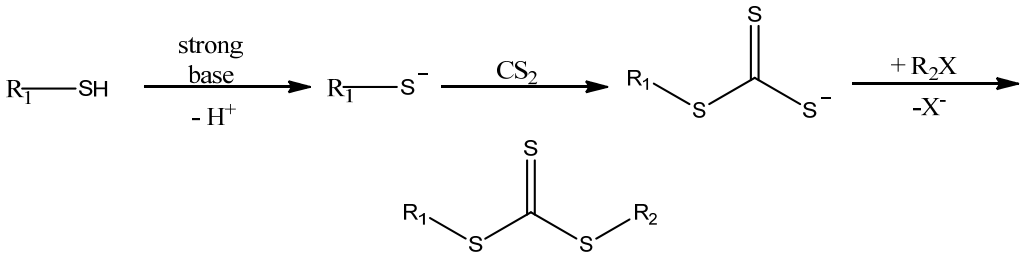

Figure 38: Synthesis of a trithiocarbonate via alkylation of carbodithioate salts

- Radical induced decomposition of a bis(thioacyl)disulfide (figure 39). This method is especially useful for the synthesis of RAFT agents bearing tertiary trithiocarbonates [32, 439]. Applying this method, a RAFT agent can also be generated in situ during the polymerization process [440].

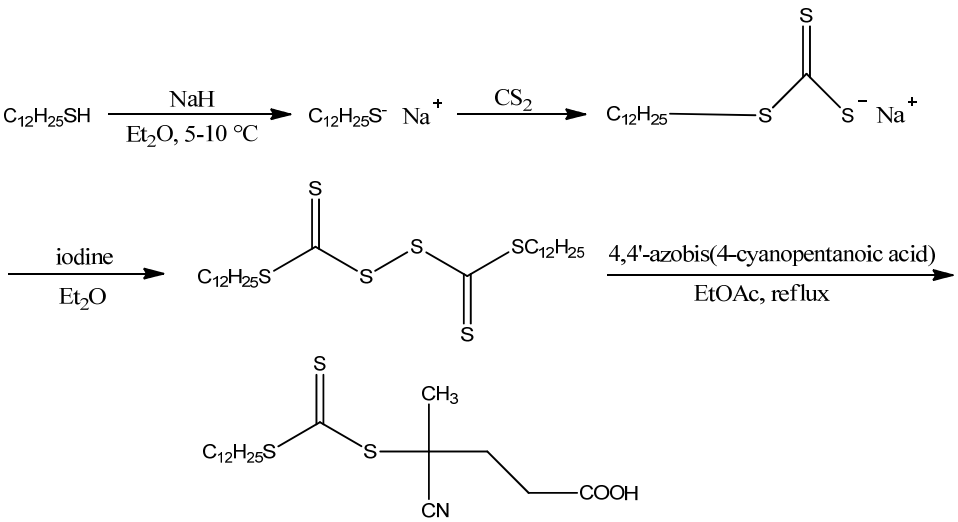

Figure 39: Synthesis of a trithiocarbonate, in this case 4-cyano-4-(dodecylthiocarbonothioylthio) pentanoic acid, by radical substitution of perthiolated acyl peroxides [441].

- The ketoform reaction [442] (figure 40):

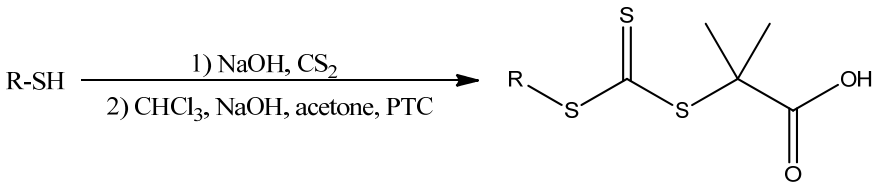

Figure 40: Synthesis of a trithiocarbonate by the ketoform reaction applying a strong base such as NaOH, followed by addition of CS_2, chloroform, acetone and phase transfer catalyst (PTC). Addition of phase transfer catalyst enables better mixing of the aqueous and organic liquids present in the reaction [442].

10.2.1 Synthesis of non-symmetric trithiocarbonates with a fluorinated R- and Z-group

In order to obtain the desired structures, the synthesis was performed by deprotonation of thiols applying strong bases followed by addition of CS_2 and alkylation by benzyl bromides as described in figure 41 according to references [32, 443]:

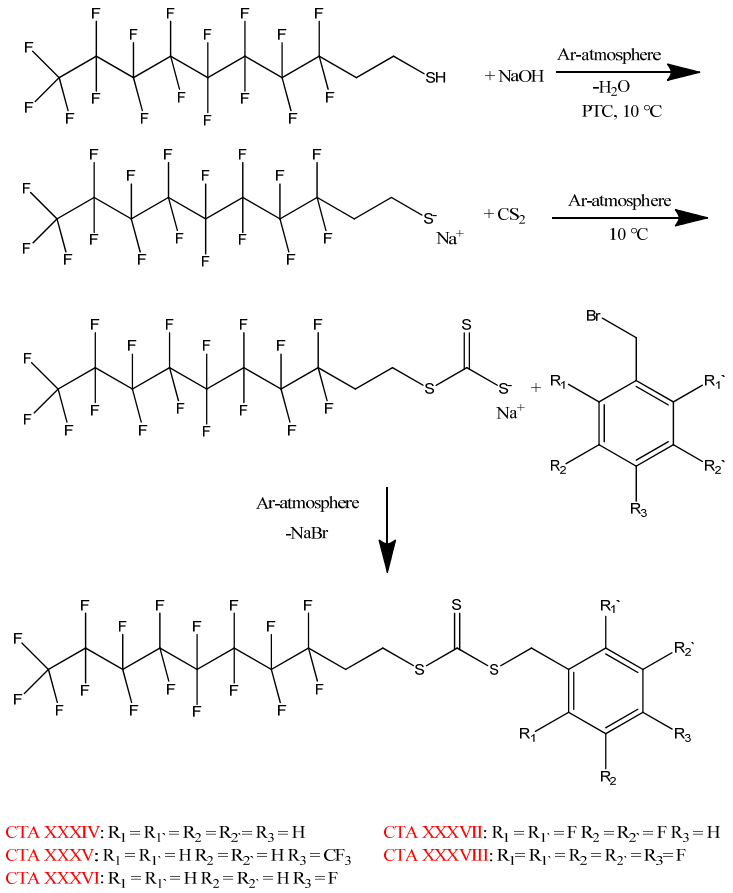

Figure 41: Synthetic route towards the synthesis of non-symmetric, monofunctional CTAs by deprotonation of a fluorinated thiol followed by the alkylation of the carbodithioate salt with various benzyl bromides bearing different substitution patterns at the aromatic ring [32, 443, 444].

The non-symmetric, monofunctional CTAs leading to fluorine end-capped polymers are all of almost the same composition. 1H,1H,2H,2H–heptadecafluoro-1-decanethiol was chosen for the introduction of both a fluorinated label, in particular of the CF_3-terminus of the chain, and the introduction of a hydrocarbon fluorocarbon chain avoiding synthetic effort. For the Z-group, benzyl-bromides with different substitution patterns were chosen in order to introduce various fluorinated labels in the R-group and to study possible effects of the different substitution patterns on the polymerization behaviour in general. Benzyl bromide, 4-(trifluoromethyl) benzyl bromide, 4-fluorobenzyl bromide, 2,3,5,6-tetrafluorobenzyl bromide and 2,3,4,5,6-pentafluorobenzyl bromide were chosen for variation of the R-group.

All products could be easily cleaned by recrystallization from methanol obtaining good yields. The synthetic process and the amounts of chemicals needed (table 6) as well as the NMR spectra are described in detail in the experimental section.

10.2.1.1 Description of the non-symmetric CTAs

CTA XXXIV: This RAFT agent consists of a CF_3-$(CF_2)_7$-CH_2-CH_2-chain for the Z-group but the benzyl (R-) group remains unsubstituted. The CF_3-group at the Z-group can be resolved as a separate signal with good intensity (3 F atoms on one signal (singlet) by ^{19}F-NMR (~ 81 ppm). In ^{1}H-NMR, the compound shows four signals; a multiplet (m) around 2.5 ppm from the –CH_2-CF_2-group and a triplet (t) around 3.6 ppm from the -CH_2-S-moiety as for the other CTAs originating from the Z-group. A multiplet (m) at 7.3 ppm is originating from the five protons of the aromatic ring and a singlet (s) around 4.6 ppm from the -CH_2-benzyl protons. The singlet (s) around 4.6 ppm is of less analytical value, for the position of the –CH_2-benzyl group will have changed after polymerization.

CTA XXXV: CTA XXXV is composed of a CF_3-$(CF_2)_7$-CH_2-CH_2-chain for the Z-group and a benzyl group carrying a CF_3-moiety in para position. Both CF_3-groups at the Z- and R-group can be resolved separately as one signal (two singlets) at -81,20 and -63.12 ppm with good intensity (3 F atoms each signal) applying ^{19}F-NMR. The fluorinated moieties on both Z- and R-group enable the calculation of the degree of functionality of the polymers (Z/R ratio) independently of ^{1}H-NMR. The compound displays three useful signals in ^{1}H-NMR; the signal around 2.5 ppm (m) from the –CH_2-CF_2-group and around 3.6 ppm (t) originating from the protons of the –CH_2-S-moiety and around 7.5 ppm from the multiplet of the benzyl group. The singlet (s) around 4.6 ppm results from the -CH_2-benzyl protons and is of less analytical value.

CTA XXXVI: CTA XXXVI is composed of a CF_3-$(CF_2)_7$-CH_2-CH_2-chain for the Z-group and a benzyl group bearing one F-atom in para position. The CF_3-group at the Z-group can be resolved as a separate signal (singlet) with good intensity (3 F atoms on one signal) also at ~ 81 ppm using ^{19}F-NMR as well as the para fluorine-substituted benzene ring at about -114.6 ppm. Here, the intensity of the F signal (singlet) originating from the substituated phenyl is relatively weak (one F atom on one signal). The signal originating from the aryl F atom can not be well resolved and is overlapping the signal originating from the -CF_2-$\mathbf{CF_2}$-CH_2-group. ^{19}F-NMR end-group analysis is going to be difficult in this case. In ^{1}H-NMR, the compound shows three valuable signals; the signal around 2.5 ppm (m) originating from the –CH_2-CF_2-group and a triplet (t) around 3.6 from the protons of the –CH_2-S-moiety and a multiplet (m) at ~ 7.1 ppm originating from the four protons of the aromatic ring. Also here, the singlet (s) resulting from the -CH_2-benzyl protons is less useful. The compound was synthesized to learn more about the effect of a differently fluorinated R-group on the kinetics and polymerization behaviour.

CTA XXXVII: CTA XXXVII consists of a CF_3-$(CF_2)_7$-CH_2-CH_2-chain for the Z-group and a benzyl group carrying four F atoms in 2, 3, 5 and 6-position. The CF_3-group at the Z-group can be resolved separately as one signal (singlet) with good intensity around -81 ppm (3 F atoms on one signal) in ^{19}F-NMR, whereas the fluorine-substituted benzene ring shows two signals (F_1, F_1` and $F_2$, $F_2$` = 2 F atoms on one signal) at -138.7 and -141.25 ppm. The singlets are close to each other but can be resolved. Determination of the Z/E-ratio using ^{19}F-NMR seems possible. The compound shows three valuable signals in ^{1}H-NMR; the signal around 2.5 ppm (m) from the –CH_2-S-moiety and around 3.6 ppm (t) originating from the protons of

the $–CH_2$-S-moiety and a multiplet (m) at ~ 7 ppm from the proton of the aromatic ring. The singlet (t) resulting from the $-CH_2$-benzyl protons at 4.7 ppm is –for the reason described before- less useful. The compound was synthesized to learn about the effect of a differently fluorinated R-group on the kinetics and polymerization behaviour.

CTA XXXVIII: As the aforementioned CTAs, CTA XXXVIII is also composed of a CF_3-$(CF_2)_7$-CH_2-CH_2-chain for the Z-group and a fully fluorinated benzyl group substituted by five F atoms in 2,3,4,5 and 6 position. The CF_3-group at the Z-group can be resolved as a separate signal (singlet) at ~ 81 ppm with good intensity (3 F atoms on one signal) in ^{19}F-NMR as well whereas the benzene ring shows three different signals (F_1, F_1` and $F_2$, $F_2$` and F_3)= 2* 2 F atoms on one signal at ~ 140.5 and ~ 153.8 ppm and 1 F atom on one signal at 161.6 ppm). Determination of the Z/E- ratio using ^{19}F-NMR seems possible. This compound shows no signal in ^{1}H-NMR in the aromatic region around 7 ppm, but the signal around 2.5 ppm (m) from the $–CH_2$-CF_2-group and around 3.6 ppm (t) resulting from the protons of the -CH_2-S-group are adressable . The singlet at about 4.7 ppm results from the -CH_2-benzyl protons and is of less analytical value.

10.2.2 Synthesis of symmetric trithiocarbonates with a fluorinated R-group

Also the synthesis of the symmetric trithiocarbonates was performed by deprotonation of dithiols applying strong bases followed by addition of CS_2 and alkylation by a halogenated compound as described in figure 42 according to reference [32, 443]:

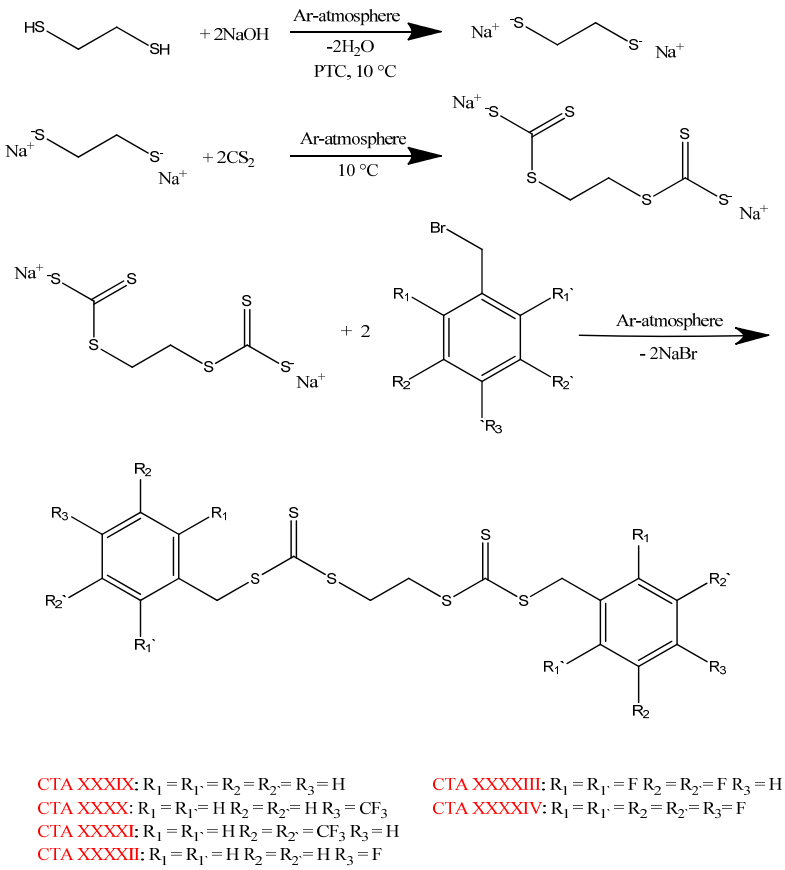

Figure 42: Synthetic route for synthesis of symmetric, bifunctional CTAs [32, 443].

The symmetric, bifunctional CTAs leading to BAB-triblock copolymers are all of almost the same composition. A bifunctional thiol, 1,2-ethanediol was chosen for Z-group addressable as a singlet in ^{1}H-NMR at a position of about 3.6 ppm; for the R-group, benzyl-bromides showing different substitution patterns were chosen in order to introduce a fluorinated label to the R-group and study a possible effect of the different substitution patterns on the kinetics and polymerization behaviour in general also for the symmetric CTAs. In addition to the reference benzyl bromide, 4-(trifluoromethyl)benzyl bromide, 4-fluorobenzyl bromide, 2,3,5,6-tetrafluorobenzyl bromide, 2,3,4,5,6-pentafluorobenzyl bromide and 3,5-bis(trifluoromethyl)benzyl bromide were chosen for the R-group.
The synthetic procedure is almost the same as described for the non-symmetric CTAs. All products could be easily cleaned by recrystallization from methanol obtaining good yields. The synthetic process and the amounts of chemicals needed (table 5) as well as the NMR spectra are described in the experimental part.

10.2.2.1 Description of symmetric CTAs

CTA XXXIX: This RAFT agent consists of a -CH_2-CH_2-chain for the Z-group but the benzyl group remains unsubstituted. In ^{1}H-NMR, the compound shows three signals; a signal around ~ 3.9 ppm (s) from the –CH_2-CH_2-moiety as for the non-symmetric CTAs originating from the Z-group, a multiplet (m) at ~ 7.3 ppm from the ten protons of the aromatic systems and a singlet (s) at 4.6 ppm originating from the four -CH_2-aryl protons. As for the non-symmetric CTAs, the signal of the CH_2-aryl protons is of less analytical value, for the position of the -CH_2-benzyl group will have changed after polymerization.

CTA XXXX: CTA XXXX is composed of a -CH_2-CH_2-moiety for the Z-group and two benzyl groups both carrying a CF_3-moiety in para position. The CF_3-moieties at both R-groups can be resolved as one signal (singlet) with good intensity (6 F atoms on one signal, symmetric molecule) applying ^{19}F-NMR at ~ 63 ppm. The fluorinated moieties enable the determination of the molar mass of fluorinated polymers via end-group analysis in ^{19}F-NMR. The compound displays three signals in ^{1}H-NMR; the singlet (s) around 3.7 ppm originating from the –CH_2-CH_2-moiety of the Z-group, a multiplet (m) at ~ 7.5 ppm resulting from the eight protons of the two aromatic systems and a singlet (s) at 4.6 ppm from the four -CH_2-aryl protons. Also here, the signal of the CH_2-aryl protons is of less analytical value.

CTA XXXXI: CTA XXXXI is composed of -CH_2-CH_2-moiety for the Z-group and a benzyl group carrying two CF_3-moieties in m-position of the phenyl ring. Both CF_3-groups attached to each of the R-groups can be resolved as one signal (singlet) with good intensity (12 F atoms on one signal originating from the CF_3-groups in m-position, symmetric molecule) applying ^{19}F-NMR at ~ -63 ppm. The fluorinated moieties enable the determination of the molar mass of fluorinated polymers via end-group analysis in ^{19}F-NMR. In ^{1}H-NMR, the compound shows two valuable signals; the singlet (s) around ~ 3.7 ppm due to the –CH_2-CH_2-moiety of the Z-group and the multiplet (m) at ~ 7.8 ppm originating from the six protons of the aromatic rings. The singlet (s) at 4.7 ppm from the four -CH_2-aryl protons is again of less useful for analytical studies. This compound was synthesized to learn more about the effect of the R-group on the kinetics and polymerization behaviour of this newly synthesized CTAs. Furthermore, the substitution of the aromatic systems with two electron withdrawing CF_3-

groups leads to a lower field shift of the aromatic signal in ^{1}H-NMR useful in poly(styrene) (**M3**) analysis.

CTA XXXXII: CTA XXXXII is composed of a -CH_2-CH_2-chain for the Z-group and two benzyl groups bearing an F-atom in para position. Using ^{19}F-NMR, the para fluorine-substituted benzene rings display one signal (s) (two F atoms on one signal) at –114.43 ppm. The intensity of the F-signal originating from the substituted phenyl rings is relatively weak (only 2 F atoms on one signal). Nevertheless, the determination of the molar mass of fluorinated polymers via end-group analysis in ^{19}F-NMR should be possible. In ^{1}H-NMR, the compound also shows three signals; the signal (s) around 3.9 ppm originating from the –CH_2-CH_2-moiety of the Z-group, a multiplet (m) at 7.5 ppm due to the eight protons of the aromatic ring and a singlet (s) at 4.8 ppm from the four -CH_2-aryl protons of limited analytical value. Also this compound was synthesized to learn more about the effect of a differently fluorinated R-group on the kinetics and polymerization behaviour.

CTA XXXXIII: CTA XXXXIII consists of a -CH_2-CH_2-moiety for the Z-group and two benzyl groups each carrying F atoms in 2, 3, 5 and 6 position. In ^{19}F-NMR, the fluorine-substituted benzene rings shows two signals (s) (2 * F_1, $F_1^{`}$ and 2 * $F_2$, $F_2^{`}$ = 4 F atoms on one signal) at -138.3 and -141.3 ppm. The determination of the molar mass of fluorinated polymers via end-group analysis in ^{19}F-NMR should be possible. The compound shows three signals in ^{1}H-NMR; the singlet (s) appearing at 3.7 ppm from the –CH_2-CH_2-moiety of the Z-group, a multiplet (m) at ~ 7 ppm resulting from the two protons in p-position of the aromatic rings and a singlet (s) at 4.7 ppm originating from the four -CH_2-aryl protons of less analytical value. The compound was synthesized to learn about the effect of differently fluorinated R-groups on the kinetics and polymerization behaviour.

CTA XXXXIV: As the aforementioned CTAs, CTA XXXXIV is also composed of a -CH_2-CH_2-chain representing the Z-group and two fully fluorinated benzyl groups bearing F atoms in 2,3,4,5 6- position. In ^{19}F-NMR, the benzene ring shows three different signals (s) (F_1, $F_1^{`}$ and $F_2$, $F_2^{`}$ and F_3) = 4* 2 F atoms on one signal, 2 F atoms on one signal) at -140.2, -153.5 and -161.9 ppm. The fluorinated moieties should enable the determination of the molar mass of fluorinated polymers via end-group analysis in ^{19}F-NMR. This compound shows no disturbing signals in the aromatic region of ^{1}H-NMR, only the singlet (s) of the Z-group (4 protons) and of the -CH_2-aryl protons (4 protons) can be detected at about 3.7 and 4.7 ppm. For the reasons explained before, the analytical use of the -CH_2-aryl protons is limited. Also this compound was synthesized to learn more about the effect of a differently fluorinated R-group on the kinetics and polymerization behaviour.

10.3 Conclusions RAFT synthesis

Two sets of non-symmetric and symmetric trithiocarbonates were successfully synthesized following the synthetic path of dehydrogenation of thiols and dithiols applying strong bases subsequently followed by addition of CS_2 and alkylation by a halogenated compound according to references [272, 361, 402] in very good yields. The raw substances can all be easily cleaned by recrystallization from methanol avoiding time consuming column chromatography.

10.4. Kinetics of styrene polymerization in the presence of CTAs

In order to study the kinetics of the newly synthesized symmetric and non-symmetric CTAs, styrene (**M3**) was chosen as model monomer. Styrene is easily purified by distillation and can be polymerized under standard conditions in both solution and bulk. In the literature, numerous CTAs have been reported to polymerize styrene successfully under good control providing polymers with narrow molecular weight distributions [445-447]. Furthermore, styrene was selected for the hydrophobic B-block of the new BAB-block copolymer systems which length has to be carefully selected to keep the later polymer water soluble. The results obtained with styrene should also serve as a kind of pre-study for the later applied fluorinated monomers 2-,3-,4-fluorostyrene (**M4, M5, M6**) and 2,3,4,5,6-pentafluorostyrene (**M7**).

The polymerization protocol followed for the kinetic studies and the amounts of chemicals used are described in the experimental part (table 9). All polymerizations were aiming at molecular weights of 10000 g/mol. The polymerizations of styrene (**M3**) were induced thermally without adding initiator (see also thermal initiation of styrene: Mayo-mechanism), whereas pentafluorostyrene (**M7**) was polymerized in presence of initiatior V 30. Before investigating the polymerizations, the thermal stabilities of the non-symmetric and symmetric **CTAs XXXV** and **XXXX** were tested applying TGA measurements. Non-symmetric **CTA XXXV** shows thermal decomposition beyond 219 °C, whereas the symmetric **CTA XXXX** is stable up to 239 °C (table 11). In order to guarantee a good radical flow, the polymerization temperature was set to 110 °C oil bath temperature [32]. The polymerization was not conducted as a one-pot reaction from which samples are taken subsequently at given time intervals, but several identical samples were prepared and the polymerizations stopped by cooling a given sample with liquid nitrogen after a distinct time interval. Part of the sample was investigated applying GPC measurements; the other part was diluted with 5 ml of THF and precipitated in methanol. The dried samples were further investigated by NMR measurements.

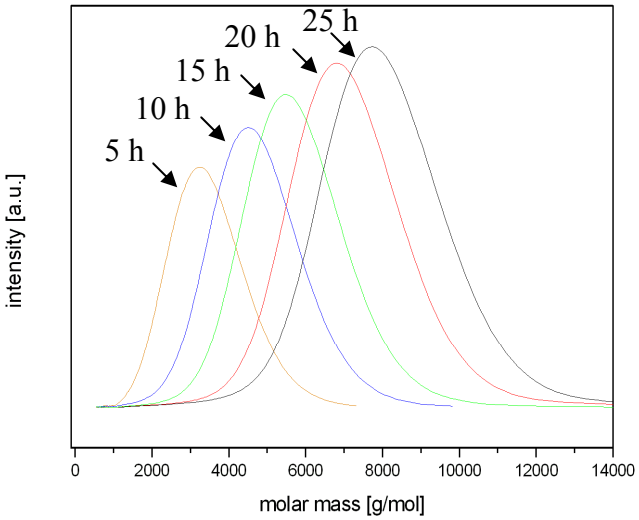

Figure 43: Evolution of GPC elugram with polymerization time (eluent: THF, internal standard: BHT) displaying the thermally initiated polymerization of styrene (**M3**) in bulk applying non-symmetric **CTA XXXV** at 110 °C after 5, 10, 15, 20 and 25 h (from left to right).

Figure 43 demonstrates the regular increase of the molar mass of the polymer within a time interval of 25 h in well defined steps. The polymerization seems to be well controlled leading to polymers with narrow molecular weight distribution (~ 1.1) (figure 44):

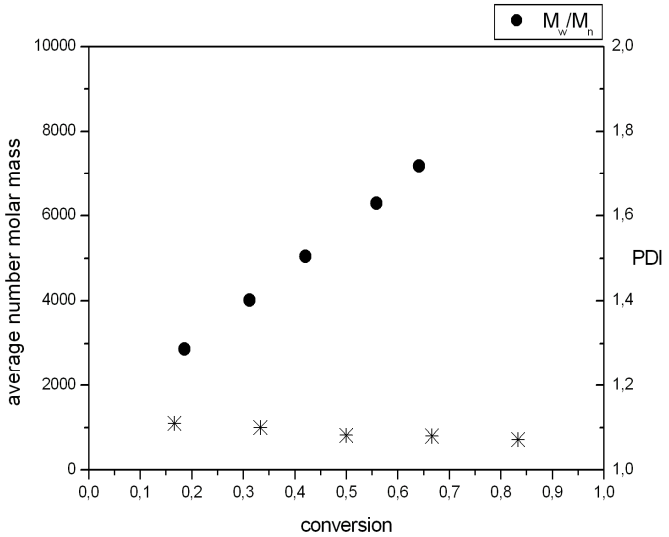

Figure 44: Polymerization of styrene (**M3**) in bulk using non-symmetric RAFT-agent **CTA XXXV** at 110 °C; average number molar mass versus conversion (values for conversion determined from IR signal ratio of monomer and polymer obtained by GPC measurements).

As shown in figure 44, the development of the molar masses follows pseudo first-order kinetics to high conversions with the number of the molar masses increasing linearly with conversion. The values calculated for M_n are comparable to the theoretically expected ones and the obtained homopolymers show low polydispersities (around 1.1). Furthermore, the symmetric **CTA XXXX** was also successful in polymerizing styrene (**M3**) (figure 45) applying thermal initiation at a bath temperature of 120 °C. Like the styrene samples prepared using the non-symmetric **CTA XXXV** before, the resulting PS-polymers showed a narrow molecular weight distribution around 1.1.

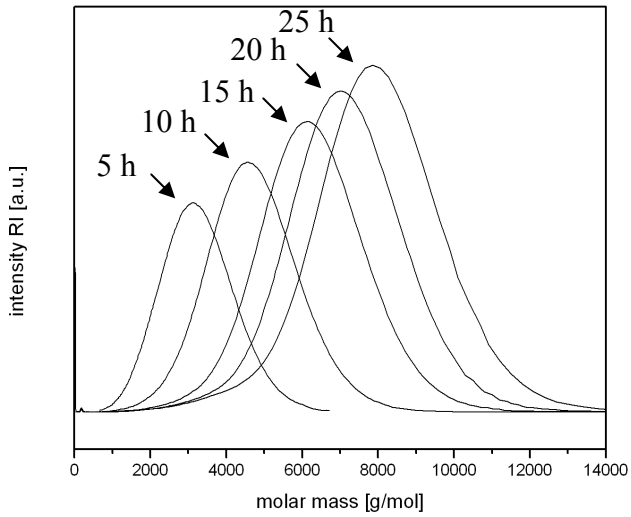

Figure 45: Evolution of the GPC elugrams with polymerization time (eluent: THF, internal standard: BHT) for the thermally initiated polymerization of styrene (**M3**) in bulk applying symmetric **CTAXXXX** at 110 °C after 5, 10, 15, 20, 25 h (from left to right). The molar mass of the polymer is increasing with time.

In a further experiment, the symmetric **CTA XXXX** was successful in polymerizing 2,3,4,5,6-pentafluorostyrene (**M7**) applying V 30 as an initiator at a bath temperature of 120 °C (figure 46).

The reasons for using an initiator for polymerization were already explained. The $[CTA]_0/[initiator]_0$ molar ratio was set to 10:1 in order to minimize the unfavourable termination reactions. Alike the styrene samples presented before, the resulting PFS (**M7**)-polymers showed a narrow molecular weight distribution around 1.1.
Compared to the PS- samples, the polymerization of PFS (**M7**) proceeded quite fast. However, the molar mass values determined by GPC measurements based on a PS-calibration are no longer reliable in this case. Therefore, ^{19}F-NMR was additionally used to determine M_n.

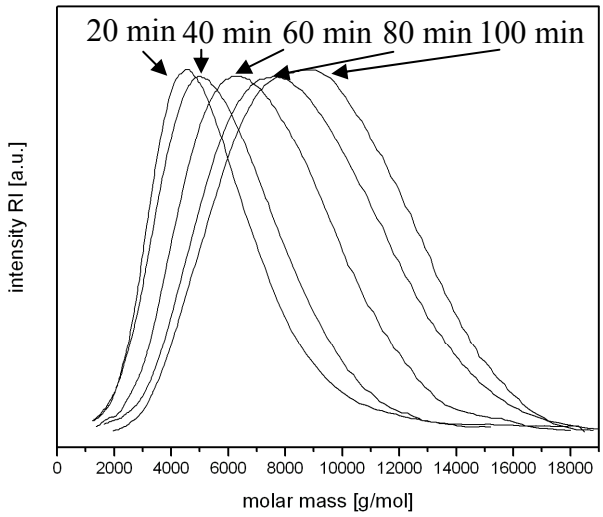

Figure 46: GPC elugramm showing a regulary increase of the molar mass in the bulk polymerization of symmetric **CTA XXXX** polymerizing pentafluorostyrene (**M7**) after 20, 40, 60, 80, 100 min at 120 °C. V 30 was chosen as an initiator. The ratio of CTA/initiator was set to 10:1. The polymerization is relatively fast (see also experimental part, table 7).

Applying non-symmetric **CTA XXXVIII** in the polymerization of styrene (**M3**) also resulted in a well-controlled polymerization yielding PS-homopolymers with narrow molecular weight distributions. The molar mass of the polymer increases with time (figure 47):

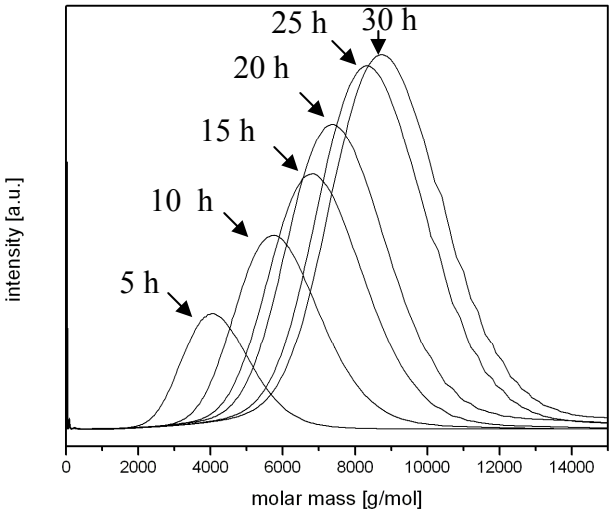

Figure 47: Evolution of GPC elugram with polymerization time (eluent: THF, internal standard: BHT) displaying the thermally initiated polymerization of styrene (**M3**) in bulk applying non-symmetric **CTA XXXVIII** at 110 °C after 5, 10, 15, 20, 25 and 30 h (in right direction).

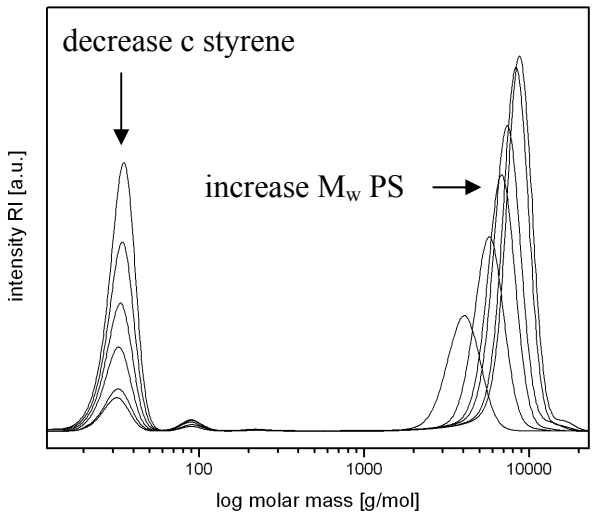

Figure 48: Evolution of GPC elugram with polymerization time (eluent: THF, internal standard: BHT) displaying the thermally initiated polymerization of styrene (**M3**) in bulk applying non-symmetric **CTA XXXVIII** at 110 °C after 5, 10, 15, 20, 25 and 30 h (from left to right). The concentration of monomer (left edge of graphics) is decreasing with time, whereas the polymer concentration (right edge of the spectrum) is increasing.

Figure 48 shows the development of the molar mass of the polymer increasing with time, whereas the amount of styrene monomer (**M3**) is decreasing (left signals) monitored by a GPC elugram.
Further examples for the controlled polymerizations of styrene (**M3**) using the newly synthesized CTAs can be found in the appendix.

In general, the thermally initiated polymerizations of styrene (**M3**) applying symmetric and non-symmetric CTAs are controlled and lead to PS-homopolymers of narrow molecular weight distribution (D~ 1.1 or 1.2). The polymerization times leading to distinct molar masses are surprisingly similar for the symmetric and non-symmetric systems (figure 49):

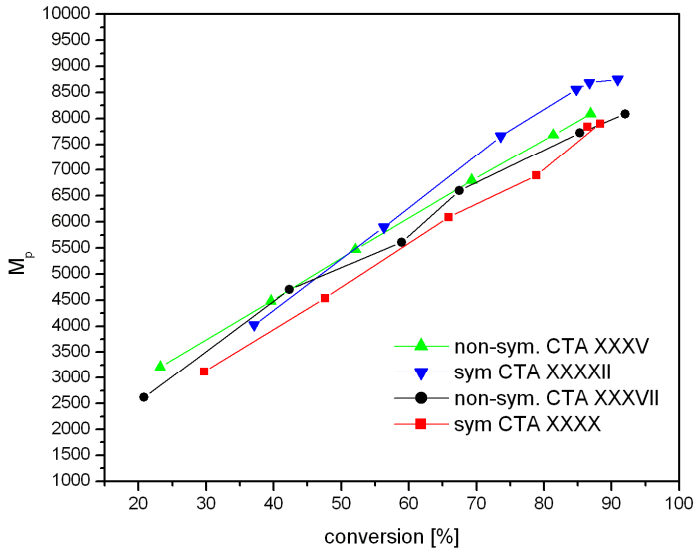

Figure 49: Comparison of the polymerization of styrene (**M3**) using non-symmetric **CTA XXXV**, sym. **CTA XXXXII**, non-sym. **CTA XXXVII** and symmetric **CTA XXXX**. The polymerization behaviour is almost similar for all CTAs, symmetric or non-symmetric.

All non-symmetric CTAs bearing a fluorinated Z- and R-group were able to polymerize styrene (**M3**) successfully under good control. The obtained polymers showed a narrow molecular weight distribution around 1.1. up to high yields. The same is valid for the samples obtained from non-symmetric **CTA XXXV**, bearing a non-fluorinated R-group. The kinetics was of pseudo-first order for all studied systems, independently of the type of label attached to the R-group, fluorinated (**CTAs XXXV-XXXVIII, XXXX-XXXXIV**) or non-fluorinated in case of the unsubstituated benzyl group (**CTAs XXXIV** and **XXXIX**). Further elugrams can be found in the appendix.

The symmetric **CTAs XXXX-XXXXIV** bearing a fluorinated R-group were able to polymerize styrene (**M3**) at 110 °C successfully under good control as well. The obtained polymers showed a narrow molecular weight distribution with PDI values around 1.1. up to high yields. The kinetics of these systems were also similar, independently of the type of fluorinated label attached. The elugram of sym. **CTA XXXXII** can be found in the appendix. The unsubstituated sample (sym. **CTA XXXIX**) was able to polymerize styrene successfully, as reported by Bivigou-Koumba [142].

10.4.1 Problems in the polymerization of styrene applying CTA XXXXIII

The problems occurring in the polymerization of styrene (**M3**) leading to a loss in control applying sym **CTA XXXXIII** labelled with fluorine in 2,3,5,6-position are still not clear. The experiment was repeated two times with the same result. The problems using this CTA might

originate from two reasons. First, the benzyl group bearing fluorine in positions 2, 3, 5 and 6 is able to form a relatively stable phenyl radical due to the +M-effect (positive mesomeric effect) of the fluorine substituents which might undergo combination or disproportionation (figure 50) reactions with other phenyl radicals leading to irreversible terminations in the RAFT process.

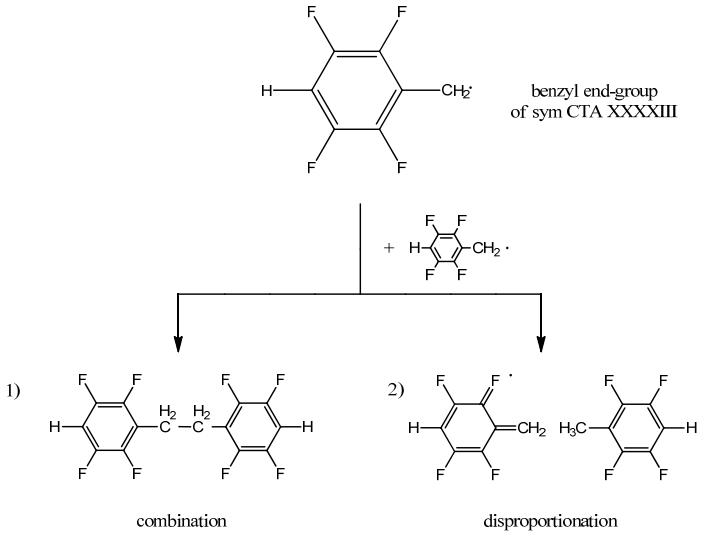

Figure 50: Combination or disproportionation reactions of the benzyl radical.

Second, the benzyl radical might be sensitive to the attack of a nucleophile due to the –I-effect (negative inductive effect) of the strongly electronegative fluorine substituents resulting in destruction of the CTA (figure 51):

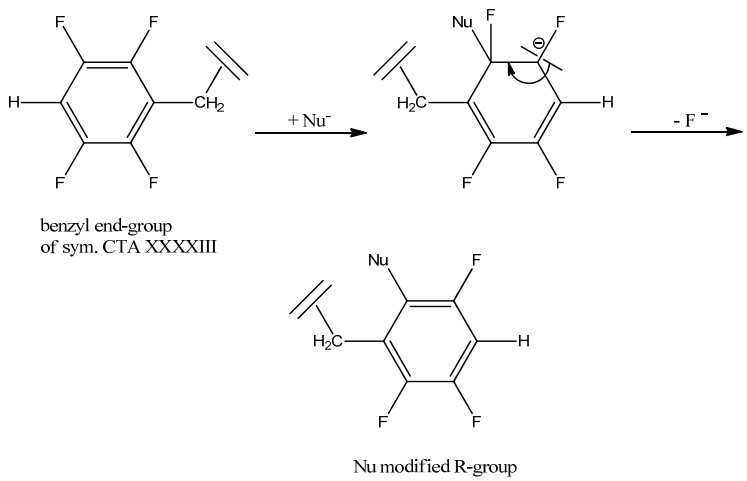

Figure 51: Hypothetic nucleophilic attack of the electron-poor benzyl system by an impurity resulting in destruction of the CTA.

As the elementary analysis of the chain transfer agent revealed no impurities, sulphur residues as possible nucleophiles can be excluded. It is therefore assumed, that the problems occurring in the polymerization process result from undesired termination- or disproportionation or the described elimination reactions.

If detailed knowledge on the reasons for the failure of the CTA is needed, NMR-measurements could help to gain further insight in the reaction mechanism using both ^{1}H-NMR spectroscopy and ^{19}F-NMR spectroscopy. Furthermore, the kinetics of the symmetric **CTA XXXXIV** should be investigated and checked for possible side reactions using ^{1}H-NMR spectroscopy and ^{19}F-NMR spectroscopy. As symmetric **CTAs XXXX** with a similar structure proved to work well, further investigations were postponed.

10.4.2 Conclusions kinetics of CTAs in the polymerization of styrene

All newly synthesized CTAs- non-symmetric and symmetric- except the symmetric **CTA XXXXIII** were able to moderate the thermally induced polymerization of poly(styrene) (**M3**) at a temperature of 110 °C successfully. For symmetric **CTAs XXXXI** and **XXXXIV** no kinetic study was performed. The polymerization process was monitored by applying GPC measurements determining the conversion with time. For the poly(styrene) polymers (**M3**-polymers) gained from the polymerizations applying the new RAFT agents the values for M_n applying a calibration on a PS-standard fit the theoretical values calculated for M_n. For 2,3,4,5-pentafluorostyrene (**M7**) the situation is different. Here, the GPC values based on a PS-calibration are no longer reliable. In this case, ^{19}F-NMR was additionally used to determine M_n. The determination of the molar mass of poly(pentafluorostyrene) polymers (**M7**-polymers) was straightforward using this method.

The fluorinated chains of the Z-group of the non-symmetric CTAs did not seem to influence GPC results; neither did the fluorinated groups of the R-groups of both symmetric and non-symmetric RAFT agents.

The reason for failing to control the polymerization process for symmetric **CTA XXXXIII** is not clear and further investigations have to be done to understand the problem, especially ^{1}H-NMR and ^{19}F-NMR spectroscopy could be instructive. Possibly, an unwanted rearrangement of the Z- or R-group takes place during the polymerization leading to a loss of control evidenced by GPC measurements. The kinetics were found to be similar for the non-symmetric and symmetric systems displaying only negligible differences.

Symmetric **CTA XXXX** was also successfully tested for the polymerization of 2,3,4,5,6-pentafluorostyrene (**M7**) applying V 30 as an initiator at a temperature of 120 °C. The attachment of fluorinated groups to both Z- and R-moiety of the RAFT agents at different positions of the aromatic ring of the R-group seems to have no negative influence on the control of the RAFT process. Therefore, functional end groups can be applied as effective labels in end-group analysis applying ^{19}F-measurements.

Chapter XI: Synthesis of amphiphilic BAB-triblock copolymers

11.1 Synthetic outline towards BAB-triblock copolymers

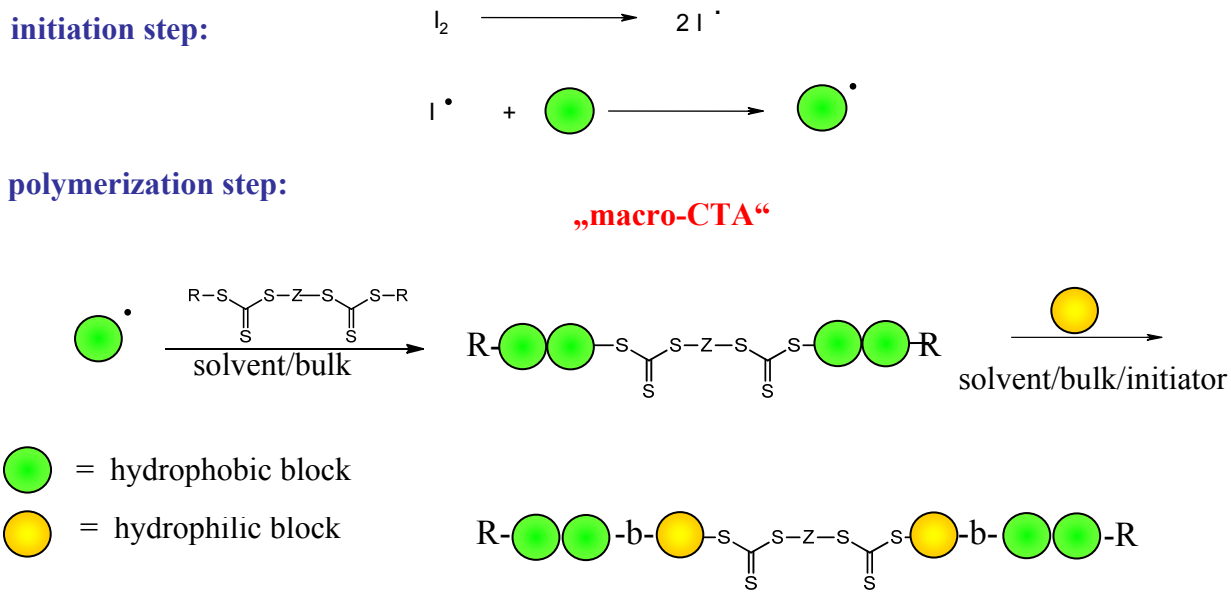

Figure 52: Synthesis of BAB-triblock copolymers in two steps applying symmetric **CTA XXXX.**

Symmetric **CTA XXXX** was used to synthesize the desired BAB-triblocks containing a thermosensitive hydrophilic A-block of poly(N-isopropylacrylamide) (**M1**) (NIPAM) or poly(N-acryloylpyrrolidine) (**M2**) (NAP) in just two steps (figure 52). The nature of the hydrophobic blocks was varied, using poly(styrene) (**M3**), poly (4-fluorostyrene) (**M6**), poly (3-fluorostyrene) (**M5**), poly (2-fluorostyrene) (**M4**) (testing if position of F has an influence on hydrophobicity) and poly (2,3,4,5,6-pentafluorostyrene) (**M7**) as an hydrophobic B-block with increasing hydrophobicity and lipophobicity. Poly(2,3,4,5,6-pentafluorostyrene) (**M7**) was tested as most hydrophobic and lipophobic monomer (figure 53). All polymers show a high T_g favouring the formation of micelles with glassy cores expecting to stabilize the structure of the eventually formed micellar gels.

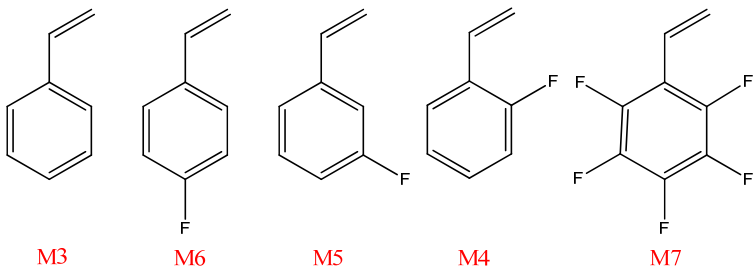

Figure 53: Styrene (**M3**) and its derivatives (**M4, M5, M6, M7**) employed in this study. The polarity of the monomers is changing from styrene (**M3**) to 2,3,4,5,6-pentafluorostyrene (**M7**). 2-, 3- and 4-fluorostyrene (**M4, M5, M6**) are probably more polar than polystrene.

Besides the analysis of the macro-RAFT agents and triblocks by GPC, conventional ^{1}H-NMR spectroscopy and the newly established end-group analysis via the fluorinated endgroups applying ^{19}F-NMR should be evaluated for the pentafluorostyrene systems (**M7**-blocks) and the results of the different methods compared.

11.1.1 Synthesis of the B-block prepared from styrene and fluorinated styrenes

In the first step, styrene (**M3**), 2-,3-,4-,5-pentafluorostyrene (**M7**) or 2-, 3- or 4-fluorostyrene (**M4, M5, M6**) homopolymers are synthesized in the presence of symmetric **CTA XXXX** (figure 54), and analyzed after purification by GPC and NMR spectroscopy. The polymerization conditions can be found in the experimental section. The solubility of the CTA in the monomer at room and elevated temperature was tested before performing the experiment. The CTA applied for polymerization was also tested for its stability before the polymerization to avoid unfavourable destruction at elevated polymerization temperatures. TGA measurements proved thermal stability of the symmetric **CTA XXXX** up to 239 °C. All polymerizations were conducted in bulk. Styrene (**M3**) polymerization was initialized thermally at an oil bath temperature of 110 °C guaranteeing a sufficient generation of radicals. The fluorinated styrene derivatives (**M4, M5, M6, M7**) were initiated using V 30 as initiator at a temperature of 120 °C. For the polymerization of 2-, 3- and 4-fluorostyrene (**M4, M5, M6**), thermal initiation might be also possible, but as problems were reported for the synthesis of 2,3,4,5,6-pentafluorostyrene (**M7**), an initiator was applied. For all polymerizations a ratio of 10:1 for CTA/initiator was chosen in order to minimize irreversible termination. Experimental data can be found in the experimental part, table 7.

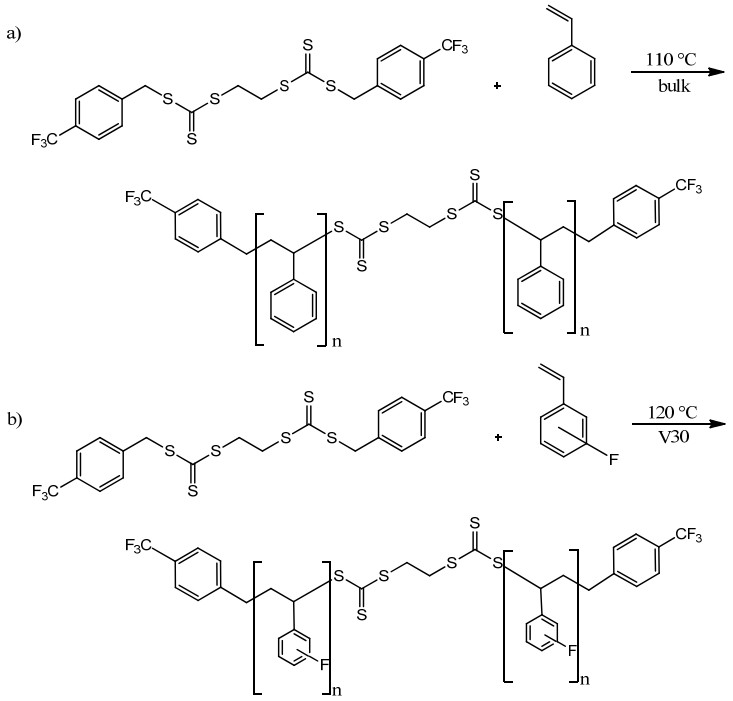

Figure 54: First step in the synthesis of BAB-triblock copolymers: synthesis of the hydrophobic B-block. a) Styrene (**M3**) was polymerized in bulk at 110 °C [32]; b) the fluorinated polymers (**M4, M5, M6, M7**) were polymerized in bulk at 120 °C applying CTA XXXX and V 30 as an initiator.

The kinetics for the polymerization of styrene (**M3**) and pentafluorostyrene (**M7**) polymerized applying symmetric **CTA XXXX** can be seen above.

11.1.2 Synthesis of the A-block prepared from NIPAM or NAP

In the second step (see figure 55), the macro-CTA was polymerized together with NIPAM (**M1**) or NAP (**M2**) in THF to achieve the BAB-triblock copolymers.

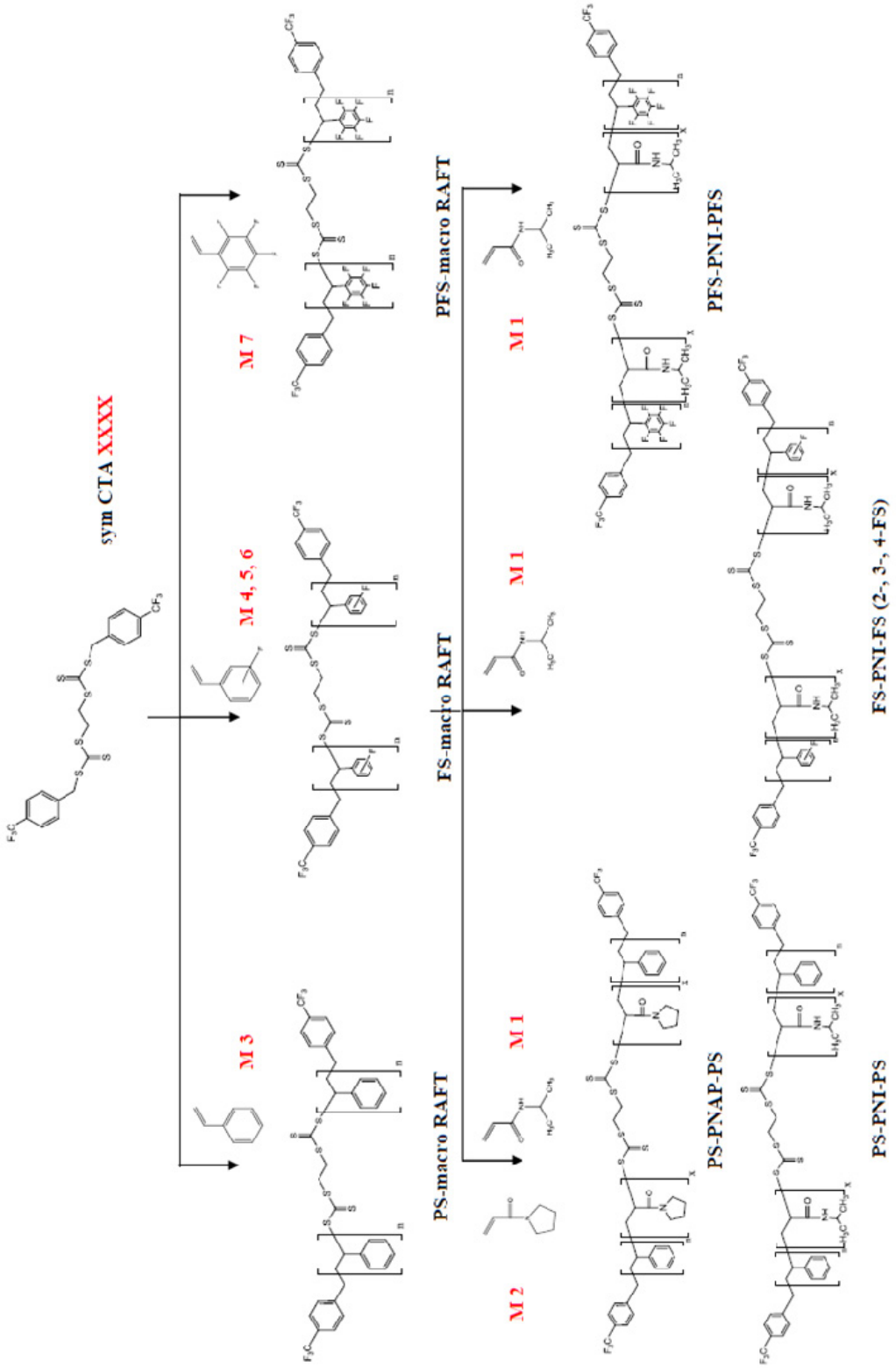

Figure 55: Synthesized homo- and BAB-triblock copolymers

Chosing THF as a solvent for radical polymerisations despite its good solubility for poly(styrenes) (**M1** blocks) and poly(pentafluorostyrenes) (**M7** blocks) may cause problems, because radical transfer reactions to the solvent and the presence of peroxides cannot be completely excluded [448].
Still, the influence of the two effects can be considered to be negligible, for the chain-transfer reactions between polymer and THF are only small and the existence of peroxides can be excluded due to freshly destilling the solvent over Na/K metal prior to use. The synthesis provided indeed polymers showing a relatively narrow molecular weight distribution. A second advantage of using THF as a solvent is the convenient cleaning of the synthesized polymers by dialysis against water directly after synthesis and subsequent freeze-drying. Furthermore, it behaved as a good solvent for the pentafluorostyrene homopolymer. Experimental data can be found in the experimental part, table 7.

The formation of block copolymer can be visualized by GPC measurements (figure 56, figure 57, figure 58). Compared to the elugrams gained from macro-CTA synthesized in step 1 (figure 54) using styrene (**M3**) or its derivatives (**M4, M5, M6, M7**) (vide supra), the formed BAB-triblock copolymers are shifted to remarkably higher molar masses for all synthesized series (**60000, 80000, 100000**). Further examples can be found in the appendix.

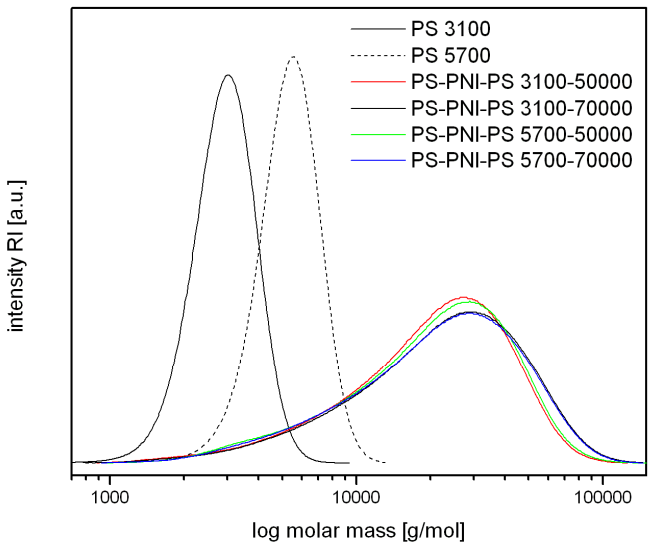

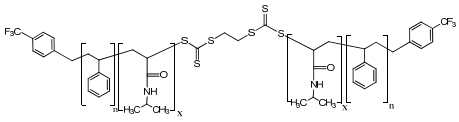

Figure 56: GPC elugram of **PS-PNI-PS 3100-50000**, **3100-70000**, **5700-50000** and **5700-70000**. Homopolymers PS 3100 and PS 5700 are the macro-RAFT precursors for the synthesis of these BAB-systems.

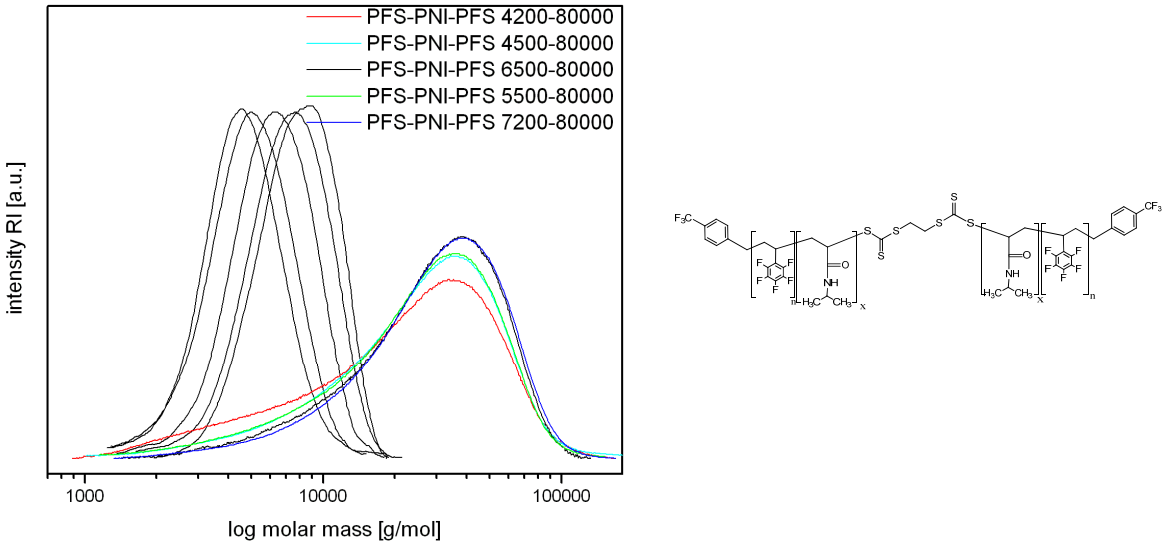

Figure 57: GPC elugram of **PFS-PNI-PFS 80000** series: **PFS-PNI-PFS 4200-80000, 4500-80000, 5500-80000, 6500-80000** and **7200-80000**. Homopolymers PFS 20 to PFS 100 (shifted to lower molecular weight, molecular weight of homopolymer increasing from left to right) resemble the PFS-macro- RAFT precursors for the synthesis of these BAB-systems.

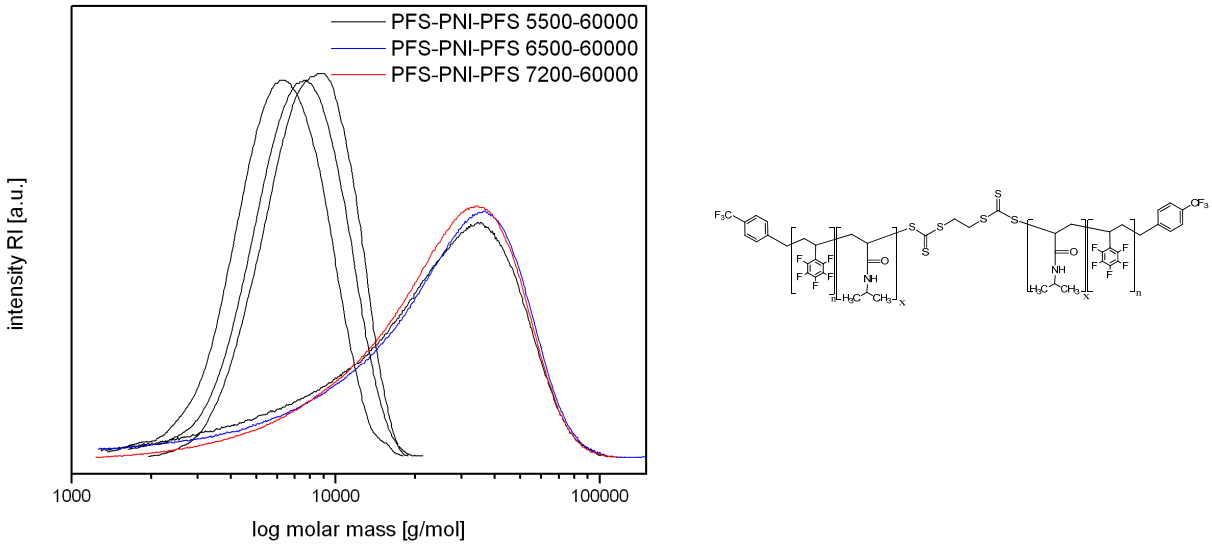

Figure 58: GPC elugram of **PFS-PNI-PFS 60000** series: **PFS-PNI-PFS 5500-60000, 6500-60000, 7200-60000**. Homopolymers PFS 60 to PFS 100 (shifted to lower molecular weight, molecular weight of homopolymer increasing from left to right) resemble the PFS-macro-RAFT precursors for the synthesis of these BAB-systems.

All BAB-triblock copolymers show a notable tailing in their GPC elugrams (Figure 54-56), whereas no tailing is observed for the macro-CTAs. The tailing of the elugrams probably results from a different retention behaviour of the block copolymers compared to homoblock

polymers as reported by Jiang et al. studying the retention behaviour of AB-, ABA- and BAB-block copolymers in liquid chromatography applying Monte Carlo simulations [449]. Another explanation could be the interaction of the BAB-polymers with the column resin.

The following BAB-triblock copolymers were synthesized in this thesis (table 1):

BAB-triblock copolymer	polymer code	information on synthesis
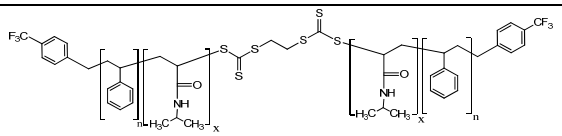	**PS-PNI-PS**	page 164, table 7
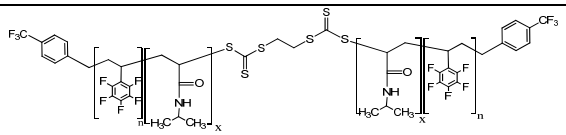	**PFS-PNI-PFS**	page 164, table 7
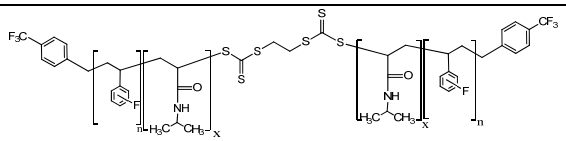	**4FS-PNI-4FS** **3FS-PNI-3FS** **2FS-PNI-2FS**	page 164, table 7
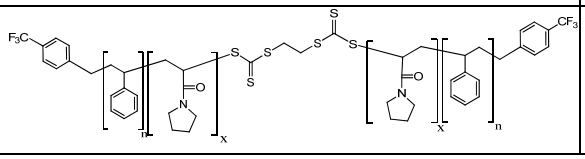	**PS-PNAP-PS**	page 165, table 7

Table 1: BAB-triblock copolymers synthesized

11.2 Synthetic strategy towards CF-end capped polymers

For the synthesis of CF-end capped polymers, several non-symmetric CTAs can be used. All CTAs were successfully tested in the polymerization of styrene (**M3**) in a kinetic study. Applying non-symmetric CTAs enables the synthesis of the CF-end capped polymers in just one step, for the fluorinated moiety is introduced by the Z-group of the CTA. For the polymer block, styrene (**M3**) was chosen.

11.2.1 Synthesis of CF end-capped polymers

The synthetic pathway towards CF-end capped polymers applying monofunctional, non-symmetric trithiocarbonate **CTA XXXV** is shown in figure 59:

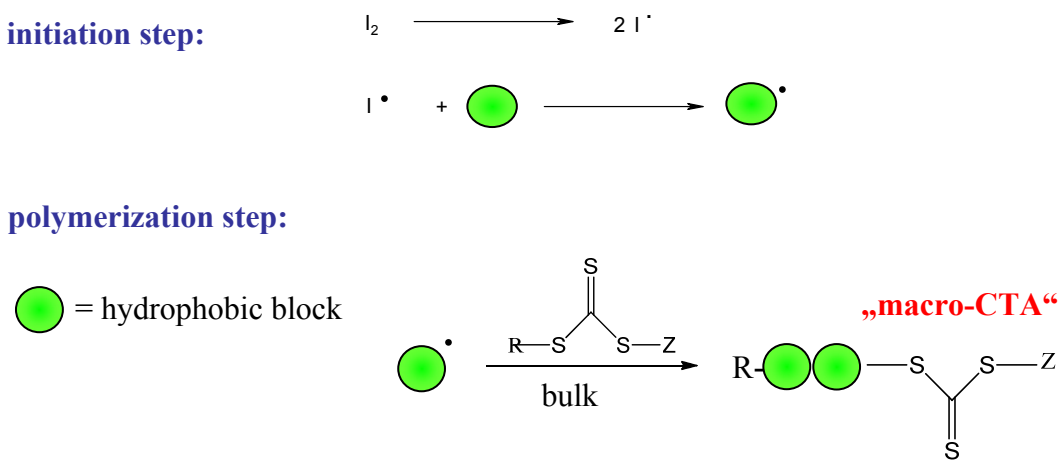

Figure 59: Synthesis of CF-end capped polymers in one polymerization step applying non-symmetric **CTA XXXV**. The fluorinated moiety is introduced by the Z-group of the monofunctional RAFT agents.

The polymerization conditions can be found in chapter experimental part. All polymerizations were conducted without solvent in bulk. The solubility of the CTA in the polymer was tested at room and elevated temperature before the polymerization. TGA measurements proved stability of **CTA XXXV** up to 219 °C. The polymerization of styrene (**M3**) (figure 60) was initiated thermally at an oil bath temperature of 110 °C [32]. The resulting polymers were analyzed after purification by GPC measurements and NMR spectroscopy.

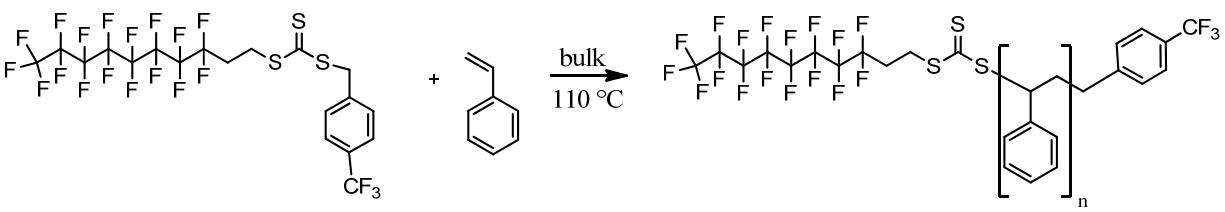

Figure 60: Synthesis of the CF-end capped hydrophobic B-block. Styrene (**M3**) was polymerized in bulk at 110 °C (thermal initiation). The used amounts and ratios can be found in the experimental part, table 8.

In contrast to the BAB-triblock copolymers, no tailing was observed. Obviously the fluorinated block is too short to show an influence on the retention behaviour.

Taking a closer look at the newly synthesized fluorinated RAFT agents, the aromatic R-groups can easily be detected via UV-measurements as well as the thiocarbonyl group. As a further obligation, the chosen R- and Z-groups -aromatic and aliphatic moieties- can be undoubtedly identified in ^{1}H-NMR spectroscopy being situated well apart from each other

(aromatic groups: ~ 7 ppm, aliphatic groups ~ 4 ppm) and thus be used as a label for end-group analysis determinating both the Z/R-ratio and the molar mass. The knowledge about the end-group functionalization is quite important; it can be estimated by the Z/R ratio of the investigated polymers assuring a high degree of functionality necessary for the further attachment of blocks (see also chapter RAFT polymerization). Fluorinated moieties are known to be electron-withdrawing shifting the proton signals of the aromatic R-group to even lower field, thus allowing a sufficient separation from proton signals originating from most aromatic polymers.

11.3 Application of labelled RAFT agents

A good example for the effectivity of using the CTAs for ^{1}H-labeling is the polymerization of styrene (**M3**) applying the symmetric **CTA XXXX** (figure 61).

The aliphatic protons originating from the $–CH_2$-CH_2-moiety are shifted in the region of 3.5 ppm displaying a sharp singulet for the symmetric CTAs, whereas the aromatic group can be resolved from the signal of the aromatic groups of poly(styrene) found around 7.5 ppm:

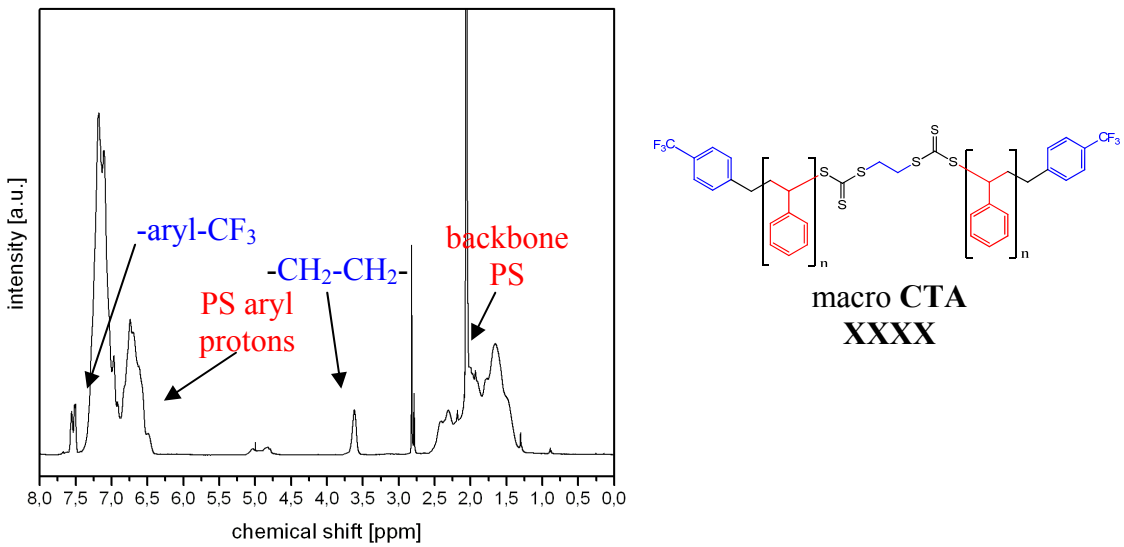

Figure 61: Poly(styrene) (**M3**) polymerized applying symmetric **CTA XXXX** enabling the determination of the molar mass using the aromatic (-aryl-CF_3) and aliphatic (-CH_2-CH_2-) CTA moiety as a label (solvent: acetone-d_6).

Nevertheless, in some cases the signals may overlap. In order to be completely independent of the position of the peaks in ^{1}H-NMR spectra, the fluorinated moieties introduced to the R- and Z-groups of the CTA provide groups still efficiently moderating the polymerization process and simultaneously provide an universal tool for end-group analysis using ^{19}F-NMR

spectroscopy, even in case fluorinated monomers are investigated. Fluorine containing groups were chosen as NMR markers, because ^{19}F, a pure element, is a half-spin nucleus with good sensitivity, small line-with, non-complicated line splitting and the possibility to investigate the block copolymers without disturbing overlaps [107-109].

Symmetric **CTA XXXX** was polymerized with 2,3,4,5,6-pentafluorostyrene (**M7**), forming the B-block of the hydrophobic, lipophobic BAB-systems. The fluorinated styrene (**M7**) shows no signal of the aromatic group around 7 ppm; only the proton containing backbone can be found around 2 ppm being of low analytical value for ^{1}H-NMR investigation.

Investigating the fluoropolymer applying ^{19}F-NMR (figure 62, 63) enables both the determination of the molar weight and the Z/R- ratio for all signals using the CF_3-moiety as a label in ^{19}F-NMR investigations. The fluorinated label can be found as a singlet in ^{19}F-NMR at -63.04 ppm:

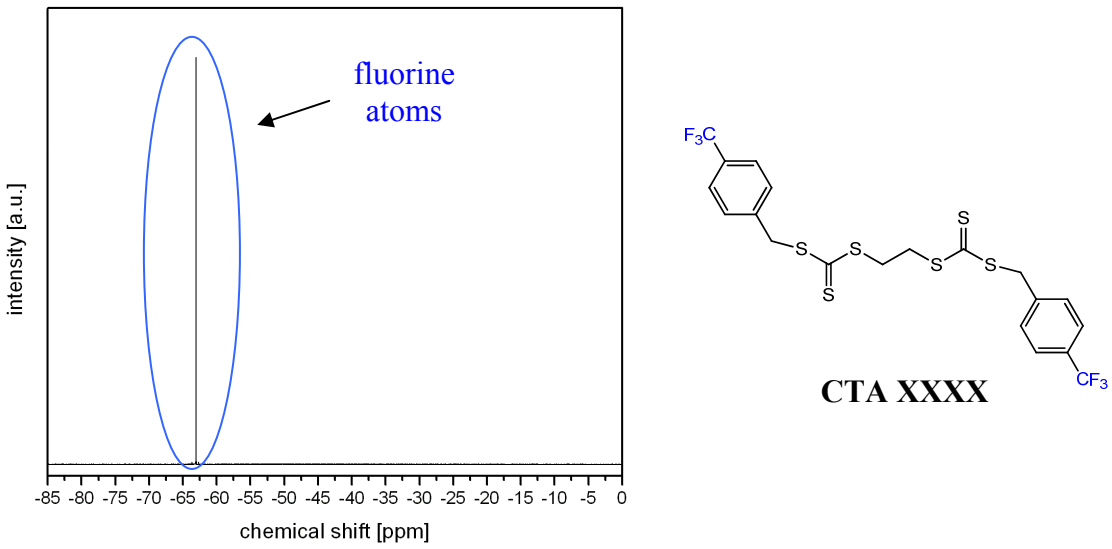

Figure 62: ^{19}F-NMR of symmetric, bifunctional **CTA XXXX**: characteristic singlet of the CF_3-moiety (solvent: chloroform-d_1).

The label can be resolved and distinguished from the F-signals originating from the polymer and successfully applied for end-group analysis (figure 63):

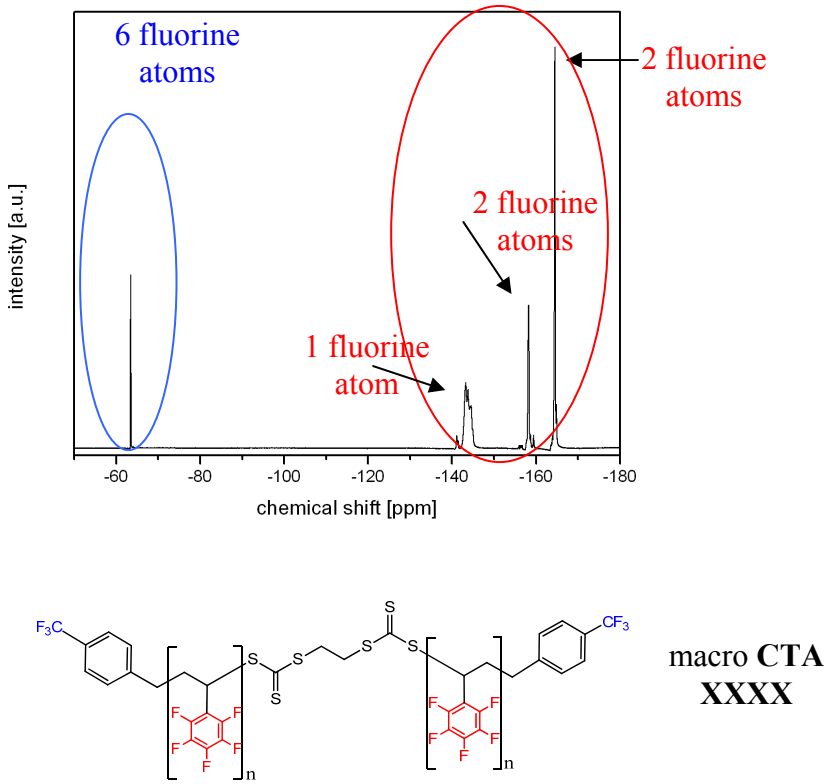

Figure 63: Determination of the molar mass of poly(pentafluorostyrene) (**M7**) polymerized applying the symmetric, bifunctional **CTA XXXX** using ^{19}F-NMR. The label can be resolved and distinguished from the F-signals originating from the polymer and successfully applied for end-group analysis (solvent: acetone-d_6).

The sensitivity of the method can be improved by choosing symmetric **CTA XXXXI**, uniting 12 fluorine atoms on one signal (figure 64):

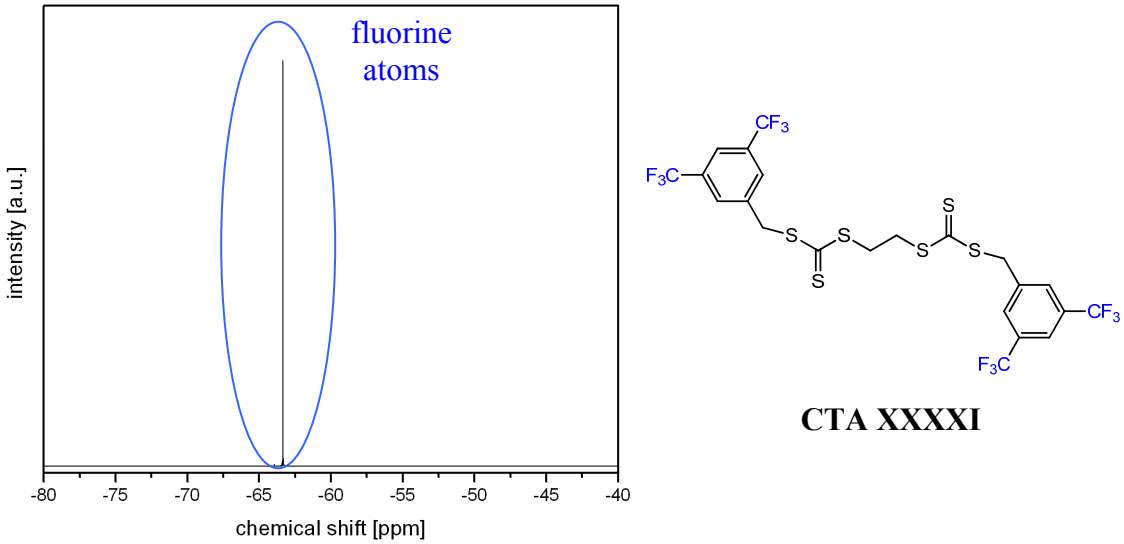

Figure 64: ^{19}F-NMR spectrum of symmetric, bifunctional **CTA XXXXI** uniting 12 fluorine atoms on one signal providing improved sensitivity (solvent: chloroform-d_1).

The monofunctional, non-symmetric **CTA XXXV** can be used following the same outline as displayed for the bifunctional, symmetric **CTA XXXX** as a useful ^{1}H- and ^{19}F-NMR label for both styrene (**M3**) and pentafluorostyrene (**M7**) polymerizations applying the p-substiutated aryl group and the alkyl group close to the fluorinated tail in ^{1}H- and the aryl-CF_3 group and the alkyl-CF_3 group in ^{19}F-NMR spectroscopy (figures 65, 66):

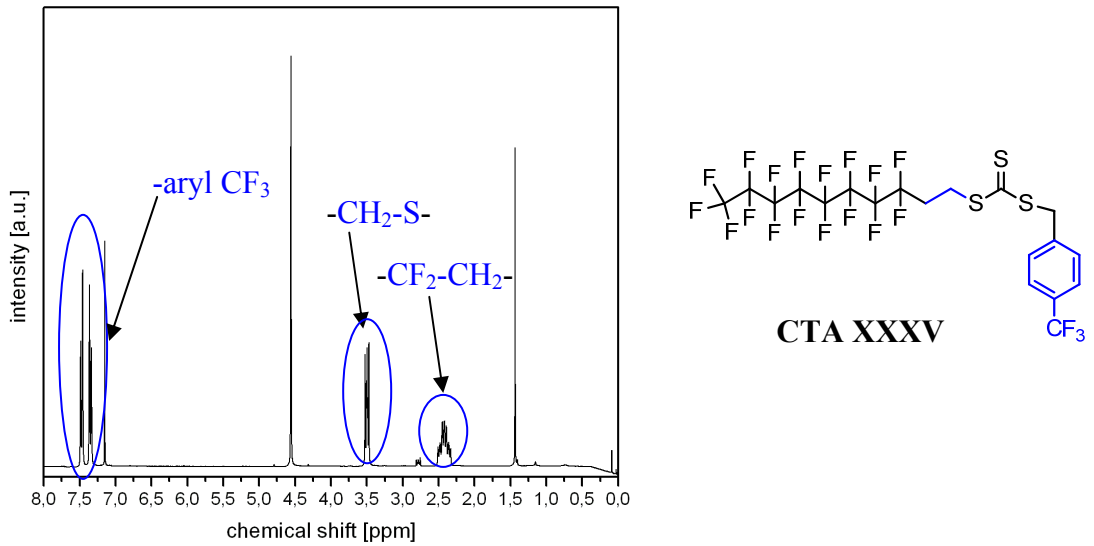

Figure 65: ^{1}H-NMR spectrum of monofunctional **CTA XXXV**. The aromatic (~ 7 ppm) and aliphatic moieties (-CH_2-S-) can be used as labels for the investigation of poly(styrene) (**M3**-block) applying ^{1}H-NMR (solvent: chloroform-d_1).

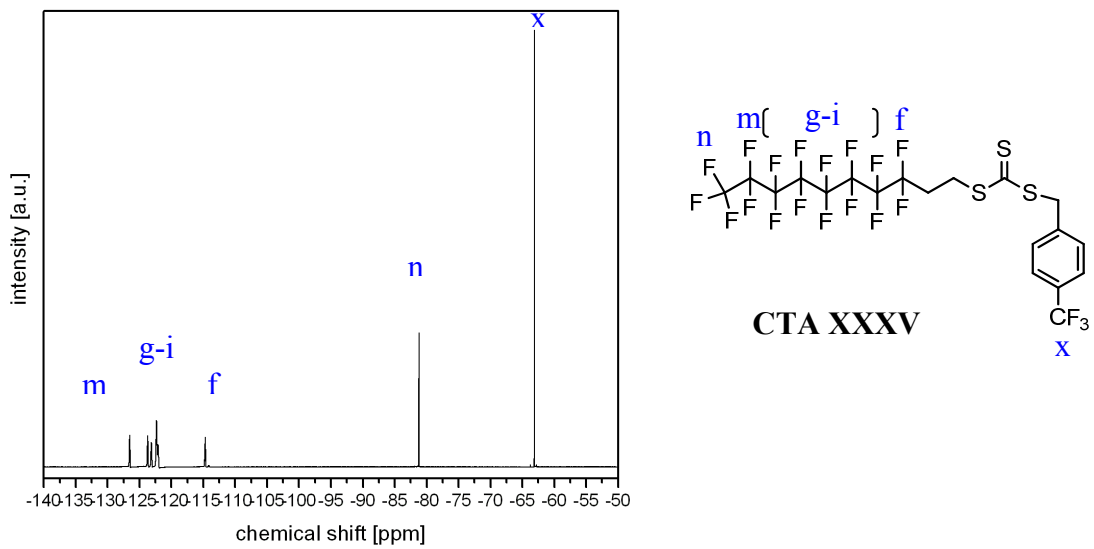

Figure 66: ^{19}F-NMR spectrum of monofunctional **CTA XXXV**. The CF_3-group at the aliphatic n and aromatic x-end of the CTA can be used as labels for the investigation of poly(pentafluorostyrene) (**M7**-block) applying ^{19}F-NMR (solvent: chloroform-d_1). Also the fluorinated m and f group are of analytical value.

The sensitivity of the method could even be improved by choosing a monofunctional CTA, uniting 6 fluorine atoms on one signal (figure 67) (not synthesized in this work):

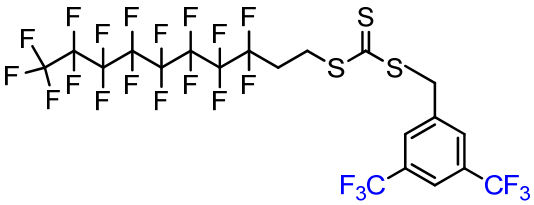

Figure 67: Non-symmetric CTA uniting 6 fluorine atoms on one signal could provide improved sensitivity.

The analysis of the BAB-triblock copolymers was nevertheless complicated due to overlapping of signals in ^{1}H-NMR (figure 68). The labelled R-group around 7 ppm could not be distinguished from the signals originating form the PS- and PNIPAM-block (NH-C=O-signals) (**M3, M1**-blocks). The same problems also occur when analyzing the **FS-PNI-FS** and **PS-PNAP-PS** systems. For the **PFS-PNI-PFS** polymers, the signals of the aromatic protons are completely missing (only visible in ^{19}F-NMR), and the signals of the polymer backbone are of low analytical value.

In this case, the C=S group of the trithiocarbonates (-S-(C=S)-S-) can be applied as an effective UV-label-provided not too much end-group is lost compromising the results.

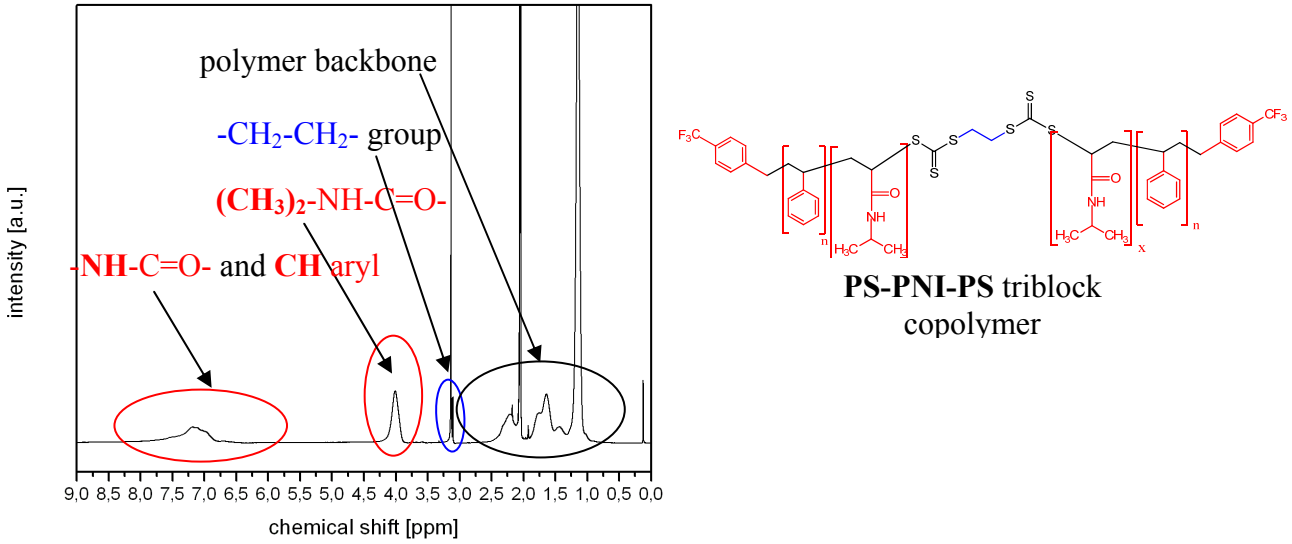

Figure 68: Analysis of BAB-triblock copolymer of type PS-PNI-PS (PS-PNI-PS 3100-70000) (solvent: acetone-d_6).

Chapter XII: Investigation of the thermosensitive solution behaviour of BAB-triblock copolymers

Depending on their block sequence and concentration of the aqueous solution, BAB-polymers are inclined to form interconnected or flower-like micelles in dilute and networks in concentrated aqueous solutions whereas the ABA-type forms core-shell micelles in diluted aqueous solutions and in concentrated ones. The BAB-type can be distinguished from mere AB-diblocks by the ability to form networks in concentrated solutions [142]. The generation of networks is favoured by the formation of bridges between the micelles due to single polymer chains not incorporated in micelles and entanglements between the micelles (requiring a sufficiently high molar mass of the triblock copolymers). These networks give rise to hydrogels which are not chemically but physically crosslinked when using a thermoresponsive A-block. Their swelling behaviour can be controlled by an external stimulus, e. g. temperature, magnetic field etc..

12.1 Turbidimetry measurements

The temperature dependent behaviour of PNIPAM-homopolymer (**M1** block) with a cloud point around 32 °C has already been discussed. Now, the temperature-dependent behaviour of the more complex BAB-block copolymer systems composed of PNIPAM-(**M1**) and PNAP (**M2**)-blocks for the hydrophilic and PS-(**M3**), PFS-(**M7**) and FS (**M4, M5, M6**)-blocks for the hydrophobic blocks of different length for both block types should be investigated applying turbidimetry measurements. The addition of hydrophobic blocks is expected to have an influence on the interactions between PNIPAM (**M1** block) and water, possibly disturbing the formation of hydrogen bonds. Effects on the cloud point and the shape of the turbidimetry graph are expected.

12.1.1 Turbidity of pure PNIPAM samples

For pure PNIPAM (**M1** block) samples, a cloud point around 32 °C is reported in the literature [305, 306]. Furthermore, Kubota and Fujishige et al. [450] and Bivigou-Koumba et al. [142] observed a small hysteresis in the cooling cycle of turbidity measurements. Fujishige postulated, that this effect could be explained by the limited free rotation on the total conformation in PNIPAM polymers according to the methylene group in the polymers main-chain. Another explanation for this phenomenon could be the conformational change from well dissolved random coils at temperatures below to closely packed particles above the cloud point delaying the hydration of the PNIPAM chains in the cooling cycle [450, 451]. The graphs gained from turbidimetry measurements were reported to be almost fully reversible.

Bivigou-Koumba reported cloud points of PNIPAM homopolymer created with different CTAs (and thus different end groups) similar to values in the literature, deducing that the influence of the end-group on the LCST is negligible [142].

12.1.2 Turbidimetry measurements of PS-PNI-PS systems

For reference, the **PS-PNI-PS** samples were investigated first. All samples are directly soluble in water, providing an optically clear solution at temperatures below the cloud point (< ~ 31 °C). At temperatures above the cloud point, the solutions became turbid. Figure 69 exemplifies this behaviour:

Figure 69: Transmission of aqueous solutions of **PS-PNI-PS 50000 and 70000** series showing samples a) **PS-PNI-PS 3100-50000** and b) **3100-70000,** c) **5700-70000** and d) **3100-70000 2g/L** as a function of temperature. (Cooling/heating rate 1 °C per minute, c= 1 g/L). The red arrow indicates the heating, the blue arrow the cooling curve.

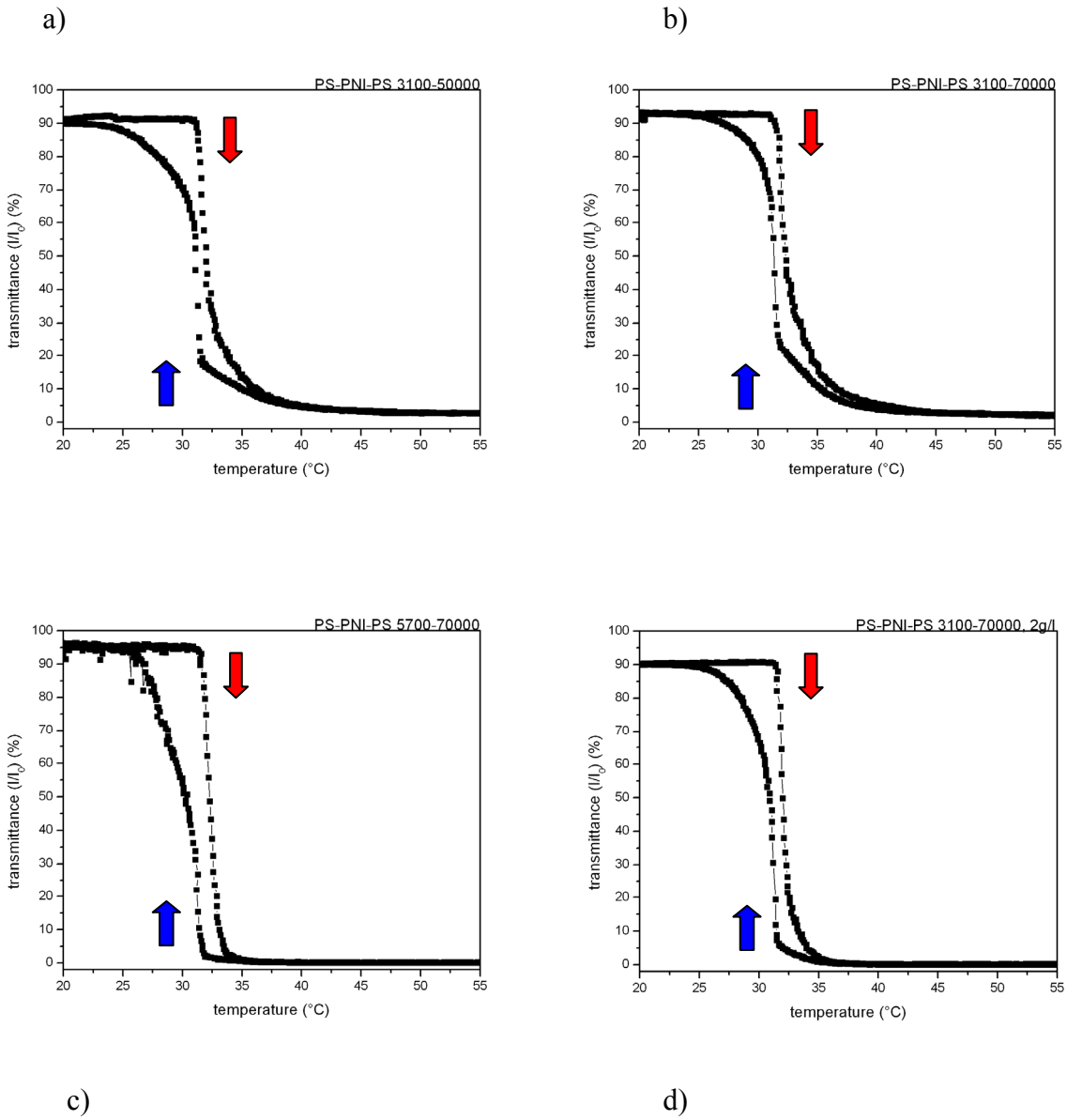

All investigated transmissions are reversible. Figure 69 displays curves of sigmoidal shape. The cloud point of the samples is marked by the solution getting turbid accompanied by a steep decrease of the transmission around 31 °C for all **PS-PNI-PS** samples. In contrast to the pure PNIPAM homopolymers, a marked hysteresis is occurring in the cooling cycle, as also described by Bivigou-Koumba [142]. Interchain association in the collapsed state of the

PNIPAM segments connected to the hydrophobic B-segments can explain this hysteresis [156]. In contrast to the samples described by Bivigou-Koumba, the values measured for transmission above the cloud point were close to zero or zero for all investigated samples. Increasing the concentration to 2 g/L did not lead to a remarkable shift in the LCST value.

Another interesting feature of the BAB-systems are the $–CF_3$-groups introduced by the symmetric **CTA XXXX** located at the polymer termini. As already discussed, some reports describe an influence of the end-group on the value of the cloud point. However, in this work no significant shift in the values measured for the cloud point could be detected. If there should be any influence originating from these groups, it is negligible. Maybe the situation is different in case bigger fluorine-containing substituents are fixed to the aromatic ring system, or when the CF_3-group is replaced by a larger fluorinated alkyl chain.

12.1.3 Turbidimetry measurements of PFS-PNI-PFS systems

In this experiment, the effect of introducing a different hydrophobic block -2,3,4,5,6-pentafluorostyrene (**M7** block)- to BAB-triblock copolymers upon thermally induced phase transition was investigated. Again, all samples are well soluble in water, providing an optically clear solution at temperatures below the cloud point (< ~ 32 °C). At higher temperatures, the solution becomes turbid as described before.

Figure 70-1): Transmission of aqueous solutions of examples of **PFS-PNI-PFS** series a) **5500-** and b) **7200-80000** as a function of temperature. (Cooling/heating rate of 1 °C per minute; sample concentration 1 g/L). The red arrow represents the heating, the blue arrow the cooling curve.

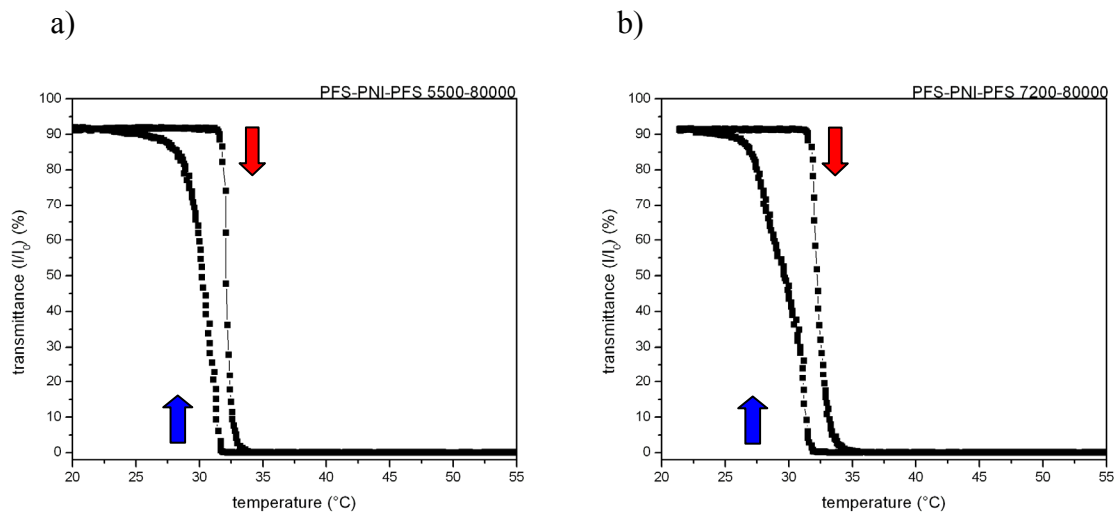

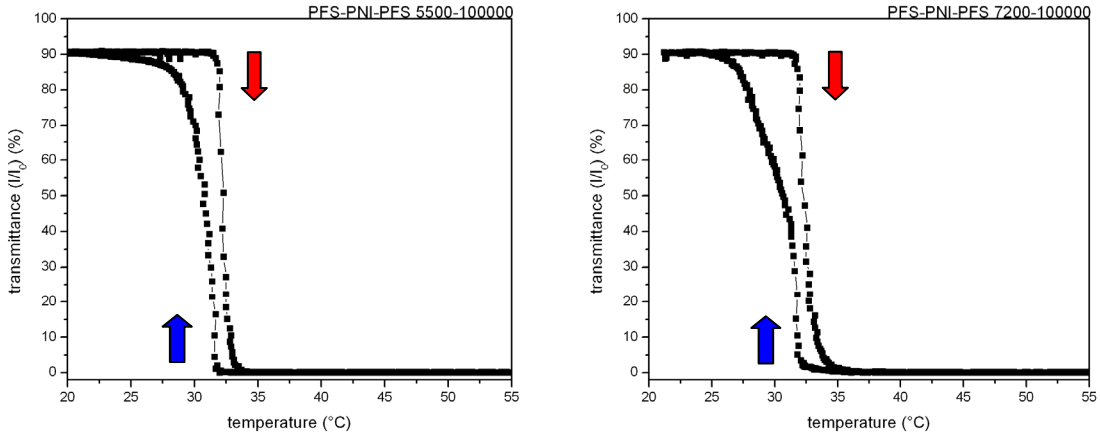

c) d)

Figure 70-2): Transmission of aqueous solutions of examples of **PFS-PNI-PFS** series c) **5500-** and d) **7200-100000** as a function of temperature. (Cooling/heating rate of 1 °C per minute; sample concentration 1 g/L). The red arrow represents the heating, the blue arrow the cooling curve.

As can be seen from figure 70, the graphs obtained from the **PFS-PNI-PFS** samples have sigmoidal shape similar to those reported for the **PS-PNI-PS** samples. The cloud point of all the investigated probes is around 32 °C, and is slightly higher compared to the **PS-PNI-PS** samples, but still within the temperature range described for PNIPAM (**M1** block) containing polymers in literature. Obviously, the hydrophobic blocks are not exposed to water in both **PS-PNI-PS** and **PFS-PNI-PFS** systems but hidden in the micellar core not counting for hydrophobic contributions to the LCST value [452].

The transitions are reversible, but a marked hysteresis can be detected in the cooling cycle which seems to be more prounounced compared to the **PS-PNI-PS** systems. Obviously the system needs a longer time to recover full hydration of the PNIPAM (**M1**)-block after collapsing. Maybe this behaviour can be related to the extremely hydrophobic fluorinated blocks.

12.1.4 Turbidimetry measurements of FS-PNI-FS systems

Here, the effect of introducing a block showing different polarity to PS (**M3**) and PFS (**M7**) to BAB-triblock copolymers upon thermally-induced phase transition was studied. Also in this case, all samples are well soluble in water forming an optically clear solution at temperatures below the cloud point (< ~ 31 °C). At high temperatures, the solution becomes turbid for reasons already described before.

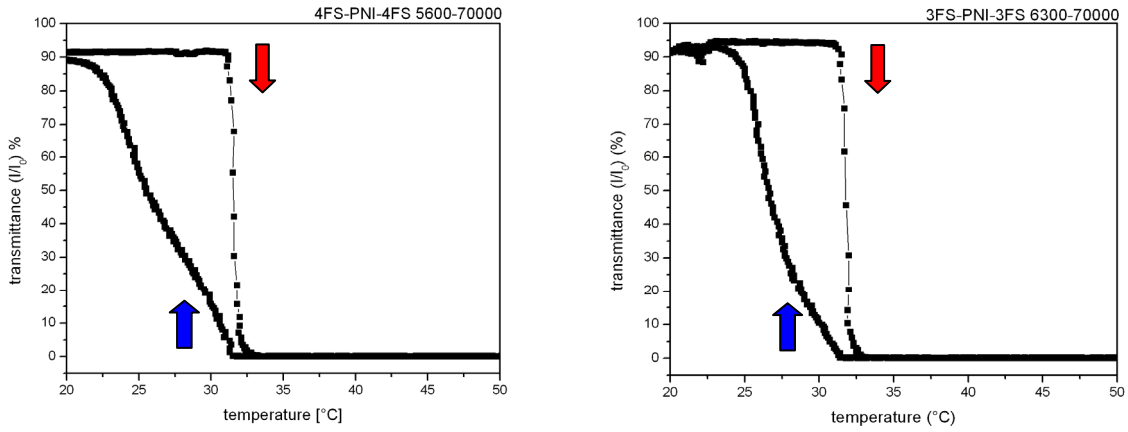

a) b)

Figure 71: Transmission of aqueous solutions of a) **4FS-PNI-4FS 5600-70000** and b) **3FS-PNI-3FS 6300-70000** as a function of temperature using a cooling/heating rate of 1 °C per minute; sample concentration 1 g/L. The red arrow represents the heating, the blue arrow the cooling curve.

All investigated transmissions are reversible (figure 71). Sample **2FS-PNI-2FS** is showing the same shape. The graph can be found in the appendix. The graphs achieved for the **FS-PNI-FS** samples are again of sigmoidal shape similar to the previously showed **PS-PNI-PS** and **PFS-PNI-PFS** samples. The cloud point of the investigated probes can be found around 31 °C matching the values for the **PS-PNI-PS** samples (vide supra). The transitions are reversible, but again a marked hysteresis can be found in the cooling cycle similar to the **PFS-PNI-PFS** systems, probably for the same reasons.

12.1.5 Turbidimetry measurements of PS-PNAP-PS systems

Only little information on the behaviour of aqueous PNAP solution and on turbidity measurements exists. For pure PNAP (**M2**-block) samples, a cloud point around 50 °C can be found in the literature [305, 306].

Here, the effect of replacing PNIPAM (**M1**-block) against another thermosensitive polymer-PNAP (**M2**-block) -in BAB-triblock copolymers upon thermally-induced phase transition was studied. All prepared samples are well soluble in water forming an optically clear solution at temperatures below the cloud point (< 50 °C). At temperatures above the cloud point, the solution becomes turbid.

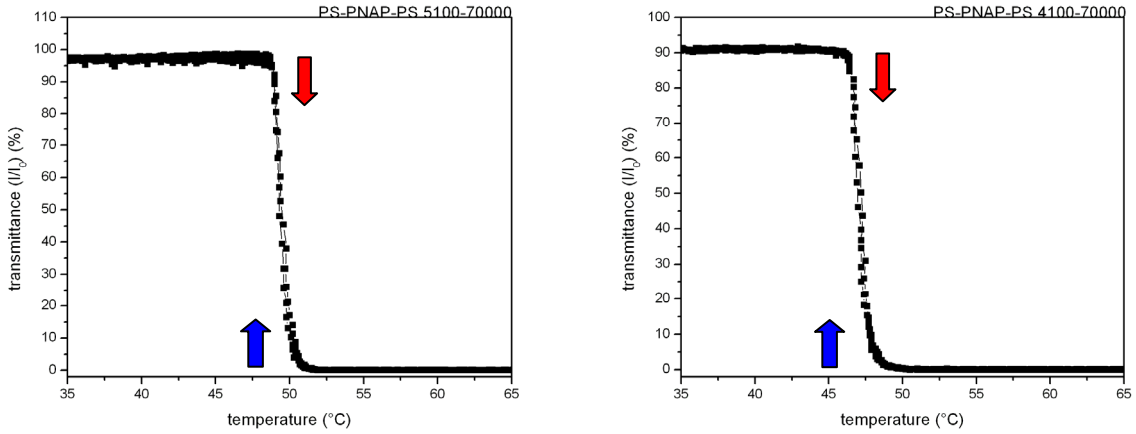

a) b)

Figure 72: Transmission of aqueous solutions of a) **PS-PNAP-PS 5100-70000** and b) **PS-PNAP-PS 4100-70000** as a function of temperature (Cooling/heating rate of 1 °C per minute; concentration 1 g/L). The red arrow represents the heating, the blue arrow the cooling curve.

All investigated transmission curves are fully reversible. Further graphs can be found in the appendix. The graphs measured for the **PS-PNAP-PS** samples (Figure 72) are again of sigmoidal shape similar to the previously displayed **PS-PNI-PS** and **PFS-PNI-PFS** analogs. The cloud point of the samples is around 50 °C; that is markedly higher than for the PNIPAM (**M1** block) containing samples. The transitions are fully reversible, showing almost no hysteresis in the cooling cycle for all PNAP (**M2** block) samples investigated. Like PNIPAM, PNAP can form hydrogen bonds with surrounding water molecules, but the structuring of the surrounding liquid is of course different compared to PNIPAM most probably leading to different effects for the phase separation temperature and turbidimetry measurements due to different destruction of the hydrogen bonds as presumed by Fujimoto et al. [318]. However, in contrast to PNIPAM, PNAP is not able to form self-consistent hydrogen bonds. PNAP represents only a hydrogen bond acceptor, which is unable to form hydrogen bonds among PNAP moieties; only interaction with the surrounding water molecules is possible. Once the PNIPAM block has collapsed, the hydrogen bonds between the PNIPAM moieties preserve the collapsed state delaying the resolving of the polymer whereas the absence of hydrogen bonds between the PNAP moieties enables a much faster rehydration. This most probably accounts for the much weaker hysteresis seen for the **PS-PNAP-PS** series.

12.1.6 Conclusions for turbidimetry measurements

The measured values can be found in table 10. The values found for the cloud point of dilute BAB-triblock copolymer solutions (c= 1 g/L) are all in the range between 30 and 31.5 °C for the PNIPAM (**M1** block) containing systems. The PNAP (**M2** block) containing systems show values between 43 and 49 °C. The polymers consisting of 2,3,4,5,6-pentafluorostyrene (PFS) (**M7**) for the hydrophobic B-block seem to be shifted towards slightly higher values

(around 31 °C) except for some polymers, whereas the non-fluorinated (**M3**) or 3 and 4-fluorostyrene (FS) systems (**M5**, **M6**) show a cloud point around 30 °C. Nevertheless, the cloud point for all polymers ranges withing the intervals described in the literature. Also Bivigou-Koumba reported no significant difference from the literature values [142]. Consequently, the influence of the nature of the hydrophobic block on the cloud point of PNIPAM (**M1** block) seems to be rather small. As all polymers were polymerized applying the same symmetric **CTA XXXX** introducing also $–CF_3$-groups as termini used for end-group analysis, the slight difference in the cloud point could probably be originating from the higher fluorinated B-blocks in case of the 2-,3-,4-,5-,6-pentafluorostyrene (**M7**) containing systems, although the influence is very small.

Furthermore, the BAB-systems composed from PNIPAM (**M1** block) for the hydrophilic A-block all show a more or less marked hysteresis. Especially in case the hydrophobic B-block is relatively long compared to the hydrophilic A-block, a strong hysteresis between heating- and cooling curve can be found. Obviously the system needs some more time for rehydration after the PNIPAM chains collapsing and dehydrating at the cloud point. In contrast, only a small hysteresis is found with the BAB-systems containing PNAP (**M2** block).

In order to find out more details, further intensive studies on this topic are necessary and further series of the BAB-sytems applying even more different thermosensitive monomers would be instructive as also double thermosensitive systems showing no hysteresis are reported by Skrabania et al. [453] and Gong et al. [454]. Especially temperature dependent ^{19}F-NMR- measurements could help to find out about the state of hydration and thus hysteresis behaviour of these BAB-systems in solution at different temperatures [145].

12.2 Studies on the size of BAB-triblock copolymer micelles using the DLS method

Applying the dynamic light scattering technique, the aggregation behaviour of the block copolymers and CF-end capped polymers was studied in solution at different temperatures.

12.2.1 DLS studies of PNIPAM homopolymer solutions

DLS studies of PNIPAM (**M1**) homopolymers were already performed by A. M. Bivigou-Koumba [142]. Below the cloud point of the solution (< 32 °C) small particles showing a size of D_h= 11 nm and a PDI of 0.6 are detected, giving evidence to the existence of single molecule coils in the solution. After increasing the temperature above the cloud point, the hydrodynamic diameter undergoes a marked sudden increase with a D_h shifting to about 300 nm and a PDI of 0.12, leaving the solution turbid. Increasing the temperature further about 60 °C lead to almost no changes of the micellar size. No precipitation of the samples was observed even at higher concentrations.

The marked change of the hydrodynamic diameter when increasing the temperature from RT above the cloud point can be explained by the fact that at temperatures below 32 °C water represents a good solvent for PNIPAM (**M1**) polymers. The polymer adopts a random coil conformation in aqueous solution and interacts preferentially with the surrounding water molecules via hydrogen bonds. After passing the cloud point, the situation becomes opposite and inter- and intramolecular interactions of the PNIPAM (**M1**) homopolymers become

dominant, while the hydrogen bonds get broken. This leads to a collapse of the random coil structure and the formation of colloidal particles of increased hydrodynamic diameter and diversity.

12.2.2 DLS studies of PS-PNI-PS systems (25-55 °C)

The BAB-triblock copolymers of type **PS-PNI-PS** additionally include two hydrophobic poly(styrene) (**M3**) blocks influencing the aggregation behaviour in aqueous solution. In order to learn about the behaviour of BAB-triblock copolymers in water, samples **PS-PNI-PS 3100-50000** and **3100-70000** were studied in detail. The samples should serve as a reference for the block copolymers of different composition. Furthermore, the influence of the small terminal CF_3-groups on the aggregation behaviour should be investigated.

Following the development of the hydrodynamic diameter D_h with increasing temperature, similar trends as described for the **PS-PNI-PS**-polymers by Bivigou-Koumba [142] can be found (figure 73, table 10):

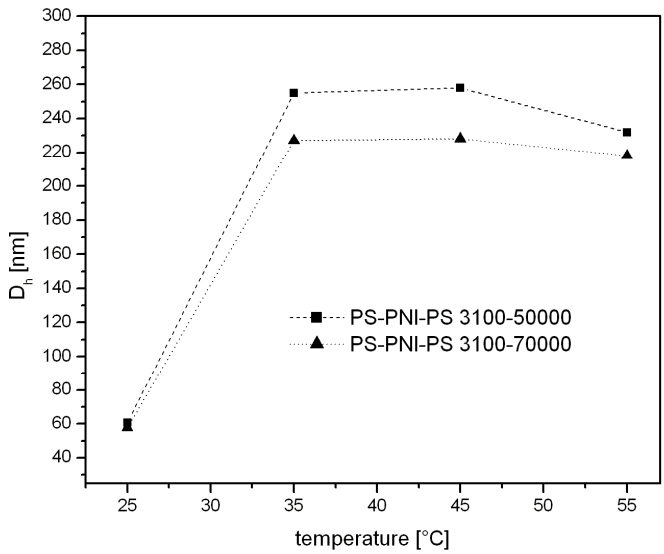

Figure 73: Temperature dependent comparison of the hydrodynamic diameter D_h of aqueous solutions of **PS-PNI-PS** systems **3100-50000** and **3100-70000** at a concentration of 1 g/L.

In figure 73, the hydrodynamic diameter changes dramatically with increasing temperature. The samples show an apparent hydrodynamic size of about 61 and 58 nm below the cloud point with a PDI of 0.23 and 0.72 (25 °C). The size of the aggregates is characteristic for the formation of micelles consisting of a PNIPAM corona and micellar core made from poly(styrene) ("flower-like micelles").

With increasing the temperature above 32 °C, the size is increasing to about 255 and 230 nm with the size distributions becoming narrower indicated by PDI values of 0.18 and 0.07. Possibly, the formed aggregates become denser and more compact leading to a more uniform size distribution. Increasing the temperature further to 55 °C results in micelles of 232 and 218 nm combined with a higher size distribution of 0.68 and 1.00. The higher PDI values

might result from the formation of large aggregates originating from a secondary association of the micelles into large clusters but not from the collapsed PNIPAM corona, as one could presume. In this context, further measurements are necessary to precisely determine the rearrangements in solution. The size of the aggregates formed above the cloud point is smaller compared to the size of pure PNIPAM samples possibly due to the formation of micellar clusters. Clusters of reduced sizes are formed as the immobilization of the hydrophobic blocks seems to hinder further aggregation on a large scale [455, 456]. None of the studied samples showed signs of precipitation, indicating the formation of stable aggregates.

In general, the studied samples display the same behaviour as the **PS-PNI-PS** systems described in the work of Bivigou-Koumba [142]. The CF_3-moiety at the polymers termini is obviously too small compared to the block copolymer segments to show any influence on the polymers aggregation behaviour. The situation might be different for bulkier fluorinated moieties or longer, stiff perfluorinated chains.

12.2.3 DLS studies of PFS-PNI-PFS systems (25-55 °C)

In order to learn about the influence of the hydrophobic block on the micellization behaviour of the BAB-systems, triblock copolymers containing 2-,3-,4-,5-pentafluorostyrene (**M7**) for the hydrophobic B-block were investigated. For this purpose, three different series of **PFS-PNI-PFS** polymers, **PFS-PNI-PFS 60000, 80000** and **100000** were studied in detail.

Following the development of the hydrodynamic diameter D_h with increasing temperature, almost the same trends as already described for the **PS-PNI-PS** systems (vide supra) can be found (figure 74, table 10):

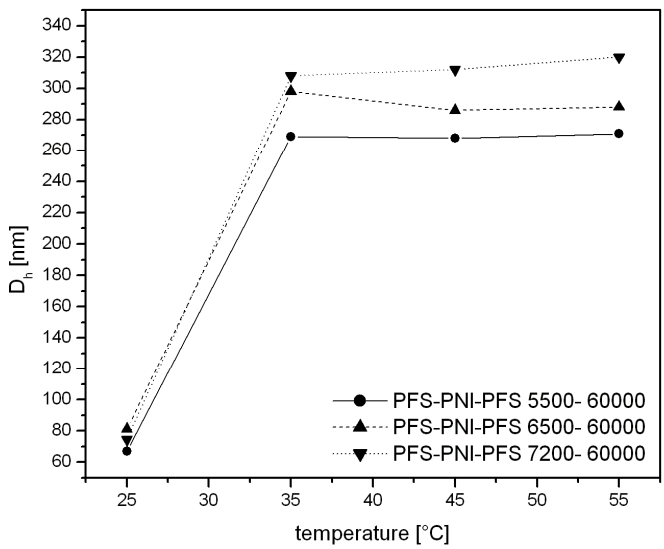

Figure 74: Hydrodynamic diameter of **PFS-PNI-PFS 60000** series at a concentration of 1 g/L.

For the **PFS-PNI-PFS 60000** series (figure 74, table 10), the hydrodynamic diameter changes with both increasing temperature and length of the hydrophobic block. The micelles show a hydrodynamic diameter of about 67, 81 and 74 nm with PDI values of 0.18; 0.2 and 0.18. At

35 °C, above the cloud point, the micellar size increased drastically to 269, 298 nm and 308 nm with PDIs of 0.04 and 0.07 indicating non–aggregated micelles. Further heating seemed to influence only the size of sample **PFS-PNI-PFS 6500-60000** showing a secondary aggregation. At 45 °C, micelles of 286 nm with a PDI of 1.0 are formed, which might give evidence for further aggregation to micellar clusters. Further measurements are necessary to precisely determine the rearrangements in solution.

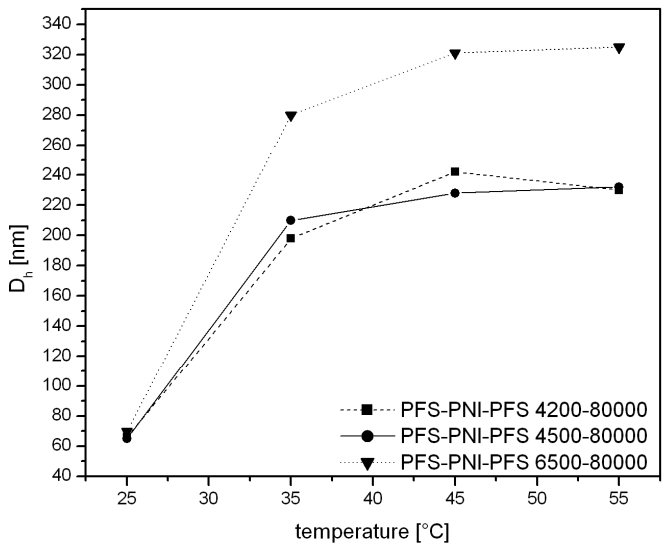

Figure 75: Comparison of the hydrodynamic diameter of **PFS-PNI-PFS 80000** series at a concentration of 1 g/L.

Within the **PFS-PNI-PFS 80000** series (figure 75, table 10), the hydrodynamic diameter changes with both increasing temperature and length of the hydrophobic block as seen before. The micelles show a hydrodynamic diameter of about 66, 65 and 70 nm with PDI values of 0.22 and 0.18. Above the cloud point, at 35 °C, the micellar size increased dramatically as described before to 198, 210 and 280 nm with PDIs of 0.02 and 0.17. Depending on the length of the hydrophilic block, the aggregation behaviour seems to be different and seems to undergo several steps. At 45 °C, well above the cloud point, hydrodynamic diameters of 242, 228 and 321 nm were detected with small PDI values of 0.17, 0.06 and 0.09 indicating still compact micellar aggregates. Here, the micelles do not seem to form large clusters but show secondary rearrangements. At 55 °C, the micellar size remained almost the same with still small PDI values. Also here, further measurements are necessary to precisely determine the rearrangements in solution. Stable micellar aggregates seem to be formed up to elevated temperatures.

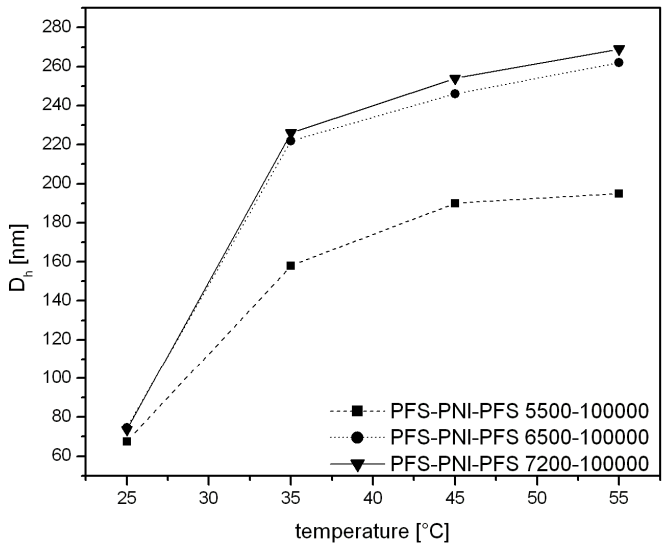

Figure 76: Temperature dependent comparison of the hydrodynamic diameter D_h of aqueous solutions of **PFS-PNI-PFS 100000** series at a concentration of 1 g/L.

Within the **PFS-PNI-PFS** series **100000** (figure 76, table 10), the hydrodynamic diameter is changing again with both increasing temperature and length of the hydrophobic block. Depending on the length of the hydrophilic block, the aggregation behaviour seems to be different from the **PS-PNI-PS** systems and seems to undergo several steps as already described for the **80000** series. At 25 °C, the micelles show a diameter of about 68, 75 and 74 nm with PDIs of 0.19, 0.2 and 0.17. At 35 °C the size enlarged to 158, 222 and 226 nm displaying small PDI values of 0.03 and 0.01 indicating micellar aggregates. Increasing the temperature further to 45 °C, values of 190, 246 and 254 nm with again small PDIs of 0.08, 0.11 still indicating micellar aggregates, were meaured. Also here, the micelles do not seem to form clusters but show secondary rearrangements. Again, further measurements are necessary to precisely determine the rearrangements in solution.

Comparing the **PFS-PNI-PFS 60000, 80000** and **100000** series (figures 74-76, table 10), the size of the aggregates is characteristic for the formation of micelles consisting of a PNIPAM corona and micellar core made from pentafluorostyrene. Increasing the temperature further above the cloud point to 35 °C, the size is increasing drastically for the **60000** series, the **80000** series the **100000** series. The size distributions become narrower indicated by smaller PDI values. The **80000** and **100000** series seem to form stable micellar aggregates instead of clusters up to 55 °C. In this context, further measurements are necessary to precisely determine the rearrangements in solution. Comparing the three different series, the temperature dependent evolution of the hydrodynamic diameter is the same within a series and can be compared to the **PS-PNI-PS** series described before, except the described secondary aggregation shown by the **80000** and **100000** series. The hydrodynamic diameter seems to change with both increasing temperature and length of the hydrophobic block. D_h is increasing with increasing length of the hydrophobic blocks within a series, as can be clearly deduced from figures 74-76. The sizes of micelles created from BAB-polymers with larger B-blocks are huger due to possessing larger cores (PFS 100 > PFS 80 > PFS 60 > PFS 40 > PFS

20). The influence of the length of the PNIPAM (**M1**)–block on the hydrodynamic diameter seems to be less emphasized than the length of the hydrophobic block. Comparing samples **PS-PNI-PS 3100-50000** with **PFS-PNI-PFS 4200-80000** (shortest B-blocks of all synthesized series) and **PS-PNI-PS 5700-70000** with **PFS-PNI-PFS 7200-100000** (largest B-blocks of all synthesized series) shows, that mainly the length of the hydrophobic B-block determines the size of the formed aggregates, whereas the length of the hydrophilic A-block seems to play only a marginal role (figure 77, table 10):

a) b)

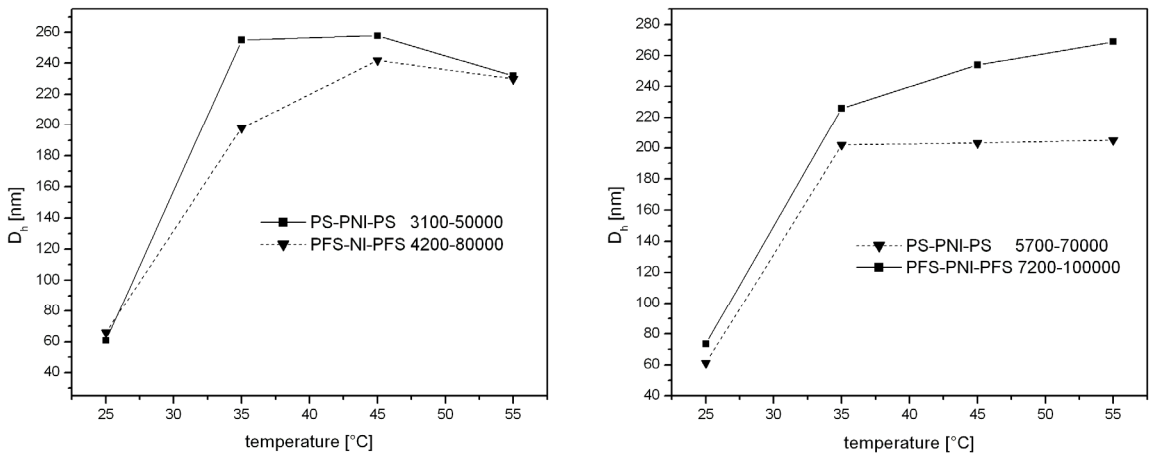

Figure 77: Samples a) **PS-PNI-PS 3100-50000** with **PFS-PNI-PFS 4200-80000** (shortest B-blocks of all synthesized series) compared to b) **PS-PNI-PS 5700-70000** with **PFS-PNI-PFS 7200-100000** (largest B-blocks of all synthesized series) at a concentration of 1 g/L.

With some samples, especially the **PFS-PNI-PFS 80000** and **PFS-PNI-PFS 100000** series, a moderate decrease or increase at temperatures above the cloud point can be detected. This behaviour might originate as already described from further association of the micelles into large clusters and thus structural changes. Also the **PFS-PNI-PFS** type samples showed no signs of precipitation indicating the formation of stable aggregates (figure 78):

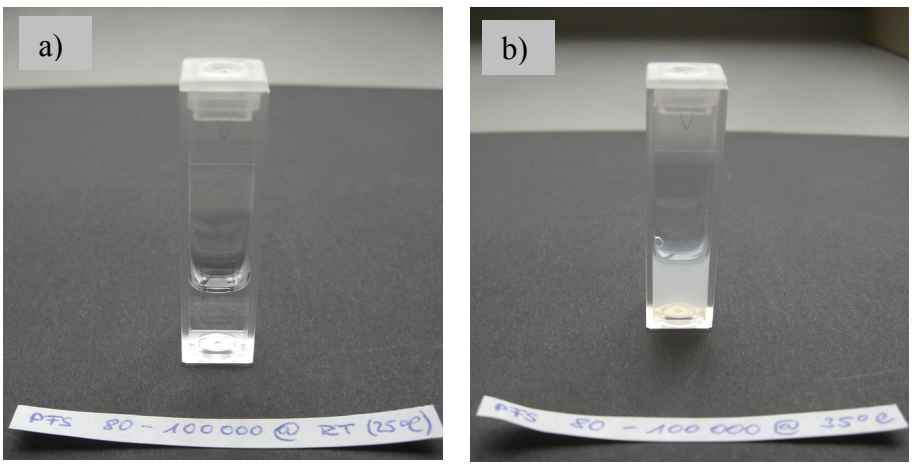

Figure 78: Triblock copolymer solution of **PFS-PNI-PFS 6500-100000** a) before and b) after reaching the cloud point. The absence of precipitation inclines the formation of stable aggregates.

12.2.4 DLS studies of FS-PNI-FS systems (25-55 °C)

In order to obtain further information about the influence of the hydrophobic block on the micellization behaviour of the BAB-systems, a B-block with a polarity different from that of the PS- and PFS-samples became interesting, namely 4-fluorostyrene (**M6**) and 3-fluorostyrene (**M5**) containing samples were investigated in detail.

In order to investigate the behaviour of FS-triblock copolymers in water, **samples 3FS-PNI-3FS 6300-70000** and were **4FS-PNI-4FS 5600-70000** studied in detail.

Recording the development of the hydrodynamic diameter D_h with increasing temperature, similar trends as already described for the **PS-PNI-PS** and **PFS-PNI-PFS** systems can be found.

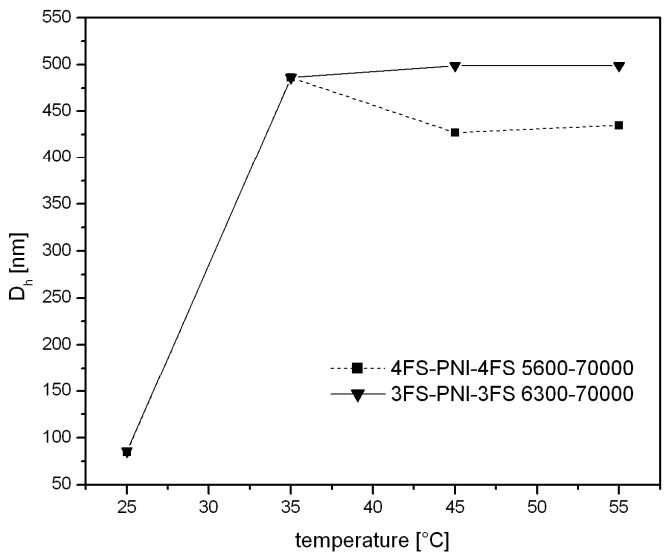

Figure 79: Change of the hydrodynamic diameter D_h of aqueous solutions of **FS-PNI-FS** systems **4FS-PNI-4FS 5600-70000** and **3FS-PNI-3FS 6300-70000** with increasing temperature at a concentration of 1 g/L.

Also for these systems, the hydrodynamic diameter changes with increasing temperature (figure 79, table 10). In case of sample **4FS-PNI-4FS 5600-70000** the micelles seem to undergo secondary aggregation. At room temperature, the samples show an apparent hydrodynamic size of 86 nm with a PDI of 0.2 and 0.22 (25 °C). With increasing the temperature further to 35 °C (above the cloud point), the size is increasing to 486 nm with the size distributions remaining almost the same or slightly higher indicated by PDI values of 0.22 and 0.36. The aggregates seem to be less uniform compared to the systems described before. At 45 °C, the micellar size is changing to 427 and 499 nm, with smaller PDI values 0.15 and 1.00. The **4FS-PNI-4FS 5600-70000** polymer seems to form more compact micellar structures, whereas the 3-FS containing polymer might already form clusters. Further measurements are necessary to precisely determine the rearrangements in solution.

The 4FS (**M6**) containing polymer is forming stable micellar solutions up to 55 °C. Also in case of the FS-systems, no studied sample showed signs of precipitation, proving the formation of stable aggregates.

12.2.5 DLS studies of PS-PNAP-PS systems (45-75 °C)

In contrast to the **PS-PNI-PS** samples, the **PS-PNAP-PS** samples possess a different hydrophilic A-block and were supposed to show similar aggregation behaviour to the PNIPAM containing samples:

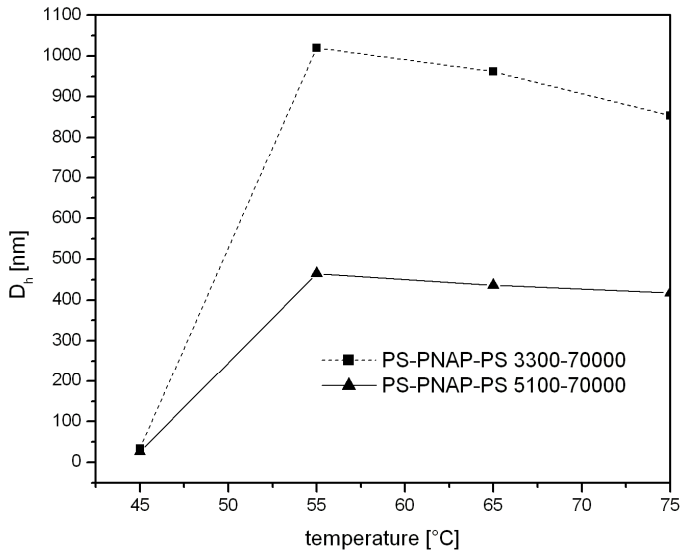

Figure 80: Change of the hydrodynamic diameter D_h of aqueous solutions of **PS-PNAP-PS** systems with increasing temperature at a concentration of 1 g/L.

The hydrodynamic diameter of the **PS-PNAP-PS** samples changes with increasing temperature and length of the hydrophobic block as described for the aforementioned systems (figure 80, table 10). At 45 °C (below the cloud point), the samples show an apparent hydrodynamic size of 33 and 26 nm with a PDI of 0.47 (**5100-70000**) and 0.71 (**3300-7000**), indicating the formation of relatively bulky aggregates. With increasing the temperature further to 55 °C (above the cloud point), the size is increasing even more drastically compared to the systems before to 1020 and 465 nm with PDI values of 0.7 and 0.35. More compact particles seem to be formed for the **3300-70000** sample, whereas the **5100-70000** sample seems to form bulkier aggregates. At 65 °C, the hydrodynamic diameter does not change too much. The **5100-70000** system (PDI 1.0) might form clusters, whereas bulkier, but still small aggregates are formed by **3300-70000** system (0.45). Also for these samples, further measurements are necessary to precisely determine the rearrangements in solution. Unlike the PNIPAM (**M1**) comtaining samples, the PNAP (**M2**)-samples show a tendency towards flocculation, indicating the formation of less stable aggregates.

12.2.6 Conclusions on DLS/turbidimetry

In this chapter, the micellization of BAB-triblock copolymers composed of PNIPAM (**M1** block) or PNAP (**M2** block) for the thermosensitive, hydrophilic A-block and PS (**M3**), PFS (**M7**) and 2-, 3-, 4-FS (**M4, M5, M6**) for the hydrophobic B-block was investigated in detail applying DLS (= dynamic light scattering). All samples are well water soluble due to the relatively short hydrophobic B-blocks compared to the long hydrophilic A-middle blocks.

DLS measurements prove the existence of small micellar aggregates showing hydrodynamic diameters D_h of about 60 nm for the **PS-PNI-PS**, 85 nm for the **FS-PNI-PS**, around 70 to 80 nm for the **PFS-PNI-PFS** and around 30 nm for the **PS-PNAP-PS** systems at room temperature with small polydispersities. The values measured for D_h tend to increase with increasing length of the hydrophobic B-block within a polymer series, independent of its type. The length of the hydrophilic PNIPAM (**M1**)-block on the evolution of the hydrodynamic diameter seems to play a negligible role, but might influence the secondary association behaviour as seen for the **PFS-PNI-PFS 80000** and **100000** series leading to the formation of micellar solutions stable up to elevated temperatures, possibly without cluster formation. In each case, further measurements are necessary to precisely determine the rearrangements in solution.
Despite insoluble in aqueous medium above the cloud point, the PNIPAM (**M1** block) containing BAB-systems did not show signs of precipitation, indicating the formation of stable aggregates. The aggregates formed above the cloud point are relatively large but display a well-defined size in case of small PDI values. As a reason for this behaviour, Winnik et al. [457] suggest kinetic effects and the tethering of both ends of the A-block on the micelles surface preventing the collapsed micelles to from larger clusters ("mesoglobule concept"). The same trends as described for the PNIPAM (**M1** block) could be found for the PNAP (**M2** block) containing samples, except that their stability against precipitation seems to be lower.

12.3 DLS studies on the stability of BAB-systems against dilution at room temperature

A well known feature about polymeric micelles is their stability against dilution [458, 459, 460]. As all investigated aqueous solutions prepared from fluorinated and non-fluorinated BAB-triblock copolymers revealed the existence of micelles, their stability against dilution was studied. The polymer solutions were stepwise diluted from 10 to 0.1 g/L from a stock solution and the micellar size compared after each dilution step applying DLS. For comparison, micellar solutions of a commercially available non-fluorinated low molecular weight surfactant, in this case Triton® X 100 and a fluorinated low molecular weight surfactant, Zonyl® FSH 300, as well as solutions of SDS, sodium dodecyl sulphate, a classical, ionic low molecular weight surfactant, were studied. Micellar solutions of Pluronic® 6400 were chosen for comparison with a polymer surfactant system.

12.3.1 DLS studies on selected BAB-systems

For preparation of solutions and DLS measurements, the protocol described in the experimental section was followed.

a) b)

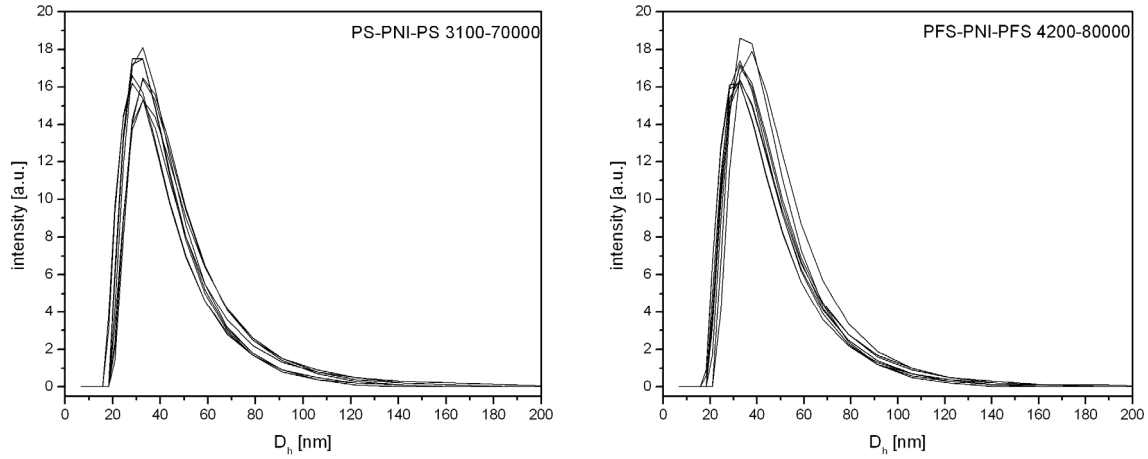

Figure 81: DLS studies of diluted aqueous solutions of a) **PS-PNI-PS 3100-70000** and b) **PFS-PNI-PFS 4200-80000**. The solutions described were stepwise diluted from 10- to 0.1 g/L.

Figure 81 exemplifies the results of the dilution experiments. The aggregates in all investigated solutions of the BAB-triblocks were stable against dilution revealing almost the same hydrodynamic diameter after each dilution step as monitored by DLS measurements (vide supra, graphs almost congruent). Further examples of **PFS-PNI-PFS**, **FS-PNI-FS** and **PS-PNAP-PS**-triblock copolymers showing the same stability against dilution can be found in the appendix.

12.3.2 DLS studies on commercially available surfactants

a) b)

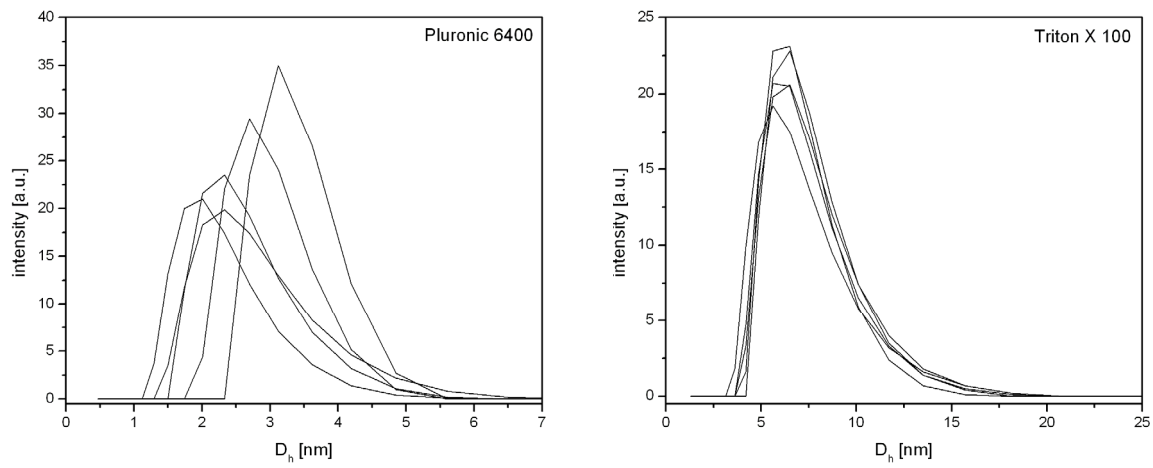

Figure 82: DLS studies of diluted aqueous solutions of a) Pluronic® 6400 and b) Triton® X 100 at concentrations from 10-1 g/L. The DLS study of Zonyl® FSH 300 can be found in the appendix.

Micellar solutions of commercially available surfactants such as SDS, Triton® X 100, Pluronic® 6400 and Zonyl® FSH 300 were also studied following the same protocol used for the BAB-systems. As expected, the low molecular weight surfactant SDS [145] is not stable against dilution as well as the studied Zonyl® fluorosurfactant and polymer surfactant Pluronic® 6400 (10-1 g/L), figure 82). Triton® X 100 proved to be the only sample of low molecular weight surfactants stable against dilution at concentrations above 1 g/L (10-1 g/L, figure 82, congruent graphs). At concentrations below 1 g/L, the micelles were no longer stable.

12.3.3 Conclusions on dilution studies

DLS measurements proved the stability of all BAB-block copolymer solutions against dilution revealing almost the same hydrodynamic diameter (congruent graphs) for the micelles after each dilution step. Some solutions were diluted to 0.01 g/L, with the micelles still showing stability against dilution.
Micelles of Triton® X 100 proved to be partially stable only at concentrations above 1 g/L (10-1 g/L), whereas Zonyl® FSH 300, Pluronic® 6400 and SDS as a low molecular weight surfactant, were not stable against dilution. The good stability of the polymeric micelles against dilution indicates very low CMCs ($< 1 \cdot 10^{-5}$ mN/m) if the polymers show a CMC at all, in agreement with the reports on diblock copolymers published by Garnier [69, 112].

12.4 SEM measurements (Scanning Electron Microscopy)

In order to find out about the structure of the micellar aggregates, SEM measurements (**S**canning **E**lectron **M**icroscopy) were performed.

The SEM works in reflection mode, applying an electron beam with an energy of 1 keV–20 keV which is focused on the probe surface to a size of about 1 nm–10 nm [461]. Spatial information can be gained by scanning the focus on the sample by scanning or deflection coil put in the optics of the microscope. Depending on the chosen detector, inelastically backscattered electrons, X-rays, Auger electrons, or true secondary electrons can be detected. The measurement conditions can be found in the experimental section.

The image (figure 83) revealed the existence of globular structures as described by ten Brinke et al. [462]. This result is in well agreement with the results gained from DLS measurements predicting globular structures.

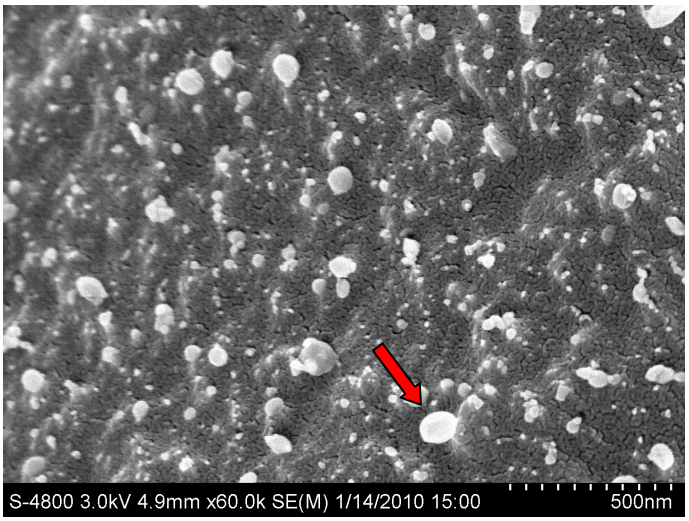

Figure 83: SEM-image of dried **PS-PNI-PS 5700-70000** micellar solutions. The globular shape of the particles is clearly visible. The sphere with radius R_B forms the inner core containing only B-monomers whereas the shell with size R_A is called the corona and contains A-blocks as described by ten Brinke et al. [462].

12.5 Mixed aggregation

Micellar solutions including mixed micelles composed of a fluorinated surfactant and a hydrocarbon-type surfactant are able to exceed the surface activity for an ideal solution in which the components do not interact [145]. The synergism observed in solutions of mixed surfactants of different types is governed by the interaction in micelles and monomer-micelle equilibra [145]; interactions between surfactant monomers are insignificant. The composition

of mixed micelles can be studied applying different methods, among them NMR-measurements, surface tension measurements, fluorescence quenching measurements and many more [145]. Observations made mixing hydrocarbon- and fluorocarbon-type micelles proved complete nonmixing of the surfactants, partial mixing and the existence of two types of mixed micelles or one single type of mixed micelle [145].

12.5.1 Mixing different micellar solutions: studying the size and shape of mixed micelles

In this experiment, the influence of mixing amphiphilic BAB-block copolymers of different block length for the hydrophobic styrene (**M3**), substituted styrenes (**M4, M5, M6, M7**) and hydrophilic PNIPAM (**M1**) or PNAP (**M2**) segments on size and shape of the flower-like micelles was investigated. The mixed systems were studied time dependent using DLS.
Experimental details on the mixing procedure can be found in the experimental section. The occurrence of newly formed mixed micelles was studied by comparing the hydrodynamic

diameters of parent and mixed solutions. If mixed micelles are formed, a new trace originating from the mixed system, often but not necessarily localized between the traces from the parent surfactants, will appear (figures 84-87). Mixing surfactants of different block lengths and thus hydrodynamic diameter D_h should lead to mixed micelles of different sizes due to changing the packing parameters of the parent systems [36, 120].

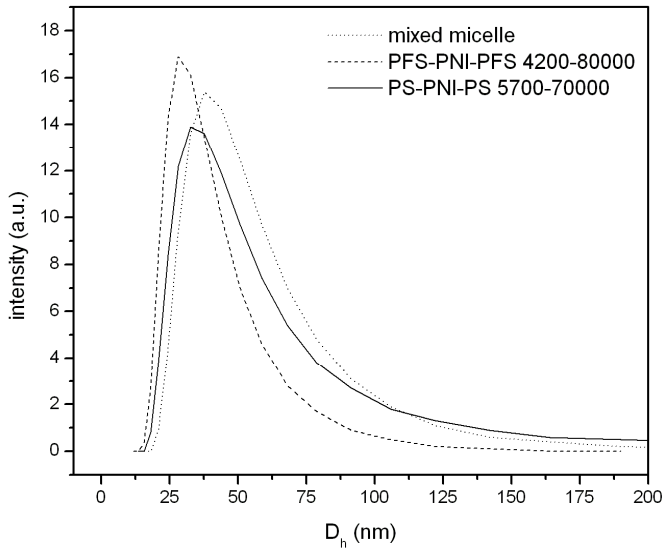

Figure 84: Comparison of DLS traces of **PS-PNI-PS 5700-70000** with **PFS-PNI-PFS 4200-80000** in aqueous solution (both 1 g/L) and mixture of both polymers (v:v/1:1).

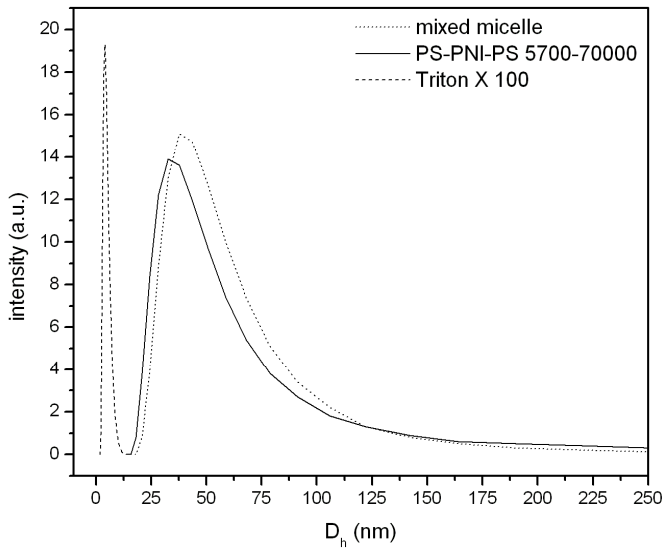

Figure 85: Comparison of DLS traces of **PS-PNI-PS 5700-70000** with **Triton® X 100** in aqueous solution (both 1 g/L) and a mixture of both polymers (v:v/1:1).

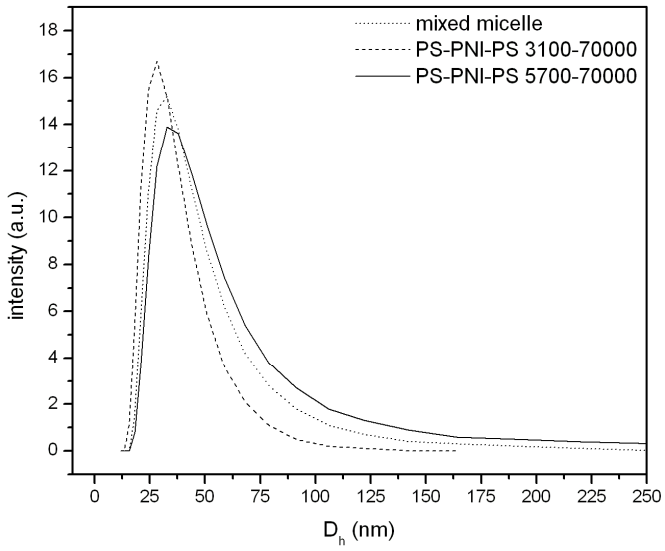

Figure 86: Comparison of DLS traces of **PS-PNI-PS 3100-70000** with **PS-PNI-PS 5700-70000** in aqueous solution (both 1 g/L) and a mixture of both polymers (v:v/1:1).

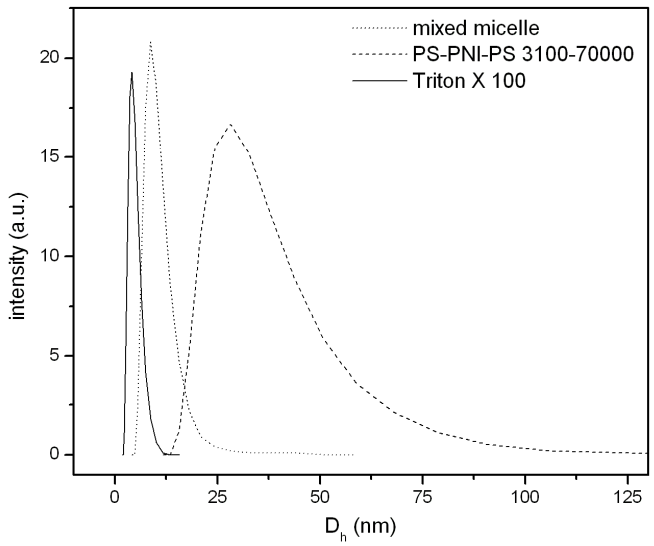

Figure 87: Comparison of DLS traces of **PS-PNI-PS 3100-70000** with **Triton® X 100** in aqueous solution (both 1 g/L) and a mixture of both polymers (v:v/1:1).

The measurements were repeated within distinct intervals (directly after preparation, after 3 days, after 7 days) in order to determine changes in the micellar size. Normally the size of these micelles should not vary due to the poly(styrene)- and poly(pentafluorostyrene) blocks

showing a high T_g (styrene (**M3**) 373 °C, pentafluorostyrene (**M7**) 378 °C) leading to the formation of micelles (figure 88) with a glassy core, the frozen micelles. Table 2 gives an overview over the prepared mixed micelles and their size after 0, 3 and 7 days.

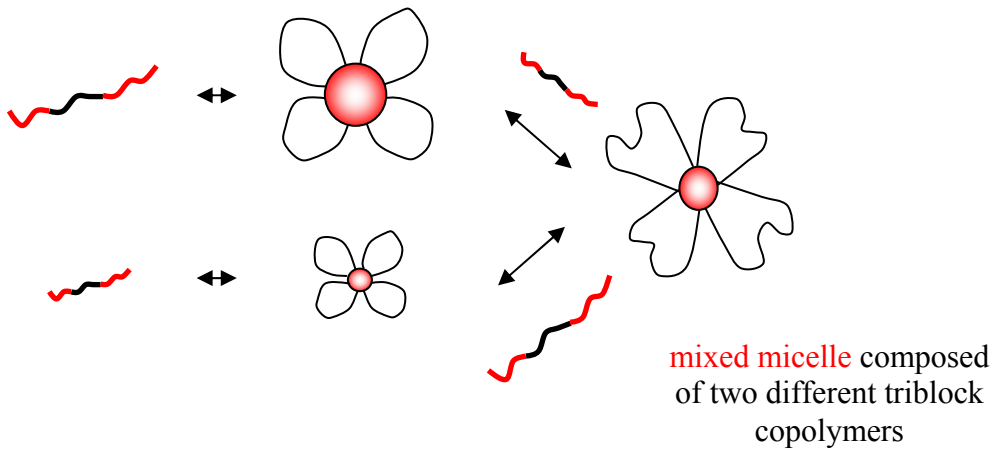

Figure 88: Flower-like micelles: possible influence on shape and size of mixing. Scheme adapted from Garnier [69].

Table 2: Evolution of mixed micellar systems as followed by DLS directly, 2 and 7 days of storage at room temperature (25 °C) after mixing:

triblock copolymers BAB	D_h [nm] [(a)] before mixing	D_h [nm] directly after mixing	D_h [nm] 3 days after mixing	D_h [nm] 7 days after mixing
PS-PNI-PS 3100-70000 + PS-PNI-PS 5700-70000	52 (100) 82 (100)	78 (100)	83 (100)	84 (100)
PS-PNI-PS 3100-70000 + PS-PNI-PS 3100-50000	52 (100) 58 (100)	55 (100)	54 (100)	57 (100)
PS-PNI-PS 3100-70000 + PFS-PNI-PFS 4200-80000	52 (100) 64,0 (100)	89 (100)	83 (100)	82 (100)
PS-PNI-PS 3100-70000 + PFS-PNI-PFS 6500-80000	52 (100) 64 (100)	77 (100)	84 (100)	77 (100)
PS-PNI-PS 3100-50000 + PFS-PNI-PFS 4200-80000	58 (100) 64 (100)	61 (100)	60 (100)	59 (100)

PS-PNI-PS 3100-50000 + PFS-PNI-PFS 6500-80000	58 (100) 64 (100)	56 (100)	63 (100)	61 (100)
PS-PNI-PS 5700-70000 + PFS-PNI-PFS 4200-80000	61 (100) 64 (100)	86 (100)	82 (100)	82 (100)
PS-PNI-PS 5700-70000 + PFS-PNI-PFS 6500-80000	61 (100) 64 (100)	77 (100)	78 (100)	80 (100)
PS-PNI-PS 3100-70000 + 4FS-PNI-4FS 5600-70000	52 (100) 84 (100)	83 (100)	84 (100)	79 (100)
PS-PNI-PS 3100-50000 + 4FS-PNI-4FS 5600-70000	58 (100) 84 (100)	75 (100)	80 (100)	86 (100)
PS-PNI-PS 5700-70000 + 4FS-PNI-4FS 5600-70000	61 (100) 84 (100)	92 (100)	89 (100)	89 (100)
PS-PNI-PS 3100-50000 + PS-PNAP-PS 3300-50000	58 (100) 33 (100)	44 (66.2) 424 (32.2)	142 (48.7) 31 (42.6)	42.0 (64) 429 (30.5)
PFS-PNI-PFS 4200-80000 + PS-PNAP-PS 3300-50000	64 (100) 33 (100)	46 (63.7) 495 (34.7)	41 (59.2) 412 (38.4)	47 (61.4) 507 (36.0)
PFS-PNI-PFS 6500-80000 + PS-PNAP-PS 3300-50000	64 (100) 33 (100)	51 (69.1) 623 (30.9)	47 (66.6) 325 (30.6)	50 (66.4) 595 (32.1)
PS-PNI-PS 3100-50000 + PS-PNAP-PS 4100-50000	58 (100) 33 (100)	45 (68.3) 352 (30.4)	44 (68,5) 400 (27.7)	45 (69) 669 (31.0)
PFS-PNI-PFS 4200-80000 + PS-PNAP-PS 4100-50000	64 (100) 33 (100)	44 (57.3) 223 (40.5)	53 (75.1) 747 (24.9)	49 (68.7) 590 (30.0)

PFS-PNI-PFS **6500-80000** + **PS-PNAP-PS** **4100-50000**	64 (100) 33.0 (100)	52 (77,5) 426 (18.2)	49 (73,9) 441 (22.8)	50 (71,2) 703 (28.8)
triblock copolymers BAB + low molar weight surfactant	D_h [nm] before mixing	D_h [nm] directly after mixing	D_h [nm] 3 days after mixing	D_h [nm] 7 days after mixing
PS-PNI-PS **3100-70000** + **Triton® X-100**	52 (100) 8 (100)	13 (48.9) 426 (41.6)	245 (55.5) 11.5 (44.5)	389 (53.8) 13 (46.2)
PS-PNI-PS **3100-50000** + **Triton® X-100**	58 (100) 8 (100)	16 (74) 238 (26)	13 (50) 257 (48)	506 (59) 15 (39)
PS-PNI-PS **5700-70000** + **Triton® X-100**	61 (100) 8 (100)	85 (100)	63 (98.7) 4670 (1.3)	41 (91.2) 4200 (8.8)
PS-PNAP-PS **3300-50000** + **PA-PNAP-PS** **4100-50000**	33 (100) 33 (100)	439 (51.0) 32 (46.8)	438 (49.7) 33 (48.3)	470 (53.4) 33 (44.8)

Table 2: Hydrodynamic diameter of mixed micelles directly after mixing, 2, 3 and 7 days of storage at room temperature (25 °C) after mixing. (100) in brackets means: 100 % by volume of aggregates with average hydrodynamic diameter D_h of X nm.

During the period of seven days no significant changes (> 10 nm) in the hydrodynamic size of the micelles could be detected except for the Triton® X 100 containing samples, which seem to be instable. This shows that a stable situation is reached within a reasonable time (i.e., within three days) and that the mixed aggregates do not grow into vesicles or bigger morphologies, as it has been often reported for other hybrid micellar systems [4]. This result is not surprising, for all the micelles are composed of blocks made of either styrene (**M3**), 4-fluorostyrene (**M6**) or pentafluorostyrene (**M7**) for the outer hydrophobic B-blocks showing a high T_g (see also chapter aggregation and rheology) and leading to the formation of micelles with a frozen core. These micelles show a reduced mobility of their unimers forming these aggregates at room temperature thus enabling only small structural changes. In order to find out about possible variations in the micellar size, long term measurements (after about 2 months, 6 months) would be necessary. Furthermore, in some cases the DLS system is not able to distinguish exactly between the distributions (see figures 84, 86). In this case, using additional fluorescence quenching measurements might be useful to determine the size of the mixed aggregates.

12.5.2 Conclusions on mixed aggregation

When mixing the various BAB-systems made within a series and among each other, no incompatibilities between different BAB-systems could be detected. Non-fluorinated (**M3**-blocks) BAB-systems are fully miscible among each other as well as fluorinated (**M5, M6, M7**)-BAB-systems. Additionally, the fluorinated BAB-systems can be mixed with non-fluorinated BAB polymers without obvious restrictions. Problems described for mixing hydrocarbon with fluorocarbon-type surfactants originating from their incompatibility could not be found [82]. Furthermore, the investigated mixtures of different BAB-systems formed mixed micelles of distinguishable hydrodynamic diameters (see table 2) and reasonable PDI values. Mixing BAB-systems of similar length of the hydrophobic B-block led to minimal changes in the hydrodynamic diameter compared to that of the larger parent system, whereas mixing with a larger B-block lead to an increase of the hydrodynamic diameter. The same is valid for mixing fluorinated and non-fluorinated systems.

The addition of the non-ionic surfactant Triton® X 100 led to different results. Whereas the **PS-PNI-PS** and **PFS-PNI-PFS** samples composed of short hydrophobic blocks (~ 3000 g/mol) do not interact with the surfactant, the samples composed of larger hydrophobic blocks (~ 5000 g/mol) are able to form mixed micelles of low molar mass polymeric polymeric surfactant. However, these micelles show no long-term stability. Surprisingly, the length of the hydrophilic A (**M1** or **M2**)-block showed no influence on the mixing behaviour. Looking at the hydrodynamic diameters (D_h) of the mixed solutions, small particle sizes of about 11 nm and a PDI of 0.6 could be detected for the systems containing the short hydrophobic blocks reflecting the size of single molecule coils, so-called unimers. Thus, no micelles are formed, which means that the two surfactants are not miscible. For the BAB-systems composed of the longer PS (**M3**)- or PFS (**M7**)-blocks, mixed micelles including Triton® X 100 surfactant molecules seem to have formed, but show only limited stability. The immiscibility might originate from unfavourable interactions between the short hydrophobic B-blocks. Further investigations are necessary to study the problem.

12.6 Rheology

12.6.1 Outline for rheology measurements of BAB-block copolymer samples

The investigation of all samples was done due to the following experimental outline:

1) Visual tests applying the TIM (tube inversion method)

2) Testing the dependence of the viscosity on the shear rate

3) Testing the dependence of the viscosity, usually as G` (gain modulus) and G`` (loss modulus) on the shear stress

⇨ Following points 1)-3) enabled the determination of the experimental data required for more detailed investigations on the samples

4) Oscillation frequency and temperature dependent investigations on G` and G``

⇨ From the ratio G`/G`` and the specific development of the parameters depending on the temperature, the sol-gel behaviour was analyzed

12.6.2 Rheology measurements applying PS-PNI-PS block copolymers

First, the system **PS-PNIPAM-PS**, which is found in the literature, was investigated as a model system. Furthermore, possible effects of the fluorinated end groups should be studied. Then, the PS blocks (**M3** blocks) in the triblock copolymers should be changed against different fluorinated blocks and the effects further investigated.

After first qualitative gelation tests on selected samples of concentrated polymer solutions (40 and 50 wt%) in tubes applying the tube inversion method (TIM) [463] were successful, the samples were subjected to rheology studies.

In the literature, the gelation behaviour in aqueous solution of only few BAB-systems were previously studied, most of them are commercially available Pluronic® systems, PPO-PEO-PPO [464, 465] or PBO-PEO-PBO systems [466, 467]. Despite these commercially available systems, Zhao et al. [468] studied the behaviour of HEMAn-NIPAAmm-HEMAn and NIPAAmm-HEMAn-NIPAAmm triblock copolymers, Kirkland et al. [469] investigated BAB-systems of type PNIPAM-DMA-PNIPAM. A great series of different BAB-systems varying in the nature and length of both blocks was recently studied in our group by A. M. Bivigou-Koumba [156].

Therefore, aqueous solutions of 20-, 30-, 40-, and 50 wt% were prepared from the BAB-triblock copolymers as described in the experimental section. A cone-plate system was chosen for measurement. Liquid samples were placed under the cone plate using a syringe, the solid ones were placed onto the Peltier-plate using a spatula. A lid was used for limiting evaporation falsifying the results due to loss of humidity during the measurement.

-Shear rate sweep measurements

First, the block copolymer solutions were studied at room temperature (25 °C) in order to get information about their general flow-behaviour.

The **PS-PNI-PS** samples of 10 wt% showed liquid like behaviour in the TIM measurements. They were difficult to measure applying the cone-plate system, for the solutions were too thin to be further investigated applying this geometry. For more detailed investigations on these systems, using the cylinder-type geometry could be favourable [470]. In order to find out about possible bridging between micelles, DLS measurements were performed using selected samples. Since no aggregation structures implying bridging between micelles could be detected, the samples can not be referred to as gels and behave like liquids. Oscillation- and frequency stress measurements were not performed with the 10 wt% samples.

Then, the flow-behaviour of the 20- and 30 wt% solutions was investigated.

In TIM experiments the **PS-PNI-PS** samples of 20 wt% samples showed liquid like behaviour but with a slightly higher viscosity compared to the 10 wt% samples. Alike the 10 wt% samples, also the 20 wt% samples were difficult to measure using the cone-plate system (figure 89). Also here, light scattering implied no bridging between the micelles. Thus it can be deduced, that also the 20 wt% samples still show liquid like behaviour.

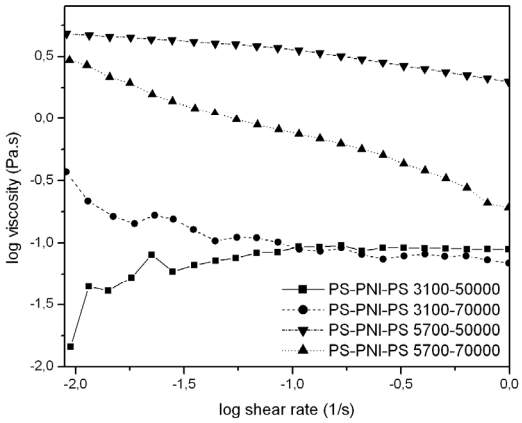

Figure 89: The viscosity depicted as a function of the shear rate of **PS-PNI-PS** samples of 20 wt% at room temperature (25 °C). The results were difficult to reproduce especially within the areas of low shear rates (left side of the graphs). All measurements for the 20 wt% samples show liquid like behaviour.

The 30 wt% measurements (figure 90) were reproducable. TIM-tests of the samples already revealed a markedly higher viscosity of the 30 wt% probes compared to the 20- and 10 wt% samples.

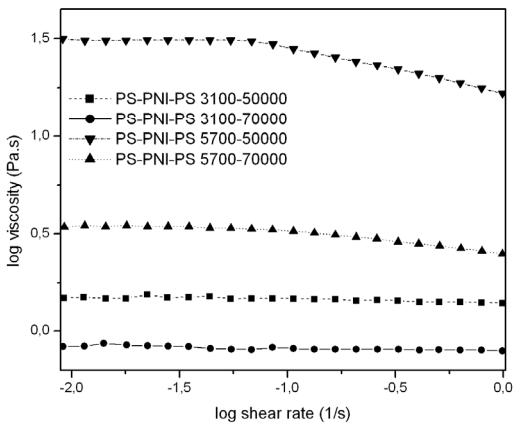

Figure 90: The viscosity of the 30 wt% samples of the **PS-PNI-PS** samples depicted as a function of the shear rate at room temperature (25 °C).

All measurements of the 30 wt% probes could be reproduced with only negligible differences. At shear rates below -1,25 1/s, all copolymers show almost constant viscosity behaving as

Newtonian liquids. At higher shear rates, the samples` behaviour leaves the Newtonian regime. Shear thinning is observed. Shear thinning often occurs due to flow orientation of particles or conformational changes of polymer molecules in dilute solution [143, 35]. When the shear rate is larger than the rate of thermal reorientation of the molecules, the molecules will align in direction of the flow, which may explain the observations in this series. Shear thinning in concentrated solution (here 40- and 50 wt%) can be found when the shear rate is larger than the rate needed to build-up the equilibrium supra-particulate structures [143, 35].

The systems viscosity seems to depend on the length of the hydrophobic block increasing with its length. Also the shear thinning effect seems to increase with the length of the hydrophobic block. It may be attributed to local restructuring and destroyment of the preliminary micellar structures and/or entanglements between the micelles. Bivigou-Koumba [142] asumed, that the disruption of the flower-like micelles might initially induce a slight increase in the share of bridged micelles leading a small dilatant maximum before the associative network structure is gradually breaking down with increasing shear deformation. Within this series, no dilatant maximum supporting this thesis could be found. As already mentioned above, the viscosity seems to depend on the length of the hydrophobic B (**M3**)-block but the type of hydrophobic block most probably plays a key role.

In the following experiment, dynamic oscillation stress measurements were performed in order to find the viscoelastic regime of the samples over which the storage modulus G` is independent of the stress. Figure 91 indicates a viscoelastic region for a stress smaller than 10 Pa.

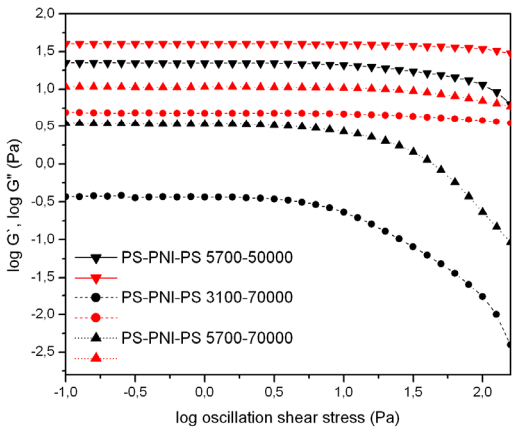

Figure 91: Oscillation shear stress dependence of the storage modulus G` and the loss modulus G`` of 30 wt% hydrogels of the **PS-PNI-PS** samples measured at 1 Hz. The loss modulus G`` is depicted in red; the storage modulus G` in black.

All following experiments were conducted at an oscillating shear stress of 1 Pa (30-, 40-, 50 wt% samples) to stay within this region.

-Oscillation frequency sweep measurements

In the following experiment, the frequency dependence of the dynamic moduli of the block copolymers was checked.

The transitions from sol to gel or vice versa were studied in the viscoelastic region of the block copolymer at an oscillating shear stress of 1 Pa (figure 92). The concentration of the investigated solutions is increasing from left to right.

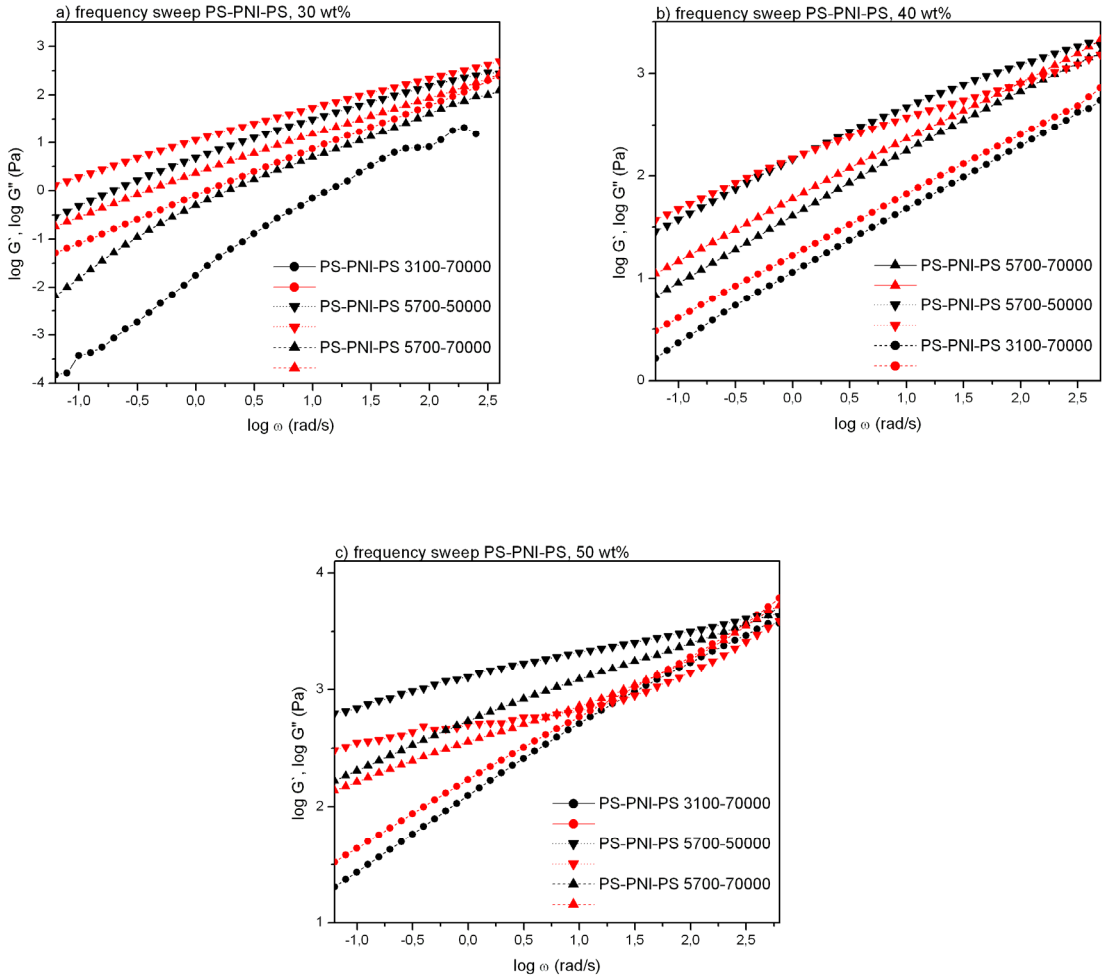

Figure 92: Frequency dependence of the dynamic moduli of aqueous micellar solutions made from **PS-PNI-PS** BAB-triblock copolymers on the concentration (30-, 40- and 50 wt%) measured at an oscillatory stress of 1 Pa at 25 °C. The loss modulus G`` is depicted in red, the storage modulus in black, a) 30 wt%, b) 40 wt%, c) 50 wt%.

Pure PNIPAM solutions of 50 wt% G` and G`` are almost parallel over the frequency window studied with G`` larger than G` at 25 °C [156]. This behaviour represents a viscous liquid. The frequency dependent measurements of the BAB-triblock copolymers of type **PS-PNI-PS** show a different behaviour compared to the pure PNIPAM samples.

Figure 92 presents the frequency dependence of the dynamic moduli for the **PS-PNI-PS** series **PS-PNI-PS 70000** and **50000**. The graphs show a general increase of the storage and the loss moduli with the concentration, especially for the storage modulus G`. At a concentration of 30 wt% both moduli are similar in size but G` is less dependent on the frequency compared to G``. At low frequencies G` is somewhat smaller than G``, but slightly higher at high frequencies indicating the substances are behaving as soft gels. With further increasing the concentration to 40- or 50 wt %, the storage modulus is in all investigated cases larger than the loss modulus indicating the samples to behave as hard gels, except for **PS-PNI-PS 3100-70000**.

As already mentioned, increasing length of the hydrophobic blocks for a certain block copolymer concentration leads to a general increase of G` compared to G`` producing harder gels.

Similar polymers differing in the nature of the end groups of the RAFT-agent chosen for polymerization (-O-CH_3 instead of –CF_3) were studied by A. M. Bivigou-Koumba [156]. Comparing the results, no significant difference in the rheology behaviour of the triblock copolymers is found, implying that the fluorinated end groups do not significantly influence the gel-formation of this polymer type. This result is not surprising, as the CF_3-groups are attached to much larger hydrophobic groups at both polymer termini which form the glassy micellar cores [471-475].

-Temperature dependent measurements of PS-PNI-PS-block copolymers investigating sol-gel and gel-sol transitions applying a temperature sweep measurements

Temperature sweep measurements reveal changes in the rheology properties of materials-here block copolymer gels -upon heating and cooling- over a moderate temperature interval. A temperature range from 15 to 45 °C was chosen for investigation of the hydrogels.

The temperature dependent change of the samples from liquid towards soft gel and finally hard gel with increasing concentration can also be followed by the change of the dynamic moduli with temperature (figure 93).

At temperatures below the cloud point, storage and loss modulus decrease steadily with temperature (figure 93). When increasing the temperature close to the cloud point, the **PS-PNI-PS** block copolymers show an abrupt change in their mechanical properties in the linear viscoelastic region independent of the sample concentration. Both storage- and loss modulus, G' and G'', display first a decay near the transition temperature of about 31 °C (see also turbiditiy measurements) coming close to each other at the cloud point, followed by a tremendous increase after the switching step. The height of the transition step depends on the concentration of the samples and diminishes with increasing polymer concentration from 20- to 50 wt% due to a change of the free volume of the sample. The hysteresis between heating and cooling curve increases with the concentration decreasing due to the tendency of the system to show macroscopic phase separation.

System **PS-PNI-PS 5700-70000**

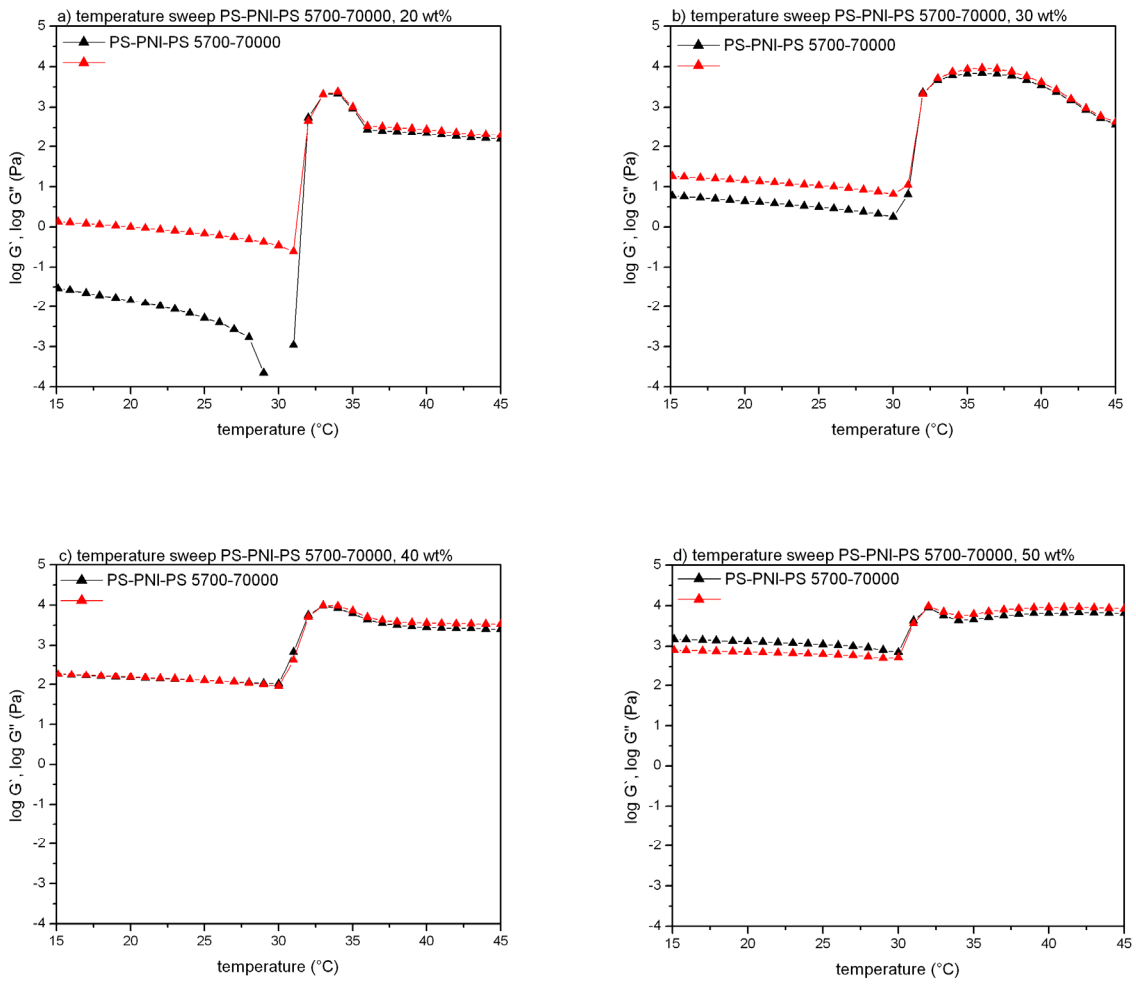

Figure 93: Temperature dependent dynamic moduli G` (red) and G`` (black) at different concentrations of sample **PS-PNI-PS 5700-70000**, a) 20 wt%, b) 30 wt%, c) 40 wt%, d) 50 wt%. The loss modulus G`` is depicted in red, the storage modulus G` in black.

As already described, the height of the transition step in figure 93 is obviously much smaller for the concentrated samples compared to the diluted ones displaying an escalating increase of the moduli G` and G``. The transition point represents the order-disorder transition of the sample T_{ODT} which is represented by the cloud point of about 31 °C in this case [476-478]. Furthermore, the point is characterized by a dramatic change of the modulus as reported by Matsuda et al. [476]. Optical observations of the samples above the cloud point show- depending on the concentration -either dull solutions (10-, 20-, 30 wt%)- or solutions, in which the collapsing polymer seems to have squeezed out the water turning the former gel into a two phase system consisting of an aqueous phase and collapsed polymer phase (40 wt% and 50 wt%).

Investigating the 30 wt% samples, both moduli G` and G`` run parallel for samples a) and b). The loss modulus G`` is larger than the storage modulus G` which is typical for liquid-like behaviour. Increasing the concentration further to 40 wt% leads to an approach of both moduli indicating the system is coming close to soft gel behaviour. At a concentration of 50 wt % the samples behave like hard gels with the storage modulus G' being much higher than the loss modulus G''. The system can also be shifted towards gel formation by increasing the length of the hydrophobic blocks. In addition to the length of the hydrophobic blocks, also their nature influences the gel formation behaviour.

12.6.3 Rheology measurements applying PFS-PNI-PFS block copolymers

In this series of experiments, the effect of replacing the poly(styrene) blocks (**M3** blocks) by the more hydrophobic poly(pentafluorostyrene) blocks (**M7-**blocks) on the rheology behaviour and gel formation behaviour of the BAB-systems was investigated. Different series of this block copolymer type varying in the size of both the hydrophobic and hydrophilic segments were measured and compared.

As found out by DLS studies and visual tests, also in this case solutions of 10 wt% are freely flowing solutions. No aggregates could be detected by DLS. The viscosity of the 10 wt% solutions was too low for applying the cone-plate geometry. The samples could be measured again using a cylindrical geometry. Also the 20 wt% samples were difficult to measure using the cone-plate geometry for measurement, leading to results which were difficult to reproduce, especially within the area of low shear rates. Light scattering implied no bridging between the micelles; therefore the 20 wt% samples behave also like flowing liquids.

-Shear rate sweep measurements

As a model series, first the block copolymers composed of a PNIPAM middle block (**M1** block) of **80000** g/mol were investigated having PFS (**M7**) end-blocks of ~ 4000-7000 g/mol (GPC). The block copolymer solutions were studied at room temperature (25°C) to get information about their flow- behaviour. Figure 94 shows the apparent viscosity as a function of the shear rate of 20-, 30-, 40- and 50 wt% solutions. All measurements could be reproduced with only negligible differences. As already mentioned above, the 20 wt% samples were again difficult to measure using the cone-plate geometry for measurement, leading to non-reproducible results within the areas of low shear rates as well as the 30 wt % measurements in the area of low shear rates.

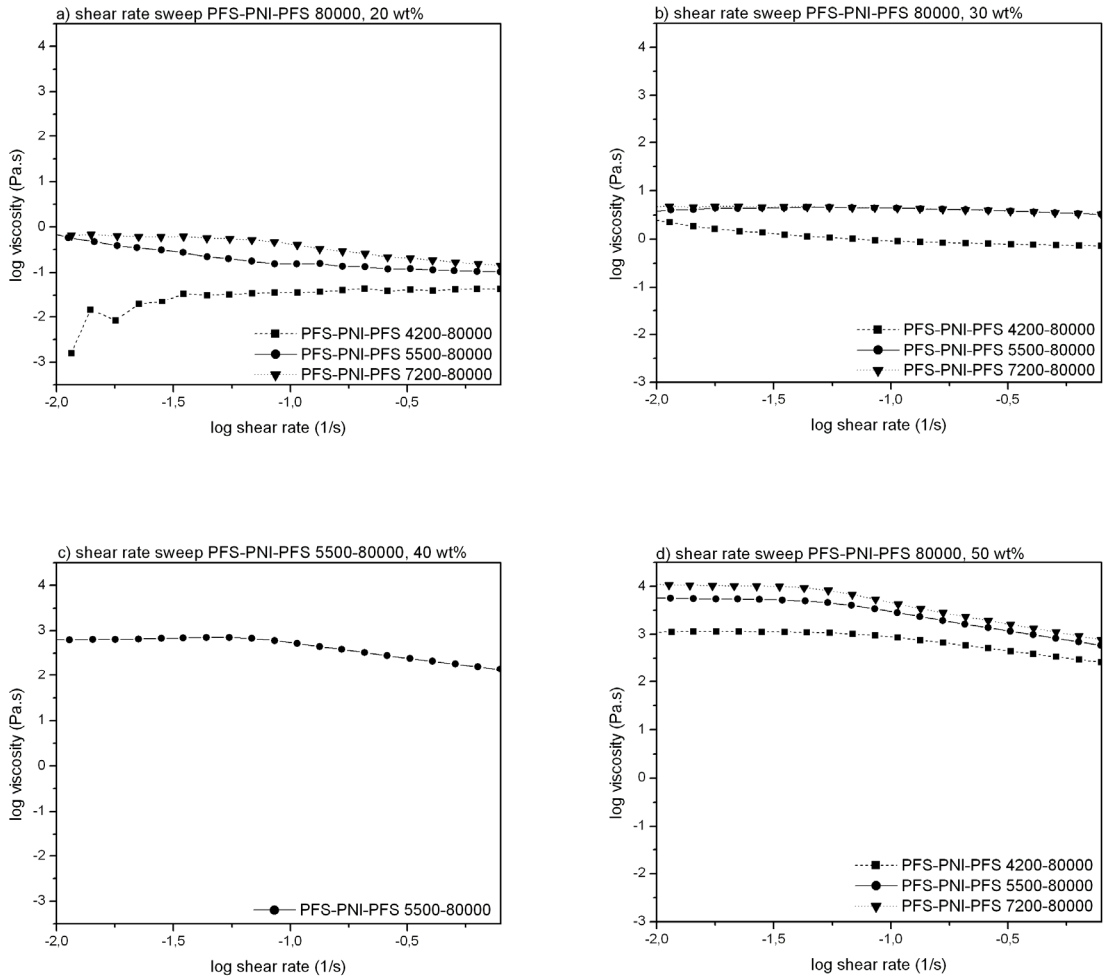

Figure 94: Development of the Newtonian behaviour of aqueous solutions for the 20- and 30 wt% samples to soft gel and gel like structures of the 40- and 50 wt% samples of the **PFS-PNI-PFS 80000** series (**PFS-PNI-PFS 4200-, 5500-** and **7200-80000**) showing a typical plateau region before shear thinning. The concentration of the investigated solutions is increasing from a)-d).

The shear rate measurements for the **80000** series (figure 94) indicate the formation of soft gels at a concentration of about 40 wt%. At higher concentrations, hard gels showing a prounounced plateau region are formed.

Then, the block copolymers composed of a PNIPAM (**M1**) middle block of **60000** g/mol were investigated (figure 95). The sizes of the hydrophobic PFS-blocks were the same as described for the **80000** series.

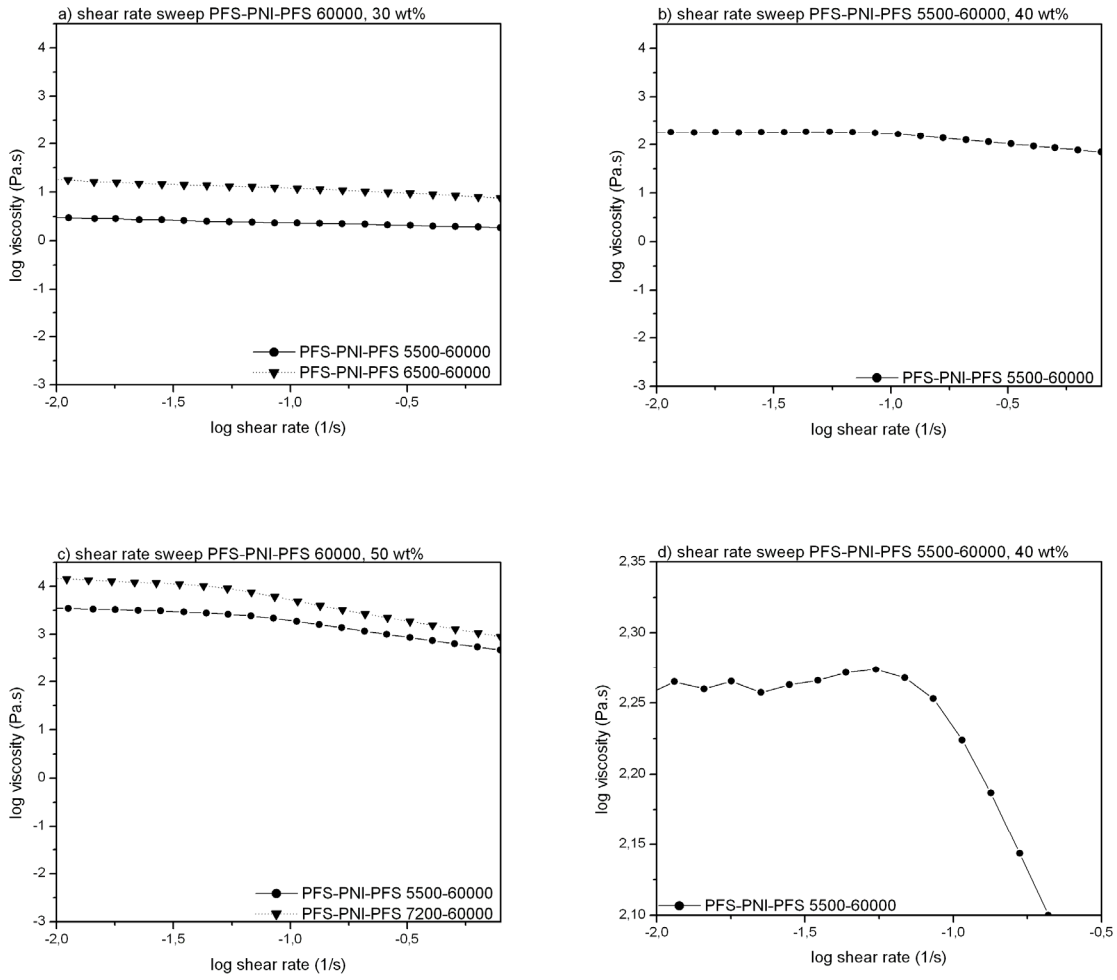

Figure 95: Development of the Newtonian behaviour of aqueous solutions for the a) 30 wt% samples to soft gel and gel like structures and of the b) 40- and c) 50 wt% samples of the **PFS-PNI-PFS 60000** series showing a typical plateau region before shear thinning, but less prounounced as for the **80000** series. For the **60000**-series a small dilatant maximum can be seen for the 40 wt% samples d).

Within this series (figure 95), the 40 wt% samples display a small dilatant maximum d) as described by Bivigou-Koumba [142], but not with the 50 wt% samples.
The shear rate measurements for the **60000** series indicates the formation of soft gels at a concentration of about 40 wt%, whereas at higher concentrations, hard gels showing a prounounced plateau-region are formed similar to the **80000** series.

Furthermore, the block copolymers composed of a PNIPAM middle block (**M1**-block) of **100000** g/mol were investigated. The sizes of the hydrophobic PFS (**M7**)-blocks were the same as described for the **80000** series.

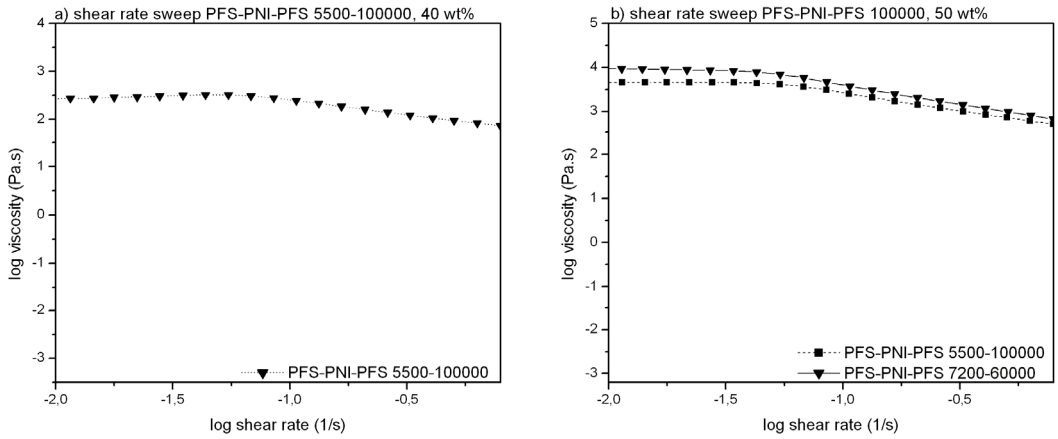

Figure 96: Development of the Newtonian behaviour of aqueous solutions of the **PFS-PNI-PFS 100000** series, examples PFS-PNI-PFS **5500-100000** and **7200-100000**. The concentration of the investigated solutions is increasing from a) 40 wt% to b) 50 wt%.

For the **100000** series (figure 96), the 40- and 50 wt% solutions show a typical plateau region before shear thinning as for the **80000** series. The 20- and 30 wt% solutions are again liquids (not shown). The 40 wt% samples display a small dilatant maximum whereas the 50 wt% samples show no dilatant maximum at all. The shear rate measurements for the **100000** series show the same trend as already described for the **60000** and **80000** series.

-Oscillation frequency sweep measurements

Next, dynamic oscillation stress measurements were performed in order to find the viscoelastic regime of the samples over which the storage modulus G` is independent of the stress. The **60000** row was studied as a model series at 1 Hz. Figure 97 displays a viscoelastic region for a stress smaller than 10 Pa.

Figure 97-1): Concentration dependent dynamic oscillation stress measurements of the **PFS-PNI-PFS 60000 (PFS-PNI-PFS 5500-60000** and **6500-60000**) series in order to find the viscoelastic regime of the samples, a) 30- and b) 40 wt% samples. The loss modulus G` is coloured red, the storage modulus G`` black.

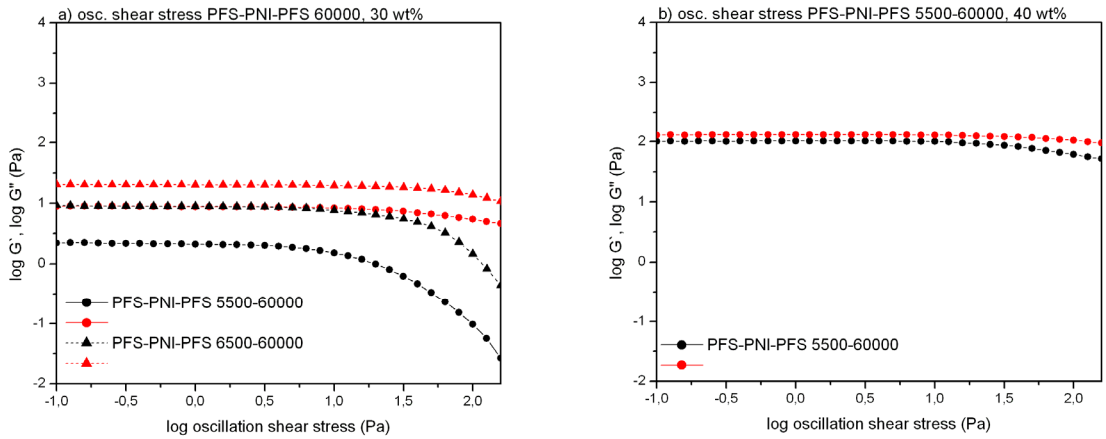

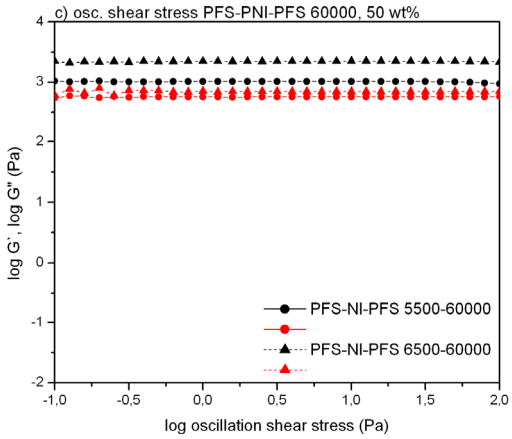

Figure 97-2): Concentration dependent dynamic oscillation stress measurements of the **PFS-PNI-PFS 60000 (PFS-PNI-PFS 5500-60000** and **6500-60000**) series in order to find the viscoelastic regime of the samples, c) 50 wt% sample. The loss modulus G` is coloured red, the storage modulus G`` black.

Investigation of sol-gel and gel-sol transitions applying frequency sweep measurements

The transitions from sol to gel or vice versa were studied in the viscoelastic region of the block copolymer at an oscillating shear stress of 1 Pa (figure 98).

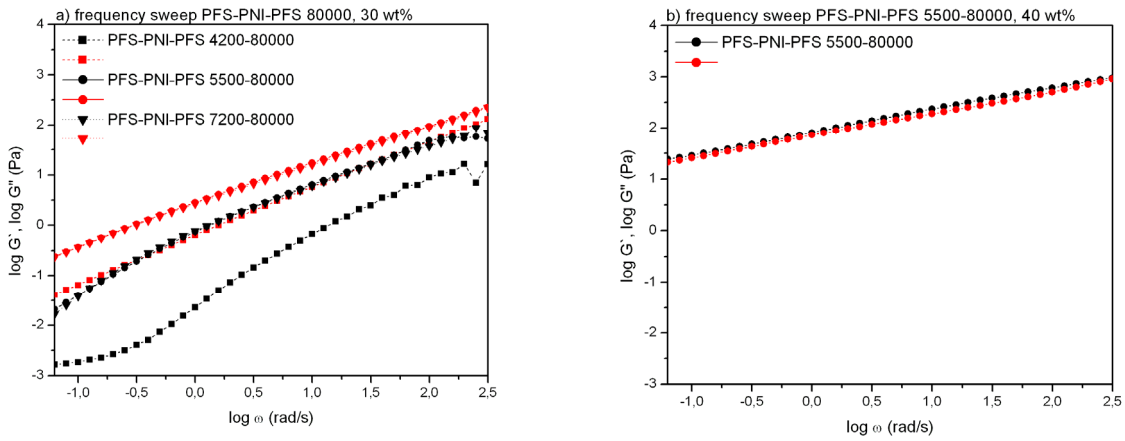

Figure 98-1): Dependence of the frequency of the dynamic moduli of aqueous micellar solutions of different concentrations a) 30- and b) 40 wt% made from **PFS-PNI-PFS triblock copolymer** of the **80000** series (**PFS-PNI-PFS 4200-, 5500-** and **7200-80000**) measured at an oscillatory stress of 1 Pa at 25 ° C. The loss modulus G`` is depicted in red, the storage modulus G` in black.

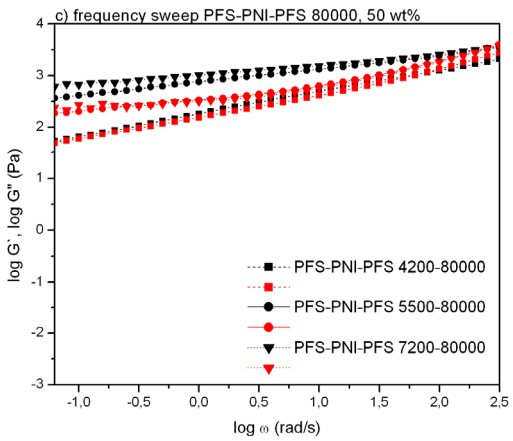

Figure 98-2): Dependence of the frequency of the dynamic moduli of aqueous micellar solutions of c) 50 wt%) made from **PFS-PNI-PFS triblock copolymer** of the **80000** series (**PFS-PNI-PFS 4200-, 5500-** and **7200-80000**) measured at an oscillatory stress of 1 Pa at 25 °C. The loss modulus G`` is depicted in red, the storage modulus G` in black.

In general, the same tendencies as described before for the **PS-PNI-PS** systems can be found, despite the introduction of the more hydrophobic pentafluorostyrene segments (**M7**-blocks) for the B-block of the BAB-triblock copolymer systems (figure 98).

At a concentration of 30 wt% both moduli are similar in size but G` is less dependent on the frequency compared to G``. At low frequencies G` is a little bit smaller than G`` but slightly higher at high frequencies indicating the substances are behaving like soft gels. With further increasing of the concentration to 40- or 50 wt%, the storage modulus is in all investigated cases larger than the loss modulus indicating the samples to behave like hard gels. As already mentioned, increasing length of the hydrophobic blocks for a certain block copolymer concentration leads to a general increase of G` compared to G`` indicating the formation of hard gels.

-Temperature dependent measurements of PFS-PNI-PFS–block copolymers investigating sol-gel and gel-sol transitions applying a temperature sweep measurements

In this experiment, a temperature range from 15- to 45 °C was chosen (figure 99):

Temperature sweep measurement for **PFS-PNI-PFS 5500-60000**

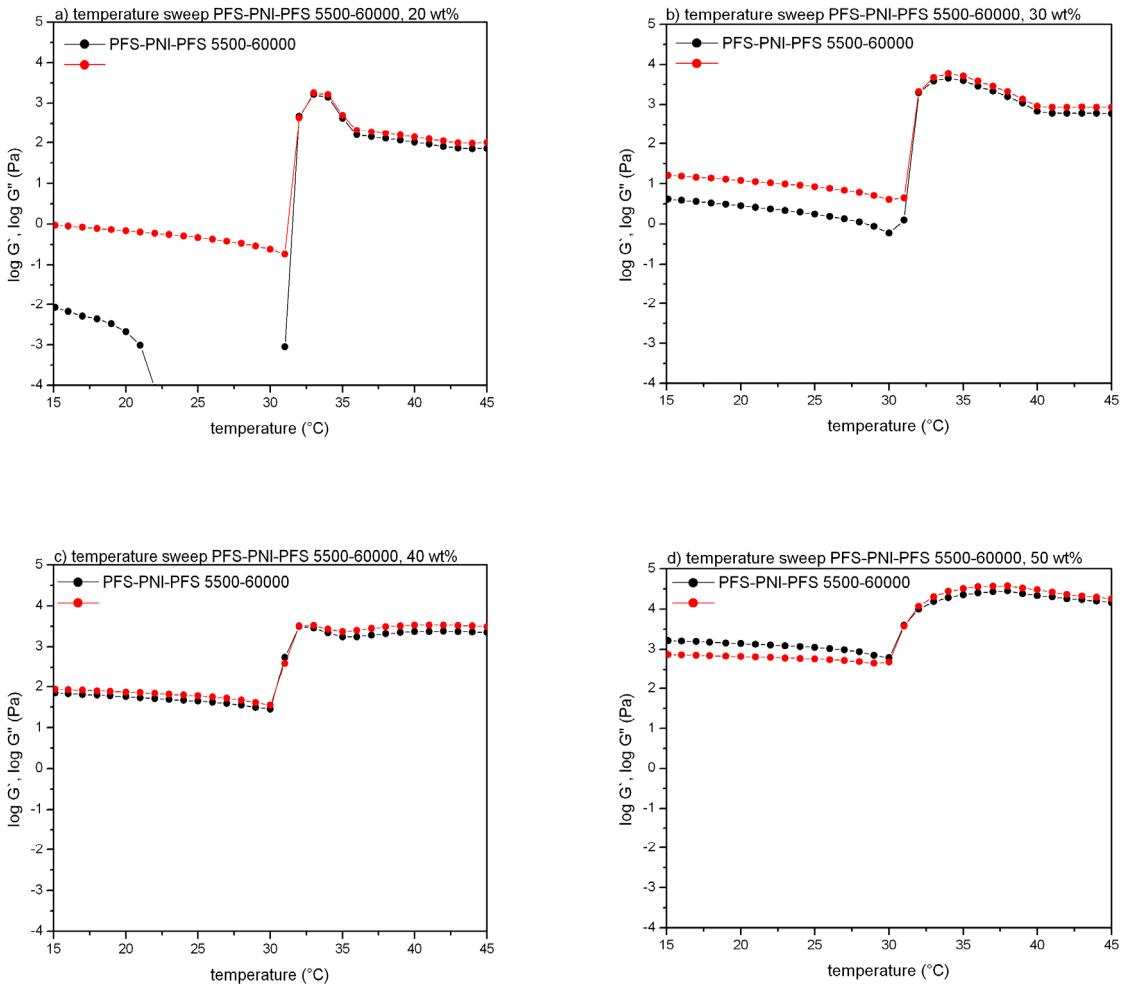

Figure 99: Temperature dependent change of the dynamic moduli G` (red) and G`` (black) at different concentrations a) 20-, b) 30-, c) 40- and d) 50 wt%) of sample **PFS-PNI-PFS 5500-60000**. The loss modulus G`` is depicted in red, the storage modulus G` in black.

As described for the **PS-PNI-PS** systems, the height of the transition step is obviously much smaller for the concentrated samples compared to the diluted ones displaying an escalating increase of the moduli G` and G``(figure 99). The transition point represents the order-disorder transition of the sample T_{ODT} which is represented by the cloud point of about 31 °C also in this case. Optical observations of the samples above the cloud point show -depending on the concentration- either dull solutions (10-, 20-, 30 wt%) or solutions, in which the collapsing polymer samples seem to have squeezed out the water turning the former gel into a two phase system consisting of an aqueous phase and collapsed polymer phase (40 wt% and 50 wt%).

12.6.4 Rheology measurements applying FS-PNI-FS block copolymers

In this experiment, the influence of introducing a block with different polarity compared to that of pentafluorostyrene (**M7**) and pure styrene (**M3**) to the BAB-systems and the influence on their rheology behaviour should be investigated. The performed TIM measurements were indicating gel-like behaviour only for the 40- and 50 wt% samples. As found out with DLS studies, no aggregates could be detected in the 10- and 20 wt% solutions as described for the **PS-PNI-PS** and **PFS-PNI-PFS** samples.

-Shear rate sweep-measurements

The block copolymer solutions were measured at room temperature (25 °C) studying their flow- behaviour first as already described for the BAB-systems measured before. Figure 100 shows the apparent viscosity as a function of the shear rate. All measurements of 30-, 40- and 50 wt% could be reproduced with only negligible differences.

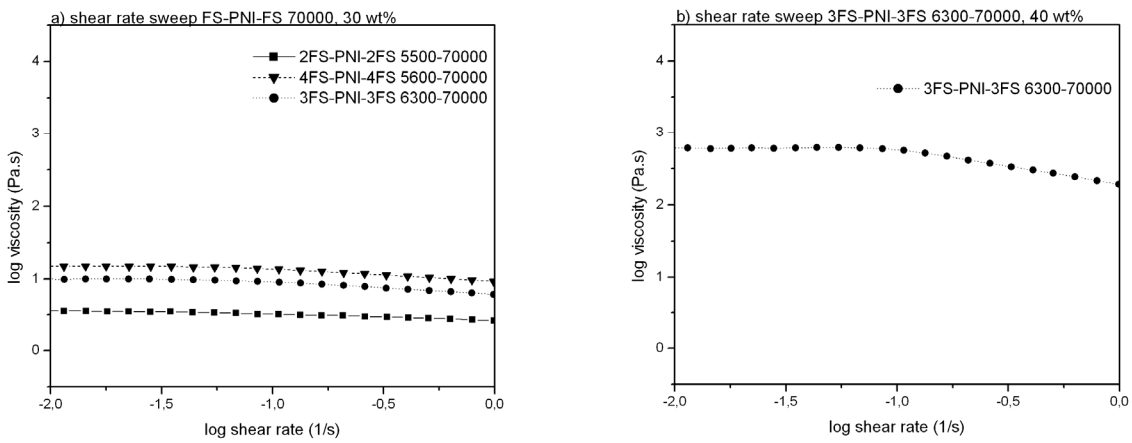

Figure 100-1): Shear rate sweep-measurement of **FS-PNI-FS 70000** series, investigating a) 30-, b) 40 wt% samples. The concentration of the investigated solutions is increasing from left to right.

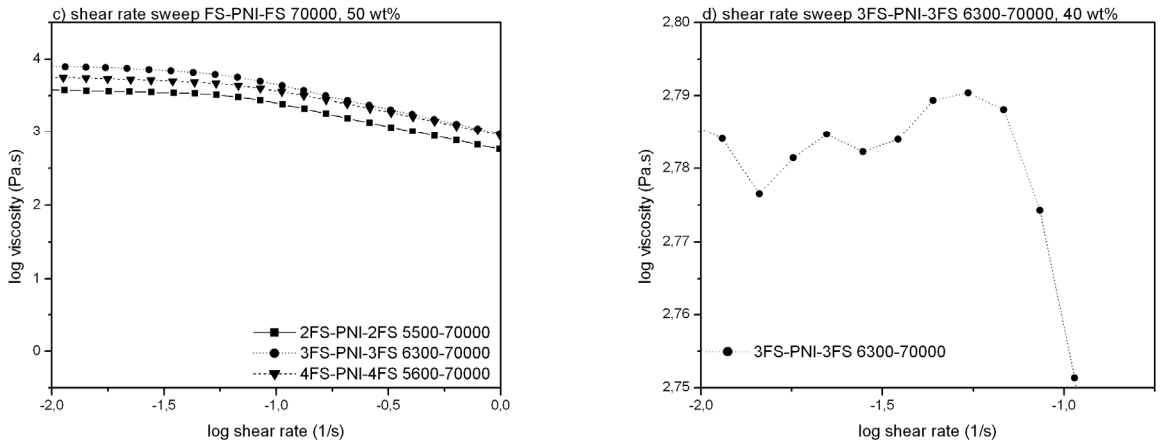

Figure 100-2): Shear rate sweep-measurement of **FS-PNI-FS 70000** series, investigating c) 50 wt% samples. Picture d) shows the small dilatant maximum of the 40 wt% series.

Comparing the graphs from figure 100 a) and b) to those of the **PS-PNI-PS** and **PFS-PNI-PS** samples, no remarkable difference in the behaviour could be found.

-Oscillation frequency sweep measurements

The transitions from sol to gel or vice versa were studied in the viscoelastic region of the block copolymers as described for the **PS-PNI-PS** and **PFS-PNI-PFS** systems before (figure 101).

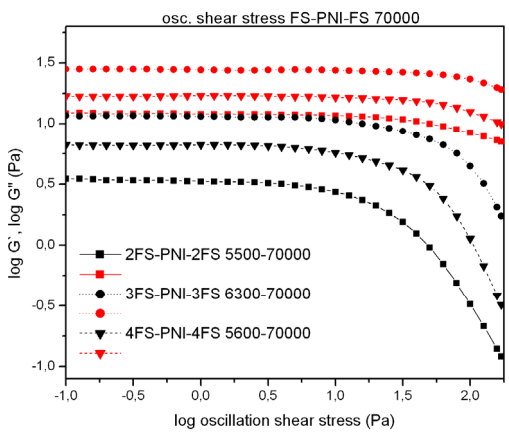

Figure 101: Oscillation shear stress measurements investigating series **FS-PNI-FS 70000** (30 wt% samples) at 1 Hz. The loss modulus G` is depicted in red, the storage modulus G`` in black.

- Frequency sweep measurements for FS-PNI-FS systems

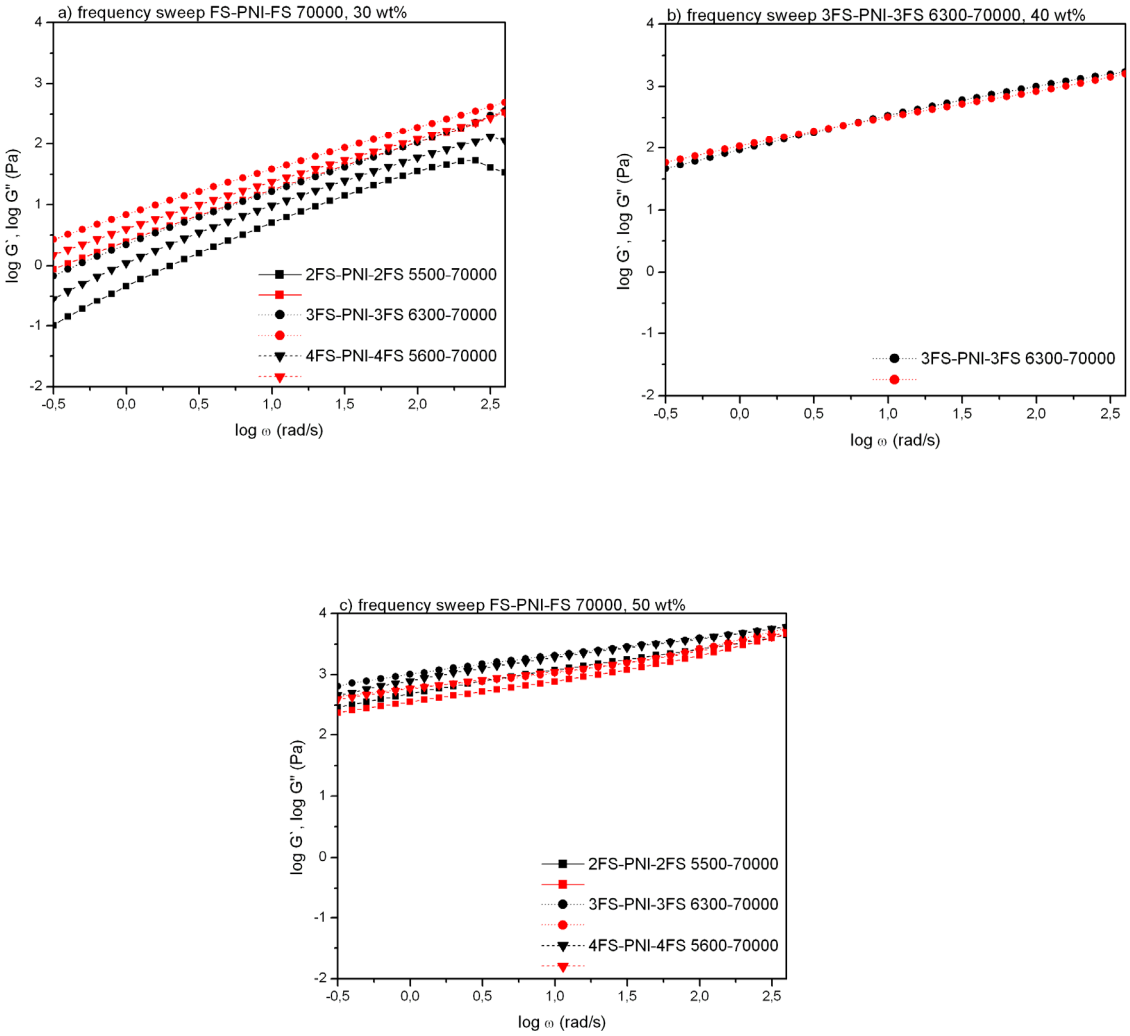

Figure 102: Frequency sweep measurements at 1 Pa for **FS-PNI-FS** systems at a) 30-, b) 40- and c) 50 wt%. The loss modulus G` is depicted in red, the storage modulus G`` in black.

The frequency sweep measurements (figure 102) showed the same tendency as for the BAB-systems reported before. The transition from a Newtonian fluid to a gel can be found around 40 wt%. At 50 wt% the **FS-PNI-FS** block copolymers are hard gels, represented by the storage modulus G` being larger than the loss modulus G''.

-Temperature dependent measurements of FS-PNI-FS–block copolymers investigating sol-gel and gel-sol transitions applying a temperature sweep measurements

Temperature sweep measurements (15-45 °C) were performed again to demonstrate the change from liquid to gel behaviour (figure 103):

Temperature sweep for **3FS-PNI-3FS 6300-70000**

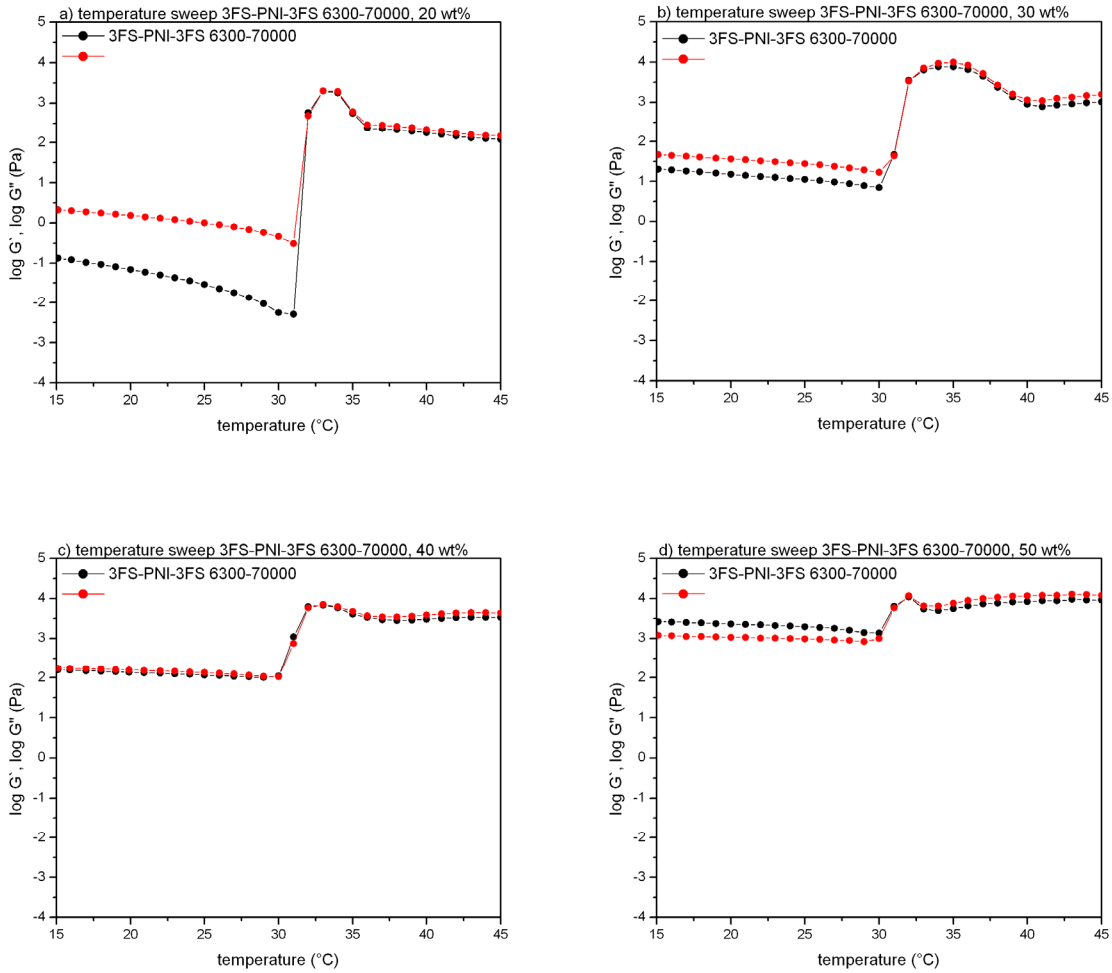

Figure 103: Temperature sweep measurements of sample **3FS-PNI-3FS 6300-70000** at concentrations of a) 20-, b) 30-, c) 40- and d) 50 wt%. The loss modulus G` is depicted in red, the storage modulus G`` in black.

Also for the temperature sweep measurements (figure 103), similar results as for the **PS-PNI-PS** and **PFS-PNI-PFS** samples can be found.

12.6.5 Rheology measurements applying PS-PNAP-PS block copolymers

The **PS-PNAP-PS** systems are different from the hydrogels studied before due to changing the PNIPAM middle block (A-block, **M1**) by a PNAP block (**M2** block). The differences between the two hydrophilic polymers have already been discussed. Now, the possible influence of changing the hydrophilic block on the rheology behaviour should be further investigated.

TIM experiments revealed liquid like behaviour for the 20 wt% samples, whereas the 50 wt% samples behaved like gels. Additionally performed DLS studies showed, that solutions of 10- and 20 wt% are freely flowing solutions as reported for the **PS-PNI-PS**, **PFS-PNI-PFS** and **FS-PNI-FS** systems before. No aggregates could be detected by DLS. Measurements applying solutions of 10 wt% were tried but as described before lead to results which are difficult to reproduce in rheology measurements.

-Shear rate sweep-measurement

As before, the block copolymer solutions were studied at room temperature (25 °C) to get information about their flow-behaviour. Figure 104 a) and b) show the viscosity as a function of the shear rate:

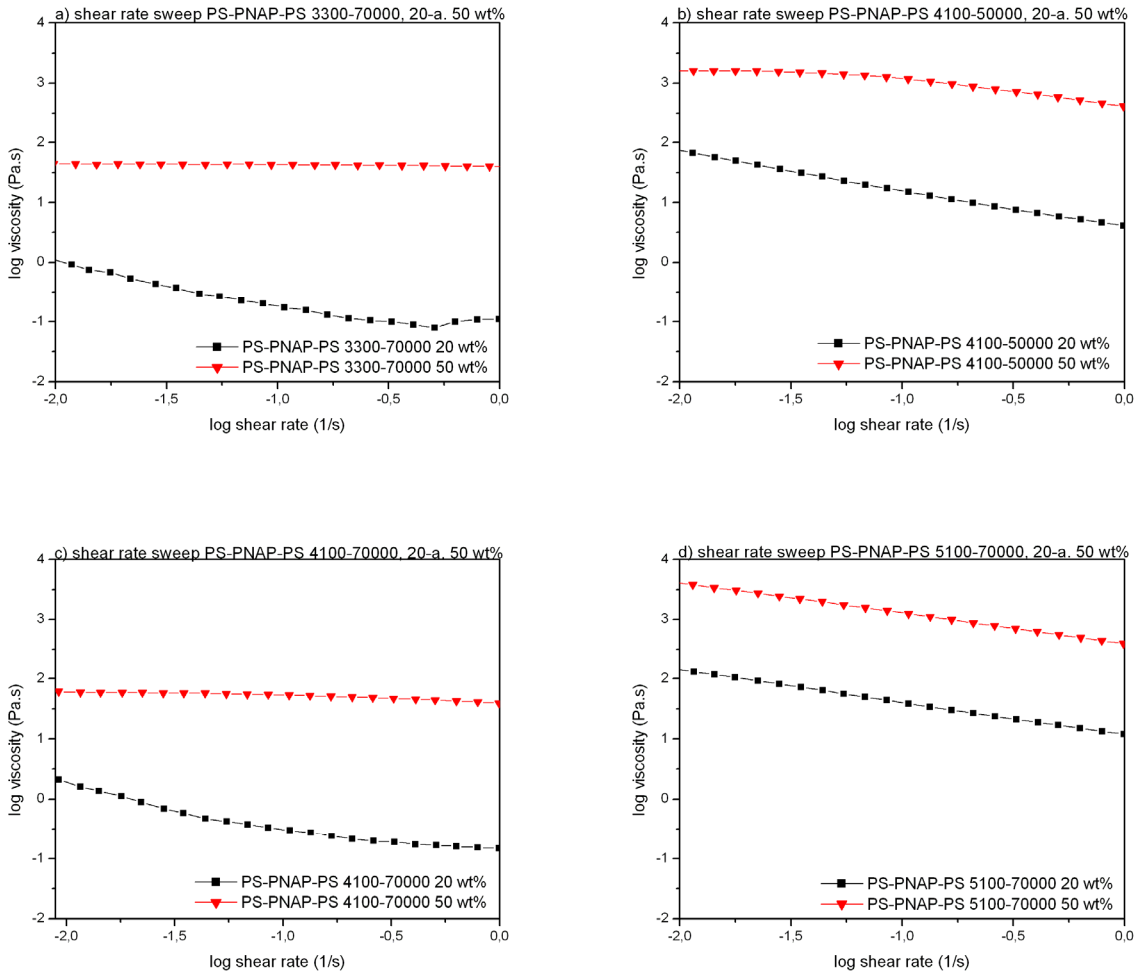

Figure 104-1): Investigation of sol-gel and gel-sol transitions of **PS-PNAP-PS** samples **3300-70000, 4100-50000**, **4100-70000** and **5100-70000** a)-d) applying frequency sweep measurements. The 20 wt% samples are depicted in black, the 50 wt% ones in red.

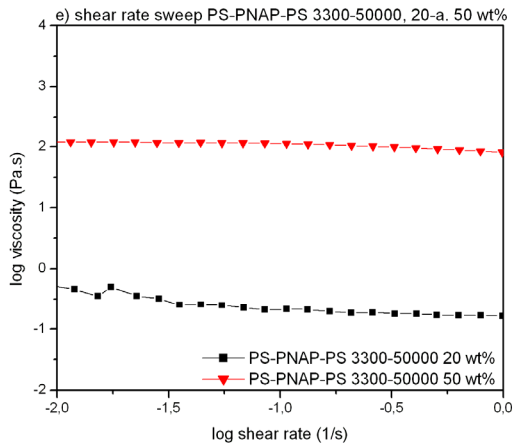

Figure 104-2): Investigation of sol-gel and gel-sol transitions of **PS-PNAP-PS** sample **3300-50000** e) applying frequency sweep measurements. The 20 wt% sample is depicted in black, the 50 wt% one in red.

-Oscillation frequency sweep measurements

The transitions from sol to gel or vice versa for the **PS-PNAP-PS** systems were studied in the viscoelastic region of the block copolymer at 1 Hz (figure 105):

Figure 105-1): PS-PNAP-PS block copolymers **3300-50000** and **3300-70000** (20- and 50 wt% samples) a)-b). The concentration of the investigated solutions is increasing from left to right. The loss modulus G` is depicted in red, the storage modulus G`` in black.

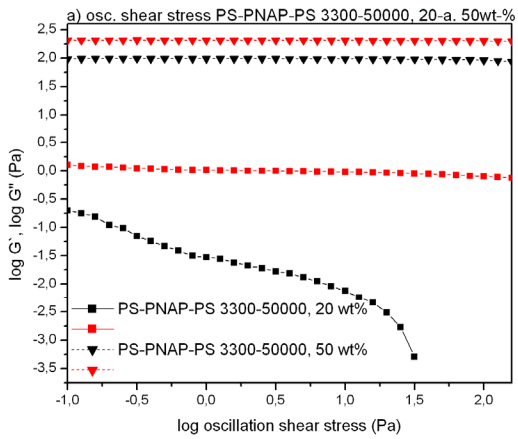

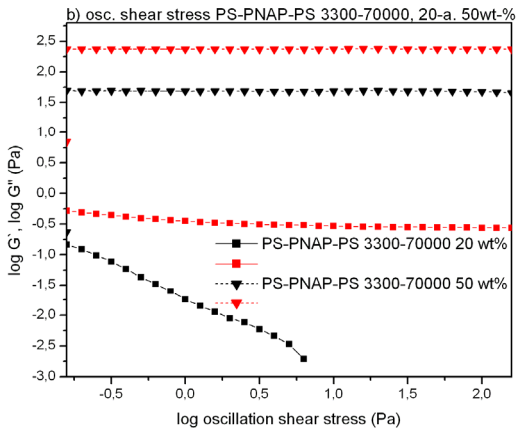

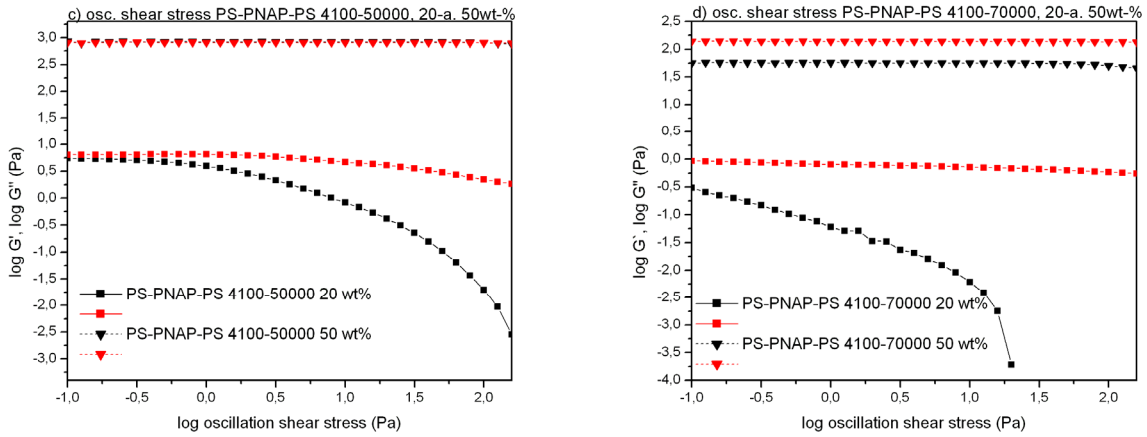

Figure 105-2): PS-PNAP-PS block copolymers **4100-50000** and **4100-70000** (20- and 50 wt% samples) c)-d). The concentration of the investigated solutions is increasing from left to right. The loss modulus G` is depicted in red, the storage modulus G`` in black.

The oscillation shear stress measurements (figure 105, 106) already display, that solutions of 50 wt% and higher are necessary to form soft hydrogels with the storage modulus G' being close to or larger than the loss modulus G'' as displayed for the **PS-PNAP-PS** samples. (The loss modulus G` depicted in red, the storage modulus G`` in black).

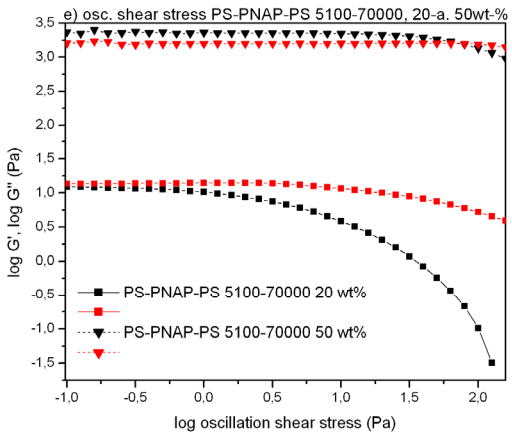

Figure 106: Oscillation shear stress measurements of **PS-PNAP-PS 5100-70000** at 20- and 50 wt%.

In order to verify the gained results, additionally frequency sweep measurements were performed at an oscillating shear stress of 1 Pa (figure 107):

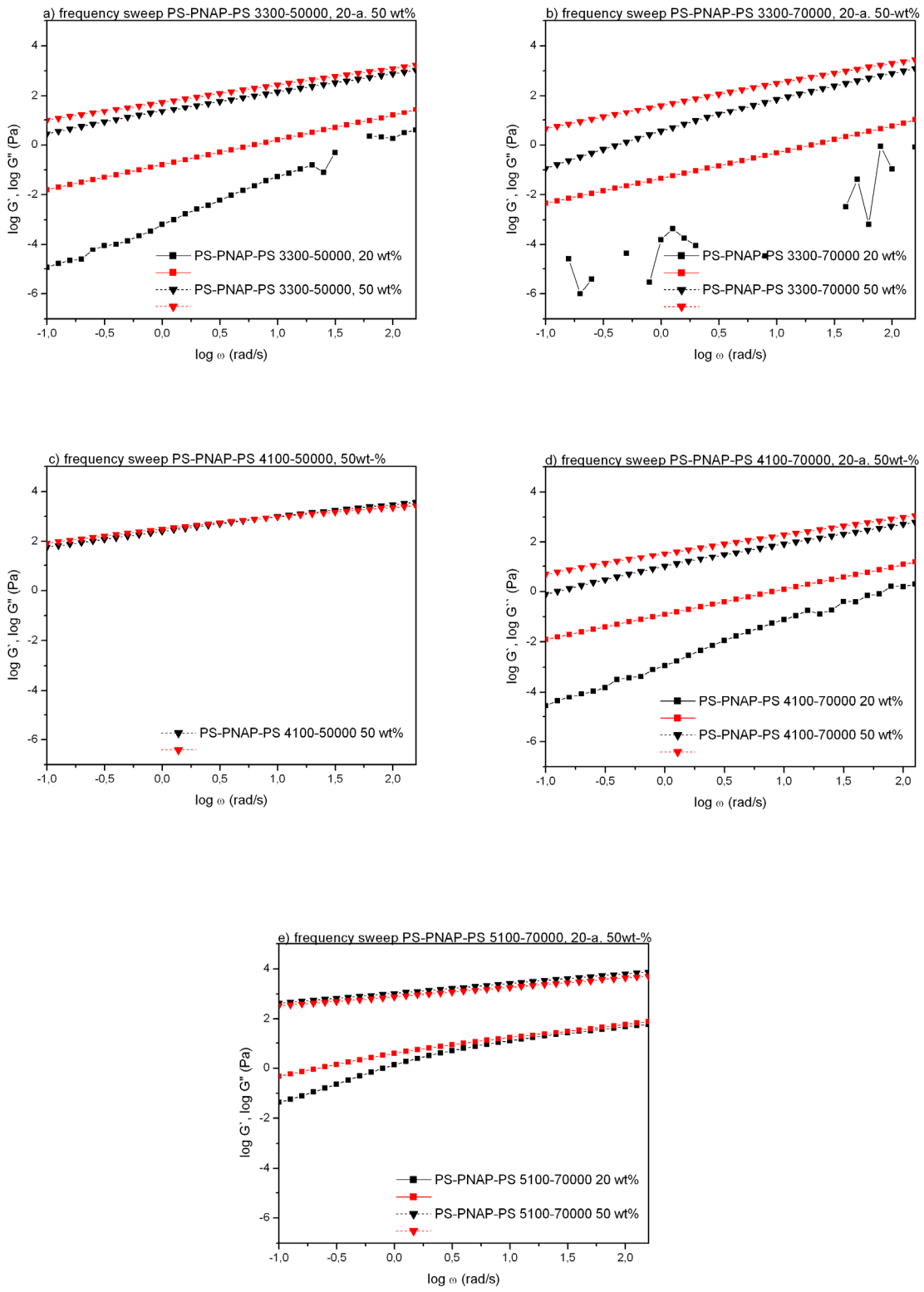

Figure 107: Frequency sweep measurements of **PS-PNAP-PS** samples **3300-50000**, **3300-70000, 4100-50000**, **4100-70000** and **5100-70000**. The loss modulus G` is depicted in red, the storage modulus G`` in black a)-e).

Temperature dependent measurements of PS-PNAP-PS–block copolymers investigating sol-gel and gel-sol transitions applying a temperature sweep measurements

Temperature sweep measurements (40- 60 °C) were performed applying the 20- and 50 wt% solutions. **PS-PNAP-PS 4100-50000** is shown as a model compound for both concentrations:

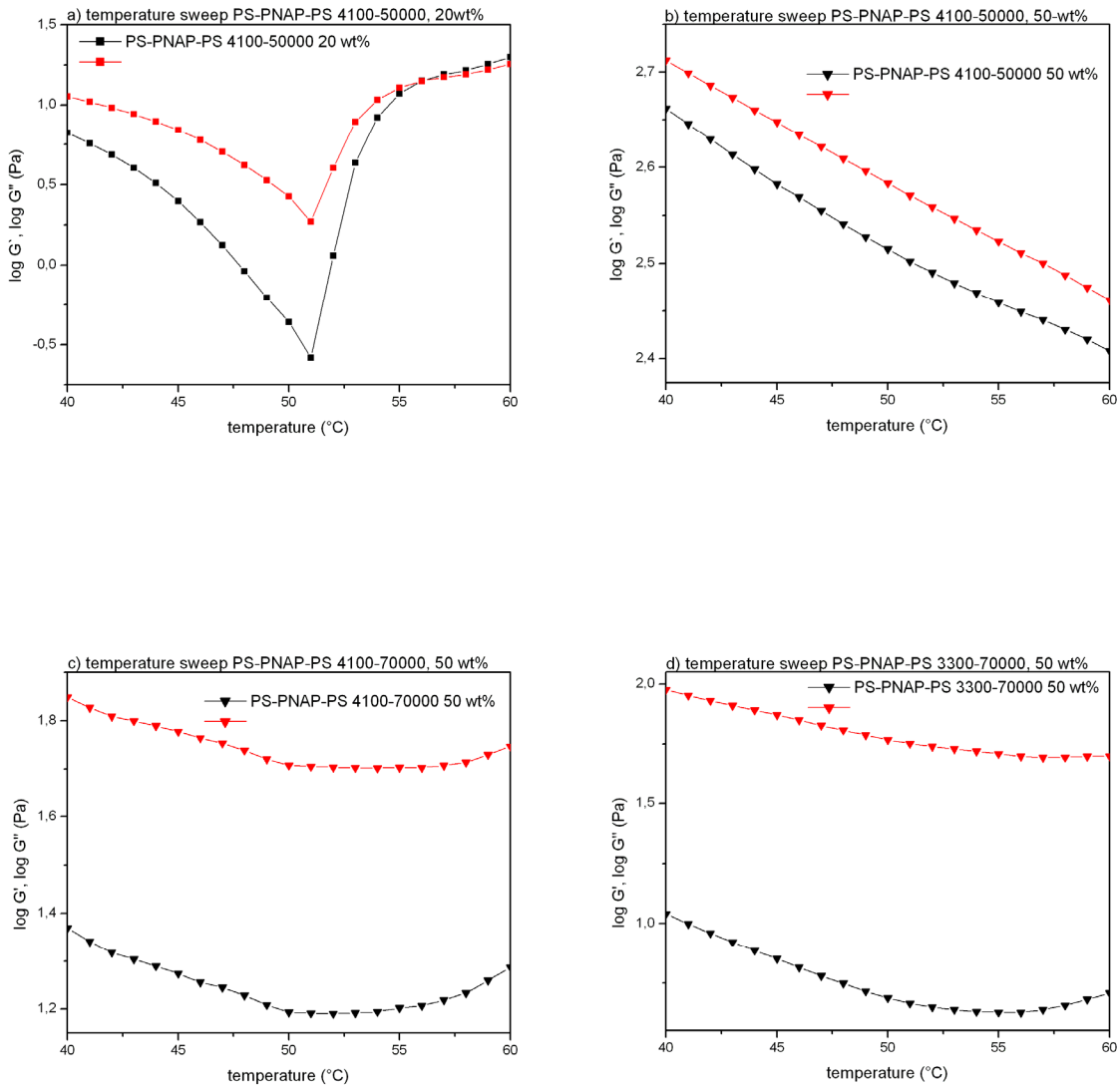

Figure 108: Temperature sweep from 40- to 60 °C of a) **PS-PNAP-PS 4100-50000** 20 wt%, b) **PS-PNAP-PS 4100-50000** 50 wt%, c) **4100-70000** 50 wt% and d) **3300-70000** 50 wt%. The loss modulus G` is depicted in red, the storage modulus G`` in black.

Whereas the graph (Figure 108 a)) of the 20 wt% solutions (example here **PS-PNAP-PS 4100-50000)** showed a marked temperature jump as shown for the BAB-systems described before, the 50 wt% solutions (figure 108 b), c), d)) unexpectedly did not show any temperature jump at all. An explanation for this behaviour could be either the system showing no elastic

properties and offering no free volume like the BAB-systems composed from PNIPAM (**M1** block) as the thermosensitive middle block or the PNAP (**M2**) blocks not being able to form secondary aggregation structures after collapsing in contrast to the PNIPAM containing systems. The reason therefore is not quite clear and more investigations on these systems are needed to gain a satisfactory explanation. Maybe this was the reason, why PNAP-PS copolymers are reported in the literature instead of block copolymers [312, 313].

12.6.6 Conclusions on rheology measurements

Applying the RAFT process, BAB-triblock copolymers composed of variable monomers and different block length showing a narrow polydispersity at the same time, were accessible in two steps only applying symmetric, bifunctional **CTA XXXX**. The long hydrophilic PNIPAM (**M1**) or PNAP (**M2**) middle-blocks compared to the short hydrophobic B-blocks enable good solubility of the BAB-systems in water. As described in detail, these micelles are hiding the hydrophobic B-ends in the micellar core while the hydrophilic A-block is exposed to water forming the characteristic flower-like structures. At concentrations between 10- to 30 wt% the samples behave like liquids proven by rheology measurements. The tendency to create bridged micelles (hydrophobic B-blocks connect two different micelles hiding in two different micellar cores) is low for the strong segregation regime applies for the polymers according to the very hydrophobic end blocks (styrene (**M3**) and 2-,3-,4-,5-,6-pentafluorostyrene (**M7**)).

At elevated and high concentrations of 40- to 50 wt% the systems are able to form soft or even hard gels (especially the 50 wt% samples). Heating slightly above the cloud point (> 32/50 °C) favours hydrogel formation according to the formation of further hydrophobic contacts between the B-blocks forming the micellar core, whereas heating well above the cloud point leads to phase separation and breakdown of the hydrogel structure due to the micellar network collapsing with increasing dehydration of the micellar coronae. The minimum concentration of block copolymer needed for gel preparation decreases with the length of the B-blocks increasing.

The mechanical strength of the hydrogels increases with increasing block length, but the main factor favouring mechanical strength and gel formation seems to be the glass transition temperature T_g of the hydrophobic blocks. Increasing the glass transition temperatures T_g (PS (**M3**) 373 K < PFS (**M7**) 378 K) [478, 479, 480, 481, 482] seems to increase the viscosity of the BAB-samples, although the temperature differences are only small. For the T_g values of 4-fluorostyrene (**M6**), different values are reported in the literature. Whereas Katritzky, Cao, García-Domenech [479, 480, 482] report a value of 379 K, Yu [481] found a value of 368 K, whereas Camelio et al. [483] reported values of 379, 384 and 386 K. For 2-FS (**M4**) and 3-FS (**M5**) no values vor T_g could be found in the literature.

The fluorinated end-groups ($-CF_3$) or fluorinated B-blocks did not show a tremendous influence on the gelation behaviour comparing to **PS-PNI-PS** samples repeated in the literature before. Substituting the F-moieties in the fluorinated B-blocks against longer chains could lead to comb-like structures which could perhaps show improved gelation behaviour already at concentrations between 10- and 30 wt%. Nevertheless, BAB-block copolymer

solutions show foaming behaviour and could probably work as solubilization agents for hydrophobic substances, due to forming free flowing micellar solutions up to a concentration of 30 wt% [142]. The BAB-systems containing PNAP for the thermoresponsive blocks seem to be more like sticky gels showing very limited elasticity at concentrations as high as 50 wt% and are thus less favourable for elastic hydrogel formation. The measured cloud points could be found around 29 to 32 °C for the PNIPAM (**M1** block) containing polymers and 44 to 50 °C for the PNAP (**M2** block) containing samples not differing notably between the diluted, semi-concentrated and concentrated solutions.

In order to follow the transitions during the temperature ramp experiment, it would be helpful to combine both rheology and optical devices. For optical investigations, the application of cryogenic transmission electron microscopy [484], X-ray techniques, such as X-ray diffraction analysis or SAXS [485-487] and FT-IR [488] or ^{1}H-NMR [489-492] as well as ^{19}F-NMR measurements for the pentafluorostyrene (**M7**) containing samples could be helpful, especially in this case studying the consistence, amount of water and ageing of this gel like samples depending on the applied temperature. The application of confocal laser scanning microscopy could give further insight in the molecular transport and distributions in the hydrogels- in case they can be fluorescently labelled or a fluorescent probe can be incorporated into the gel (preferred case). If a laser beam passes an anisotropic sample, its polarization and amplitude are be varied and detected. Changes in the anisotropy thus resemble changes in the samples properties [493-494].

Chapter XIII: Investigation of the surfactant properties of BAB-triblock copolymers and fluorine end capped polymers

Part of the newly synthesized BAB-triblock copolymers composed of 2-, 3-, 4-fluorostyrene (**M4, M5, M6**) and 2,3,4,5,6-pentafluorostyrene (**M7**) as well as the fluorine end-capped systems including a PS (**M3**) block belong to the class of fluorinated polymers due to containing also hydrocarbon-moieties [36, 145]. These fluorinated samples are reported to display good solubility in water which is in fact true for the BAB-systems [36, 145]. All samples are mixtures of homologues and the values gained from surface tension and CMC measurements must be seen as average values. As all series of BAB- and fluorine end-capped-systems have the same components, differences in the surfactant behaviour within a series most probably originate from different block length for the hydrophobic and hydrophilic blocks. Note that the BAB- and CF-end capped samples are not stable against very high or low pH-values due to the trithiocarbonate moieties linking the blocks are not stable under this conditions. Due to the relatively long hydrophilic PNIPAM (**M1**)- or PNAP (**M2**)-block, the polymers display excellent water solubility and amphiphilic properties, which can be changed to hydrophobic behaviour and unsolubility on demand by simply switching the temperature. In emulsions these amphiphiles could be added as cosurfactants forming globular aggregates at elevated temperatures which could work as stabilizing particles for the emulsions [36, 145]. The good stability of the polymeric micelles in water against dilution already indicates a very low CMC of the triblock copolymers under investigation. Therefore, CMC/CAC- measurements of the block copolymers were performed. Furthermore, the foam formation and stability of selected triblock copolymers in water was studied. The aspects of the surface active triblocks at the interface between two liquids is studied, namely the ability to work as stabilizers for emulsions with oils of different polarity. Experiments for the investigation of the application as possible efficiency boosters in microemulsion were performed additionally.

13.1 Foam experiments

As simple shaking of aqueous solutions of BAB-block copolymers revealed foam formation and thus surface activity, the foaming behaviour of these systems was studied in more detail. In order to get informations about the ability of the amphiphilic polymers to create foams and their foam stability, time dependent measurements of the foam height were performed. The systems described in this work are dispersions of air in water.

Normed glass cylinders washed with piranha acid before use had been applied as vessels for the determination of the foam height. For all experiments the same amount of liquid was filled into each tube and the same type of test tube model was chosen. For foam formation, the protocol described in the experimental section was followed.
For comparison, commercially available low molecular weight surfactants such as Triton® X 100, Zonyl® FSP, Brij® 56 and Tween® 65 and SDS were chosen. Pluronic® 6400 was investigated as a polymer surfactant (Figure 109):

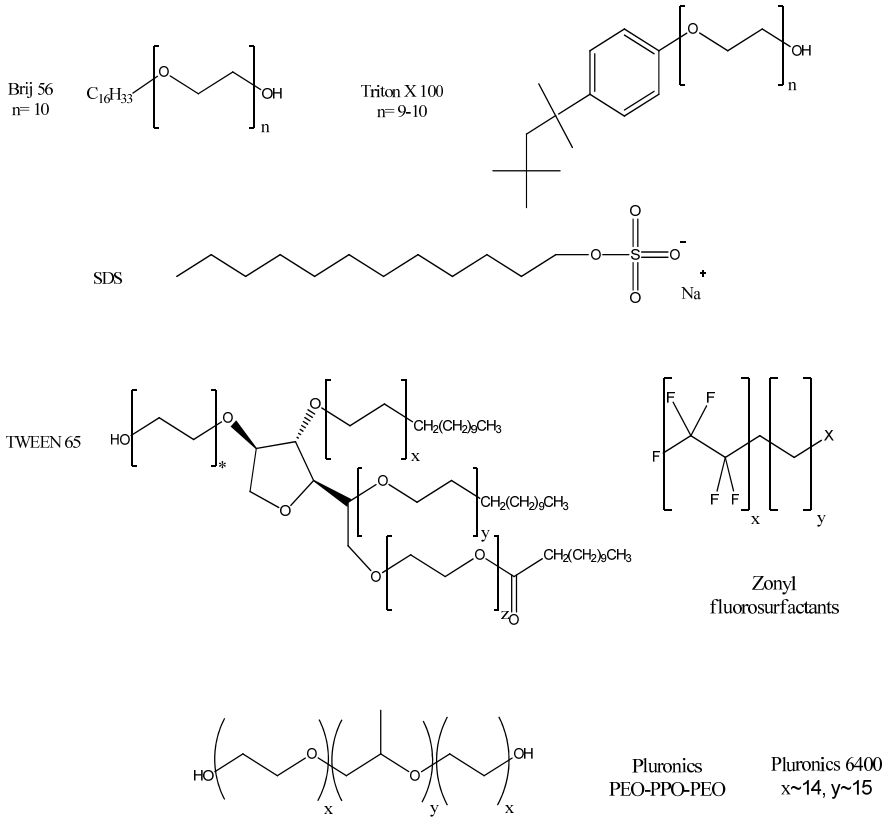

Figure 109: Commercially available low molecular weight surfactants such as Triton® X 100, Zonyl® FSP, Brij® 56, Tween® 65 and SDS were chosen as low molecular weight surfactants [495, 496], Zonyl® FSP is a very low foaming surfactant [497] whereas Triton® X 100 is a better foaming agent, with an HLB of 13.5 [495, 496]. Pluronic® 6400, a polymer surfactant containing 40 % of polyethylene glycol is a very low foaming polymeric surfactant [498].

All tested BAB-triblock copolymers –fluorinated and non-fluorinated- are able to form stable foams (figure 110-112). The tested BAB-triblock copolymers all displayed a fine pored structure directly after shaking. Defined, spherical gas bubbles with thick liquid lamellae were observed indicating low foam numbers for this type of polymeric surfactant. With longer observation times, a polyhedral foam crown developed as described above due to liquid leaving the interface due to gravitation [36, 158].

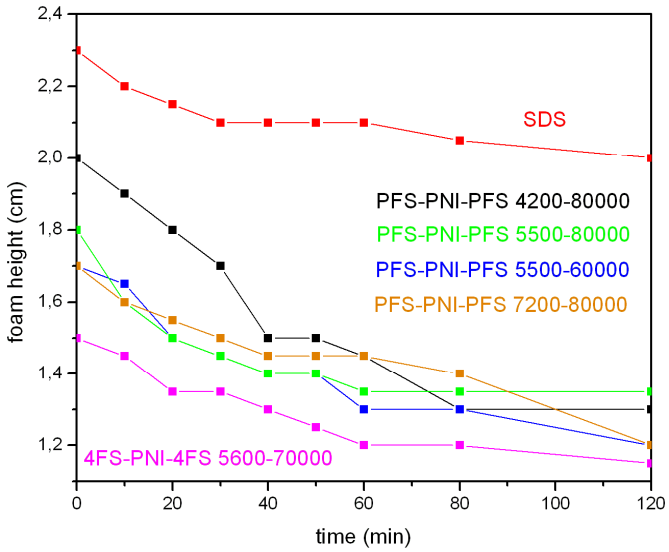

Figure 110: Foam decay of aqueous polymer solutions of fluorinated BAB-systems as a function of time (concentration of solutions= 1 g/L). Lines are meant as guides for the eye.

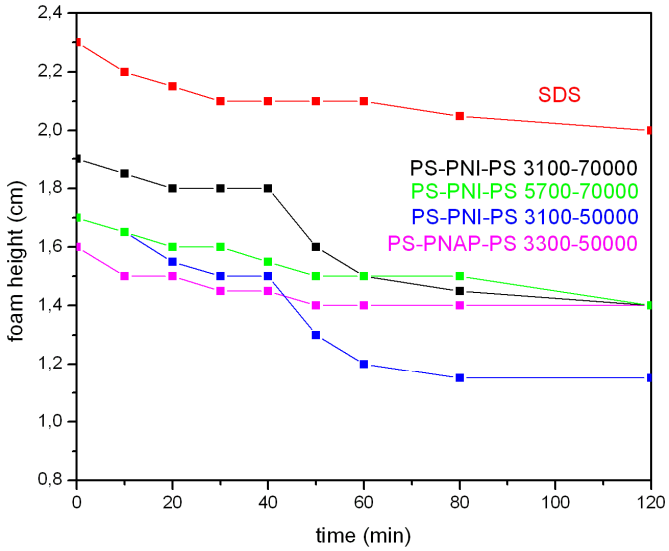

Figure 111: Foam decay of aqueous polymer solutions of non-fluorinated BAB-systems as a function of time (concentration of solutions= 1 g/L). Lines are meant as guides for the eye.

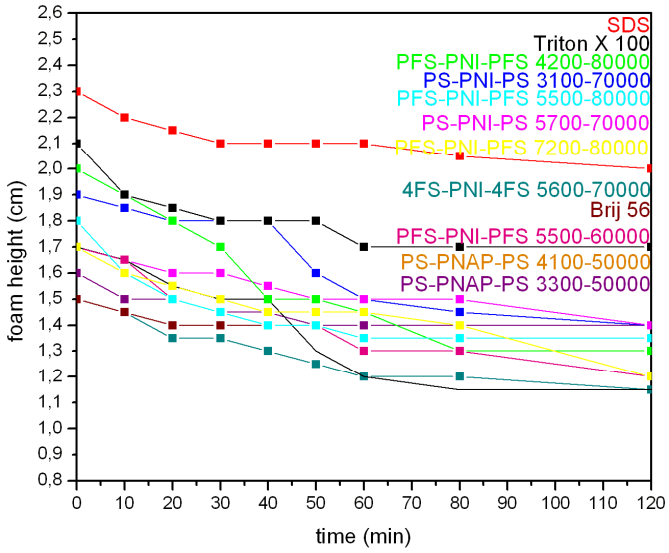

Figure 112: Comparison of foam decay of aqueous polymer solutions of non-fluorinated and fluorinated BAB-systems as a function of time (concentration of solutions= 1 g/L). Lines are meant as guides for the eye.

Figures 110-112: the foam composition is almost similar in all cases, which means that neither the type and length of the hydrophobic B-blocks, styrene (**M3**) or 2,3,4,5,6-pentafluorostyrene (**M7**), nor the length of the hydrophilic PNIPAM (**M1**) middle- block has an influence on the quality of the foaming behaviour of the BAB-systems. The foam of all investigated systems is stable for over two hours until total foam decay (zero-level) as typical for transient foams (see chapter on foams). In contrast, Pluronic® 6400, a surfactant of type PEO-PPO-PEO, Zonyl® FSP, representing a fluorinated surfactant (for detailed information about both surfactants vide supra and see appendix) and Tween 65® show very low foaming activity which is an advantage in many industrial applications [36, 145]. The compounds are not depicted in the graphs. Compared to the latter ones, Triton® X 100 and Brij® 56 reveal better foam composition and activity.

Nevertheless, the quantity of the foaming behaviour seems to be influenced by the type and length of the applied blocks as shown by figures 110, 111 and 112.

As expected, the foams created from SDS, an ionic surfactant, show the best foam formation and stability [36], followed by Triton® X 100. Both foams display a slow, continuous decay. The foams created from **PFS-PNI-PFS 4200-80000** and **PS-PNI-PS 3100-70000**, **PFS-PNI-PFS 5500-80000** showed the best foaming behaviour of the BAB-systems, but also rapid foam decay. Especially **PFS-PNI-PFS 4200-80000** foams decrease rapidly. Foams prepared from **PFS-PNI-PFS 5500-80000, 5500-60000, 7200-80000** show medium foam formation and a relatively continuous decay. The foams created from the PS-PNAP-PS polymer and Brij® 56 displayed the lowest foam formation and stability.

Obviously the samples created from the BAB-polymers with short hydrophobic B-blocks show the best foam formation but also the lowest stability. Increasing the length of the hydrophobic B-block leads to a reduced foaming behaviour, but simultaneously increases foam stability.

As a rough estimation, the value for the HLB of the systems can be estimated between the HLB-value described for Triton® X 100 and Brij® 56, this means between 13.5 and 16 (vide supra). The HLB-value for the BAB-systems is relatively low explaining their moderate to poor foaming properties [466]. Figures 108 and 109 display the low molecular weight surfactant SDS as the surfactant creating the highest and most stable foams showing better diffusion behaviour at the interface compared to the relatively slow macromolecules. More graphs for comparison can be found in the appendix.

13.1.1 Foam experiments applying mixtures of amphiphilic polymers and SDS (v:v/1:1)

In this experiment, the effect of the addition of SDS, sodium dodecyl sulphate, a well known commercially available low molecular weight surfactant, on the foam formation and stability of aqueous solutions of BAB-triblock copolymers should be studied. SDS itself shows both good foam formation and foam stability and is therefore an ideal candidate for comparison as shown above.

For foam formation and mixing of SDS- and copolymer solutions, the protocol described in the experimental part was followed. All investigated BAB-triblock copolymers –fluorinated (**M5, M6, M7** blocks) and non-fluorinated (**M3** blocks)- are still able to form stable foams, also in the presence of the low molecular weight surfactant (figures 113, 114). The tested BAB-triblock copolymers also displayed a fine pored structure directly after shaking, similar to the samples without SDS-additive.

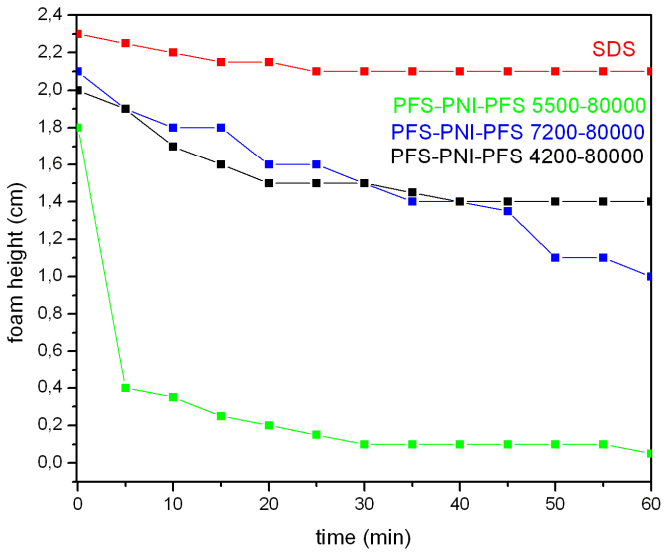

Figure 113: Foam decay of aqueous polymer solutions of fluorinated BAB-systems including SDS (v:v= 1:1) as a low molecular weight surfactant as a function of time (concentration of solutions= 1 g/L). Lines are meant as guides for the eye.

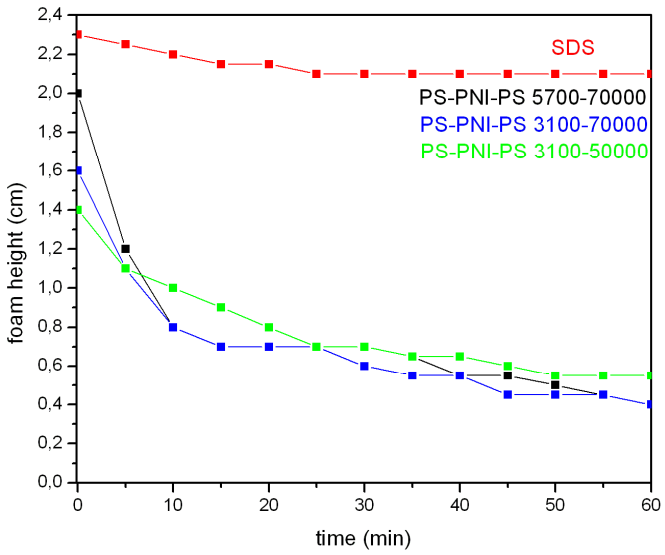

Figure 114: Foam decay of aqueous polymer solutions of fluorinated BAB-systems including SDS (v:v= 1:1) as a low molecular weight surfactant as a function of time (concentration of solutions= 1 g/L). Lines are meant as guides for the eye.

Figures 113, 114: The time for the decay of the foam height is obviously faster compared to the SDS-free samples (vide supra) and the overall foaming behaviour of all studied samples is reduced. Also this type of foam belongs to the class of transient foams. Also in this case neither the type and length of the hydrophobic B-blocks, styrene (**M3**) or 2,3,4,5,6-pentafluorostyrene (**M7**), nor the length of the hydrophilic PNIPAM (**M1**) A-block has an influence on the quality of the foaming behaviour. The foam of all SDS-polymer systems is stable for over two hours until total foam decay. The quantity of the foaming behaviour seems to be influenced by the type and length of the applied blocks as already discussed for the SDS-free samples. Whereas the fluorinated samples **PFS-PNI-PFS 7200-80000** and **4200-80000** show a continuous, gradual decay, the foams generated by the non-fluorinated samples **PS-PNI-PS 3100-50000, 3100-70000** and **5700-70000** together with those of Pluronic® 6400 show a rapid decay.

In general it can be deduced, that the addition of SDS reduces the foaming ability and lifetime of the foams created from aqueous solutions of BAB-triblock copolymers. The reason therefore is not known. A possible explanation could be the introduction of a smaller molecule leading to a higher dynamics at the interface simultaneously resulting in a reduced stability of the foam bubbles and thus foam crown. Alltogether, the mixed polymer/SDS-surfactant systems are even poorer foaming agents than the pure polymer systems.

13.1.2 Conclusions on the foam formation of BAB-triblock copolymers

The foaming properties of polymeric surfactants of various BAB-types were compared to ionic low molecular weight surfactant SDS, being a very good foaming agent, and the commercially available non-ionic surfactants Triton® X 100, Tween® 56, Zonyl® FSP fluorosurfactant and Pluronic® 6400 as a polymer surfactant.

All investigated BAB-triblock copolymers show foam formation, but are in general no good foamers indicating towards a low HLB-value of these systems. The **PS-PNI-PS** and **PFS-PNI-PFS** systems are able to create homogeneous transient foams with a limited lifetime. PS-PNI-PS systems show almost the same foam stability as the **PFS-PNI-PFS** systems. The chemical nature of the fluorinated block seems to have only limited influence on the foaming properties. As a rough estimation, the value for the HLB of the systems can be estimated between the HLB-value described for Trition® X 100 and Brij® 56, this means between 13.5 and about 16 (vide supra). The HLB-value for the BAB-systems is relatively low explaining their moderate to poor foaming properties [36]. Compared to the BAB-systems, SDS as an ionic surfactant shows the best foam formation and stability. In contrast, Pluronic® 6400, Tween® 56 and Zonyl® FSP fluorosurfactant can be seen as non-foaming surfactants creating almost no foam even after intensive shaking. The addition of SDS to the **PS-PNI-PS** and **PFS-PNI-PFS** systems still leads to homogeneous transient foams but of reduced foam stability. The reason for this behaviour is still unknown.

13.2 Amphiphilic BAB-triblock copolymers as surfactants in emulsions

As a closer look into literature revealed only restricted knowledge about the behaviour of fluorinated and non-fluorinated amphiphilic BAB-triblock copolymers on emulsions, the ability of these polymers to stabilize o/w- and w/o-emulsions created of various types of oil has shifted into focus. The broad spectrum of studies was finished by testing **PS-PNI-PS** and **PFS-PNI-PFS** polymers for their possible efficiency boosting effect in miniemulsions and as stabilizers in miniemulsions.

13.2.1 Investigation of emulsion stabilization applying BAB-triblock copolymers

The stability of a typical emulsion without a stabilizing additive, e. g. an amphiphile, is only poor [36, 144]. A high viscosity of the continuous phase is favoured for making emulsions more stable due to a reduced coalescence; i.e. the collision between the droplets is reduced. For this reason, polymer or other additives increasing the viscosity are added [36]. Here polymers are introduced for steric stabilization, also called polymer stabilization, of the particles [36].

In this experiment, the ability of the fluorinated and non-fluorinated BAB-block copolymers to stabilize emulsions was investigated. BAB-block copolymers shifted into focus after Klapper et al. [171] reportet successfully applying the BAB-systems for emulsion stabilization, whereas He et al. [328] report the use of poly(ethylene glycol)-poly(lactic acid)-poly(ethylene glycol) systems (PEG-PLA-PEG) for pharmaceutical applications. The non-ionic BAB-samples should enable steric stabilization of emulsions [36]. The theory about emulsion formation and stabilization has already been described in the previous chapter. The newly synthesized BAB-triblock copolymers could stabilize emulsions in the following ways (figure 115, 116):

-oil–in-water emulsions (o/w-emulsions)

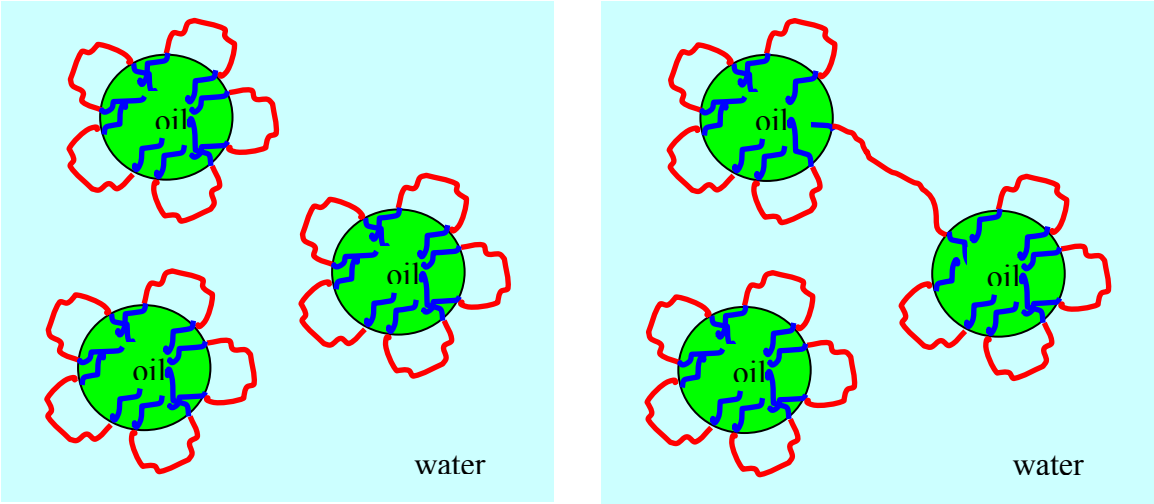

Figure 115: Stabilization of the oil droplets in oil-in-water systems. The size of the droplets is enlarged compared to the true, smaller size for explanation reasons.

a) The hydrophobic B-blocks (**M3, M7**-blocks) (blue) interact with the oil droplets (green) dispersed in the aqueous phase (light blue).The hydrophilic, but lipophobic part resembled by the PNIPAM (**M1**)-middle block (red) enables good interaction with water.

b) The B-blocks (**M3, M7**-blocks) (blue) can also be located in two different oil droplets leading to bridging-structures.

Figure 115: The hydrophobic B-blocks (blue) interact with the oil of the oil droplets (green) spread in the aqueous phase (light blue), whereas the hydrophilic, but lipophobic part, which is formed by the PNIPAM-middle block (red), enables good interaction with water. Both B-blocks (blue) can be located at the interface of one oil droplet similar to the flower-like structures already described for the micellization of these polymers in aqueous solution or in two different oil droplets leading to bridging-structures as already described for these systems for the gelation of BAB-triblock copolymers. The bridging structures are more likely to occur with high surfactant concentrations.

- water–in-oil emulsions (w/o-emulsions)

This emulsion type is the opposite type to the described oil-in-water systems (figure 116):

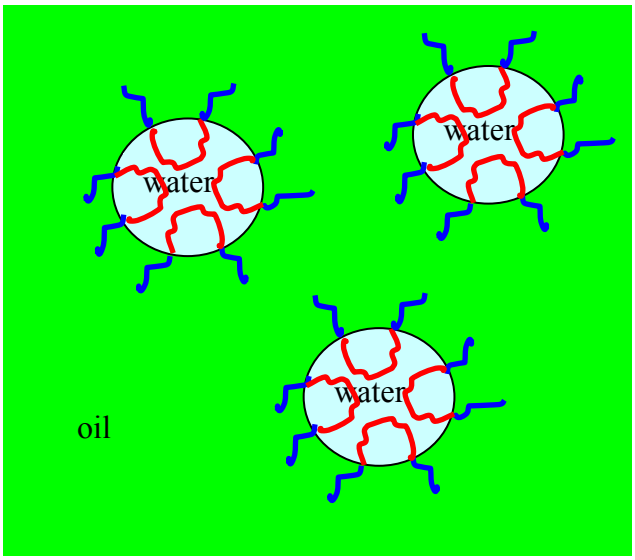

Figure 116: The hydrophobic B-blocks (**M3, M7**-blocks) (blue) interact with the oil (green) surrounding the aqueous droplets (light blue) spread in the oil. The hydrophilic, but lipophobic part resembled by the PNIPAM (**M1**)-middle block (red) enables good interaction with the water droplets. The size of the droplets is enlarged compared to the true, smaller size for explanation reasons.

Figure 116: The hydrophilic PNIPAM (**M1**)-block (red) interacts with the water of the water droplets (light blue) spread in the oil phase, whereas the hydrophobic, lipophobic part, which is formed by the poly(styrene) (**M3**) or poly(pentafluorostyrene) (**M7**) B-blocks (blue), enables good interaction with the applied oil. Both B-blocks are located at the interface of one water droplet similar to flower-like structures but forming reverse "flowers" in this case. Bridging-structures as described for the oil-in-water systems (vide supra) cannot be formed in these systems.

In order to learn more about the ability of BAB-systems to stabilize emulsions, oil-in-water (o/w) and water-in-oil (w/o) emulsions were prepared from fluorinated and non-fluorinated BAB-triblock copolymers, destilled water and different kinds of oils according to the procedure described in the experimental part. As sonication of the samples might destroy the block copolymers, the time of sonication was limited to three and five minutes. Furthermore, short sonication times avoid a warming of the solution above the cloud point of the solution leading to precipitation of the polymer and falsifying the results. Waxy oils such as methyl-palmitate or n-nonane were not heated to improve emulsion formation for the same reasons.

The chosen triblock copolymers vary in length and type of the hydrophobic styrene (**M3**) and 2,3,4,5,6-pentafluorostyrene (**M7**) B-blocks and the length of hydrophilic A-block prepared from PNIPAM (**M1**). Polymers **PS-PNI-PS 3100-70000**, **PFS-PNI-PFS 4200-80000** and **PFS-PNI-PFS 6500-80000** were selected for performing the emulsion experiments. The types of oils chosen for emulsion preparation were varied in their polarity, lipophilicity and consistence (figures 117, 118).

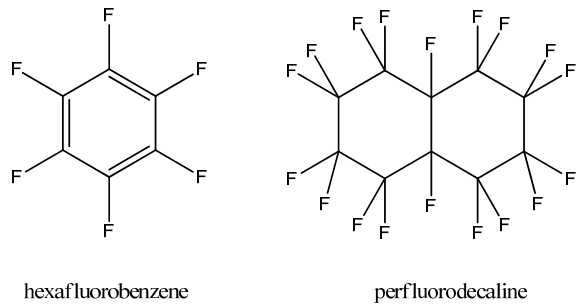

Figure 117: Compounds chosen as fluorinated oils: hexafluorobenzene and perfluorodecaline.

The fluorinated compounds (figure 118) hexafluorobenzene and perfluorodecaline can be found in e. g. medical applications as a marker or as solvating agents or in microemulsions [499-502]. They are highly unpolar and lipophobic oils.

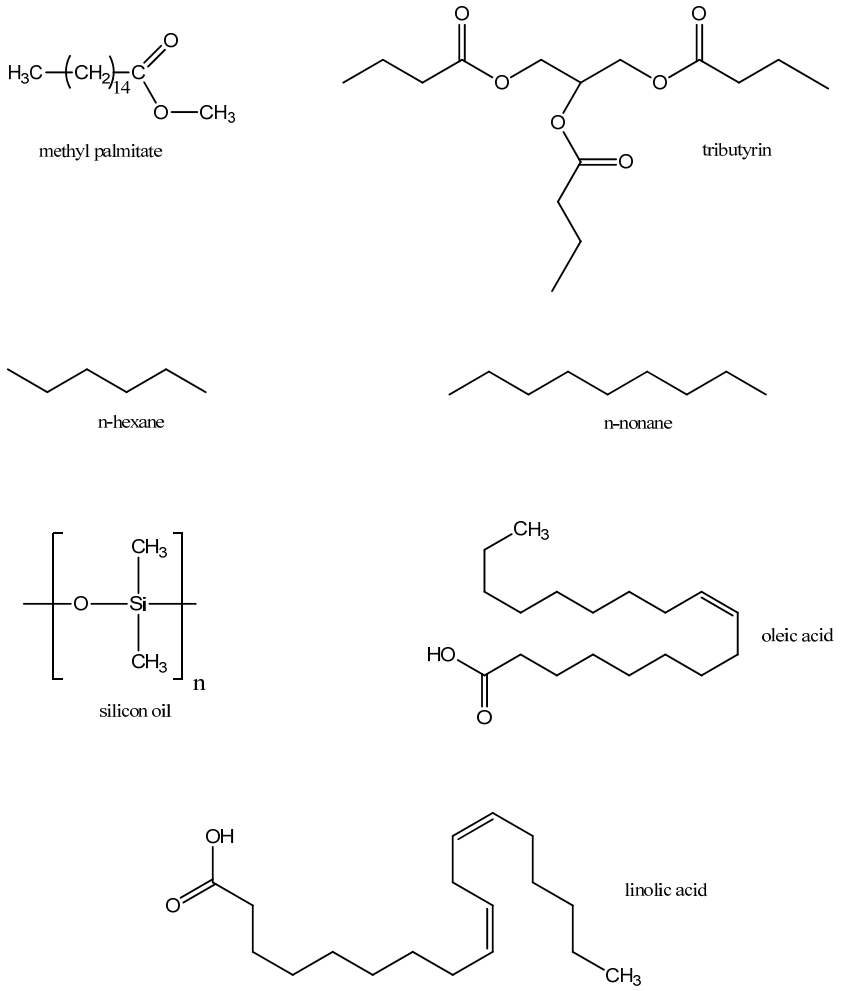

Figure 118: Non-fluorinated, lipophilic oils of variable polarity chosen for emulsion formation.

Despite methyl palmitate and nonane showing a more waxy character, all other oils are liquids (figure 118). Methyl palmitate is often applied in medical- and pharmaceutical applications and cosmetics [503-505], whereas sunflower and rapeseed oil find different applications e. g. in food industry and the latter one also in bio diesel [506-510]. Sunflower oil and rapeseed oil contain mixtures of fatty acids [511, 512]. The main ingredient of sunflower oil is mostly linolic acid, whereas rapeseed oil contains oleic acid as the most part. Silicon oil is used for medical applications such as ophthalmologic and plastic surgery [513, 514]. Tributyrin has been reported in pharmaceutical applications [515, 516]. N-hexane and n-nonane are common hydrocarbons used as solvents, in extraction and synthesis.

As a general rule for the formulation of an emulsion, the mixture of emulsifiers should have an HLB-value similar to that of the ingredient to be emulsified [36, 144]. Methyl palmitate and n-nonane represent relatively unpolar, waxy substances, whereas sunflower- and tributyrin oil, rapeseed oil, hexane and silicon oil are substances of also low polarity but liquid. Emulsions prepared from these unpolar oils were expected to be well stabilized especially from polymers containing styrene **(M3)** as the hydrophobic but not lipophobic B-block. As highly fluorinated compounds, both hexafluorobenzene and perfluorodecaline resemble very unpolar, hydro- and lipophobic liquids [223] and emulsions prepared from these fluorinated oils were expected to be stabilized especially by the fluorinated BAB-triblock copolymers prepared from monomer **M7**. Furthermore, the fluorinated systems were expected to stabilize the oil compounds worse compared to the styrene containing samples due to their not only hydrophobic, but also lipophobic character [223].

All emulsions prepared from styrene (**M3**) containing BAB-triblock copolymers were able to form stable emulsions after three minutes of sonication from sunflower-oil (o/w and w/o), rapeseed-oil (o/w and w/o), tributyrin (o/w and w/o), and silicon oil (o/w and w/o). From methyl-palmitate, nonane and hexane only oil-in-water systems could be prepared. Directly after preparation, the described solutions -except the hexane containing one which was opaque- appeared as a single white uniform phase indicating the block copolymers adsorbing onto the interface between the liquid and oil phase providing steric stabilization [144]. The generation of emulsions was verified by investigating samples under the light microscope (figures 119, 120). Sample preparation was done according to the procedure described in the experimental section. The type of emulsion could be investigated using conductivity measurements, in which the water-in-oil-emulsions showed almost no conductivity, whereas a current could be measured for the oil-in-water systems.

Water-in-oil-emulsions of only poor stability could be formed with the perfluorinated oil hexafluorobenzene. The formation of more stable oil-in-water-emulsions was possible but resulting also in emulsions of restricted stability after sonication for five minutes. Emulsions prepared under the same conditions decomposing within minutes were formed using perfluorodecaline, whereas the oil-in-water systems again proved to be the more stable ones. It seems that these oils, especially the fluorodecaline, are too unpolar and thus the oil droplets in solution are not well stabilized by the polymers composed of styrene (**M3**)-blocks, despite two outer blocks can interact at the interface. Applying the waxy oils methyl palmitate and nonane, emulsions could be formed after sonication of the samples for four minutes. Unfortunately the quality of these emulsions suffers from greater wax particles still present in

the samples (samples were not heated due to avoiding solutions warming over the cloud point).

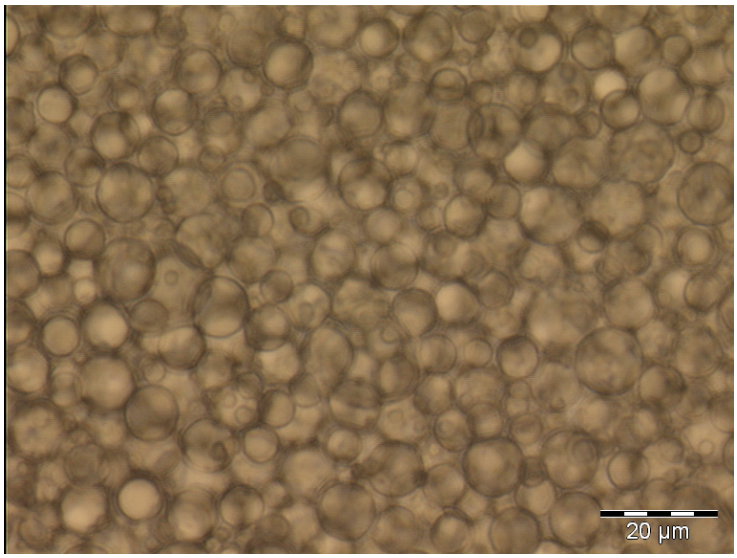

Figure 119: Optical micrograph of emulsions made using **PS-PNI-PS 3100-70000**, 1 g tributyrin as oil (oil-in-water emulsion).

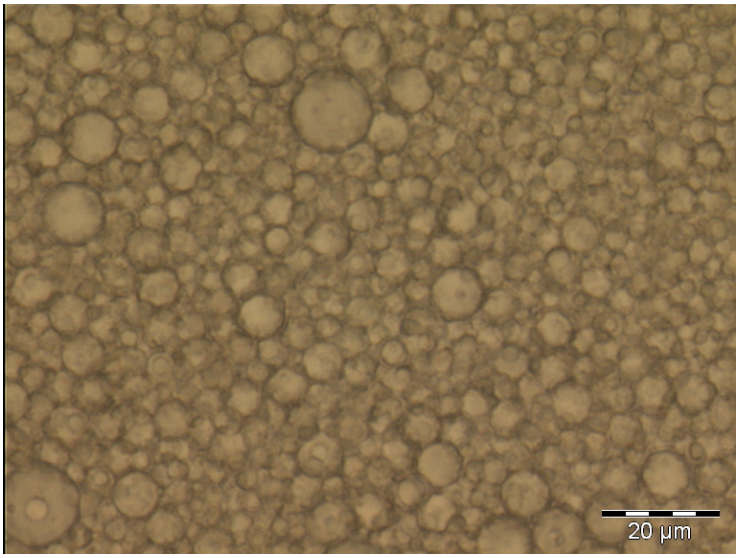

Figure 120: Optical micrograph of emulsions made using **PS-PNI-PS 3100-70000**, 4 g tributyrin as oil (water-in-oil emulsion).

Within the first two days after preparation, the height of the emulsion decreased quite fast until the equilibrium volume phase was reached for the samples prepared from non-fluorinated oils.

All o/w and selected w/o-emulsions prepared from the non-fluorinated systems were stable for two days (interval of observation). After one week, emulsions began to show signs of separation, creaming and sedimentation in this case. In general, most emulsions were showing signs of degradation, whereas the emulsions prepared from silicone oil, rapeseed oil and sunflower oil were still stable. As already mentioned, the oil-in-water-emulsions prepared using hexafluorobenzene and perfluorodecaline showed only limited stability. The height of the emulsions decreased within minutes and most of the emulsions had decomposed within a day, the perfluorodecaline containing w/o samples within two hours. The same was found for the hexane containing emulsions.

BAB-triblock copolymers containing 2,3,4,5,6-pentafluorostyrene (**M7**) as the hydrophobic B-block were showing similar behaviour compared to the non-fluorinated BAB-systems. Stable emulsions were obtained after three minutes of sonication from sunflower oil (o/w and w/o), rapeseed oil (o/w and w/o), tributyrin (o/w and w/o), hexane (o/w) and silicon oil (o/w). From methyl palmitate, nonane and hexane also in this case only oil-in-water systems could be prepared. With hexafluorobenzene and perfluorodecaline, w/o and o/w emulsions were prepared. Directly after preparation, the described solutions -except the hexane containing one- appeared as a single white uniform phase as described for the styrene containing BAB-systems. The generation of emulsions was checked by investigating samples of the prepared emulsions under the light microscope (figures 121, 122). Sample preparation was done following the same routine as described before. The type of emulsion was investigated using conductivity measurements, in which the water-in-oil-emulsions showed almost no conductivity, whereas a current was measured for the oil-in-water systems.

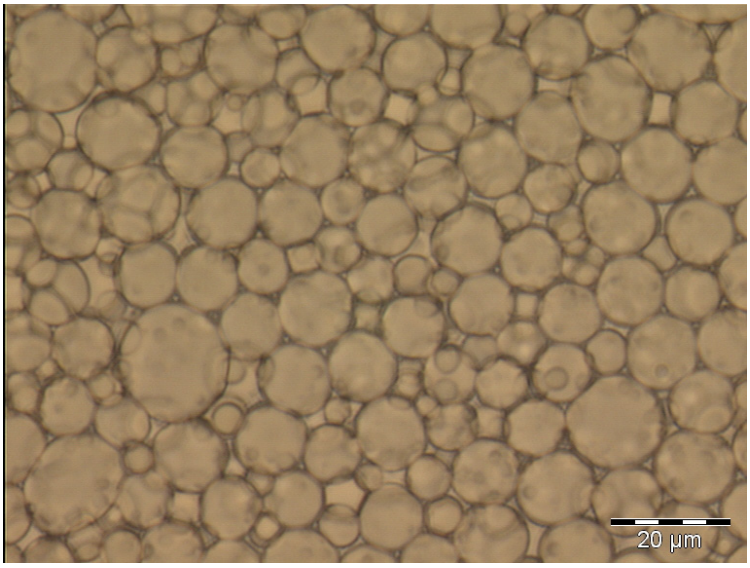

Figure 121: Optical micrograph of emulsions made using **PFS-PNI-PFS 4200-80000**, 1 g tributyrin as oil (oil-in-water emulsion).

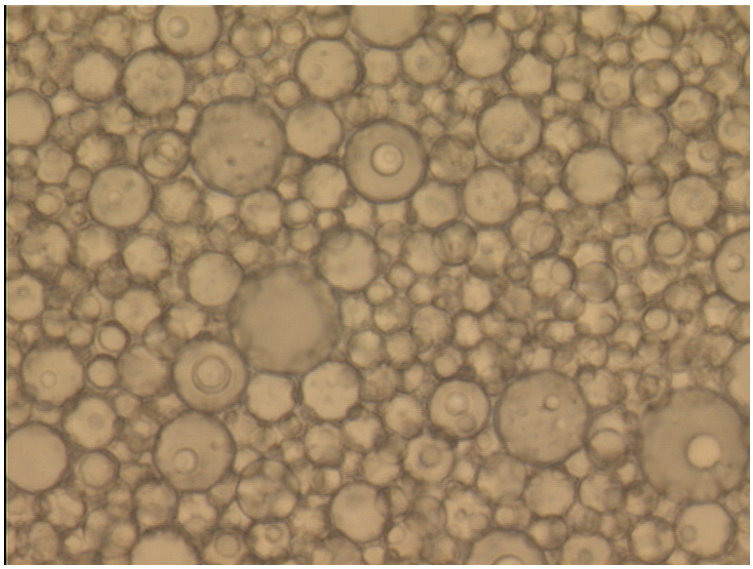

Figure 122: Optical micrograph of emulsions made using **PFS-PNI-PFS 4200-80000**, 4 g tributyrin as oil (water-in-oil emulsion).

Within the first two days after preparation, the height of the emulsion decreased quite fast until the equilibrium volume phase was reached for the samples prepared from non-fluorinated oils as described for the styrene (**M3**) containing systems.
All o/w and selected w/o-emulsions were at least stable for two days (interval of observation). After one week, also these emulsions began to display signs of creaming and sedimentation, except the ones prepared from sunflower oil, rapeseed oil, silicon oil and tributyrin. The oil-in-water emulsions prepared using hexafluorobenzene and perfluorodecaline showed only limited stability despite now using fluorinated block copolymers for steric stabilization. As seen before, the height of the emulsion decreased within minutes and most of the emulsions had decomposed within a day. The water-in-oil systems showed even worse stability and decomposed within an hour. Applying block copolymer **PFS-PNI-PFS 6500-80000**, including a longer PFS-block did not lead to better results. The same was found for the hexane containing emulsions.

Furthermore, the preparation of emulsions applying BAB-triblock copolymers offers the possibility to destroy the emulsion on demand by just heating it above the cloud point of PNIPAM changing the HLB of the triblock copolymers with temperature (see appendix).

In general, BAB-triblock copolymers can be applied for the preparation of emulsions, especially oil-in-water emulsions, in which no long-term stability is required. The preparation of water-in-oil emulsions was not possible for the waxy samples. The emulsions prepared from liquid oils- oil in water and water in oil- are of good quality according to light-microscopy investigations. The emulsions using silicon oil, rapeseed oil and tributyrin as the oil phase show good stability about one week. Neither the styrenic (**M3**) nor the perfluorinated (**M7**) BAB-triblock copolymers formed long-term stable oil-in-water

emulsions with hexafluorobenzene and perfluorodecaline. The reverse systems showed even worse stability. The same is valid for the preparation of emulsions applying hexane. The emulsions decomposed within 1 h. The reason for the limited stability could be the hydrophobic styrene (**M3**) or perfluorinated (**M7**) B-block being too short for well stabilization of the fluorinated oils. Enlargement of the styrenic and perfluorinated blocks could probably solve the problem. Another explanantion could be limited compartibility between the styrene (**M3**) blocks and the perfluorinated oils and the pentafluorostyrene (**M7**)-blocks with fluorodecaline. In general, enlargement of the hydrophobic blocks but keeping the polymer easily water- soluble by tuning the length of the hydrophilic PNIPAM-block could lead to emulsions of improved stability by shifting the HLB of the polymeric BAB-surfactants.

13.2.2 Conclusions on emulsions prepared from BAB-systems

The preparation of o/w and w/o emulsions applying fluorinated (**M7** block copolymers) and non-fluorinated (**M3** block) BAB-systems and a liquid oil phase- except for pentane and the fluorinated oils- leads to good results as monitored by light microscopy studies, whereas the long-term stability of most emulsion systems is only limited and a crucial drawback for the application of this type of amphiphilic polymers in emulsion formulation.
In general, polymeric surfactants usually show no good emulsifying properties being unable to diffuse rapidly to fresh created interfaces [36]. Some emulsions were stable for two days only; the emulsions prepared from pentafluorostyrene and perfluorodecaline only for hours or a day. Especially for the emulsification of hexafluorobenzene and fluorodecaline, the length of the hydrophobic-lipophilic fluorinated B-block was probably not enough to stabilize the oil water interface sufficiently. Applying polymers composed of a longer B-block could help but might lead to solubility problems due to negatively shifting the HLB-value. The emulsions prepared from the silicon oil, rapeseed oil and tributyrin surprisingly showed the best long term stability. In general, the BAB-systems show no satisfying behaviour in the formulation of emulsions with long term stability, which might originate from the fact that their diffusion coefficients are too slow compared to low molecular weight surfactants efficiently stabilizing the oil-water interface in emulsions leading to a soon breakdown of the emulsions due to decomposition mechanisms such as creaming, etc. described in chapter emulsion. The emulsions should be prepared again with different ratios of oil to water or water to oil and the formed emulsions tested for their stability. Maybe an improvement of the emulsions stability is possible following this way or by preparing mixtures together with other non-ionic surfactants. The combination of both a low- and a high-HLB surfactant could help to support the newly developed oil-water interface by offering stabilizing surfactants from both sides at the same time. Further pictures of the emulsions formed applying the BAB-triblocks can be found in the appendix.

13.3 BAB-triblock copolymers for efficiency boosting in microemulsions

In the following experiments the behaviour of the non-fluorinated BAB-triblock copolymers as boosting agents in microemulsion at room temperature (25 °C) and elevated temperature (40 °C) were investigated.

The triblock copolymers are spread uniformly in the surfactant membranes increasing their bending rigidity [517] and curvature elasticity [186]. Efficiency boosting has been investigated so far applying block copolymers made from PPO or PEO [186, 518] the AB-diblock-polymers synthesized and studied by S. Garnier [69] and other di- and triblock copolymers. The nature and length of the oil soluble block seems to play an important role for the use of the polymer as efficiency boosters [519]. Hydrophobic or hydrophilic homopolymers showing non-adsorbing behaviour are reported to lead to the opposite effect when used in microemulsions [520]. Oil and water are expelled due to the osmotic pressure resulting in a growing of the excess phase of the microemulsion phase.

Choosing the composition of the amphiphilic block copolymers should enable a smart fine tuning of the efficiency of microemulsions. Nevertheless, more systems should be studied to gain further information in this challenging field. Frank et al. [521] report efficiency boosting for block copolymers with a long hydrophilic block. Therefore, the effect of amphiphilic **PS-PNI-PS** block copolymers of BAB-type with a relatively long hydrophilic PNIPAM (**M1**) block on microemulsion systems- in this case based on toluene as the oil phase and **PS-PNI-PS 3100-50000** as the amphiphilic block copolymer, SDS, sodium docecyl sulphate, as low molecular weight surfactant and pentanol as a co-surfactant (pentanol/oil:50/50 w/w)- should be investigated following the protocol described in the experimental section.

Figure 123 displays the behaviour of the macrosurfactants **PS-PNI-PS 3100-50000** and **PS-PNI-PS 3100-70000** in the microemulsion system SDS/pentanol/toluene. The partial phase diagram of the microemulsion is compared to the partial phase diagram of the microemulsion including 10 % (w/w) of triblock copolymer.

The diagrams were recorded in cooperation with Dr. M. Fechner (UP, AK Prof. Koetz).

a) **T= 25 °C**

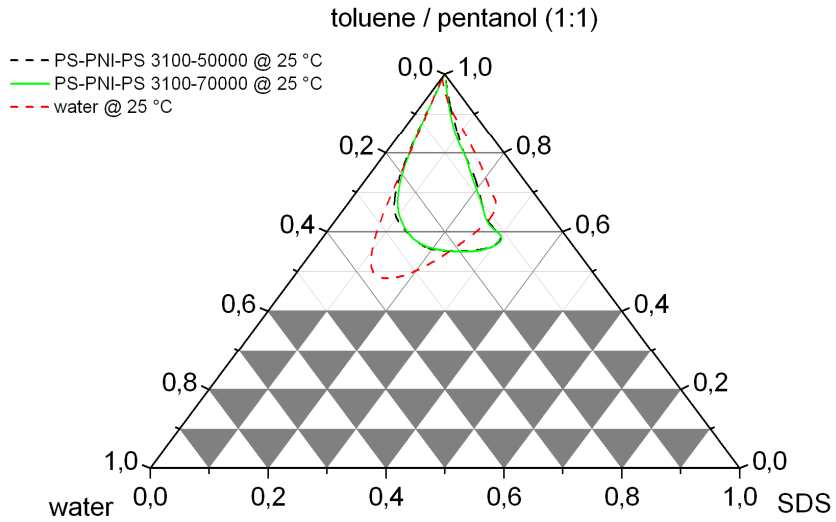

Figure 123-1): Partial phase diagram of the microemulsion system SDS/pentanol/toluene compared to the phase diagram of the microemulsion including 10 % (w/w) of triblock copolymer **PS-PNI-PS 3100-50000** (- - -) and **PS-PNI-PS 3100-70000** (——) at room temperature (25 °C). The red dotted line represents the system without polymer additive. The grey part of the diagram was not further investigated.

b) **T= 40 °C**

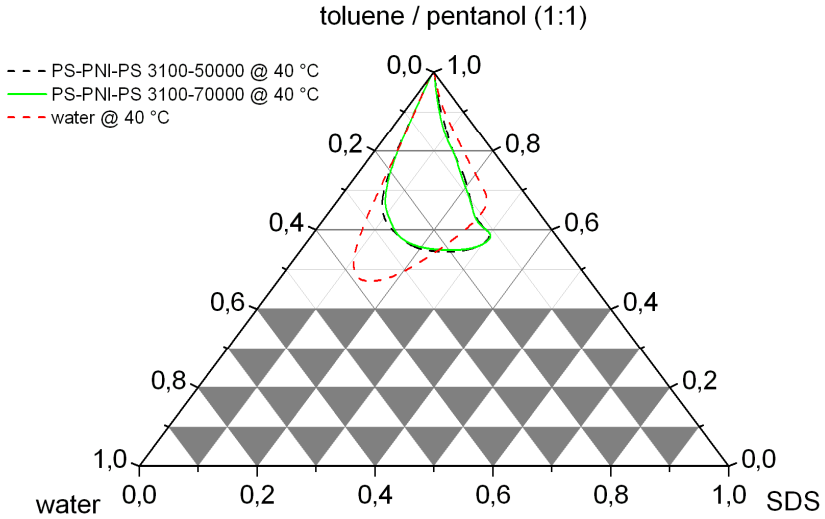

Figure 123-2): Partial phase diagrams of the microemulsion system SDS/pentanol/toluene compared to the phase diagram of the microemulsion including 10 % (w/w) of triblock copolymer **PS-PNI-PS 3100-50000** (- - -) and **PS-PNI-PS 3100-70000** (——) at elevated temperature (40 °C). The red dotted line represents the system without polymer additive. The grey part of the diagram was not further investigated.

Figure 123 shows that the domains of the partial phase diagram representing the basic microemulsion (red) is not congruent to the phase diagrams gained from the systems containing the amphiphilic BAB-block copolymers **PS-PNI-PS 3100-50000** and **3100-70000** at both room temperature (25 °C) and elevated temperature (40 °C). At room temperature and elevated temperature the phase diagrams of the microemulsions with or without polymer additive are almost congruent. Obviously the influence of the slightly longer PNIPAM (**M1**) chain length of the **PS-PNI-PS 70000** series compared to the **50000** series on the phase behaviour is negligible. The domains are shifted towards the surfactant corner, indicating a reduced water uptake of the system. The reason for observing the same effect at room and elevated temperature (above the cloud point of the PNIPAM (**M1**)-middle block) could be originating from strong hydrophobic interactions between the B-blocks (styrene (**M3**)) not depending on the polarity of the PNIPAM (**M1**)-block preventing interaction and adsorption of the block copolymers on the interfacial film of the surfactant in the microemulsion. Most probably the polymer is located inside the droplets. In case it was able to stabilize the interface, the domain of the polymer containing microemulsion would be shifted in direction of the water edge (left corner of the triangular phase diagram), indicating a larger water uptake capacity and thus a boosting effect.

13.3.1 Conclusions on microemulsions

The preparation of microemulsions applying fluorinated and non-fluorinated BAB-systems using toluene/pentanol= 1:1 as a liquid oil phase leads to no boosting effect of the microemulsion at room temperature (25 °C) and elevated temperature (40 °C). The influence of the slightly longer PNIPAM (**M1**) chain length of the **PS-PNI-PS 70000** series compared to the **50000** series on the phase behaviour is obviously negligible. Strong hydrophobic interactions between the B-blocks (styrene (**M3**)) not depending on the polarity of the PNIPAM (**M1**)-block seem to prevent interaction and adsorption of the block copolymers on the interfacial film of the surfactant in the microemulsion. Possibly, recording the phase diagrams using different oils than toluene/pentanol could provide further insights in the influence on the phase behaviour of these polymers in microemulsions.

13.4 Behaviour of BAB-triblock copolymers at the air-water interface

When accumulating at the interface between air and water, the BAB-systems expose their hydrophilic segments (PNIPAM (**M1**)- and PNAP (**M2**)-blocks) towards water and hide their hydrophobic blocks away (PS (**M3**)- and PFS (**M7**)-blocks) from water by orientating them towards the gas phase.

13.4.1 Surface activity of amphiphilic BAB-block copolymer systems

For the aqueous solutions of BAB-triblock copolymer, foam formation was already indicating weak but existing surface activity. The stability of the block copolymer solutions against dilution in aqueous solution proven by DLS measurements was indicating very low CMCs ($< 1 \cdot 10^{-5}$) or the polymers showing no CMC at all [69]. In order to find the CMC values of the BAB-systems, concentration dependent measurement of the surface tension keeping the temperature constantly at 25 °C were tried.

13.4.2 Determination of the CMC

Compared to low molecular weight surfactants, amphiphilic di- and triblock copolymers show a reduced mobility and slower diffusion rates leading eventually to longer equilibration times [522]. Therefore, the systems should be given enough time to equilibrate before performing the measurement. Furthermore they show lower CMCs/CACs compared to their low molecular weight equivalents [69, 523]. It can be found at concentrations from 10^{-9} to 10^{-4} mol·L (SDS/CTAB: 10^{-3} mol·L) [524, 525, 526]. It is also possible that the CMC/CAC can not be detected at all as described by Rager et al. [527]. Low CMCs/CACs are favourable for many applications because only small amounts of polymers are needed for micelle formation [112]. The CMC gained for fluorinated surfactants is approximately equal to hydrocarbon analogues with 1.5 to 1.8 times longer hydrocarbon chain [98].

The CMC/CAC can be determined by measuring changes in the surface tension applying the plate or ring method, the hanging drop tensiometer, measurements of the equivalent conductance [528, 529], potentiometric titration [530, 531] optical methods like UV-vis spectroscopy based on the Tyndall effect [532, 533], time resolved fluorescence quenching measurements (TRFQ) [534, 535] and dye solubilization methods [536] applying fluorescent dyes such as N-phenyl-1-naphthylimine [537] or others [538]. In this case, the CAC of different BAB-systems varying in the nature and length of the hydrophilic and hydrophobic blocks was investigated at room temperature (25 °C) applying the Du-Nuoy-ring tensiometer for surface tension measurements [82, 120, 539, 540]. The temperature was kept constant important for these measurements for the surface tension being temperature dependent [82, 120]. The systems were equilibrated overnight before the measurement creating an undisturbed, equilibrated surface. All samples were prepared freshly. Exhaustive cleaning avoiding dust or any other impurities, especially residues of organic solvents and grease, are obligatory for obtaining reliable results.

CMC-measurements of BAB-triblock copolymers in aqueous solution (figure 124):

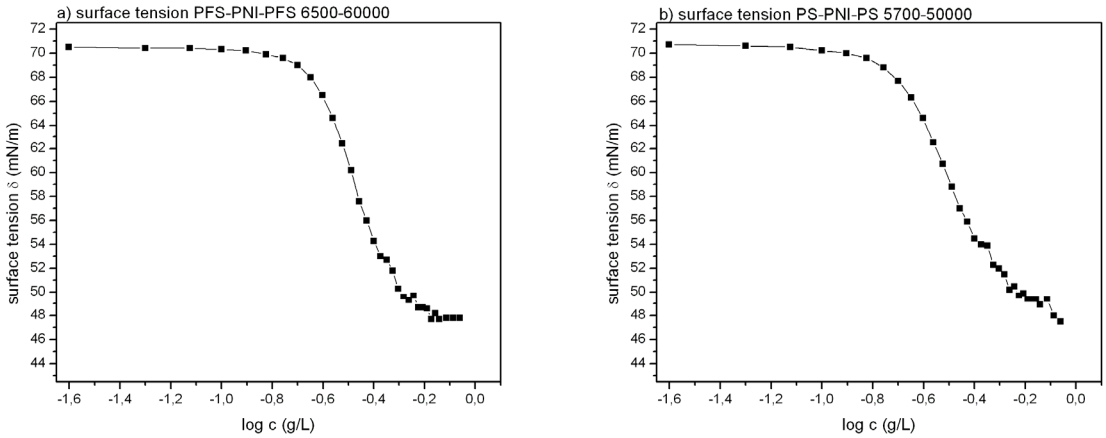

Figure 124: CMC-measuements of polymer a) **PFS-PNI-PFS 6500-60000** and b) **PS-PNI-PS 5700-50000** in water applying the ring method. The stock solution (0.1 g/L) was stepwise diluted (x 0,5 microliters on 20 ml of Millipore water). The temperature was kept constantly at 25 °C. Graphs determined for BAB-systems **PS-PNI-PS 3100-50000**, **3100-70000**, **5700-50000**, **5700-70000**; **PFS-PNI-PFS 4200-80000**, **5500-80000**, **5500-60000**, **FS-PNI-FS** and **PS-PNAP-PS** can be found in the appendix.

All studied samples showed almost the same sigmoidal shape (figure 124). The irregularities observed in the graphs may originate form transitions from [59, 541] U-structure (described in context with adsorption phenomena) to hairpin shape [542] of the polymers localized at the interface, but not indicating the CMC of the polymers. In this context, the ring method does not seem to be useful for determination of the CMC-values of these polymer surfactant systems, as also found by Garnier et al. [69]. Sievers et al. [543, 544] described a smart method for CMC determination applying AFM measurements. Despite on dry surfaces, AFM measurements can also be conducted in solution and the point of micelle formation, which represents the CAC, can be clearly visualized.

Another, different reason explaining the graphs (figure 124) could be the samples still including residues of the surface active poly(PNIPAM) (**M1**) homopolymer. Surface active poly(PNIPAM) homopolymer could be originating from the second step of the block copolymer synthesis. During the chain extension with NIPAM also some PNIPAM homopolymer is generated due to the initiator AIBN (4,4`-azobisisobutyronitrile) starting the polymerization process of the RAFT polymerization (see also chapter RAFT). This problem unfortunately cannot be circumvented when starting the RAFT process using initiators. In order to remove these impurities the samples were homogenized and dialyzed for four days. Since GPC-elugrams revealed no low molecular weight components, the mentioned impurities can be excluded.

13.4.3 Surface tension measurements

The dynamic surface tension can be measured by applying the maximum bubble pressure method or oscillating yet method [145, 180]. For measurements of the equilibrium surface tension, the du-Nuoy-ring method, the Wilhelmy-plate method, the pendant drop method and the capillary rise method can be applied [145, 180]. Another convenient possibility for suface tension measurements are contact angle measurements. [145, 180]. The sessile drop-, adhering bubble method and hanging drop method are frequently used for measuring contact angles.
Applying the hanging drop method, a drop of the liquid is pressed out of a syringe and the shape of the drop recorded using a camera. Tailored analysis software enables the calculation of the surface tension from the drop shape. The apparent contact angle on a surface can also be measured as a function of time [399].

In the literature, most articles found provide data about BAB-systems such as Pluronics® [546-548] or ABA-systems [548, 549] only, but no information about the CMC and surface tension can be found for the new BAB-systems of the synthesized type, neither for the **PS-PNI-PS** nor the **PFS-PNI-PFS** triblock copolymers. The surface tension of the polymers was determined using the hanging drop method [180, 145] (table 3). Prior to measurement all used glassware was exhaustively cleaned and polymer solutions were prepared following the protocol described in the experimental section.

polymer solution in water	surface tension [mN/m]
PS-PNI-PS 3100-70000	45,0
PS-PNI-PS 3100-50000	44,8
PFS-PNI-PFS 6500-80000	44,8
PFS-PNI-PFS 4200-80000	45,0
4FS-PNI-4FS 5600-70000	45,1

Table 3: Values gained for the surface tension applying the hanging-drop method. The concentration of the investigated solutions was 0.1 g/L.

For the hanging drop method, the surface tension was calculated from drop shape pictures applying Image J® analysis software [550, 551]. For all investigated samples, a value of about 45 mN/m (± 0,5) was found independently of the type and length of hydrophobic B (**M3, M6, M7**)-block or length of the hydrophilic PNIPAM (**M1**)-block applying the hanging drop method. This means that the BAB-systems- as described before- show only weak surface activity. The values gained are average values for each sample consisting of a mixture of homologues.

13.4.4 Conclusions surface tension and CMC measurements

Despite the different nature of both hydrophilic A (**M1**)- and hydrophobic B (**M3, M7**)-block, the values found for the surface tension applying the hanging drop method are around 45 mN/m for all systems with only negligible deviations from this value. The amphiphilic molecules show only weak surface activity compared to conventional surfacant systems. It seems that the influence of the fluorinated (**M7)** B-blocks on diminishing the surface tension is almost equal to that of the styrene ones. Maybe prolonged fluorinated blocks might show a more significant influence due to tuning the HLB but might also lead to solubility problems for the fluorinated **PFS-PNI-PFS** and styrene **PS-PNI-PS** systems. For the CMC of the systems, no value could be achieved applying ring-tensiometer measurements. The system seems to have a very low CMC/CAC- if it exists at al. The measurements should be repeated applying more sensitive characterization methods [552, 553].

13.4.5 Fluorine end-capped polymers as surfactants in organic solvents

The use of non-symmetric **CTA XXXV** enabled the smart introduction of the fluorinated moiety via the Z-group of the RAFT agent. The gained fluorine end-capped polymers are not water soluble due to their composition from PS (**M3**) and a fluorinated moiety. Despite the widespread application of surfactants in aqueous systems, these systems could be tried as surfactants in organic solvents [120]. Aggregation studies of these systems in a solvent selective for one of the blocks were performed applying DLS.

Several organic solvents were studied as a selective solvent for either the PS (**M3**) or the fluorinated block. As described for the BAB-systems, also the surfactants carrying a fluorinated moiety consist of a mixture of homologues. Isooctane, decane, heptane, hexane, dioxane, xylene and toluene were tried as solvents. Whereas the first five solvents did not dissolve the polymers at all, toluene and xylene turned out to be good solvents. Toluene turned out to be a selective solvent for the poly(styrene) (**M3**)-block. DLS (table 4) proved the existence of aggregates (probably globular micelles as described for AB-systems) at a block length for the PS (**M3**)-block > 20000 g/mol.

poly(styrene) (PS) (M3)	PDI	Z-average	D_h volume average (nm)
10000	-	-	-
20000	-	-	-
30000	0.07	8.3	7.4
40000	0.16	10	9.5
50000	0.13	10.9	10.5
60000	0.10	12.3	11.7
100000	0.05	17.6	13.9

Table 4: Investigation of the hydrodynamic diameter D_h of micelles prepared from fluorine end-capped polymers choosing toluene as a selective solvent. The concentration of the samples was 1 g/L.

13.4.6 Conclusions on fluorine end-capped polymers as surfactants in organic solvents

The fluorine end-capped polymers are not water soluble due to their composition from PS and a fluorinated moiety. These systems were tried as surfactants in organic solvents applying DLS for the investigation of aggregates. Toluene proved to be a selective solvent for the styrene B (**M3)**-block. DLS proved the existence of aggregates (most probably globular micelles as described for AB-systems) at a block length for the PS block > 10000 g/mol. All studied samples showed no foaming, which can be an advantage in some applications.

Chapter XIV: Conclusions and perspectives

14.1 Conclusions

In this thesis fluorinated and non fluorinated mono- and bifunctional trithiocarbonates of the structure Z-C(=S)-S-R and Z-C(=S)-S-R-S-C(=S)-Z were synthesized for the use as chain transfer agents (CTAs) in the RAFT process. All newly synthesized polymers successfully moderated the radical polymerization process of styrene (**M3**). In order to enable convenient and reliable determination of the molecular masses besides GPC measurements, end-group analysis of the synthesized block copolymers via ^{1}H-, ^{19}F-NMR and UV-vis spectroscopy could be performed by attaching suitable fluorinated groups to the R-groups of the symmetric CTAs and both R- and Z-groups of the non-symmetric CTAs. A further advantage of all the newly prepared RAFT agents is their simple preparation in a one- pot reaction in high yields and the easy purification step by just recrystallizing the raw product from methanol.

Using the RAFT process, symmetric triblock copolymers of type BAB- and fluorine end-capped polymers could be synthesized in just two or one polymerization steps. The RAFT-process enabled the polymerization of hydrophilic monomers such as N-isopropylacrylamide (NIPAM) (**M1**) as well as N-acryloylpyrrolidine (NAP) (**M2**) for the A-blocks and of the hydrophilic styrene (**M3**), 2-fluorostyrene (**M4**), 3-fluorostyrene (**M5**), 4-fluorostyrene (**M6**)

and 2,3,4,5,6-pentafluorostyrene (**M7**) for the B-blocks. All polymers could be synthesized with good control of the molar mass and narrow molar mass distributions.

The properties of the triblock copolymers were investigated using DLS, turbidimetry, rheology, foam height- and surface tension measurements. Furthermore their ability to stabilize emulsions and microemulsions was investigated. The self-assembly behaviour of the block copolymers was studied in dilute, concentrated and high concentrated aqueous solutions. In dilute aqueous solutions the polymers form micelles which could be investigated using DLS and NMR measurements for characterizing their size. The cloud point was determined via turbidimetry and DLS. It is found around 31 °C for the NIPAM (**M1**)- and around 50 °C for the NAP (**M2**) based polymers. The fluorinated end-groups did not shift the cloud point temperature for NIPAM and NAP notably.

Dilute aqueous polymer solutions were showing surface activity; they form foams of only limited stability indicating weak surface activity studied in foam height measurements. The micelles are -typical for polymeric surfactants- stable against dilution to 0.1 g/L, proven by DLS investigations. Furthermore, the foam stability and stability against dilution was compared to standard surfactants such as Triton® X 100, Zonyl® fluorosurfactants, Pluronic® 6400 and others. Other commercially available fluorinated and non-fluorinated polymeric surfactants did not show this foam stability and stability against dilution. Surface tension measurements applying the drop method showed a value of about 45 mN/m for all samples, which points at weak surface activity as already deduced from the foam stability measurements.

At high concentrations, the polymers are able to form hydrogels, which properties were compared depending on their composition. For the investigation of hydrogels, aqueous solutions of the triblocks containing of 10 wt%, 20 wt%, 30- and 40 wt% and finally 50 wt % of polymer were prepared. Among those, the rheology studies showed that physical networks and thus hydrogels are only formed at concentrations around 40 wt% and higher. The 10 wt% solutions were too thin to perform rheology studies; they were investigated using DLS. DLS proved normal solution behaviour showing no bridging. The minimum concentration needed for hydrogel formation decreases with the length of the hydrophobic end-blocks. It seems that high glass transition temperatures favour hydrogel formation, the achieved hydrogels show high mechanical strength. The concentrated samples of the NAP (**M2**) based BAB-systems showed no elasticity during rheology measurements and are not suitable for the preparation of hydrogels.

Furthermore, the BAB-block copolymers were positively tested as emulsifiers for different oils- fluorinated or non-fluorinated. However, the prepared emulsions show only short-term stability.

14.2 Perspectives for further investigations-outlook

The synthesized BAB-triblock copolymers and fluorine end-capped polymers turned out to be polymers possessing interesting features. Some more experiments and measurements should be done to complete the knowledge about these interesting polymers:

- Triblock copolymers with switched block sequence, leading to ABA-systems should be synthesized and compared to the BAB-systems.

- The PNIPAM/PNAP-block (A-block) (**M1, M2**) could be replaced by other polymers, like e.g. PMDEGA or other stimuli-sensitive polymers, comparing the properties of the different systems.

- The PS-block (**M3**) in the fluorine end-capped polymers could be substituted by another hydrophobic polymer such as BuA, comparing the properties of the different polymers, also as surfactants in non-aqueous systems.

- The pentafluorostyrene-blocks (**M7**) should be modified e.g. by attaching glycopolymers or POSS and the effect on micellization and LCST behaviour tested.

- The fluorinated monofunctional RAFT agents should be tried in emulsion polymerization and polymerization in supercritical CO_2, due to the fluorinated tail might provide good solubility in this medium.

- In order to complete investigations on kinetics applying ^{19}F-NMR-studies with fluorinated RAFT-agents, also fluorinated initiators should be synthesized (e. g. labelled V 501). An example is shown in figure 125:

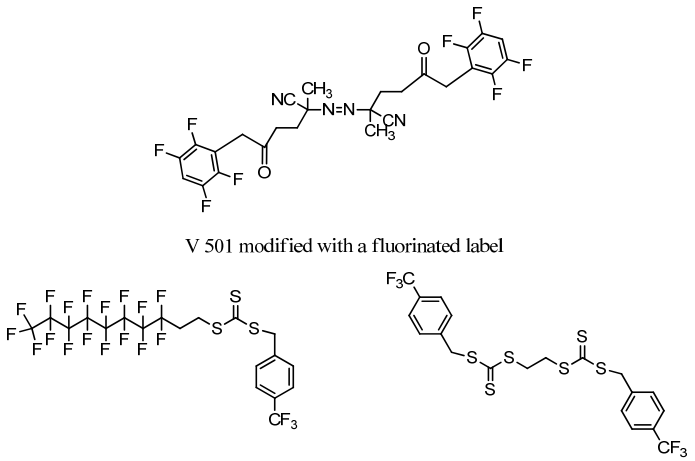

Figure 125: Example for fluorinated initiator and RAFT-agents for ^{19}F-NMR investigations.

- Double fluorinated symmetric RAFT-agents should be synthesized and evaluated, e.g. as shown in figure 126:

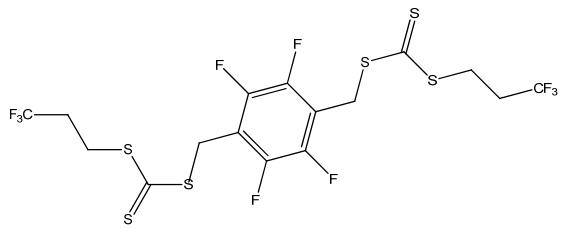

Figure 126: Example for double fluorinated, symmetric RAFT-agent.

- AFM-measurements could be performed for characterization of mechanical properties of gels and determination of the very low (if existing) CMC values.

- The CMC-values should be measured again using a more sensitive method.

- The chosen water-to-oil-ratio may also influence the type of emulsion formed. Other ratios could be tested to improve the emulsions stability.

- Measurement of the surface tension with fluorine end-capped polymers in solvents different from toluene could be tried.

- The wetting behaviour of aqueous solutions containing the newly synthesized BAB-triblock copolymers (fluorinated and non fluorinated) on various high- and low-energy surfaces should be tried.

- Solubilization experiments with fluorinated- and non-fluorinated BAB-block copolymers applying different kinds of oils should be tried.

Chapter XV: Experimental part

15.1 Analytical methods

^{1}H-(300 MHz), **^{13}C-**(75 MHz) and **^{19}F-**(282 MHz) **NMR-spectra** of the synthesized RAFT-compounds and polymers were recorded using a Bruker Avance 300 apparatus (128 scans for ^{1}H-, 10000 scans for ^{13}C- and 19 scans for ^{19}F-spectra).

IR-spectra of the newly synthesized RAFT agents and a selection of polymers were recorded using a Bruker IFS FT-IR spectrometer 66/s.

Mass spectra were tried to be taken using a TSQ Quantum spectrometer from Thermo Finnigan in Louvain-la-Neuve by Raoul Rozenberg (Prof. Dr. Habib-Jiwan) and M. Winkler from Waters using the APCI ionization method.

Elementary analysis was made using a Model EA 1110 (CHNS-O) from CE Instruments (Dr. H. Wetzel, Fraunhofer-Institut für Angewandte Polymerforschung, Potsdam-Golm).

The thermal properties of CTAs, homo- and block copolymers were recorded using a **TGA/SDTA 851** thermal gravimetric analyzer (TGA) from Mettler-Toledo and a DSC 822 differential scanning calorimeter (DSC) from Mettler Toledo under a nitrogen atmosphere. For the TGA analysis, the products were scanned at a rate of 20 °C min^{-1} from 25 °C to 700 °C. The calibration was done on indium and zinc standards. For DSC measurements, the samples were put into an aluminium pan sealed with a lid. The mass of the full pan was noted. The scanning interval was between 25 °C and 180 °C at a rate of 5 °C min^{-1} or 10 °C min^{-1}, respectively.

Gel permeation chromatography (GPC) was performed using an Agilent 1200 isocratic pump equipped with an Agilent 1200 refractive index detector, an Agilent UV detector and a set of Styragel columns pore size 100 and 1000 from PSS GmbH, Mainz, Germany. Eluent: THF (HPLC grade from Acros/Roth). Flow rate 1.0 ml min^{-1}. The calibration was done with poly(styrene) standards from Polymer Standards Service (PSS), Mainz, Germany for all kinds of measured polymers. The measurements were performed at 45 °C for the BAB-triblocks, the other block copolymers were measured at room temperature in THF. The BAB-triblocks were measured applying N,N-dimethylacetamide (DMAc) as an eluent, 0,1 % LiBr was added.

Turbidimetry studies were conducted applying a temperature controlled turbidimeter model TP1 from E. Tepper (Mainz, Germany). As heating and cooling rates 1 °C min were chosen at concentrations of 1 and 2 g/L of polymer solutions, respectively.

Dynamic light scattering measurements were performed applying a High Performance Particle Sizer (HPPS from Malvern Instruments) using a light scattering apparatus equipped with a He-Ne (633 nm) laser and a thermo-electric Peltier temperature controller. The temperature interval lies between 10 to 90 °C degrees. The measurements were performed at the scattering angle of 173 °C ("backscattering detection") at 25 °C (0.1 °C) using the autocorrelation functions analyzed with the CONTIN method . For all the samples the results

were calculated first applying the "multi-modal distribution mode". For monomodal size distributions, the measurement was repeated using the "monomodal distribution mode". Aqueous solutions of the polymers were filtered with a disposable filter and placed in a poly(styrene) or glass cuvette for analysis.

Scanning electron microscopy (SEM) pictures of the prepared micellar solutions were recorded applying a Hitachi "S-4800" equipped with a cryo-device from Gatan Alto 2500 and a sandwich sample holder without cave. For measurement the cryo-preparation was chosen. The sample was sputtered for 120 seconds using a platine source at 3 kV acceleration voltage.

For **rheology measurements** a rheometer AR-G2 from TA Instruments was used. A cone plate made from Titanium (diameter 40 mm, cone angle 1° with gap 30 µm) was applied. Temperature control was achieved applying a Peltier element. A solvent trap filled with water was used to limit solvent evaporation during the experiments. Shear flow measurements under stress control: range between 0.01-100 s^{-1}. Oscillation stress sweep experiment: range 0.01-1000 Pa at 25 °C, frequency 1 Hz. Frequency sweep experiments: range 0.001-100 Hz at 25 °C, oscillatory stress 1 Pa at 1 Hz. All temperature dependent experiments between 15-45 °C (PNIPAM containing samples) and 39-60° C (PNAP containing samples) were performed with a heating/cooling rate of 2 °C/min., ocillatory stress 5 Pa at 1 Hz in controlled gap compensation mode.

Ultrasonication for preparing of the investigated emusions and microemulsions was performed using a US50 from IKA Labortechnik (Germany).

Microscopy was applied for characterizing the emulsions of the prepared block copolymers using a Olympus® BHS light microscope.

Foaming experiments were performed in 10 ml glass cylinders of the same diameter (~ 7 mm) cleaned with piranha acid before use. The samples were sealed with a stopper and homogeneously shaken for 2 min. The height of the foam diminishing with time was compared. All investigated triblock copolymers, polymer- and low-molecular weight surfactants displayed a very good solubility in water. Aqueous micellar solutions of 1 g/L with a constant volume were prepared by directly dissolving the desired amount of copolymer in Millipore water and stirring the aqueous solution overnight. The liquids were transferred into glass tubes (volume 5 ml) and mechanically shaken for one minute. The glass tubes were cleaned applying piranha acid and rinsing with milipore water before use to avoid any contamination with surfactant or polymer residues. For evaluation, the height of the foam was plottet against time and compared with that of the reference surfactants listed. Mixtures of surfactants (polymer/polymer and polymer/low molecular weight surfactant) were investigated, too, mixing two different surfactant solutions (1/1:v/v) and stirring overnight before measurement.

Surface tension data of polymers was collected using a hanging drop tensiometer of S. Karpitschka (MPI-MPG). The measurements were conducted at room temperature. For measurement, a drop of the polymer solution is squeezed out of syringe and the changing contact angle of the drop is measured and compared to pure MILLIPORE water. Image J® was used as an analysis software.

CMC data of the polymer solutions was collected at room temperature (about 296 K) using a Du Nuoy ring-tensiometer K12 from Krüss (Hamburg, Germany).

15.2 Sample preparation

For the preparation of **NMR-samples**, 35 mg of dry polymer or 15 mg of dry CTA were dissolved in about 2 ml of an appropriate deuterated solvent for the measurement of ^{1}H-, ^{13}C- and ^{19}F- spectra. P_4O_{10} was applied as a drying agent for the samples in vacuuo at RT.

IR-spectra were taken from the pure, dry CTA or polymer sample. P_4O_{10} was applied as a drying agent for the samples in vacuuo at RT.

Elementary analysis (EA) was made using pure, dry polymer and CTA samples (dried over P_4O_{10} under vacuo at RT before measurement)

TGA- and DSC-measurements were performed from about 8 and 10 mg of CTA/polymer dried over P_4O_{10} under vacuo at RT shortly before measurement.

Gel permeation chromatography (GPC) elugrams were recorded using solutions of 1 g/mol of polymer in destilled THF. The samples were allowed to dissolve in THF overnight under soft shaking.

Investigations on the turbidity of the polymer samples were performed by preparing polymer solutions of 1 g/L and 2 g/L in MILLIPORE water from dry polymer (dried prior to use in vacuuo over P_4O_{10}). To assure complete dissolution of the polymers, the solutions were shaken overnight.

DLS measurements were performed from aqueous solutions of 1 g/L or 2 g/L of dry BAB-block copolymers at different concentrations by dissolving the samples in MILLIPORE water. The samples were allowed to dissolve overnight under gentle shaking. From the fluorine end-capped systems, solutions of 1 g/L in toluene were prepared from the dry polymers. For the dilution studies, a stock solution of 10 g/L was prepared and stepwise diluted to 1 g/L, 0.1 g/L and some samples to 0.01 g/L. Each sample was equilibrated for 10 minutes before measurement. The solutions of the CF end-capped samples were dissolved in toluene.

SEM samples were prepared from polymer solutions of 1 g/L using MILLIPORE water. The polymer was allowed to dissolve overnight under gentle shaking at room temperature. For measurement the cryo-preparation was chosen. The sample was shock-frozen applying liquid nitrogen to avoid the formation of crystals. The frozen sample was broken at a temperature of -180 °C and subsequently etched for 4 seconds at – 98 °C.

For **rheology measurements**, all used triblock copolymers were dried under vacuo over P_4O_{10} at RT before use. Samples including 10-, 20-, 30-, 40- and 50 wt% of polymer were prepared by dissolving the polymer sample in small jars filled with about 2 ml of pure acetone. The samples were allowed to dry at room temperature for about eight days. Afterwards, the calculated amount of MILLIPORE water was added using a syringe and the jar tightly closed using PARAFILM for sealing. The water was allowed to diffuse into the dry polymer for 14 days resulting in clear liquids or gels depending on the concentration. The gels obtained from the PS-PNAP-PS polymers were slightly yellow.

For the preparation of the oil-in-water (o/w) **emulsions**, 0.015 g of dry polymer (dried over P_4O_{10} under vacuuo), 4.0 g of water and 1.0 g of different oils (sunflower, rapesseed, hexane, nonane, tributyrin, methyl palmitate, hexafluorobenzene and fluorodecaline) were united in

sealable test tubes of the same size and diameter. For preparing the water-in-oil- emulsions (w/o), 0.015 g of dry polymer (dried over P_4O_{10} under vacuuo), 1.0 g of water and 4.0 g of different oils (sunflower, rapesseed, hexane, nonane, tributyrin, methyl palmitate, hexafluorobenzene and fluorodecaline) were united in test tubes of the same size. The non-fluorinated samples were sonicated for 3 min, the fluorinated ones and hexane for 5 min. Short sonication times were chosen in order to avoid destruction of the polymer chains and warming of the sample (thermosensitive PNIPAM blocks might collapse and falsify results)

Microscopic investigations of the emulsions and microemulsions were done by investigation of the emulsion/microemulsion samples directly after preparation on glass slides. A drop of a distinct emulsion was placed between two glass slides (cleaned with ethanol before use) and spread between them. Best results are gained from thin, homogeneously spread samples.

For the preparation of **microemulsions**, MILLIPORE water was applied for the aqueous phase, toluene as the oil phase and SDS, sodium dodecyl sulphate, as surfactant. Pentanol was used as a co-surfactant. The phase diagrams were recorded by titration of the mixture with water or the corresponding solution including the polymeric surfactant **PS-PNI-PS 3100-50000** and **PS-PNI-PS 3100-70000** at RT and 40 °C. A mixture including oil, surfactant and alcohol was prepared first (oil/alcohol:50/50w/w). Then, water or the aqueous polymer solution was added to the system and the mixture was stirred or exposed to an ultrasonic bath (only short time!) until the mixture appeared optically clear (sometimes it is good to wait for some minutes). The isotropic phase in the phase diagram was investigated by dropwise addition of water or the aqueous polymer solution to the mixture.

Foaming experiments were performed using polymer solutions of 1 g/L. The polymers were dried prior to use in vacuuo under P_4O_{10} and dissolved in exactly 2 ml of MILLIPORE water. The solutions were gently shaken at room temperature overnight. For the mixtures of polymeric surfactants with SDS, 1:1 mixtures (v:v) of polymeric surfactants and SDS (1 g/L) were prepared.

For **surface tension measurements**, 0.0050 g of dry polymer was dissolved in 50 ml of MILLIPORE water (0.1 g/L). The samples were gently shaken overnight at room temperature. All used glassware was cleaned with piranha acid prior to use in order to avoid any organic pollution. The tensiometer syringe was cleaned after each measurement using pure acetone and MILLIPORE water for complete removement of impurities.

For **CMC** determination via surface tension, 0.0050g of dry polymer was dissolved in 50 ml of MILLIPORE water (0.1 g/L) for preparing the stock-solution. The solutions were gently shaken overnight at room temperature. For measurement the stock solutions were diluted (x 5 microliter/20 ml) The diluted solutions were stirred for 10 minutes and allowed to equilibrate overnight at room temperature. All used glassware was cleaned with piranha acid prior to use in order to avoid any organic pollution. The tensiometer ring was cleaned after each measurement using pure acetone and glowing using a Bunsen-burner for complete removement of impurities.

For the mixed micelle samples, samples of 1 g/L were prepared and stirred overnight. Then, the solutions were united (v:v= 1:1) and equilibrated overnight before measurement.

15.3 Synthesis of CTAs (+ tables)

15.3.1 Synthesis of symmetric CTAs (see figure 127 and table 5)

W, X, Y, Z values for the precise amounts of reagents are given in table 5. A 500 ml three necked round- bottom flask equipped with a magnetic stirring bar, silicon septum and a silicon oil bubbler was purged with nitrogen for 30 minutes. Then, phase-transfer catalyst Aliquat® 336 (Acros Organics, average MW 442 g/mol) (4 drops) and W g 1,2-ethanediol (Fluka, > 98 %) (0.053 mol) were added using a liquipipette/syringe under nitrogen flow. Y g of sodium hydroxide microprills (Riedel-de-Haën, purum) (0.106 mol) were completely dissolved in 15 ml of distilled water and added dropwise to the reaction mixture under vigorous stirring and cooling the flask at 10 °C (isopropanol-dry ice bath).The solution was stirred for one hour under nitrogen atmosphere before X g of carbon disulfide (Aldrich, low in benzene-content, > 99.9 %) (0.106 mol) were added dropwise. The colour of the reaction mixture immediately turned into bright yellow. The reaction was stirred one further hour at RT before adding Z g of benzyl bromide (Aldrich, 98 %) (0.106 mol) dissolved in a solvent mixture of benzene/hexane (1:1= 150 ml:150 ml) and 50 ml of CS_2. The mixture was stirred at RT overnight. The reaction mixture was completely clear after this time containing a yellow phase.

Purification

First, part of the solvent was removed under vacuuo. Then, the crude product got washed with 200 ml of distilled water for three times. Residual water was removed drying with magnesium sulphate powder (Aldrich, > 97 %). The sulphate powder was filtered off afterwards. In order to remove salt residues completely, the dried liquid was passed over a column of neutral alumina (Acros, mesh 50-200 microns), turning a bit brownish/yellow. The column was washed with hexane/benzene to make sure that no product remained on the column. Solvent residues were then removed in vacuuo and the raw product, a bright yellow solid, dried in the vacuum oven at RT for 24 h. Yield of the crude raw product ~ 100 %.

For further purification, the substance was recrystallized from methanol. 5 g of product were completely dissolved in about 500 ml of methanol (Aldrich, ACS-grade).

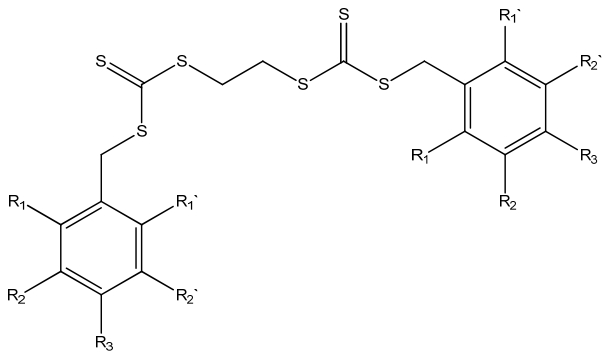

CTA XXXIX: $R_1 = R_{1'} = R_2 = R_{2'} = R_3 = H$
CTA XXXX: $R_1 = R_{1'} = H$ $R_2 = R_{2'} = H$ $R_3 = CF_3$
CTA XXXXI: $R_1 = R_{1'} = H$ $R_2 = R_{2'} = CF_3$ $R_3 = H$
CTA XXXXII: $R_1 = R_{1'} = H$ $R_2 = R_{2'} = H$ $R_3 = F$
CTA XXXXIII: $R_1 = R_{1'} = F$ $R_2 = R_{2'} = F$ $R_3 = H$
CTA XXXXIV: $R_1 = R_{1'} = R_2 = R_{2'} = R_3 = F$

Figure 127: General formula of symmetric trithiocarbonate RAFT agents

symmetric CTA	$HS-(CH_2)_2-SH$ [g] W	CS_2 [g] X	NaOH [g] Y	benzylbromide [g] Z	yield (after recrystalliz.) [%]
CTA XXXIX	5	8.08	4.25	18.16	-*
CTA XXXX	5	8.08	4.25	25.37	89 %
CTA XXXXI	5	8.08	4.25	32.6	82 %
CTA XXXXII	5	8.08	4.25	20.07	81 %
CTA XXXXIII	5	8.08	4.25	25.8	80 %
CTA XXXXIV	5	8.08	4.25	27.71	83 %

Table 5: Amount of chemicals used for synthesis of symmetric trithiocarbonate RAFT agents.* **CTA XXXIX** is a liquid and was not recrystallized from MeOH, yield ~ 97 %.

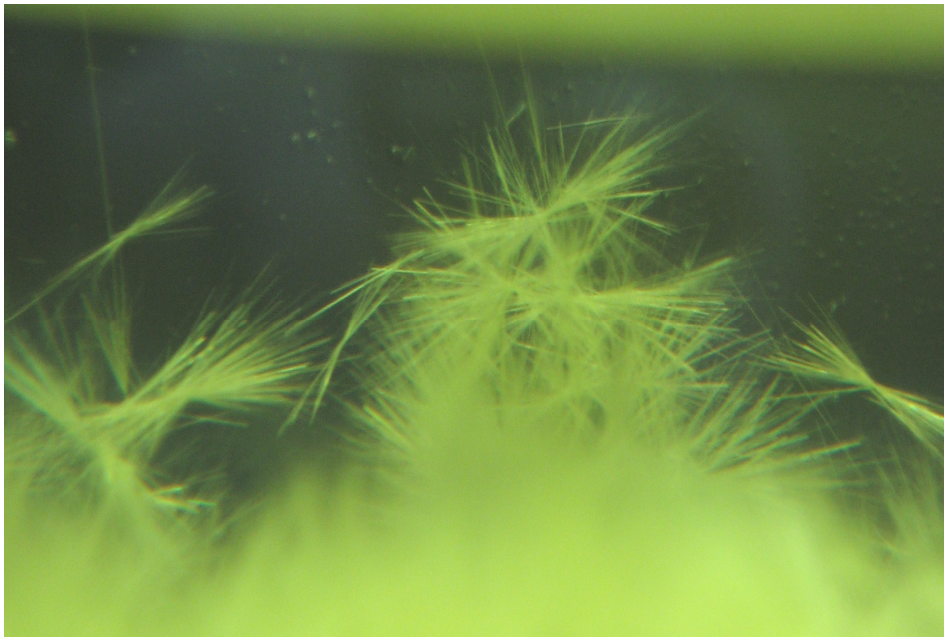

Figure 128: Especially the symmetric CTAs crystallize in shape of long, yellow needles when recrystallized from methanol. The picture shows the crystallisation of bifunctional, symmetric **CTA XXXX**.

15.3.2 Synthesis of non-symmetric CTAs (see figure 129 and table 6)

W, X, Y, Z values for the precise amounts of reagents are given in table 6. A 500 ml three necked round-bottom flask equipped with a magnetic stirring bar, silicon septum and a silicon oil bubbler was purged with nitrogen for 30 minutes. Then, phase-transfer catalyst Aliquat® 336 (Acros Organics, average MW 442 g/mol) (4 drops) and W g 1H,1H,2H,2H-heptadecafluoro-1-decanethiol (Fluka, > 98 %) (0.010 mol) were added using a liquipipette/syringe under nitrogen flow. X g of sodium hydroxide microprills (Riedel-de-Haën, purum) (0.010 mol) were completely dissolved in 15 ml of distilled water and added dropwise to the reaction mixture under vigorous stirring and cooling the flask at 10 °C (isopropanol-dry ice bath).The solution was stirred for one hour under nitrogen atmosphere before Y g of carbon disulfide (Aldrich, low in benzene-content, > 99.9 %) (0.010 mol) were added dropwise. The colour of the reaction mixture immediately turned into bright yellow. The reaction was stirred one further hour at RT before adding Z g of benzyl bromide (Aldrich, 98 %) (0.010 mol) dissolved in a solvent mixture of benzene/hexane (1:1= 150 ml:150 ml) 50 ml of CS_2. The mixture was stirred at RT overnight. The reaction mixture was completely clear after this time containing a yellow phase.

Purification

First, part of the solvent was removed under vacuuo. Then, the crude product got washed with 200 ml of distilled water for three times. Residual water was removed by drying with magnesium sulphate powder (Aldrich, > 97 %). The sulphate powder was filtered off afterwards. In order to remove salt residues completely, the dried liquid was passed over a column of neutral alumina (Acros, mesh 50-200 microns), turning a bit brownish/yellow. The column was washed with hexane/benzene in order to ensure no product remaining on the column. Solvent residues were then removed in vacuuo and the raw product, a bright yellow solid, dried in the vacuum oven at RT for 24 h. Yield of the crude raw product ~ 100 %.

For further purification, the substance was recrystallized from methanol. 5 g of product were completely dissolved in about 500 ml of methanol (Aldrich, ACS grade).

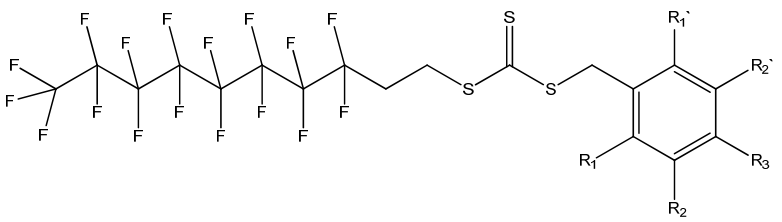

CTA XXXIV: $R_1 = R_{1'} = R_2 = R_{2'} = R_3 = H$
CTA XXXV: $R_1 = R_{1'} = H$ $R_2 = R_{2'} = H$ $R_3 = CF_3$
CTA XXXVI: $R_1 = R_{1'} = H$ $R_2 = R_{2'} = H$ $R_3 = F$
CTA XXXVII: $R_1 = R_{1'} = F$ $R_2 = R_{2'} = F$ $R_3 = H$
CTA XXXVIII: $R_1 = R_{1'} = R_2 = R_{2'} = R_3 = F$

Figure 129: General formula of non-symmetric trithiocarbonate RAFT agents bearing a fluorinated tail

non-symmetric CTA	$F_3C-(CF_2)_7-(CH_2)_2-SH$ [g] W	CS_2 [g] Y	NaOH [g] X	benzyl-bromide [g] Z	yield (after recrystalliz.) [%]
CTA XXXIV	5	0.79	0.42	1.78	85 %
CTA XXXV	5	0.79	0.42	2.49	80 %
CTA XXXVI	5	0.79	0.42	1.97	80 %
CTA XXXVII	5	0.79	0.42	2.53	83 %
CTA XXXVIII	5	0.79	0.42	2.72	83 %

Table 6: Amount of chemicals used for synthesis of non-symmetric trithiocarbonate RAFT agents.

15.4 Monomer synthesis: N-acryloylpyrrolidine (NAP) (M2)

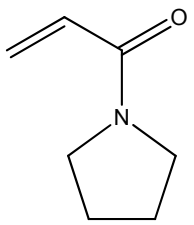

Figure 130: N-acryloylpyrrolidine (NAP) (**M2**)

Synthesis of N-acryloylpyrrolidine (figure 131)

A 500 ml three-necked round bottom flask equipped with a magnetic stirring bar, a silicon bubbler and a thermometer was dried under nitrogen flow with a heating gun for 30 minutes. Afterwards the flask is cooled with an isopropanol-dry ice bath to 10 °C and 86.9 g of acryloyl chloride (0.96 mol, M= 90.51 g/mol, Aldrich, 97 %) in 30 ml of benzene are added dropwise to 68.3 g of pyrrolidinee (0.96 mol, M= 71.12 g/mol, Acros, 98 %) dissolved in 30 ml of dry benzene and 93.25 g of triethylamine (0.96 mol, M= 97.14 g/mol) under vigorous stirring (~ 2 h). The solution must be cooled well because the reaction is strongly isothermic! (figure 131). Under nitrogen atmosphere, the reaction is kept one hour at 5 °C and one further hour at RT to complete the reaction.

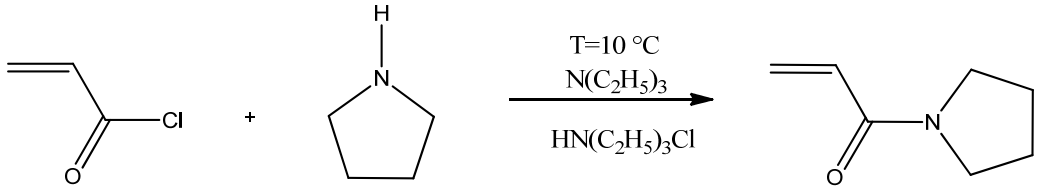

Figure 131: Synthetic path towards N-acryloylpyrrolidine **(M2)**. Strict temperature control is necessary during the synthesis.

Purification

In order to remove the salt residue, the solution is filtered applying a Büchner funnel. The filter cake is washed with benzene (3* 50 ml) until the washings are colourless. The solvent is then removed in vacuuo yielding a brownish-yellow liquid. The substance is mixed with calcium hydride and carefully destilled in vacuuo (0.33-0.29 mbar, T= 63 °C).

Yield: 40 %

15.5 Purification of initiators, solvents and monomers

Before the polymerization or reaction,

2,2`-azobisisobutyronitrile (**AIBN**) (Fluka) was recrystallized from MeOH (reagent plus, > 99 % from Aldrich) and dried under vacuuo at RT. The initiator was stored in the fridge (4 °C)

2-(carbamoylazo)-isobutyronitrile, (**V 30**), was used without further purification (Wako Chemicals). The initiator was kept in the fridge (4 °C) before use.

Tetrahydrofuran (**THF**, Baker, ultra resi analyzed) was destilled over Na/K before use in order to remove the inhibitor BHT as well as dangerous peroxides. The liquid was stored under argon in brown bottles.

N,N-isopropylacrylamide (**NIPAM**) (**M1**) was recrystallized from hexane/benzene three times. 10 g of NIPAM were dissolved completely in 800 ml of hexane (Baker) and 30 ml of benzene (Aldrich, thiophene-free, ≥ 99 %) for removing the stabilizer MEHQ (methyl hydroxyquinone). The white needles were dried in vacuuo at RT for 48 h. The stock was stored in the fridge (4 °C)

N-acryloylpyrrolidine (**NAP**) (**M2**) was purified by distillation before the polymerization in order to remove amine and salt residues originating from the synthesis. The destilled monomer was stored in the fridge (-20 °C).

2,3,4,5,6-pentafluorostyrene (**M7**) was purified by distillation before the polymerization in order to remove the added stabilizer p-tert.-butylcatechol. The destilled monomer was stored in the fridge (-20 °C).

2-fluorostyrene (**M4**) was purified by distillation before the polymerization in order to remove the added stabilizer p-tert.-butylcatechol. The destilled monomer was stored in the fridge (-20 °C).

3-fluorostyrene (**M5**) was purified by distillation before the polymerization in order to remove the added stabilizer p-tert.-butylcatechol. The destilled monomer was stored in the fridge (-20 °C).

4-fluorostyrene (**M6**) was purified by distillation before the polymerization in order to remove the added stabilizer p-tert.-butylcatechol. The destilled monomer was stored in the fridge (-20 °C).

Styrene (**M3**) was purified by distillation before the polymerization in order to remove the added stabilizer. The destilled monomer was stored in the fridge (-20 °C).

15.6 Polymer synthesis (+ tables)

All polymerizations were performedin a 50- or 100 ml round bottom flask equipped with a magnetic stirring bar, sealed with a silicon septum. After purging the samples with nitrogen, the septum was sealed with parafilm and the flask was located in a tempered silicon oil bath for a given time. The oil bath was tempered at the needed temperature for at least one hour before use.

15.6.1 Synthesis of homopolymers (figure 132, 133 + table 7)

W, X, Y, Z values for the precise amounts of reagents are given in table 7).
The monomers were polymerized in bulk applying the symmetric, bifunctional RAFT-agent **CTA XXXX** (figure 132, 133). In order to remove oxygen present in the reaction mixture, each flask was purged with nitrogen for 20 minutes (pressure 1 bar) prior to polymerization. Polymerizations performed with fluorinated monomers (**M4, M5, M6, M7**) W (**M4, M5, M6, M7**) were initiated using initiator V 30 (WAKO) Y; styrene (**M3**) W (**M3**) was initiated thermally. The polymerization temperatures were 120 °C for the initiator-initiated Y and 110 °C for the thermally initiated case. M_{wth} should not exceed 10000 g/mol. The polymerizations were stopped by cooling the flasks with liquid nitrogen. For purification, the cooled down samples were diluted with about 10 ml of pure, destilled THF and precipitated three times in 250 ml of methanol. The polymer was then separated with a Büchner funnel and dried under vacuo for 48 h at RT. The ratio and amount of CTA, monomer and initiator used can be found in table 7. The end-group functionalization was checked applying ^{19}F-NMR.

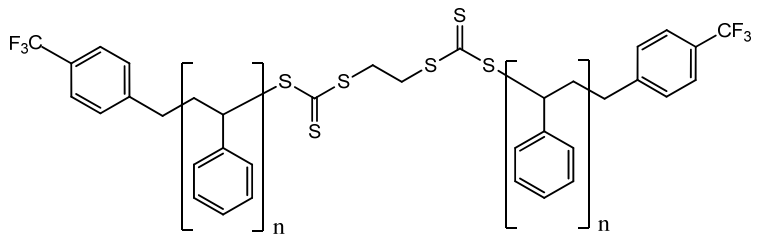

Figure 132: Poly(styrene) (**M3**) homopolymer gained using bifunctional, symmetric **CTA XXXX.**

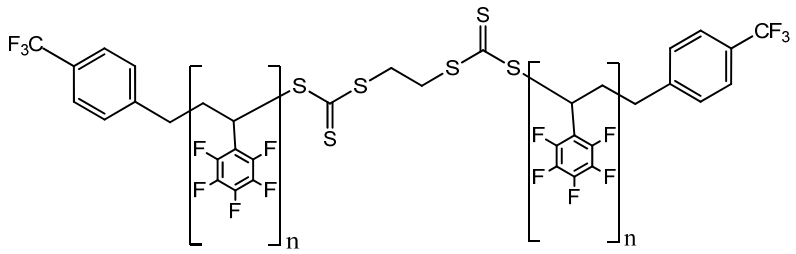

Figure 133: 2,3,4,5,6-poly(pentafluorostyrene) (**M7**) homopolymer gained using bifunctional, symmetric **CTA XXXX.**

15.6.2 Synthesis of BAB-triblock copolymers (Figure 134, 135, 136 + table 7)

W, X, Y, Z values for the precise amounts of reagents are given in table 7, page 166). For the synthesis of the BAB-triblock copolymers (figure 134, 135), the macro-PS-RAFT/macro-PFS-RAFT agent/macro-FS-RAFT agent X and Y g of recrystallized AIBN, W g of recrystallized NIPAM (**M1**) and Z g of THF (destilled over Na/K) were united in a 50 ml round bottom flask, equipped with a silicon septum. The flask was purged with nitrogen for 20 minutes. The silicon septum was fixed using some additional wire. The polymerization was conducted at a temperature of 65 ° C for 48 h for the **PS-PNI-PS** and at 60 °C for 48 h for all other samples. The ratio and amount of macro-CTA, monomer and initiator used can be found in table 7. M_{wth} of **50000**, **70000**, **80000** and **100000** were chosen.
The polymerization was stopped by cooling the flasks with liquid nitrogen. The contents of the flask was dialyzed (THF against destilled water) for 3-4 days applying a dialysis-membrane with a cut-off of 3500 g/mol. The water was changed three times a day. Afterwards the gained, clear solutions were freeze-dried.

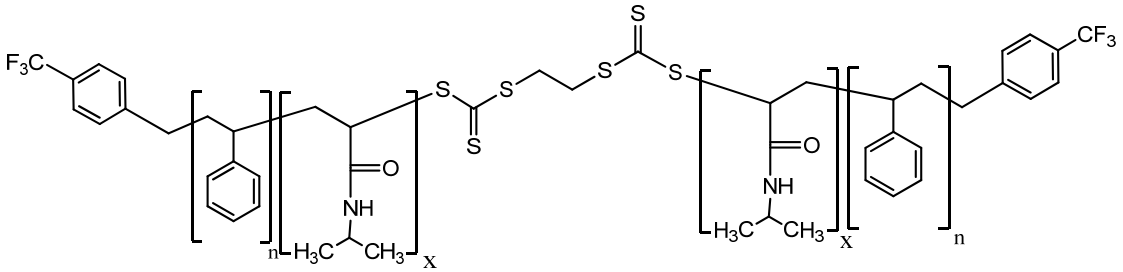

Figure 134: PS-PNI-PS triblock copolymer gained using bifunctional, symmetric **CTA XXXX.**

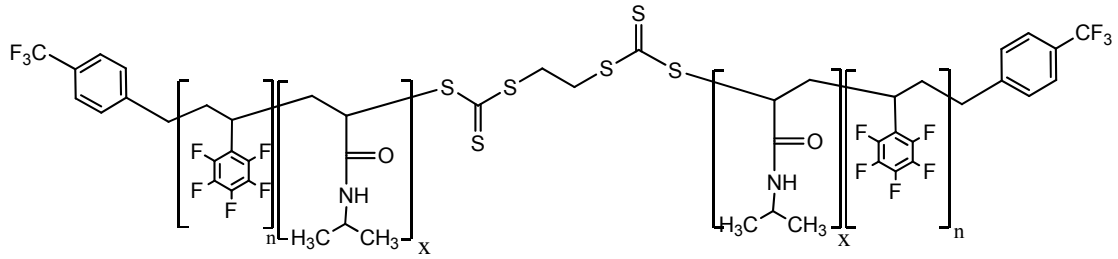

Figure 135: PFS-PNI-PFS triblock copolymer gained using bifunctional, symmetric **CTA XXXX.**

For the synthesis of the BAB-triblock copolymer containing NAP (**M2**) (figure 136) for the thermosensitive block, X g of the macro-PS-RAFT agent, W g of destilled NAP (**M2**), Z g of THF (destilled over Na/K) and Y g of AIBN were united in a 50 ml round bottom flask, equipped with a silicon septum. The flask was purged with nitrogen for 20 minutes. The silicon septum was fixed using some additional wire. The polymerization was conducted at a temperature of 60 ° C for 48 h. The ratio and amount of macro-CTA, monomer and initiator used can be found in table 7. M_{wth} of **50000** and **70000** were chosen for the hydrophilic block. The polymerization was stopped by cooling the flasks with liquid nitrogen. The contents of the flask was dialyzed (THF against destilled water) for 3-4 days using a dialysis- membrane with a cut-off of 3500 g/mol, changing the water three times a day. Afterwards the gained solutions were freeze-dried.

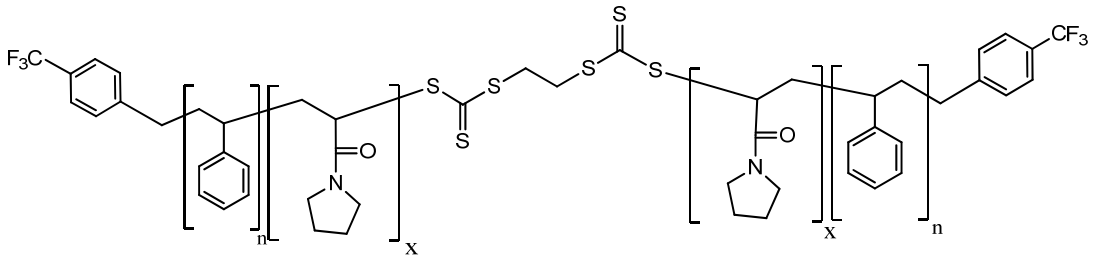

Figure 136: PS-PNAP-PS triblock copolymer gained using bifunctional, symmetric **CTA XXXX.**

polymer **PS-PNI-PS**	**monomer** [mmol] [g] W	**RAFT agent/** **macroRAFT agent [mmol]** [g] X	**AIBN** [mmol] or **V 30** [mmol] [g] Y	**solvent/** **bulk** [ml] Z	**polym. time** [min] [h]	**molar mass** [g/mol] GPC	**molar mass** [g/mol] NMR	**molar mass** [g/mol] calc. [theo.]	**D**
PS(M3) **3100**	96 10 b)	0.2 1.13	thermal initiation @ 110 °C	bulk	1020	3076 (d)	3520	2750 (g)	1.1

PS(M3) **5700**	96 10 b)	0.1 0.56	thermal initiation @ 110 °C	bulk	1080	5710 (d)	5720	5410 (g)	1.1
PS(M3) **4400**	96 10 b)	0.1 0.56	thermal initiation @ 110 °C	bulk	780	4410 (d)	4360	4100 (g)	1.1
PS-PNI-PS **3100-50000**	44 a) 5 b)	0.10 0.31	0.01 0.0016	THF c) 25g	48h	13510 f)	-	41500 (g)	1.8
PS-PNI-PS **3100-70000**	44 a) 5 b)	0.071 0.22	0.0071 0.0012	THF c) 25g	48 h	14300 f)	-	58500 (g)	1.9
PS-PNI-PS **5700-50000**	44 a) 5 b)	0.10 0.57	0.01 0.0016	THF c) 25g	48 h	13770 f)	-	43400 (g)	1.8
PS-PNI-PS **5700-70000**	44 a) 5 b)	0.071 0.41	0.0071 0.0012	THF c) 25g	48 h	14150 f)	-	61000 (g)	1.9
PS-PNI-PS **4400-50000**	44 a) 5 b)	0.10 0.45	0.01 0.0016	THF c) 25g	48 h	14600 f)	-	42200 (g)	1.7
PS-PNI-PS **4400-70000**	44 a) 5 b)	0.071 0.32	0.0071 0.0012	THF c) 25g	48 h	14700 f)	-	63500 (g)	1.9
polymer **PFS-PNI-PFS**	**monomer** [mmol] [g] W	**RAFT agent/** **macroRAFT agent** [mmol] [g] X	**AIBN** [mmol] or **V 30** [mmol] [g] Y	**solvent/** **bulk** [ml] Z	**polym. time** [min] [h]	**molar mass** [g/mol] GPC	**molar mass** [g/mol] NMR	**molar mass** [g/mol] calc. [theo.]	**D**
PFS 4200 (M7)	20.6 4 b)	0.40 0.23	0.399 0.0056	bulk	21 min	4200 d)	5140 e)	1340 (g)	1.2

			@ 120 °C						
PFS 4500 (M7)	20.6 4 b)	0.40 0.23	0.399 0.0056 @ 120 °C	bulk	40 min	4450 d)	5760 e)	2460 (g)	1.2
PFS 5500 (M7)	20.6 4 b)	0.40 0.23	0.399 0.0056 @ 120 °C	bulk	60 min	5540 d)	6980 e)	4100 (g)	1.2
PFS 6500 (M7)	20.6 4 b)	0.40 0.23	0.399; 0.0056 @ 120 °C	bulk	80 min	6460 d)	7660 e)	5000 (g)	1.2
PFS 7200 (M7)	20.6 4 b)	0.40 0.23	0.399 0.0056 @ 120 °C	bulk	100 min	7190 d)	8150 e)	5700 (g)	1.2
PFS-PNI-PFS 5500-60000	26.5 a) 3 b)	0.05 0.35	0.005 0.008	THF c) 15	48 h	13700 f)	-	49600 (g)	2
PFS-PNI-PFS 6500-60000	26.5 a) 3 b)	0.05 0.38	0.005 0.008	THF c) 15	48 h	14700 f)	-	51900 (g)	2
PFS-PNI-PFS 7200-60000	26.5 a) 3 b)	0.05 0.41	0.005 0.008	THF c) 15	48 h	17300 f)	-	52200 (g)	1.7
PFS-PNI-PFS 4200-80000	26.5 a) 3 b)	0.04 0.19	0.004 0.0006	THF c) 15	48 h	12100 f)	-	72300 (g)	2.3
PFS-PNI-PFS 4500-80000	26.5 a) 3 b)	0.04 0.22	0.004 0.0006	THF c) 15	48 h	15600 f)	-	72400 (g)	2.0
PFS-PNI-PFS 5500-80000	26.5 a) 3 b)	0.04 0.26	0.004 0.0006	THF c) 15	48 h	15700 f)	-	71100 (g)	1.7
PFS-PNI-PFS 6500-80000	26.5 a) 3 b)	0.04 0.29	0,004 0,0006	THF c) 15	48 h	19500 f)	-	73500 (g)	2

PFS-PNI-PFS **7200-80000**	26.5 a) 3 b)	0.04 0.31	0.004 0.0006	THF c) 15	48 h	20200 f)	-	69200 (g)	1.7
PFS-PNI-PFS **5500-100000**	26.5 a) 3 b)	0.03 0.21	0.003 0.0005	THF c) 15	48 h	16600 f)	-	88900 (g)	2
PFS-PNI-PFS **6500-100000**	26.5 a) 3 b)	0.03 0.23	0.003 0.0005	THF c) 15	48 h	21700 f)	-	89500 (g)	1.7
PFS-PNI-PFS **7200-100000**	26.5 a) 3 b)	0.03 0.24	0.003 0.0005	THF c) 15	48 h	23600 f)	-	95200 (g)	1.7
polymer **FS-PNI-FS**	**monomer** [mmol] [g] W	**RAFT agent/** **macroRAFT agent** [mmol] [g] X	**AIBN** [mmol] or **V 30** [mmol] [g] Y	**solvent/** **bulk** [ml] Z	**polym. time** [min] [h]	**molar mass** [g/mol] GPC	**molar mass** [g/mol] NMR	**molar mass** [g/mol] calc. [theo.]	**D**
4FS (M6)	24.6 3 b)	0.3 0.17	0.03 0.0042 @ 120 °C	bulk	80 min	5600 d)	-	5280 (g)	1.1
3FS (M5)	24.6 3 b)	0.3 0.17	0.03 0.0042 @ 120 °C	bulk	80 min	6300 d)	-	5930 (g)	1.1
2FS (M4)	16.4 2 b)	0.2 0.11	0.02 0.0028 @ 120 °C	bulk	80 min	5500 d)	-	5190 (g)	1.1
4FS-PNI-4FS **5600-70000**	26.5 a) 3 b)	0.04 0.24	0.004 0.0007 @ 60 °C	THF c) 15	48 h	17700 f)	-	57000 (g)	1.6
3FS-PNI-3FS **6300-70000**	26.5 a) 3 b)	0.04 0.24	0.004 0.0007 @ 60 °C	THF c) 15	48 h	14800 f)	-	61300 (g)	1.9

2FS-PNI-2FS **5500-70000**	26.5 a) 3 b)	0.04 0.24	0.004 0.0007 @ 60 °C	THF c) 15	48 h	19500 f)	-	63500 (g)	1.6
polymer **PS-PNAP-PS**	**monomer** [mmol] [g] W	**RAFT agent/** **macroRAFT agent** [mmol] [g] X	**AIBN** [mmol] or **V 30** [mmol] [g] Y	**solvent/** **bulk** [ml] Z	**polym. time** [min] [h]	**molar mass** [g/mol] GPC	**molar mass** [g/mol] NMR	**molar mass** [g/mol] calc. [theo.]	**D**
PS (M3) **3300**	28.8 3 b)	0.3 0.17	thermal initiation @ 110 °C	bulk	5 h	3300	-	2790 (g)	1.1
PS (M3) **4100**	28.8 3 b)	0.3 0.17	thermal initiation @ 110 °C	bulk	10 h	4100	-	3810 (g)	1.1
PS (M3) **5100**	28.8 3 b)	0.3 0.17	thermal initiation @ 110 °C	bulk	15 h	5100	-	4750 (g)	1.1
PS-PNAP-PS **3300-50000**	2 a) 16 b)	0.04 0.13	0.004 0.0007 @ 60 °C	THF c) 10	48 h	8900 f)	-	40600 (g)	1.8
PS-PNAP-PS **3300-70000**	2 a) 16 b)	0.03 0.09	0.003 0.0005 @ 60 °C	THF c) 10	48 h	10300 f)	-	61400 (g)	1.7
PS-PNAP-PS **4100-50000**	2 a) 16 b)	0.04 0.16	0.004 0.0007 @ 60 °C	THF c) 10	48 h	10600 f)	-	39800 (g)	1.6
PS-PNAP-PS **4100-70000**	2 a) 16 b)	0.03 0.12	0.003 0.0005 @ 60 °C	THF c) 10	48 h	10000 f)	-	63500 (g)	1.8
PS-PNAP-	2 a)	0.04	0.004	THF c)	48 h	12700	-	64100	1.6

PS **5100-70000**	16 b)	0.22	0.0007 @ 60 °C	10		f)		(g)	

Table 7: Amounts of CTA, monomer and initiator, polymerization times and analysis results

a) For diblock copolymers, amount of macro RAFT agent in mmol, with the assumption of 100 % functionalization. Conversion determined by gravimetry.

b) degassing time 20 minutes (pressure of N_2 1 bar)

c) THF was freshly destilled over Na/K prior to use in order to remove residues of peroxide and stabilizer thoroughly.

d) after precipitation (3x) in MeOH from a THF solution

e) molar mass determined applying ^{19}F-NMR

f) molar mass after dialysis against water for three days

g) molar mass calculated from sample weight after freeze-drying

15.6.3 Synthesis of CF-end capped polymers (figure 137 + tables 8 and 9)

For the synthesis of the fluorine end-capped systems (figure 137), the monomers were polymerized in bulk applying the non-symmetric, monofunctional RAFT agent **CTA XXXV**. Therefore, the flask was purged with nitrogen for 20 minutes (pressure 1 bar) in each case. Polymerizations were performed using styrene (**M3**) and thermal initiation. The polymerization was conducted at 110 °C. The reactions were stopped by cooling the flasks with liquid nitrogen. For purification, the cooled down samples were diluted with about 10 ml of pure, destilled THF and precipitated three times in 250 ml of methanol. The polymer was then separated with a Büchner funnel and dried under vacuuo for 48 h at RT.

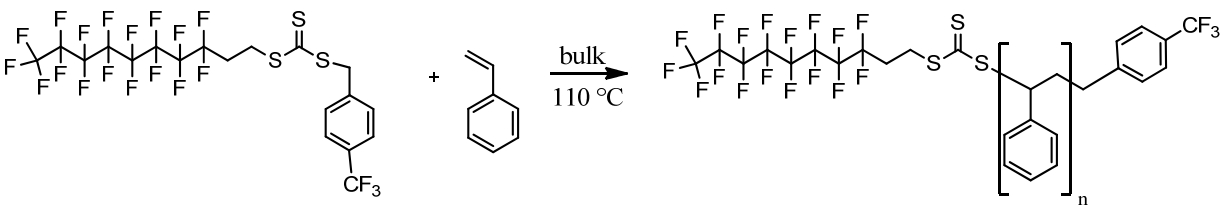

Figure 137: Polymerization of styrene (**M3**) in bulk at 110 °C applying monofunctional, non-symmetric **CTA XXXV.**

sample	momomer (**M3**) [mmol] [g]	RAFT [mmol] [g]	initiator [mmol] [g]	polymerization temperature [°C]	polymerization time [h]	M_nGPC [g/mol]
10000	28.8 ; 3 a)	0.15; 0.107	thermal	110 °C	17	11300 b)
20000	28.8 ; 3 a)	0.075; 0.054	thermal	110 °C	17	21100 b)
30000	28.8 ; 3 a)	0.05; 0.036	thermal	110 °C	17	29500 b)
40000	28.8 ; 3 a)	0.038; 0.027	thermal	110 °C	17	37200 b)
50000	28.8 ; 3 a)	0.030; 0.021	thermal	110 °C	17	44800 b)
60000	28.8 ; 3 a)	0.025; 0.017	thermal	110 °C	17	50000 b)
100000	28.8 ; 3 a)	0.015; 0.011	thermal	110 °C	17	90000 b)

a) degassing time 20 minutes (pressure of N_2 1 bar)

b) after precipitation (3x) in MeOH from a THF solution

Table 8: Polymerization of styrene applying **CTA XXXV**, aiming at Mw_{th}100000.

The kinetic studies were performed using the CTAs and conditions listed in table 9:

CTA	momomer (**M3**) [mmol] [g]	RAFT [mmol] [g]	initiator [mmol] [g]	polymerization temperature [°C]	polymerization time [h]
CTA XXXIV	19.2 ; 2 a)	0.2 ; 0.129	thermal	110 °C	5,10,15,20,25
CTA XXXV	28.8 ; 3 a)	0.3 ; 0.214	thermal	110 °C	5,10,15,20,25
CTA XXXVI	19.2 ; 2 a)	0.2 ; 0.133	thermal	110 °C	5,10,15,20,25
CTA XXXVII	19.2 ; 2 a)	0.2 ; 0.144	thermal	110 °C	5,10,15,20,25
CTA XXXVIII	19.2 ; 2 a)	0.2 ; 0.147	thermal	110 °C	5,10,15,20,25
CTA XXXX	28.8 ; 3 a)	0.3 ; 0.169	thermal	110 °C	5,10,15,20,25
CTA XXXXII	19.2 ; 2 a)	0.2 ; 0.114	thermal	110 °C	5,10,15,20,25
CTA XXXXIII	19.2 ; 2 a)	0.2 ; 0.093	thermal	110 °C	5,10,15,20,25

Table 9: Polymerization of styrene applying non-symmetric CTAs, aiming at Mw_{th}10000. The samples were polymerized 5,10,15,20 and 25 h for kinetic studies.

a) degassing time 20 minutes (pressure of N_2 1 bar)

Polymerizations were performed using styrene (**M3**) and thermal initiation. Again, the reactions were stopped by cooling the flasks with liquid nitrogen. For purification, the cooled down samples were diluted with about 10 ml of pure, destilled THF and precipitated three

times in 250 ml of methanol. The polymer was separated with a Büchner funnel and dried under vacuuo for 48 h at RT.

15.7 DLS- and turbidimetry data

triblock copolymer PS-PNI-PS	**DP_n of hydrophobic block**	**cloud point** [°C]	**D_h** [nm] **25 °C**	**PDI 25 °C**	**D_h** [nm] **35 °C**	**PDI 30 °C**	**D_h** [nm] **45 °C**	**PDI 40 °C**
PS (M3) 3100	30	-	-	-	-	-	-	-
PS (M3) 5700	55	-	-	-	-	-	-	-
PS (M3) 4400	42	-	-	-	-	-	-	-
PS-PNI-PS 3100-50000	30	31.0	60.6	0.23	255	0.18	258	0.43
PS-PNI-PS 3100-70000	30	29.9	57.7	0.72	225	0.07	228	0.37
PS-PNI-PS 5700-50000	55	29.8	162	0.30	686	0.15	698	0.21
PS-PNI-PS 5700-70000	55	30.1	61.1	0.22	202	0.04	203	0.03
PS-PNI-PS 4400-50000	42	-	-	-	-	-	-	-
PS-PNI-PS 4400-70000	42	-	-	-	-	-	-	-
triblock copolymer PFS-PNI-PFS	**DP_n of hydrophobic block**	**cloud point** [°C]	**D_h** [nm] **25 °C**	**PDI 25 °C**	**D_h** [nm] **35 °C**	**PDI 30 °C**	**D_h** [nm] **45 °C**	**PDI 40 °C**
PFS 4200 (M7) 4200	22	-	-	-	-	-	-	-
PFS 4500 (M7) 4450	23	-	-	-	-	-	-	-
PFS 5500 (M7) 5540	29	-	-	-	-	-	-	-

PFS 6500 (M7) 6460	33	-	-	-	-	-	-	-
PFS 7200 (M7) 7190	48	-	-	-	-	-	-	-
PFS-PNI-PFS 5500-60000	29	31.1	66.9	0.18	269	0.04	268	0.59
PFS-PNI-PFS 6500-60000	33	31.5	81.1	0.20	298	0.07	286	1.00
PFS-PNI-PFS 7200-60000	48	29.3	74.4	0.18	308	0.07	312	1.00
PFS-PNI-PFS 4200-80000	22	31.1	65.9	0.22	198	0.02	242	0.17
PFS-PNI-PFS 4500-80000	23	31.3	65.1	0.18	210	0.02	228	0.06
PFS-PNI-PFS 5500-80000	29	31.2	69.7	0.18	280	0.17	321	0.09
PFS-PNI-PFS 6500-80000	33	30.3	62.4	0.20	199	0.02	211	0.04
PFS-PNI-PFS 7200-80000	48	30.3	-	-	-	-	-	-
PFS-PNI-PFS 5500-100000	29	31.1	67.6	0.19	158	0.03	190	0.08
PFS-PNI-PFS 6500-100000	33	31.2	74.5	0.20	222	0.01	246	0.11
PFS-PNI-PFS 7200-100000	48	31.1	73.6	0.17	226	0.01	254	0.11
triblock copolymer FS-PNI-FS	**DP_n of hydrophobic block**	**cloud point** [°C]	**D_h** [nm] **25 °C**	**PDI 25 °C**	**D_h** [nm] **35 °C**	**PDI 30 °C**	**D_h** [nm] **45 °C**	**PDI 40 °C**
4FS (M6) 5600	46	-	-	-	-	-	-	-
3FS (M5) 6300	52	-	-	-	-	-	-	-
2FS (M4) 5500	45	-	-	-	-	-	-	-

4FS-PNI-4FS **5600-70000**	46	30.5	85.7	0.20	486	0.22	427	0.15
3FS-PNI-3FS **6300-70000**	52	30.9	85.9	0.22	486	0.36	499	1.00
2FS-PNI-2FS **5500-70000**	45	30.7	104	0.34	374	0.14	392	0.06
triblock copolymer **PS-PNAP-PS**	**DP_n of hydrophobic block**	**cloud point** [°C]	**D_h** [nm] **25 °C**	**PDI 25 °C**	**D_h** [nm] **35 °C**	**PDI 30 °C**	**D_h** [nm] **45 °C**	**PDI 40 °C**
PS (M3) **3300**	32	-	-	-	-	-	-	-
PS (M3) **4100**	39	-	-	-	-	-	-	-
PS (M3) **5100**	53	-	-	-	-	-	-	-
PS-PNAP-PS **3300-50000**	32	48.1	25.9	0.71	465	0.35	436	0.45
PS-PNAP-PS **3300-70000**	32	49.4	711	0.82	562	0.74	493	1.00
PS-PNAP-PS **4100-50000**	39	48.8	327	0.92	560	1.00	559	627
PS-PNAP-PS **4100-70000**	39	43.9	338	0.63	445	0.26	376	0.30
PS-PNAP-PS **5100-70000**	53	48.4	33.3	0.47	1020	0.70	962	1.00

Table 10: Turbidimetry and DLS data of BAB-block copolymer systems

15.8 Reference oils

- rapeseed oil (Cargill)
- sunflower oil (conventionally available)
- tributyrin (Aldrich, ≥ 97 %)
- methyl palmitate (Aldrich, ≥ 97 %)
- n-nonane (Aldrich, 99 %)
- n-hexane (Baker, 98 %)
- hexafluorobenzene (Aldrich, 99 %)
- perfluorodecaline (Aldrich, 95 %)
- silicone oil M100, medium viscosity (Roth)

15.9 Reference surfactants [495-498]

Triton® X-100 (figure 138) is a widely used non-ionic surfactant. It is applied for example in biochemistry and biotechnology for the recovery of membrane components under mild non-denaturating conditions:

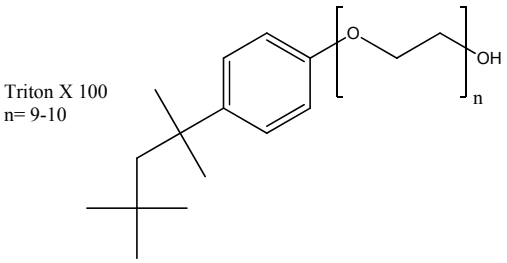

Figure 138: Triton® X-100

SDS (figure 139) is a commonly used low molecular weight surfactant for various applications:

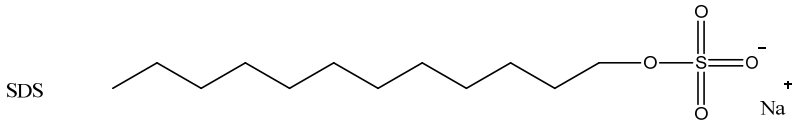

Figure 139: SDS (= sodium dodecyl sulphate)

Brij® 56 (figure 140) is a non-ionic detergent which can be used for example in biochemistry and biotechnology for protein extraction of cells:

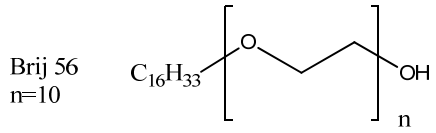

Figure 140: Brij® 56 (several types available)

Tween® 65 (figure 141) is a non-ionic surfactant used for many purposes:

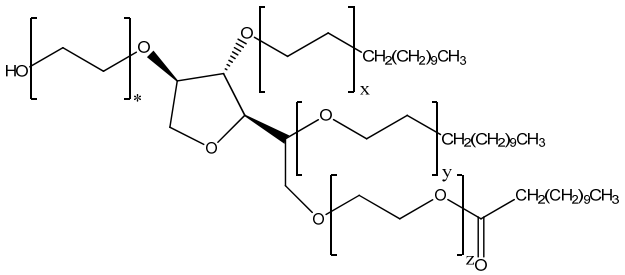

Figure 141: Tween® 65 (several types available)

Pluronics® from BASF (figure 142) are low foaming, non ionic block copolymers showing surfactant properties. They are consisting of a central polypropylene glycol group flanded by two polyethylene glycol groups. The length of the blocks is adapted due to the desired HLB.

The used surfactant Pluronic® PE 6400 is a colorless liquid consisting of a polypropylene glycol block of 1750 g/mol representing 40 % in the molecule and 60 of % polyethylene glycol.

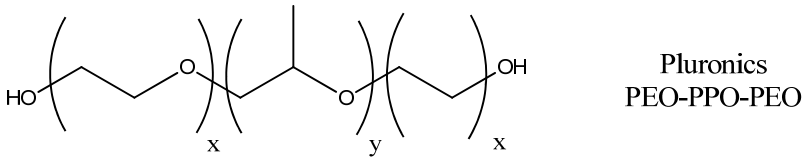

Figure 142: Pluronics® (several types exist)

Zonyl® fluorosurfactants (figure 143) are tailor-made surfactants for different kinds of applications. These fluorosurfactants are block copolymers consisting of a perfluorinated alkyl block. They are available in anionic, kationic, zwitterionic and neutral form. The following fluorosurfactants were used:

Zonyl® FSP is a water soluble anionic phosphate fluorosurfactant giving low aqueous surface tensions with minimal foaming. It can be used as a defoamer. Because of its excellent wetting performance it can be used for coatings, floor waxes, industrial finishes and wood-coatings as well as metal cleaning applications.

Zonyl® FSH 300 is a non-ionic water soluble fluorosurfactant showing very low surface tension in aqueous or solvent based products enabling good wetting, spreading levelling and other useful properties in cleaning products.

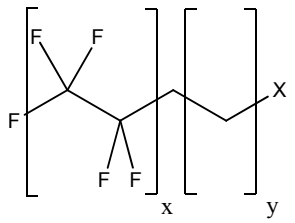

Zonyl
fluorosurfactants

Figure 143: General formula of Zonyl® fluorosurfactants. They are available in anionic, cationic, zwitterionic and neutral form.

15.10 Decomposition temperatures

compound	decomposition temperatures [°C]
PS-PNI-PS **3100-50000**	382
PS-PNI-PS **5700-70000**	387
PFS-PNI-PFS **7200-100000**	374
4FS-PNI-4FS **5600-70000**	185
PFS (**M7**) **4500**	409
PFS (**M7**) **7200**	411
PS-PNAP-PS **4100-50000**	418
PS-PNAP-PS **3300-50000**	417
CF3-RAFT (**CTA XXXX**)	239
CF3-RAFT (**CTA XXXV**)	219
PS (**M3**) mit **CTA XXXX**	355

Table 11: Onset of decomposition temperatures of RAFT agents and polymers

NMR, IR, EA and melting points of newly synthesized non-symmetric and symmetric CTAs and monomer NAP

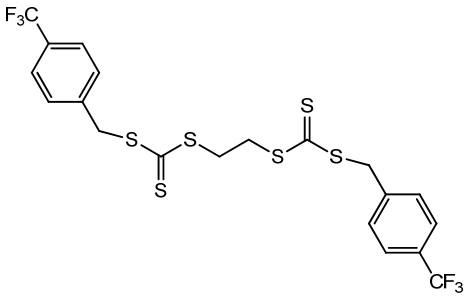

CTA XXXX

MS m/z = 562 (M-1). **EA** ($C_{20}H_{16}F_6S_6$), **M$_r$**= 562.72. Calcd: %C= 42.69; %H= 2.87; %S= 34.19; %F= 20.26. Found: %C= 42.92; %H= 2.65; %S= 35.35
^{1}H-NMR (300 MHz in $CDCl_3$, δ in ppm): δ= 3.71 (s, 4H, -S-CH_2-CH_2-S-), 4.65 (s, 4H, -S-CH_2-aryl), 7.46 (d, 4H, -C-CH=CH- aryl), 7.57 (d, 4H, -CH=C-CF_3 aryl). **^{13}C-NMR** (75 MHz in $CDCl_3$, δ in ppm): δ = 34.90 (-S-CH_2-CH_2-S-), 40.60 (-S-CH_2-aryl), 125.66, 129.52, 139.3 (=C-aryl), 221.63 (-S-(C=S)-S-). **^{19}F-NMR** (282 MHz in $CDCl_3$, δ in ppm): δ= -63.04 (s, 6F, aryl-CF_3). **Melting point**= 105 °C. **IR**= ν (C-H aromat.) ~ 2900 cm^{-1} (w), (aromat.) 1616 cm^{-1} (m), δ (CH_2 def.) 1423 cm^{-1} (m), 1318 cm^{-1}, ν (C-F) 1160 cm^{-1} (s), ν (C=S) 1116 cm^{-1} (s), 1048 cm^{-1} (s), 1019 cm^{-1} (s), 891 cm^{-1} (m), 802 cm^{-1} (s), (CH_2-rocking) 749 cm^{-1} (m), (C=C monosubst. arom.) 704 cm^{-1} (m), 622 cm^{-1} (w), 592 cm^{-1} (w)

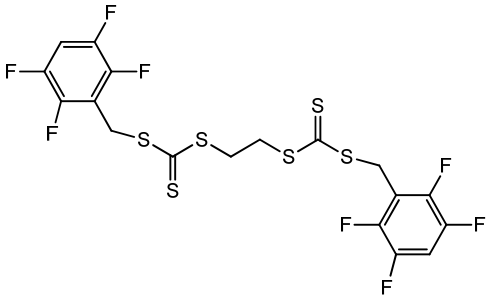

CTA XXXXIII

MS not possible. ($C_{18}H_{10}F_8S_6$), **M$_r$**= 570.65. Calcd: %C= 37.89; %H= 1.77; %S= 33.71; %F= 26.63. Found: %C= 38.09; %H= 1.72; %S= 34.48; %F= 25.72
^{1}H-NMR (300 MHz in $CDCl_3$, δ in ppm): δ= 3.72 (s, 4H, -S-CH_2-CH_2-S-), 4.72 (s, 4H, S-CH_2-aryl), 7.04 (m, 2H, -CF=CF-CH-aryl). **^{13}C-NMR** (75 MHz in $CDCl_3$, δ in ppm): δ= 28.45 (-S-CH_2-CH_2-S-), 34.68 (-S-CH_2-aryl), 105.5, 105.8, 106.1 (-**C**-CF=CF-aryl, **CH**-CF=CF), 114.5 (-CF=CF-aryl), 220.29 (-S-(C=S)-S-). **^{19}F-NMR** (282 MHz in $CDCl_3$, δ in ppm): δ= -138.29 (s, 4F, aryl-**oF**), -141.3 (s, 4F, aryl-**mF**). **Melting point**= 125 °C. **IR**= ν (C-H aromat.) ~ 2900 cm^{-1} (w), (aromat.) 1650 cm^{-1} (w), δ (CH_2 def.) 1504 cm^{-1} (s), 1454 cm^{-1} (m), 1409 cm^{-1} (m), 1382 cm^{-1} (m), ν (C-F) 1258 cm^{-1} (m), 1212 cm^{-1} (m), ν (C=S) 1169 cm^{-1} (m), 1057 cm^{-1} (s), 1012 cm^{-1} (m), 945 cm^{-1} (s), (C-H arom. isolated) 800 cm^{-1} (s), (CH_2-rocking) 711 cm^{-1} (s), 677 cm^{-1} (m), 609 cm^{-1} (m)

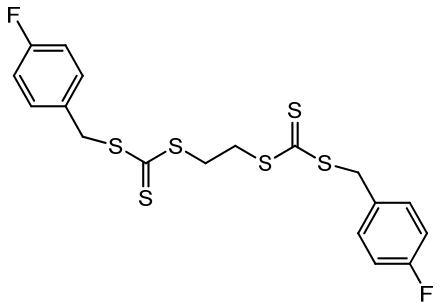

CTA XXXXII

MS not possible. **EA** ($C_{18}H_{16}F_2S_6$), M_r= 462.71. Calcd: %C= 46.72; %H= 3.49; %S= 41.58; %F= 8.21. Found: %C= 47.06; %H= 3.52; %S= 42.08; %F= 7.34
^{1}H-NMR (300 MHz in $CDCl_3$, δ in ppm): δ= 3.95 (s, 4H, -S-CH_2-CH_2-S-), 4.83 (s, 4H, -S-CH_2-aryl), 7.28, 7.53 (m, 8H, CH= CH-aryl, -CH-CF-aryl). **^{13}C-NMR** (75 MHz in $CDCl_3$, δ in ppm): δ= 33.76 (-S-CH_2-CH_2-S), 39.75 (-S-CH_2-aryl), 114.5, 114.79 (-CH=**CH**-CF-aryl), 129.84, 129.95 (-C-**CH**=CH-aryl), 159.68 (-**C**=CH=CH-aryl), 162.95 ((-CH=CH-**C**F-aryl), 221.09 (-S-(C= S)-S-). **^{19}F-NMR** (282 MHz in $CDCl_3$, δ in ppm): δ= -114.43 (s, 2F, aryl-pF). **Melting point**= 108 °C. **IR**= ν (C-H aromat.) ~ 2900 cm^{-1} (w), (aromat.) 1597 cm^{-1} (m), δ (CH_2 def.) 1499 cm^{-1} (m), 1390 cm^{-1} (m), ν (C-F) 1218 cm^{-1} (m), ν (CS) 1157 cm^{-1} (m), 1048 cm^{-1} (s),(C-H aromat. monosubst.) 828 cm^{-1} (s), (CH_2-rocking) 791 cm^{-1} (s), 755 cm^{-1} (s), 718 cm^{-1} (m), 657 cm^{-1} (m)

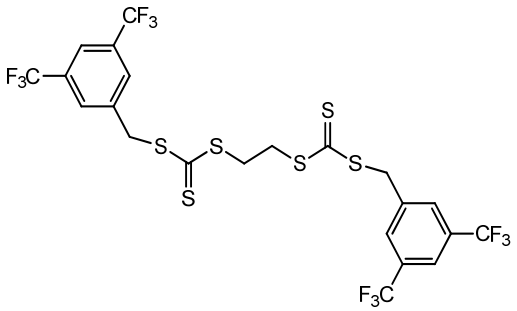

CTA XXXXI

MS not possible. EA ($C_{22}H_{14}F_{12}S_6$), **M_r**= 698.72. Calcd: %C= 37.82; %H= 2.02; %S= 27.53; %F= 32.63. Found: %C= 37.86; %H= 1.93; %S= 27.54; %F= 32.67
^{1}H-NMR (300 MHz in $CDCl_3$, δ in ppm): δ= 3.71 (s, 4H, -S-CH_2CH_2-S-), 4.70 (s, 4H, -S-CH_2-aryl), 7.79 (m, 6H, -C=CH-aryl). **^{13}C-NMR** (75 MHz in $CDCl_3$, δ in ppm): δ= 34.98 (-S-CH_2-CH_2-S-), 39.84 (-S-CH_2-aryl), 121.67 (-C(CF_3)-**C**H-C(CF_3)-), 124.88 (**C**F_3), 129.24 (-C-**C**H=CH-aryl), 132.23 (-C-CH=**C**-(CF_3)-aryl), 138.24, (-**C**-CH=C-(CF_3)-aryl), 220.98 (-S-(C=S)-S-). **^{19}F-NMR** (282 MHz in $CDCl_3$, δ in ppm): δ= -63.34 (s, 12F, aryl-CF_3). **Melting point**= 105 °C. **IR**= ν (C-H aromat.) ~ 2900 cm^{-1} (w), (aromat.) 1627 cm^{-1} (w), δ (CH_2 def.) 1471 cm^{-1} (w), 1370 cm^{-1} (m), ν (C-F) 1280 cm^{-1} (s), ν (CS) 1113 cm^{-1} (s), 1035 cm^{-1} (s), 922 cm^{-1} (w), 901 cm^{-1} (s), 867 cm^{-1} (m), (aromat. isolated H) 800 cm^{-1} (s), (CH_2-rocking) 699 cm^{-1} (s), 677 cm^{-1} (s), 622 cm^{-1} (s)

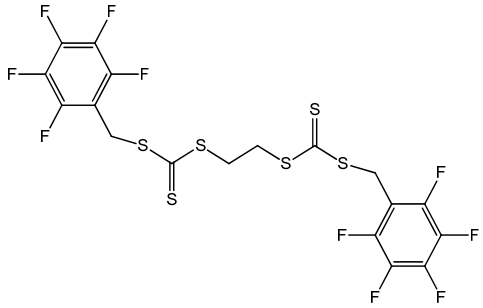

CTA XXXXIV

MS not possible. **EA** ($C_{18}H_8F_{10}S_6$), $\mathbf{M_r}$= 606.63. Calcd: %C= 35.64; %H= 1.33; %S= 31.71; %F= 31.32. Found: %C= 35.89; %H= 1.28; %S= 32.36, %F= 30.47
^{1}**H-NMR** (300 MHz in $CDCl_3$, δ in ppm): δ= 3.73 (s, 4H, -S-CH_2CH_2-S-), 4.7 (s, 4H, -S-CH_2-aryl). ^{13}**C-NMR** (75 MHz in $CDCl_3$, δ in ppm): δ= 27.41 (-S-**C**H_2-**C**H_2-S-), 34.18 (-S-**C**H_2-aryl), 219.55 (-S-(C=S)-S-). ^{19}**F-NMR** (282 MHz in $CDCl_3$, δ in ppm): δ= -140.19 (s, 4F, aryl-**o-F**), 153.49 (s, 4F, aryl-**m-F**), -161.93 (s, 2F aryl-**p-F**). **Melting point**= 106 °C. **IR**= ν (C-H aromat.) ~ 2900 cm^{-1} (w), (aromat.) 1616 cm^{-1} (m), δ (CH_2 def.) 1423 cm^{-1} (m), 1318 cm^{-1}, ν (C-F) 1160 cm^{-1} (s), ν (C= S) 1116 cm^{-1} (s), 1048 cm^{-1} (s), 1019 cm^{-1} (s), 891 cm^{-1} (m), 802 cm^{-1} (s), (CH_2-rocking) 749 cm^{-1} (m), (C=C monosubst. arom.) 704 cm^{-1} (m), 622 cm^{-1} (w), 592 cm^{-1} (w)

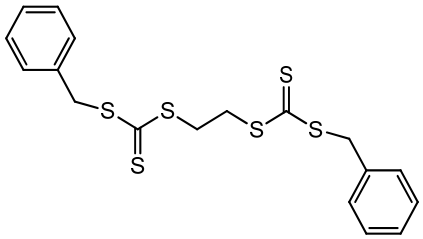

CTA XXXIX

EA ($C_{18}H_{18}S_6$), $\mathbf{M_r}$= 426.73. Calcd: %C= 50.66; %H= 4.25; %S= 45.09
^{1}**H-NMR** (300 MHz in $CDCl_3$, δ in ppm): δ= 3.88 (s, 4H, -S-CH_2-CH_2-S-), 4.56 (s, 4H, -S-CH_2-aryl), 7.27 (m, 10H, -C-CH=CH-aryl). ^{13}**C-NMR** (75 MHz in $CDCl_3$, δ in ppm): δ= 41.34 (-S-CH_2-CH_2-S-), 43.54 (-S-CH_2-aryl), 127.6, 128.52, 129.06 (=C-aryl), 134.73 (-**C**-CH=CH-aryl), 221.82 (-S-(C=S)-S-). **Melting point**= liquid at RT. **IR**= ν (C-H aromat.) ~ 2900 cm^{-1} (w), (aromat.) 1597 cm^{-1} (w), δ (CH_2 def.) 1487 cm^{-1} (m), 1450 cm^{-1} (m), 1401 cm^{-1} (w) 1279 cm^{-1} (w), 1243 cm^{-1} , 1146 cm^{-1}, ν (C=S) 1072 cm^{-1} (s), 950 cm^{-1} (w), 876 cm^{-1} (m), 853 cm^{-1} (m), 804 cm^{-1} (m), (CH_2-rocking) 767 cm^{-1} (w), (C=C unsubst. arom.) 706 cm^{-1} (s)

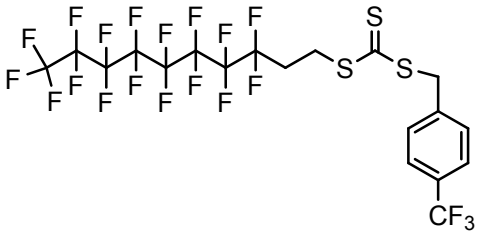

CTA XXXV

MS not possible. **EA** ($C_{19}H_{10}F_{20}S_3$), $\mathbf{M_r}$= 714.45. Calcd: %C= 31.94; %H= 1.41; %S= 13.46; %F= 53.18. Found: %C= 31.64; %H= 1.07; %S= 13.48; %F= 53.81.
^{1}H-NMR (300 MHz in $CDCl_3$, δ in ppm): δ= 2.53 (m, 2H, -CF_2-**CH_2**-), 3.61 (t, 2H, -CH_2-**CH_2**-S-(C=S)-S-), 4.67 (s, 2H, -S-CH_2-aryl), 7.47 (d, 2H, -C-C= CH-aryl), 7.57 (d, 2H, -CH=C-CF_3-aryl). **^{13}C-NMR** (75 MHz in $CDCl_3$, δ in ppm): δ= 27.25 (-S-**CH_2**-CH_2-), 30.30 (-CH_2-**CH_2**-CF_2-), 40.35 (-S-CH_2-aryl), 121.38, 121.95, 125.45 (-CH=CH-aryl), 139.01 (-**C**-CH=CH-aryl), 221.01 (-S-(C=S)-S-). **^{19}F-NMR** (282 MHz in $CDCl_3$, δ in ppm): δ= - 63.12 (s, aryl-CF_3), -81.20 (s, **CF_3**-CF_2-), -114.69 (-CH_2-**CF_2**-CF_2-), -122.28-126.56 (-CF_2-), -126.57 (CF_3-**CF_2**-). **Melting point**= 55 °C. **IR**= ν (C-H aromat.) ~ 2900 cm^{-1} (w), (aromat.) 1609 cm^{-1} (w), δ (CH_2 def.) 1413 cm^{-1} (w), 1316 cm^{-1} (s), ν (C-F) 1194 cm^{-1} (s), ν (C=S) 1157 cm^{-1} (s), 1072 cm^{-1} (s), 1023 cm^{-1} (m), 999 cm^{-1} (m), 950 cm^{-1} (m), (C=C monosubst. arom.) 791 cm^{-1} (m), (CH_2-rocking) 706 cm^{-1} (m), 644 cm^{-1} (w), 560 cm^{-1} (w)

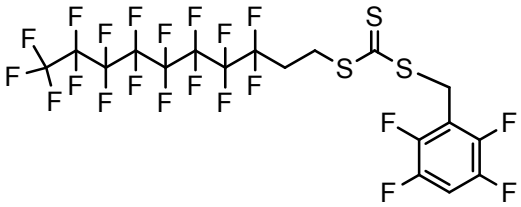

CTA XXXVII

MS not possible. **EA** ($C_{18}H_7F_{21}S_3$), $\mathbf{M_r}$= 718.41. Calcd: %C= 30.09; %H= 0.98; %S= 13.39; %F= 55.53. Found: %C= 29.98; %H= 1.10; %S= 13.50; %F= 55.53.
^{1}H-NMR (300 MHz in $CDCl_3$, δ in ppm): δ= 2.54 (m, 2H, -CF_2-**CH_2**-), 3.62 (t, 2H, CH_2-**CH_2**-S-(C=S)-S-), 4.73 (s, 2H, -S-CH_2-aryl), 7.05 (m, 1H, -CF=CF-CH-aryl). **^{13}C-NMR** (75 MHz in $CDCl_3$, δ in ppm): δ= 27.47 (-S-**CH_2**-CH_2-), 28.63 (-CH_2-**CH_2**-CF_2-), 30.55 (-S-CH_2-aryl), 106.05 (-CF=**C**H-aryl), 220.1 (-S-(C=S)-S-).**^{19}F-NMR** (282 MHz in $CDCl_3$, δ in ppm): δ= -81.20 (s, **CF_3**-CF_2-), -114.7 (-CH_2-**CF_2**-CF_2-), -122.28-123.7 (-CF_2-), -126.51 (CF_3-**CF_2**-), -138.75 (aryl C-**oF**), -141.25 (aryl C-**mF**) . **Melting point**= 71 °C. **IR**= ν (C-H aromat.) ~ 2900 cm^{-1} (w), (aromat.) 1633 cm^{-1} (w), δ (CH_2 def.) 1509 cm^{-1} (s), 1362 cm^{-1} (w), 1338 cm^{-1} (w), ν (C-F) 1191 cm^{-1} (s), ν (C=S) 1142 cm^{-1} (s), 1055 cm^{-1} (m), 1018 cm^{-1} (m), (C-H arom. isolated H) 957 cm^{-1} (s), 847 cm^{-1}, (CH_2-rocking) 798 cm^{-1} (m), 700 cm^{-1} (m), 639 cm^{-1} (w), 552 cm^{-1}

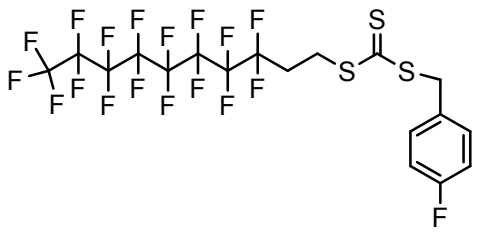

CTA XXXVI

MS not possible. **EA** ($C_{18}H_{10}F_{18}S_3$), $\mathbf{M_r}$= 664.44. Calcd: %C= 32.54; %H= 1.52; %S= 14.48; %F= 51.47. Found: %C= 33.03; %H= 1.36; %S= 14.74; %F= 50.87
^{1}H-NMR (300 MHz in $CDCl_3$, δ in ppm): δ= 2.53 (m, 2H, -CF_2-**CH_2**-), 3.60 (t, 2H, -CH_2-**CH_2**-S-(C=S)-S-), 4.59 (s, 2H, -S-CH_2-aryl), 7.01 (d, 2H, -C-C=CH-aryl), 7.26 (d, 2H, -CH=C-CF-aryl). **^{13}C-NMR** (75 MHz in $CDCl_3$, δ in ppm): δ= 27.52 (-S-**CH_2**-CH_2-), 30.85 (-CH_2-**CH_2**-CF_2-), 40.06 (-S-CH_2-aryl), 115.87, 116.16 (-CH=CH-aryl), 131.19, 131.3 (-**C**-CH=CH-aryl), 221.96 (-S-(C=S)-S-). **^{19}F-NMR** (282 MHz in $CDCl_3$, δ in ppm): δ= -81.17 (s, **CF_3**-CF_2-), -114.37 (-CH_2-**CF_2**-CF_2-), -114.67 (s, aryl C-F) -122.27-126.53 (-CF_2-), -126.54 (CF_3-**CF_2**-). **Melting point**= 70 °C. **IR**= ν (C-H aromat.) ~ 2900 cm^{-1} (w), (aromat.) 1597 cm^{-1} (w), δ (CH_2 def.) 1499 cm^{-1} (m), 1376 cm^{-1} (w), 1328 cm^{-1} (w), ν (C-F) 1194 cm^{-1} (s), ν (C=S) 1146 cm^{-1} (s), 1060 cm^{-1} (s), 1023 cm^{-1} (m), 950 cm^{-1} (m), (C=C monosubst. arom.) 816 cm^{-1} (m), (CH_2-rocking) 706 cm^{-1} (m), 644 cm^{-1} (w), 560 cm^{-1} (w)

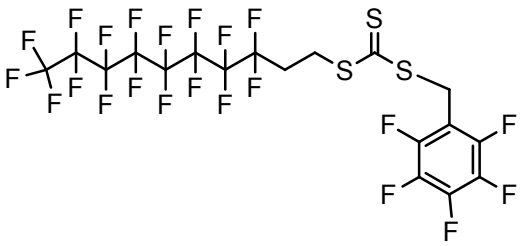

CTA XXXVIII

MS not possible. **EA** ($C_{18}H_6F_{22}S_3$), $\mathbf{M_r}$= 736.40. Calcd: %C= 29.36; %H= 0.82; %S= 13.06; %F= 56.76. Found: %C= 29.46; %H= 0.73; %S= 11.84; %F= 57.97
^{1}H-NMR (300 MHz in $CDCl_3$, δ in ppm): δ= 2.54 (m, 2H, -CF_2-**CH_2**-), 3.62 (t, 2H, -CH_2-**CH_2**-S-(C=S)-S-), 4.69 (s, 2H, -S-CH_2-aryl). **^{13}C-NMR** (75 MHz in $CDCl_3$, δ in ppm): δ= 27.64 (-S-CH_2-aryl), 30.04 (-S-CH_2-CH_2-), (-CF), 127.5 (=C-aryl), 219.53 (-S-(C=S)-S-). **^{19}F-NMR** (282 MHz in $CDCl_3$, δ in ppm): δ= -81.21 (s, **CF_3**-CF_2-), -114.69 (-CH_2-**CF_2**-CF_2-), -122.29-126.56 (-CF_2-), -126.54 (CF_3-**CF_2**-), -140.5 (aryl C-**oF**), -153.85 (aryl C-**mF**), -161,64 (aryl C-**pF**). **Melting point**= 73 °C. **IR**= ν (C-H aromat.) ~ 2900 cm^{-1} (w), (aromat.) 1657 cm^{-1} (w), δ (CH_2 def.) 1499 cm^{-1} (s), 1401 cm^{-1} (w), 1365 cm^{-1} (w), 1328 cm^{-1} (w), ν (C-F) 1206 cm^{-1} (s), ν (C=S) 1132 cm^{-1} (s), 1060 cm^{-1} (m), 974 cm^{-1} (s), 864 cm^{-1} (w), (C=C monosubst. arom.) 816 cm^{-1} (m), (CH_2-rocking) 706 cm^{-1} (m), 632 cm^{-1} (w), 560 cm^{-1} (w)

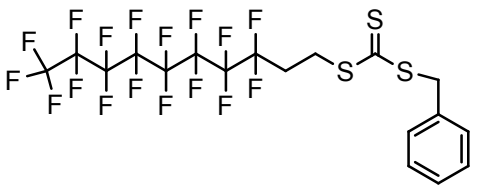

CTA XXXIV

MS not possible. **EA** ($C_{18}H_{11}F_{17}S_3$), M_r= 646.45. Calcd: %C= 33.44; %H= 1.72; %S= 14.88; %F= 49.96. Found: %C= 33.09; %H= 1.52; %S= 14.76, %F= 50.63
^{1}H-NMR (300 MHz in $CDCl_3$, δ in ppm): δ= 2.53 (m, 2H, -CF_2-**CH_2**-), 3.60 (t, 2H, -CH_2-**CH_2**-S-(C=S)-S-), 4.63 (s, 2H, -S-CH_2-aryl), 7.26, 7.33 (m, 5H, -CH=CH-aryl and -C-C=CH-aryl).**^{13}C-NMR** (75 MHz in $CDCl_3$, δ in ppm): δ= 26.31 (-S-CH_2-CH_2-), 29.88 (-CH_2-**CH_2**-CF_2-), 40.96 (-S-CH_2-aryl), 127.22 ,128.07, 128.57 (-S-CH_2-aryl), 221.14 (-S-(C=S)-S-). **^{19}F-NMR** (282 MHz in $CDCl_3$, δ in ppm): δ= -81.18 (s, **CF_3**-CF_2-), -114.7 (-CH_2-**CF_2**-CF_2-),-122.27, -126.5 (-CF_2-), -126.51 (CF_3-**CF_2**-). **Melting point**= 72 °C. **IR**= ν (C-H aromat.) ~ 2900 cm^{-1} (w), (aromat.) 1438 cm^{-1} (w), δ (CH_2 def.) 1353 cm^{-1} (w), ν (C-F) 1194 cm^{-1} (s), ν (CS) 1146 cm^{-1} (s), 1097 cm^{-1} (s), 1060 cm^{-1} (m), 1035 cm^{-1} (w), 999 cm^{-1} (w), 950 cm^{-1} (m), (CH_2-rocking) 791 cm^{-1}, 1060 cm^{-1} (m), (C=C 5H) 706 cm^{-1} (s), 644 cm^{-1} (s), 560 cm^{-1} (m)

Monomer NAP

^{1}H-NMR (300 MHz in $CDCl_3$, δ in ppm): δ= 2.38 (s, 3H, CH_3-), 2.5 (s, 1H, -CH=C(CH_3)-), 3.73 (t, 2H, -CH_2-), 4.10 (t, 2H, -CH_2-OH), 4.92 (s, 1H, HO-), 6.19 (s, 1H, -CH=CH-aryl),6.95 (d, 1H, -CH=CH-aryl), 7.65 (s, 1H, -CH=CH-aryl)

Melting point= substance is a liquid at RT.

NMR- and IR-spectra of RAFT agents

^{1}H-, ^{13}C-, ^{19}F-NMR spectra and IR-spectra of non-symmetric and symmetric CTAs

non-symmetric, monofunctional **CTA XXXV**

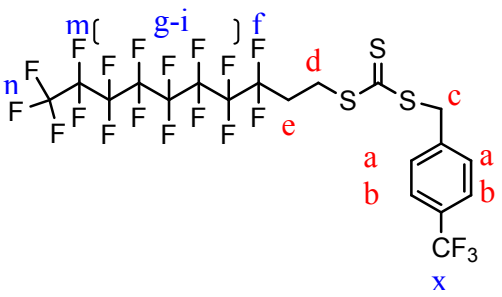

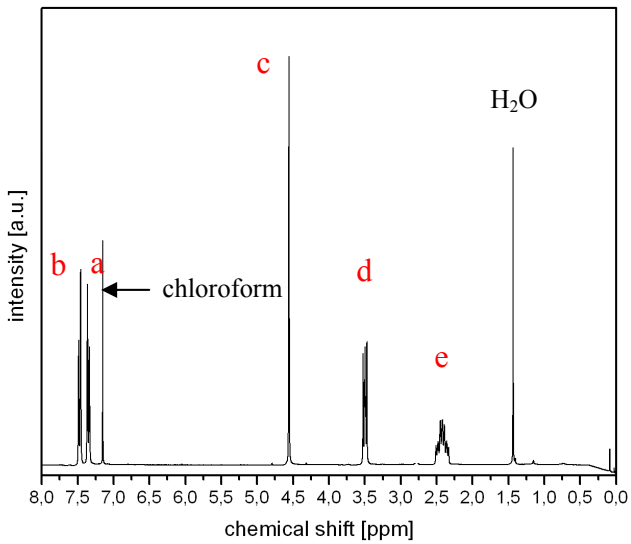

Figure 144: ^{1}H-NMR spectrum of monofunctional **CTA XXXV** in chloroform-d

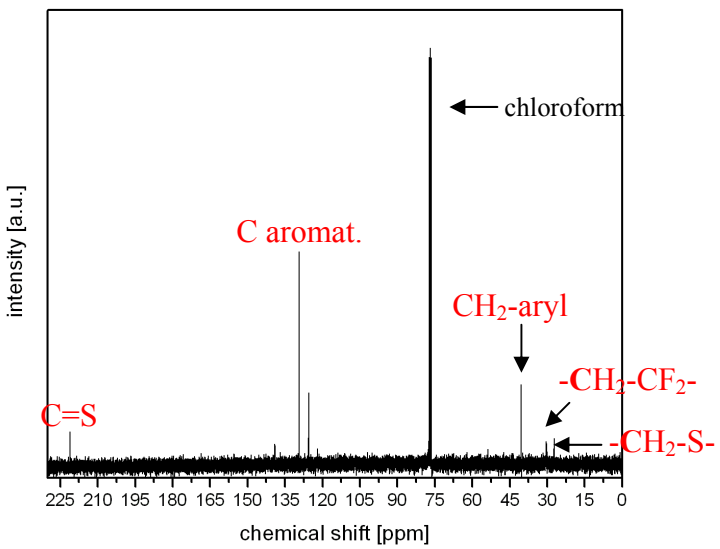

Figure 145: ^{13}C-NMR spectrum of monofunctional **CTA XXXV** in chloroform-d

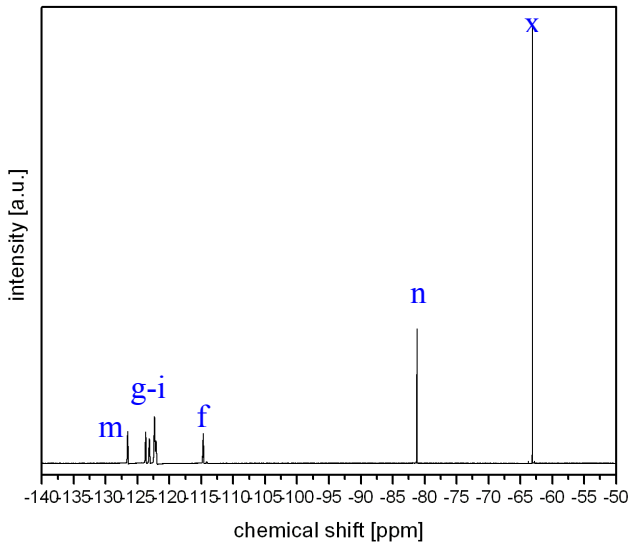

Figure 146: ^{19}F-NMR spectrum of monofunctional **CTA XXXV** in chloroform-d

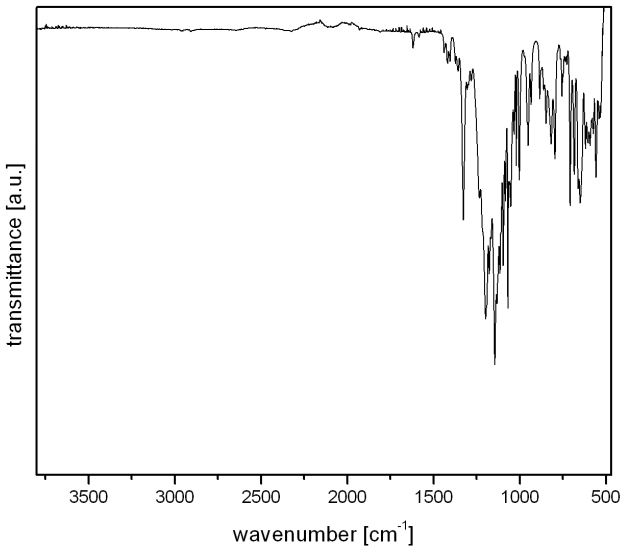

Figure 147: IR-spectrum of monofunctional **CTA XXXV**

symmetric, bifunctional **CTA XXXX**

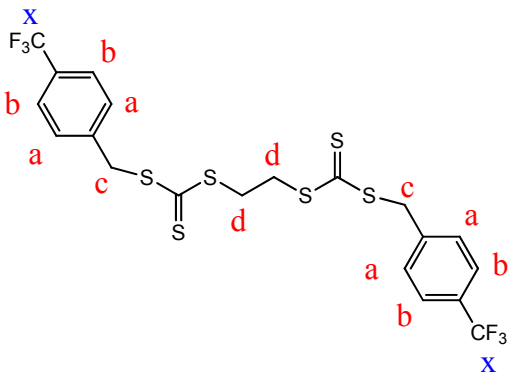

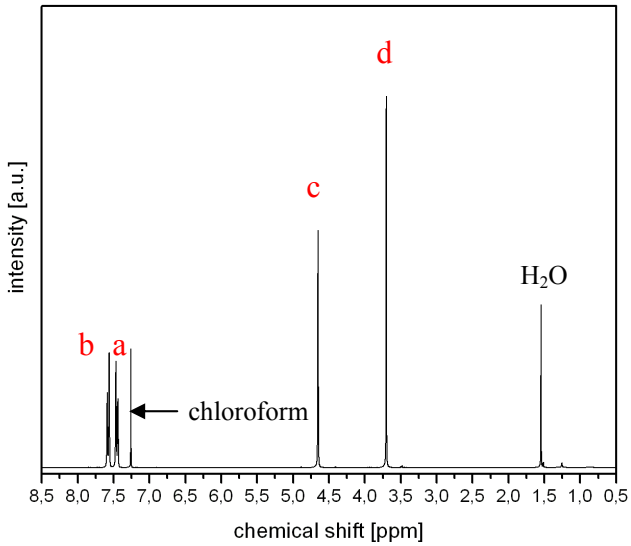

Figure 148: ^{1}H-NMR spectrum of symmetric, bifunctional **CTA XXXX** in chloroform-d

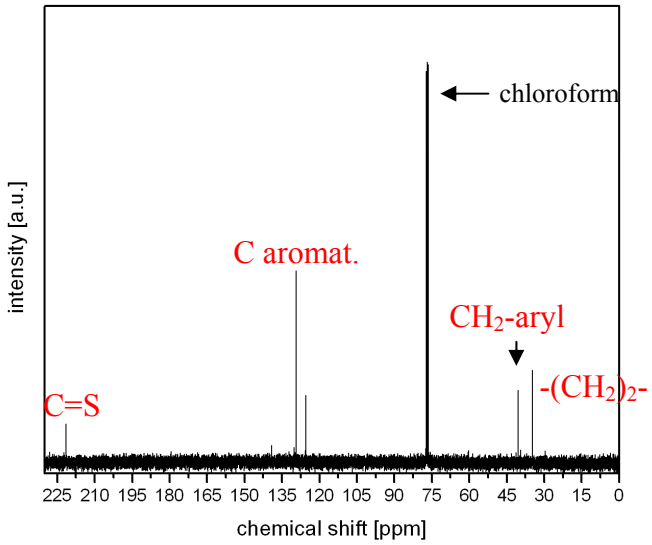

Figure 149: ^{13}C-NMR spectrum symmetric, bifunctional **CTA XXXX** in chloroform-d

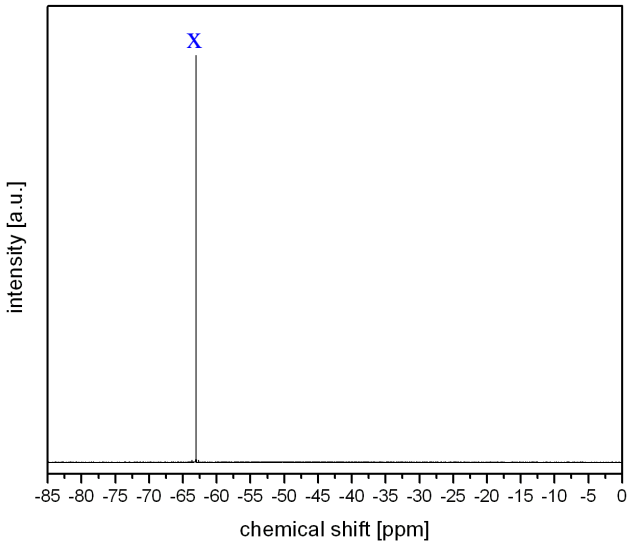

Figure 150: ^{19}F-NMR symmetric, bifunctional **CTA XXXX** in chloroform-d

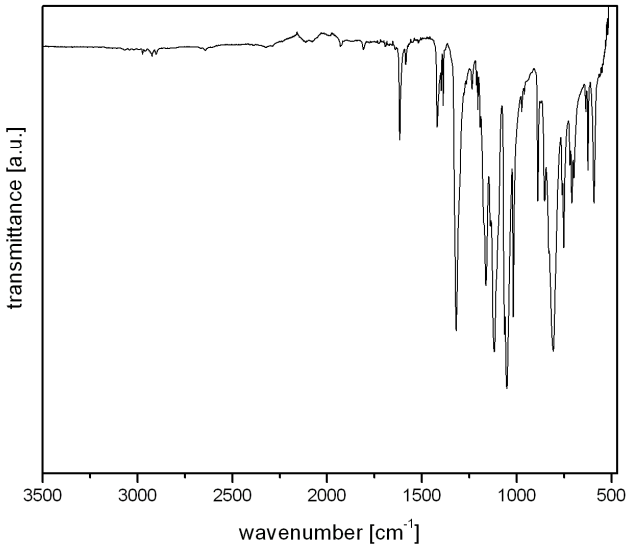

Figure 151: IR-spectrum of symmetric, bifunctional **CTA XXXX** in chloroform-d

non-symmetric, monofunctional **CTA XXXVII**

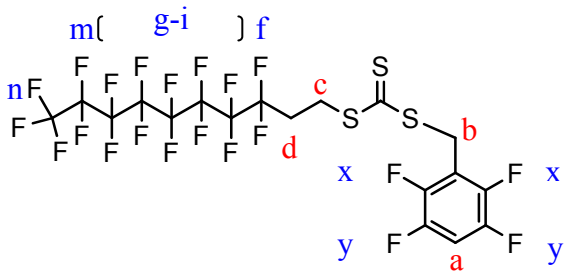

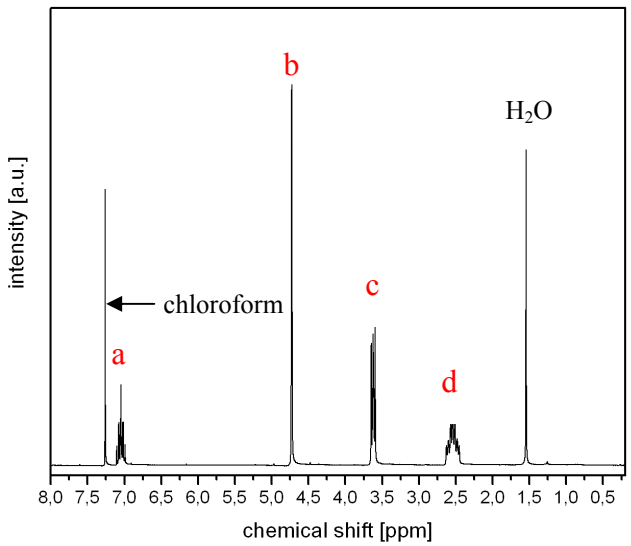

Figure 152: ^{1}H-NMR spectrum of monofunctional **CTA XXXVII** in chloroform-d

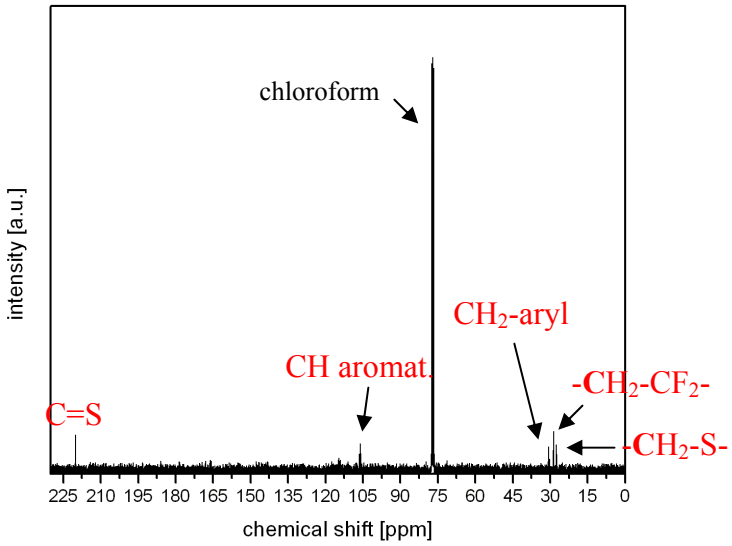

Figure 153: ^{13}C-NMR spectrum of monofunctional **CTA XXXVII**

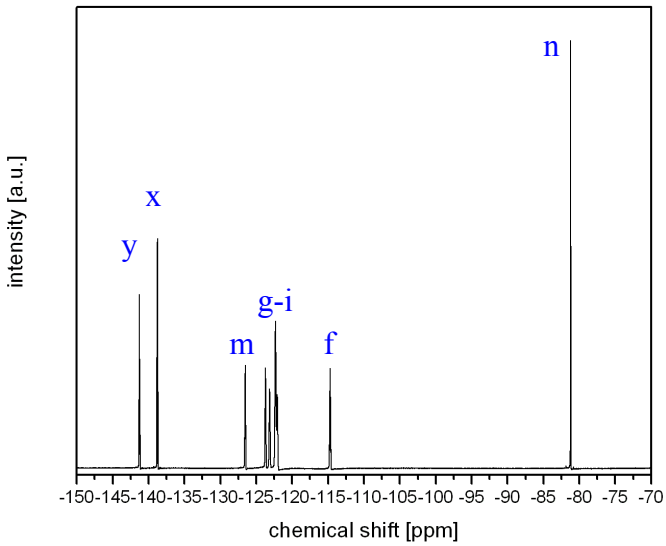

Figure 154: ^{19}F-NMR spectrum of monofunctional **CTA XXXVII** in chloroform-d

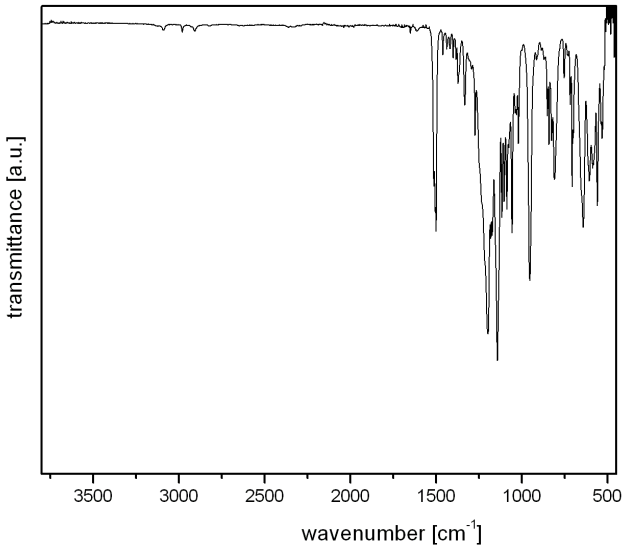

Figure 155: IR-spectrum of monofunctional **CTA XXXVII**

symmetric, bifunctional **CTA XXXXIII**

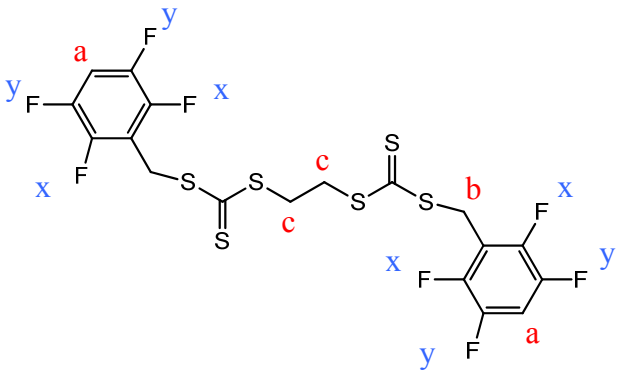

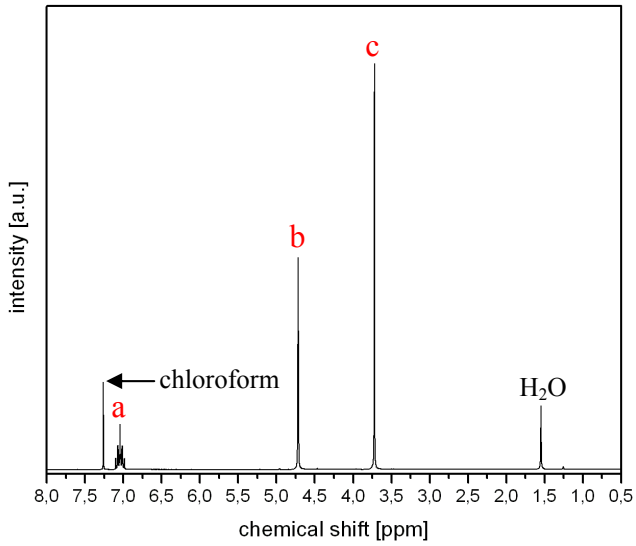

Figure 156: ^{1}H-NMR spectrum of symmetric, bifunctional **CTA XXXXIII** in chloroform-d

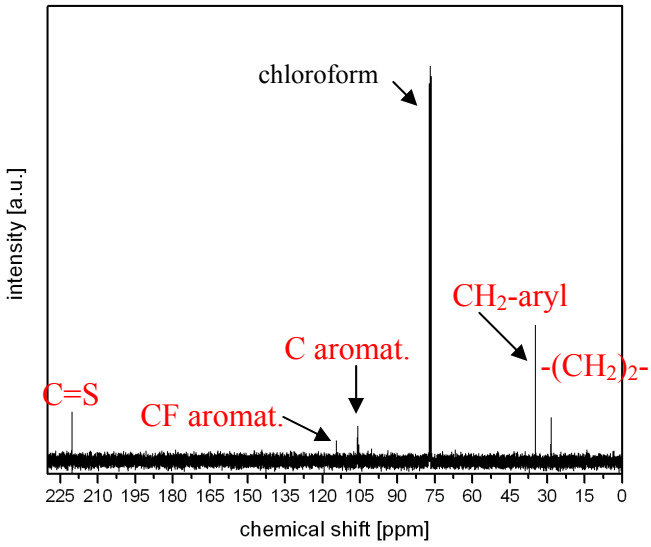

Figure 157: ^{13}C-NMR spectrum of symmetric, bifunctional **CTA XXXXIII** in chloroform-d

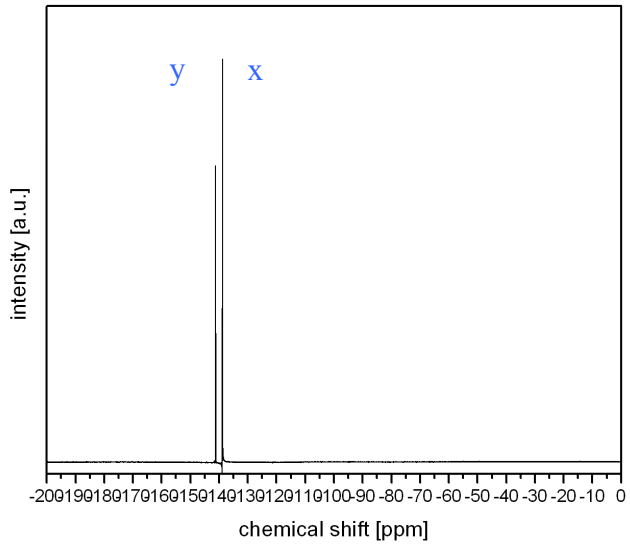

Figure 158: ^{19}F-NMR spectrum of symmetric, bifunctional **CTA XXXXIII**

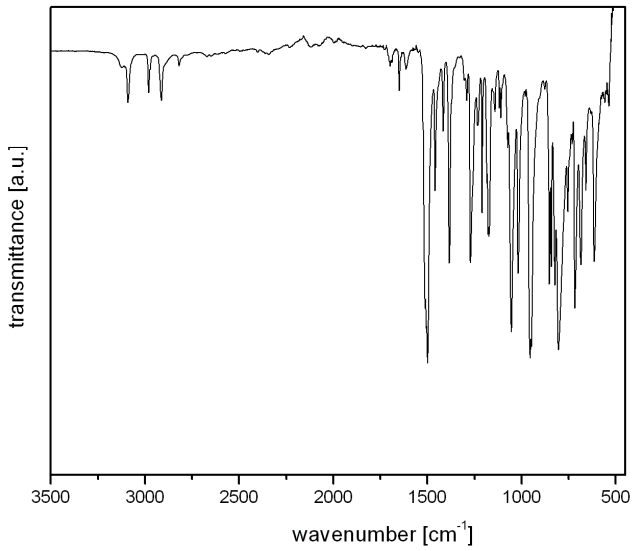

Figure 159: IR-spectrum of symmetric, bifunctional **CTA XXXXIII** in chloroform-d

non-symmetric, monofunctional **CTA XXXVI**

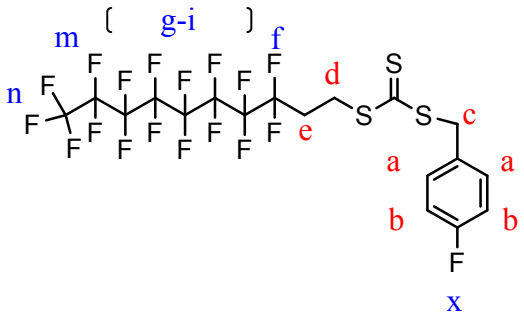

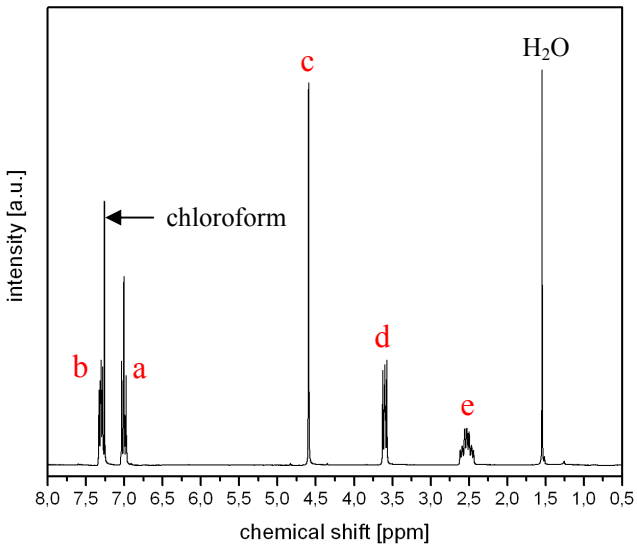

Figure 160: ^{1}H-NMR spectrum of monofunctional **CTA XXXVI** in chloroform-d

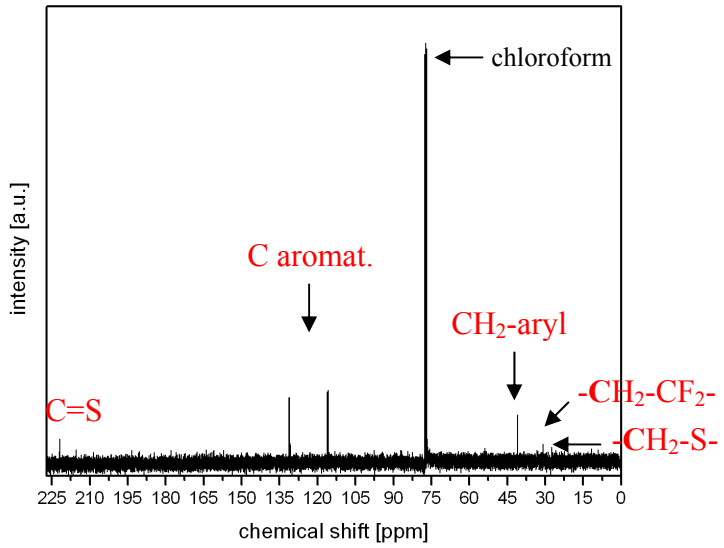

Figure 161: ^{13}C-NMR spectrum of monofunctional **CTA XXXVI** in chloroform-d

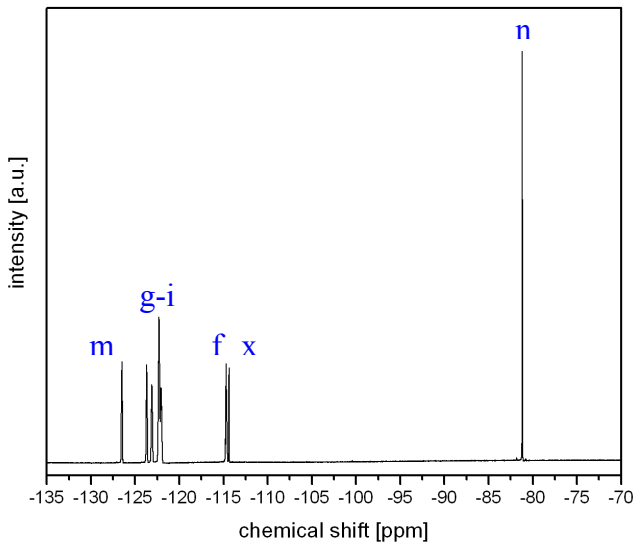

Figure 162: ^{19}F-NMR spectrum of monofunctional **CTA XXXVI** in chloroform-d

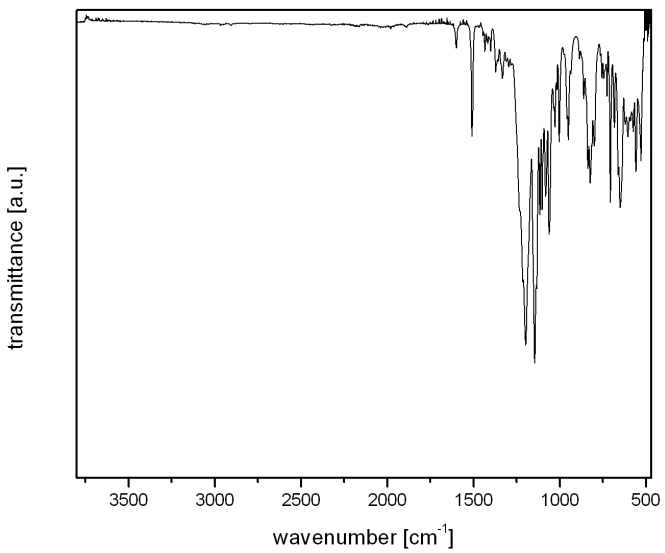

Figure 163: IR-spectrum of monofunctional **CTA XXXVI**

symmetric, bifunctional **CTA XXXXII**

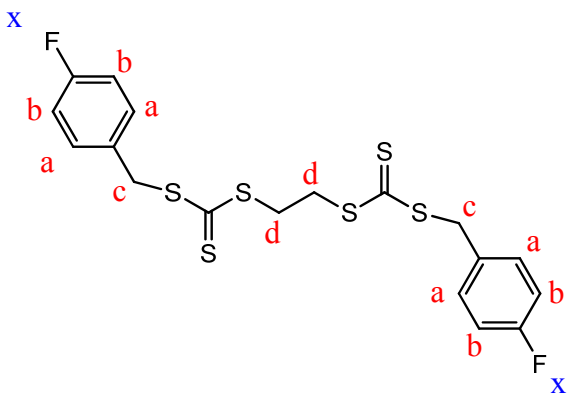

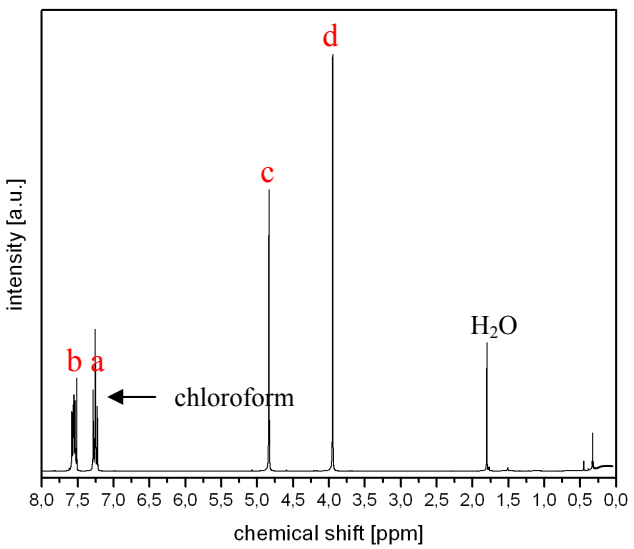

Figure 164: ^{1}H-NMR spectrum of symmetric, bifunctional **CTA XXXXII** in chloroform-d

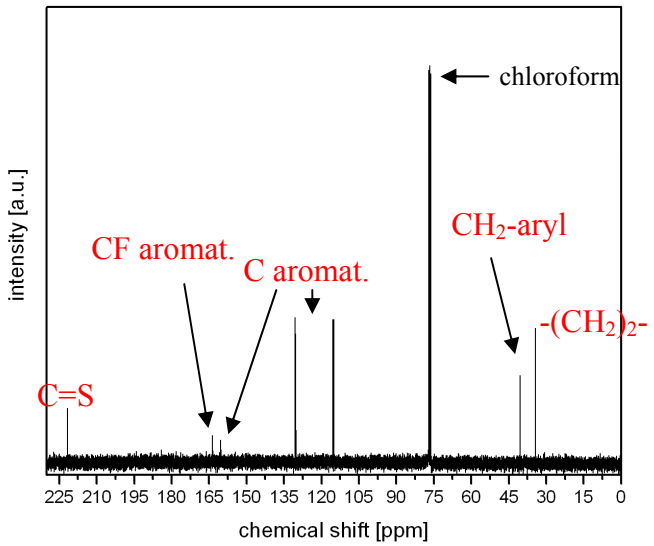

Figure 165: ^{13}C-NMR spectrum of symmetric, bifunctional **CTA XXXXII** in chloroform-d

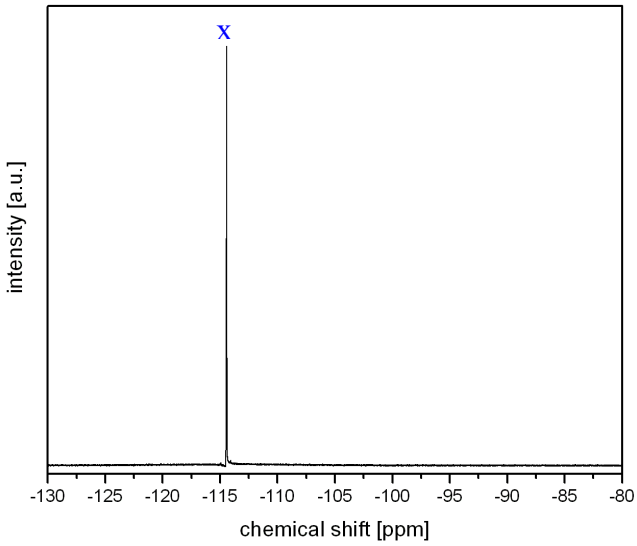

Figure 166: ^{13}C-NMR spectrum of symmetric, bifunctional **CTA XXXXII** in chloroform-d

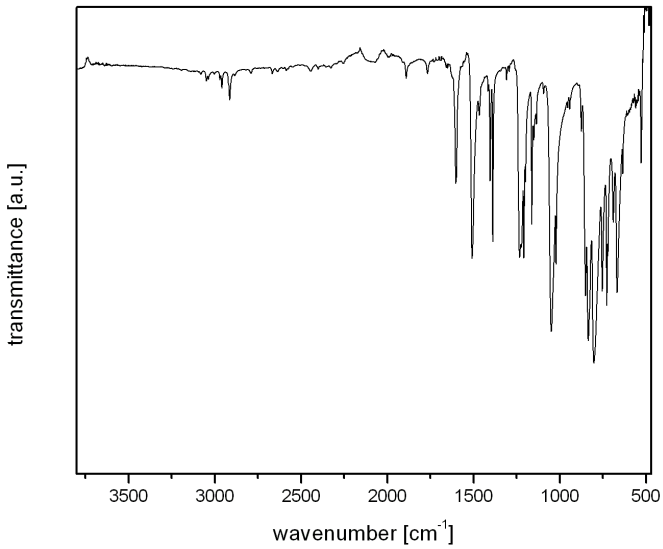

Figure 167: IR-spectrum of symmetric, bifunctional **CTA XXXXII**

Non-symmetric, monofunctional **CTA XXXVIII**

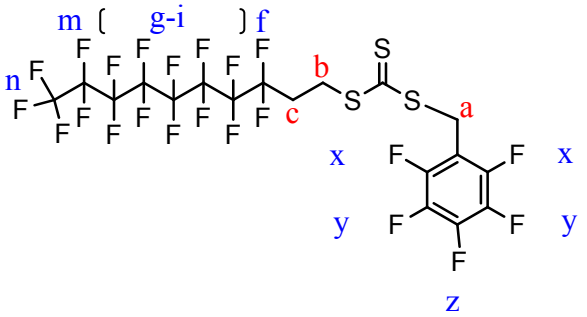

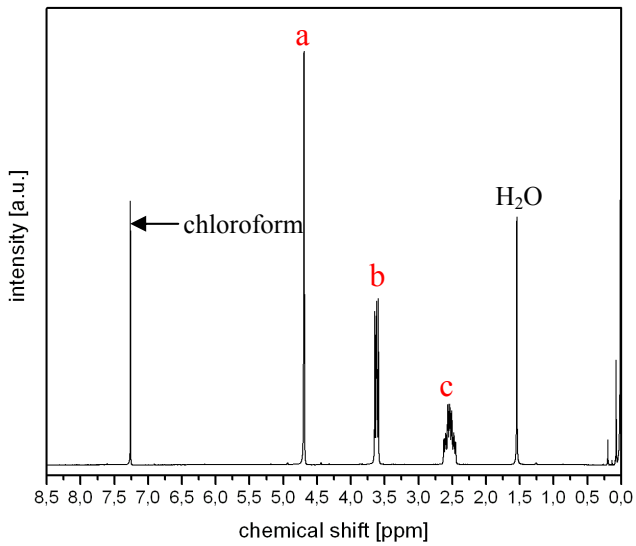

Figure 168: ^{1}H-NMR spectrum of monofunctional **CTA XXXVIII** in chloroform-d

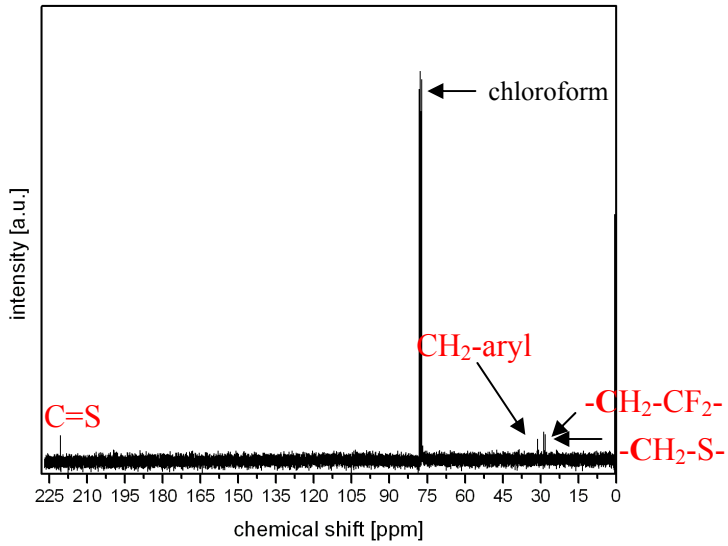

Figure 169: ^{13}C-NMR spectrum of monofunctional **CTA XXXVIII** in chloroform-d

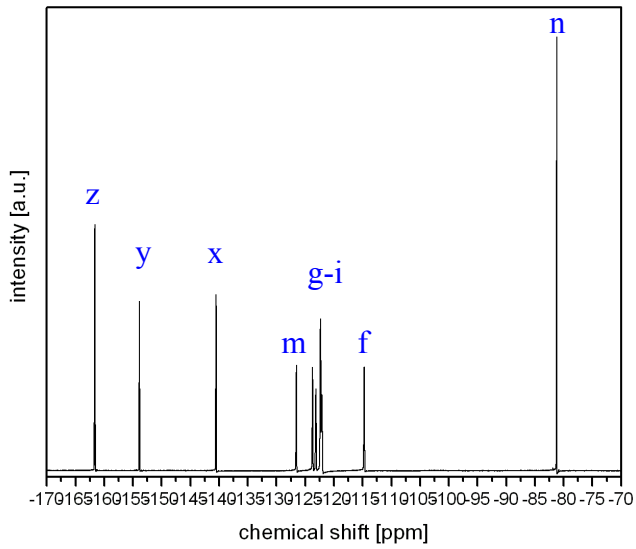

Figure 170: ^{19}F-NMR spectrum of monofunctional **CTA XXXVIII** in chloroform-d

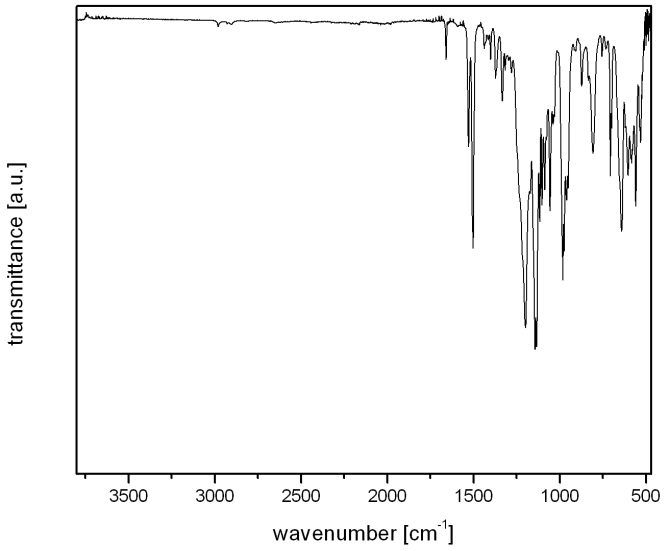

Figure 171: IR-spectrum of monofunctional **CTA XXXVIII**

symmetric, bifunctional **CTA XXXXIV**

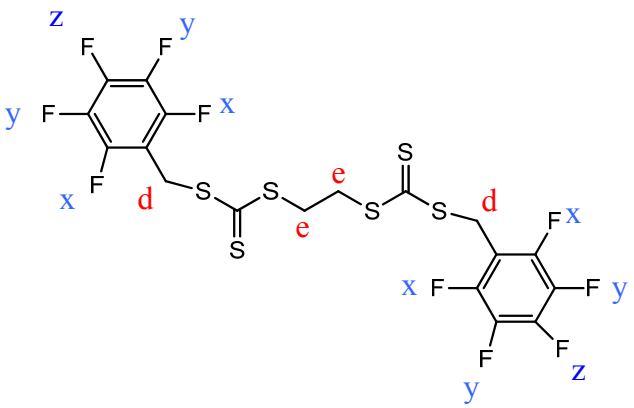

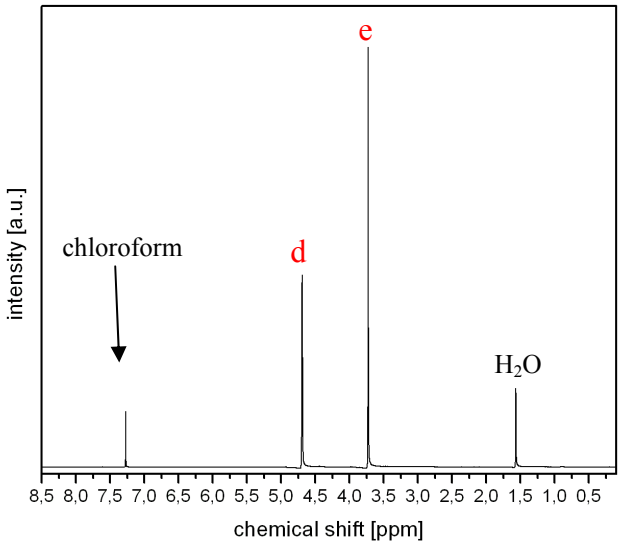

Figure 172: ^{1}H-NMR spectrum of **CTA XXXXIV** in chloroform-d

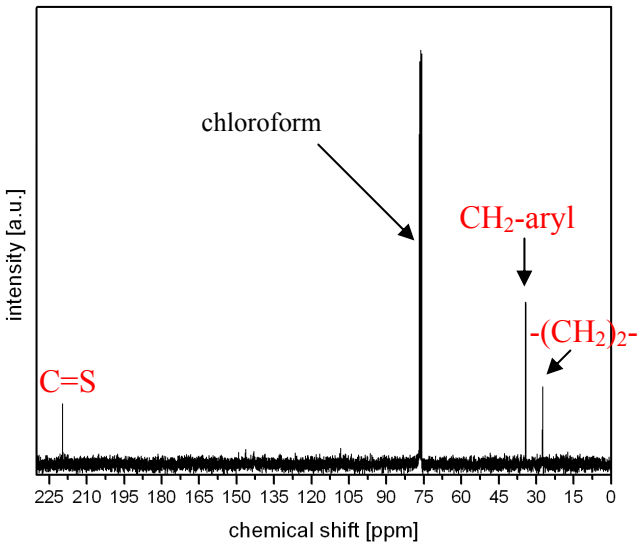

Figure 173: ^{13}C-NMR spectrum of **CTA XXXXIV** in chloroform-d

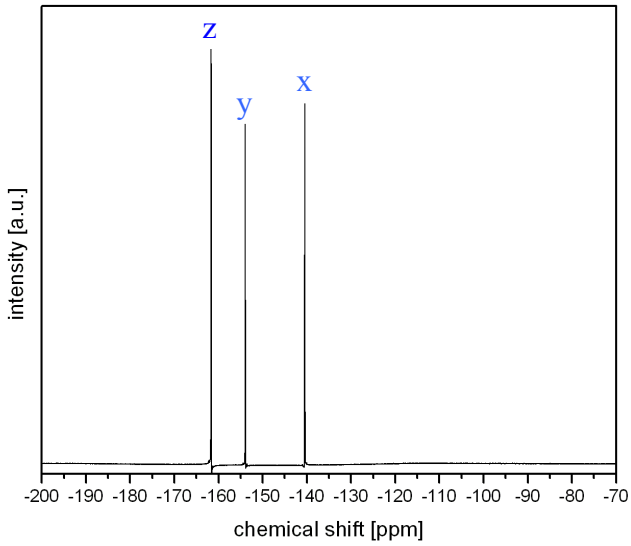

Figure 174: ^{19}F-NMR spectrum of **CTA XXXXIV** in chloroform-d

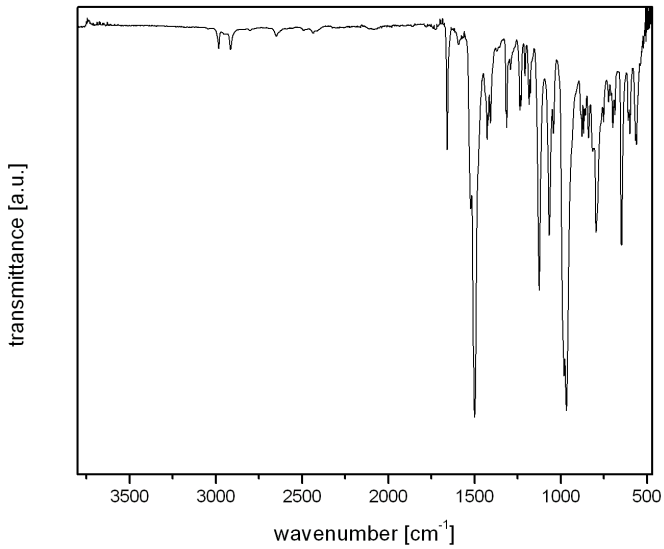

Figure 175: IR-spectrum of symmetric, bifunctional **CTA XXXXIV**

non-symmetric, monofunctional **CTA XXXIV**

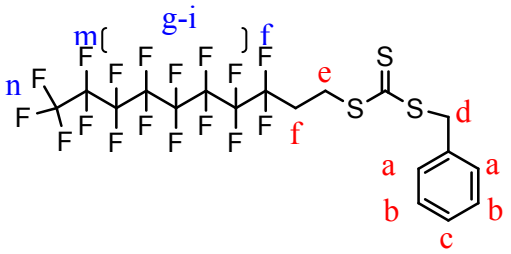

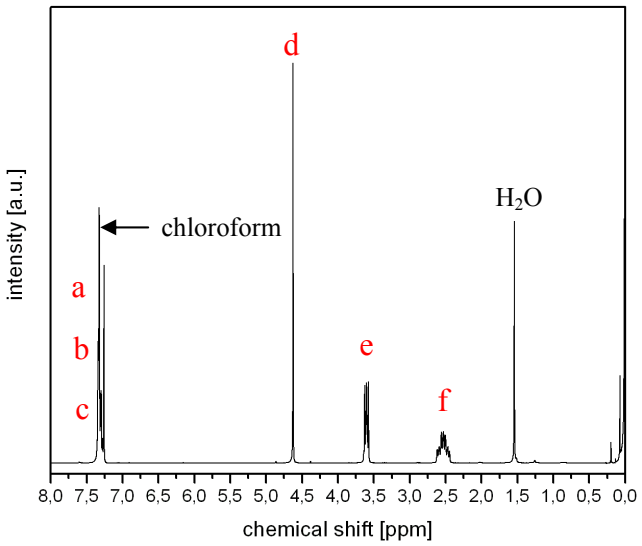

Figure 176: ^{1}H-NMR spectrum of monofunctional **CTA XXXIV** in chloroform-d

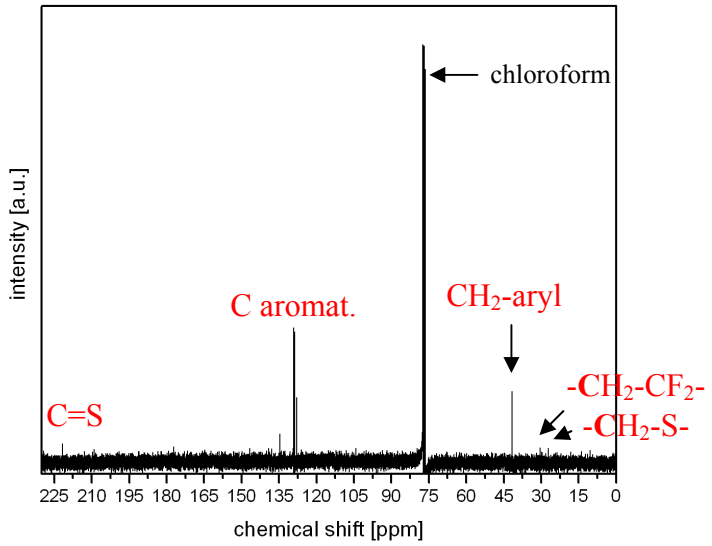

Figure 177: ^{13}C-NMR spectrum of monofunctional **CTA XXXIV** in chloroform-d

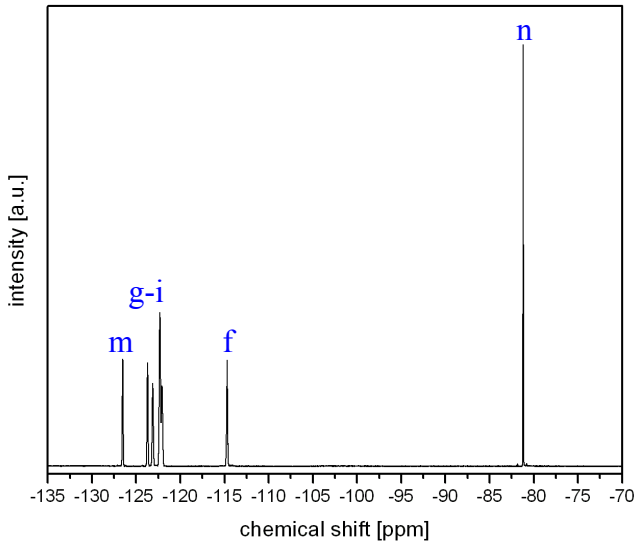

Figure 178: ^{19}F-NMR spectrum of monofunctional **CTA XXXIV** in chloroform-d

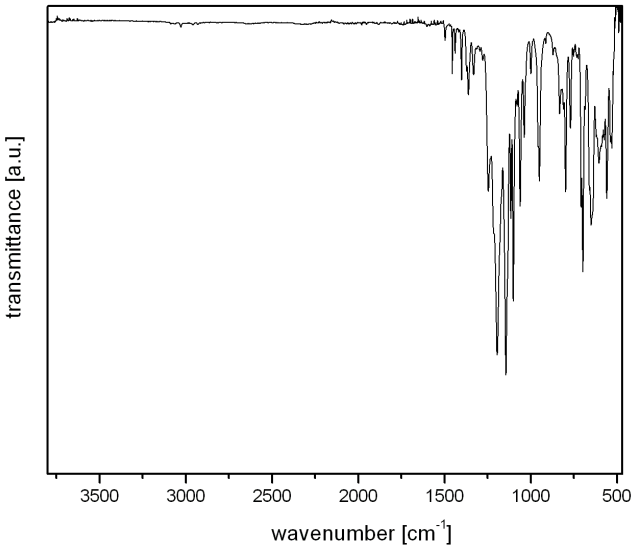

Figure 179: IR-spectrum of monofunctional **CTA XXXIV**

symmetric, bifunctional **CTA XXXIX**

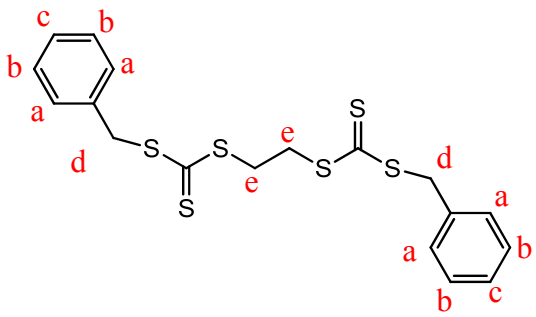

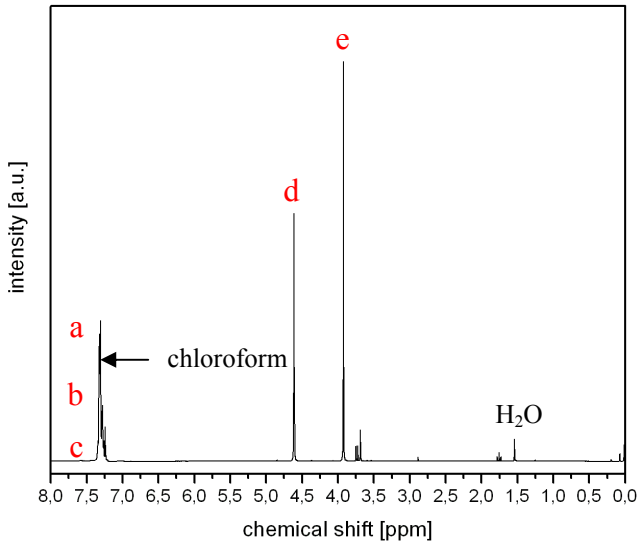

Figure 180: ^{1}H-NMR spectrum of symmetric bifunctional **CTA XXXIX** in chloroform-d

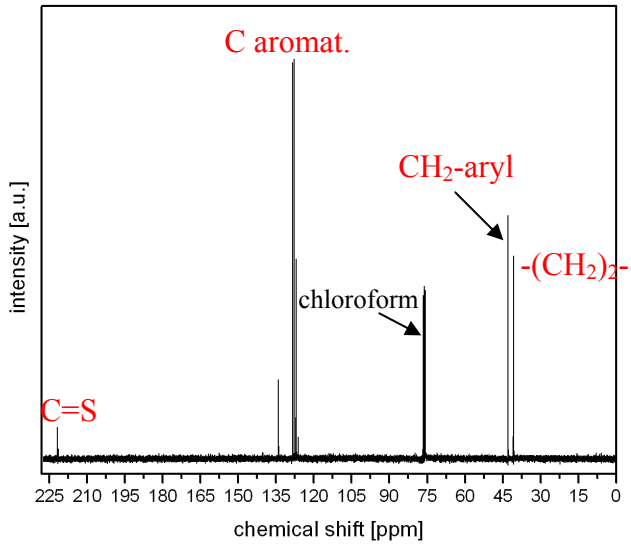

Figure 181: ^{13}C-NMR spectrum of symmetric bifunctional **CTA XXXIX** in chloroform-d

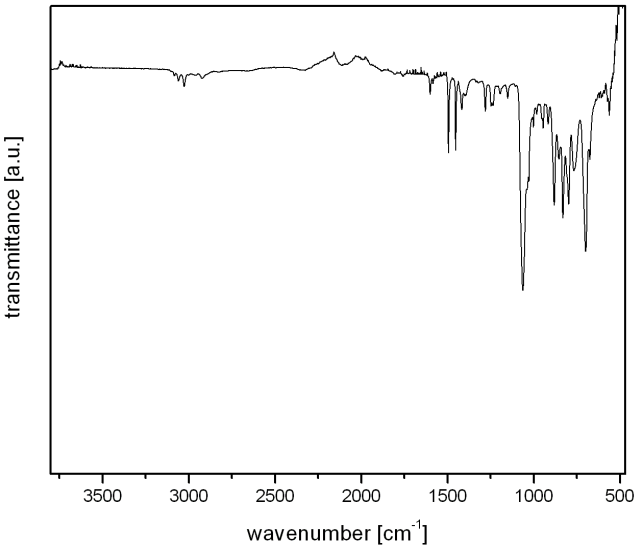

Figure 182: IR-spectrum of symmetric bifunctional **CTA XXXIX**

symmetric, bifunctional **CTA XXXXI**

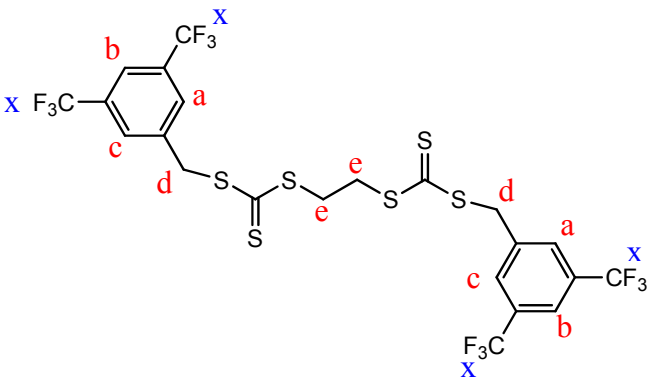

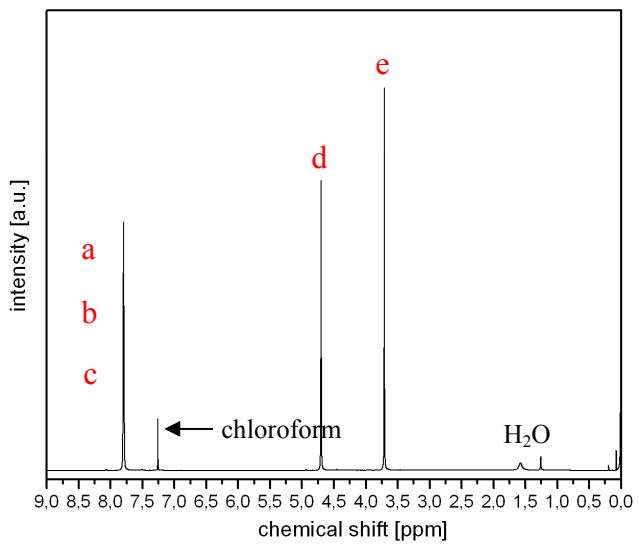

Figure 183: ^{1}H-NMR spectrum of symmetric, bifunctional **CTA XXXXI** in chloroform-d

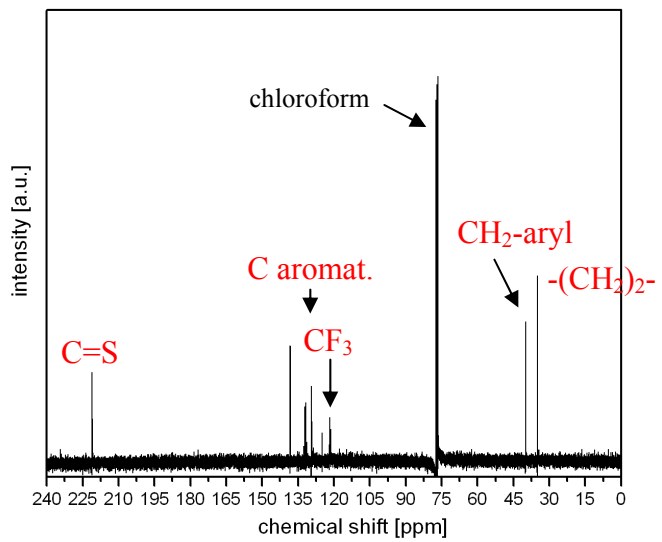

Figure 184: ^{13}C-NMR spectrum of symmetric, bifunctional **CTA XXXXI** in chloroform-d

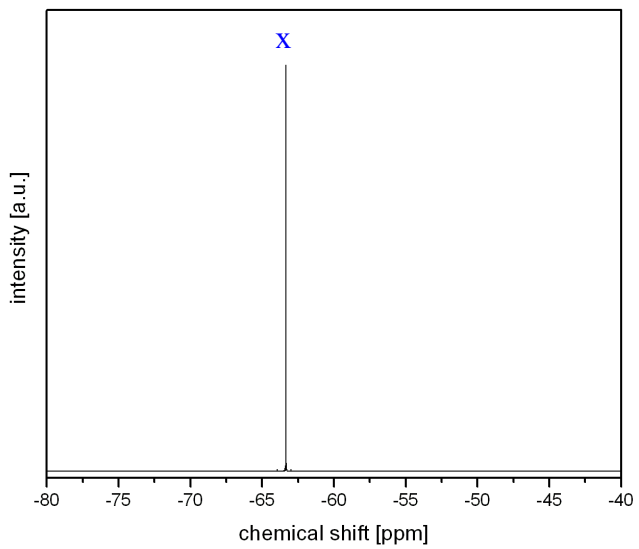

Figure 185: ^{19}F-NMR spectrum of symmetric, bifunctional **CTA XXXXI** in chloroform-d

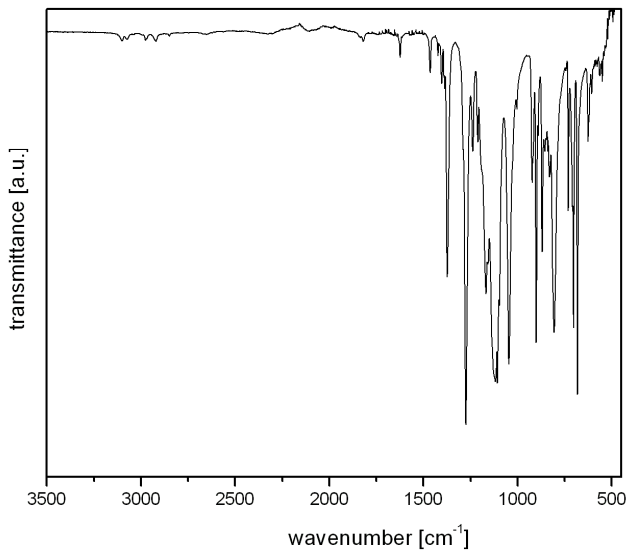

Figure 186: IR-spectrum of symmetric, bifunctional **CTA XXXXI**

IR-spectra of polymers

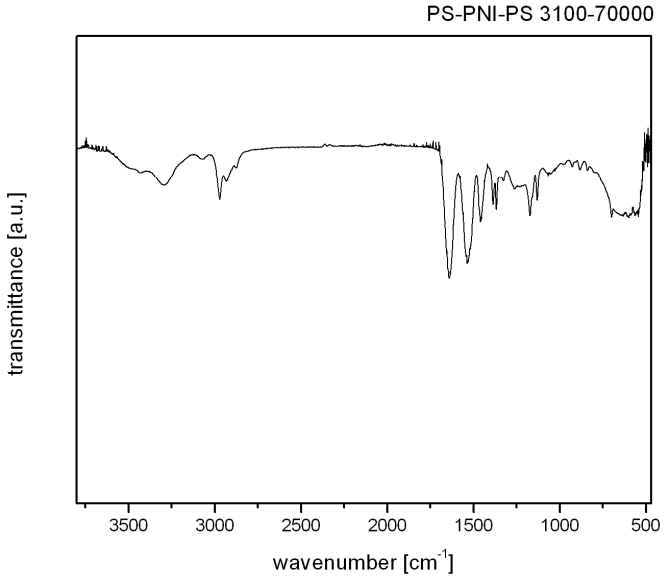

Figure 187: IR-spectrum of **PS-PNI-PS 3100-70000**

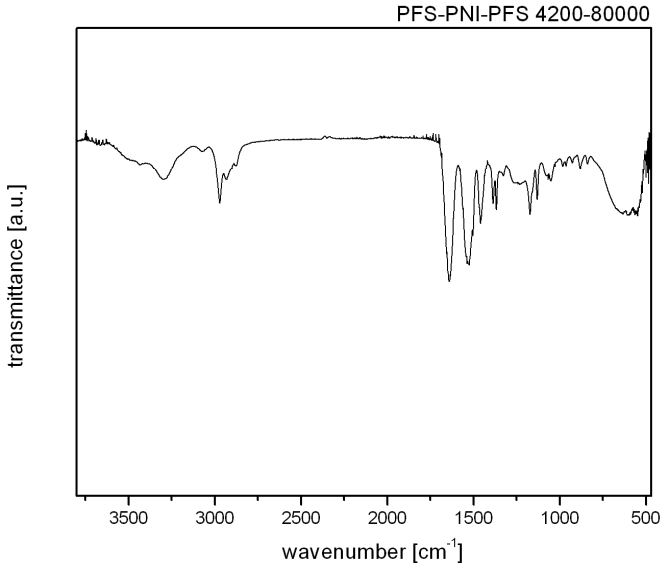

Figure 188: IR-spectrum of **PFS-PNI-PFS 4200-80000**

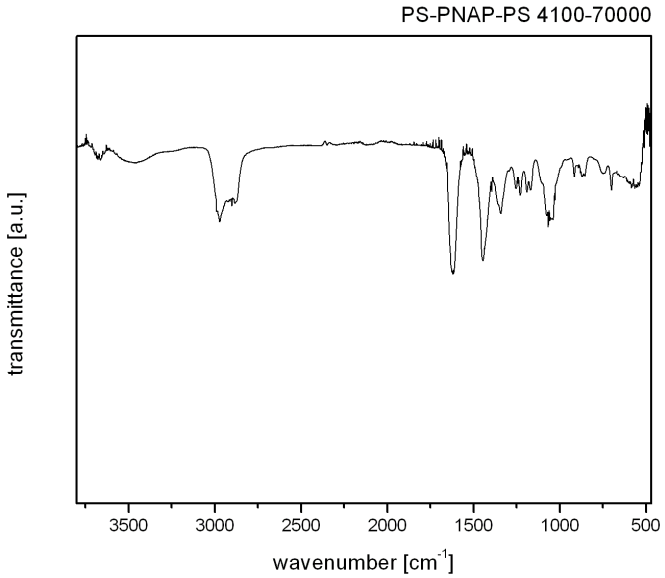

Figure 189: IR-spectrum of **PS-PNAP-PS 4100-70000**

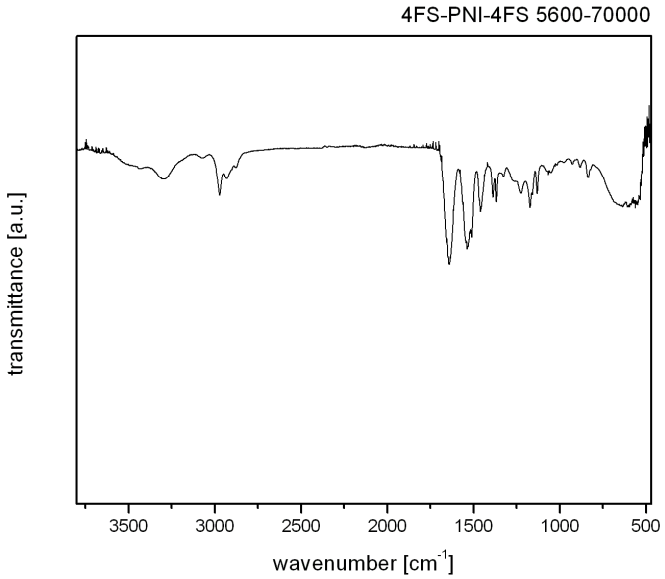

Figure 190: IR-spectrum of **4FS-PNI-4FS 5600-70000**

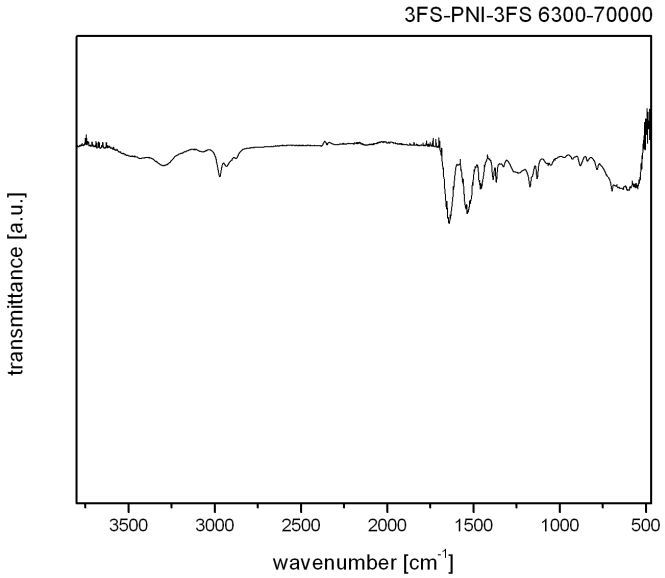

Figure 191: IR-spectrum of **3FS-PNI-3FS 6300-70000**

References

1. J. H. Johnson, *US-Patent 2,269,342*, **1942**
2. E. L. Skov, *US-Patent 6,911,266B1*, **2005**
3. V. Siracusa, P. Rocculi, S. Romani and M. Dalla Rosa, *Trends Food Sci. Technol.* **2008**, 19, 634-643
4. J. Lunt, *Polym. Deg. Stab.* **1998**, 59, 145-152
5. M. M. Davoodi, S. M. Sapuan, R. Yunus, *Mat. Des.* **2008**, 29, 1447–1452
6. T. M. Keller, D. D. Dominguez, *Polymer* **2005**, 46, 4614–4618
7. E. S. Weiser, T. F. Johnson, T. L. St. Clair, Y. Echigo, H. Kaneshiro and B. W. Grimsley, *High Perform. Polym.* **2000**, 12**,** 1–12
8. M. Fahlman, W.R. Salaneck, *Surf. Sci.* **2002**, 500, 904–922
9. Lehmann et al., *US-Patent 5,175,285*, **1992**
10. A. Benicou, A. Aserin, N. Garti, *Polym. Adv. Technol.* **2002**, 13, 1019-1031
11. L. Szente, J. Szejtli, *Trends Food Sci. Technol.* **2004**, 15, 137–142
12. H. Bader, H. Ringsdorf, B. Schmidt, *Angew. Makromolek. Chem.* **1984,** 123/124, 457-485 (2062)
13. I. Chianella, K. Karim, E. V. Piletska, C. Preston, S. A. Piletsky, *Anal. Chim. Acta* **2006**, 559, 73–78
14. J. M. Rosiak, F. Yoshii, *Nucl. Instr. and Meth. in Phys. Res. B* **1999**, 151, 56-64
15. L. J. Suggs, S. A. Moorey, and A. G. Mikos, *Handbook of Physical Properties of Polymers* **2007**, Part **IX**, 939-950
16. T. Lippert, M. Hauer, C. R. Phipps, A. Wokaun, *Appl. Phys. A* **2003**, 77, 259–264
17. R. D. Lentz, I. Shainberg, R. E. Sojka, and D. L. Carter, *Soil Sci. Soc. Am. J.* **1992**, 56, 1926-1932
18. E. Armelin, R. Oliver, F. Liesa, J. I. Iribarren, F. Estrany, C. Alemán, *Prog. Org. Coat.* **2007**, 59, 46–52
19. A. Hiraoa, K. Sugiyama, Hideaki Yokoyam, *Prog. Polym. Sci.* **2007**, 32, 1393–1438
20. C. Boyer, V. Bulmus, J. Liu, T. P. Davis, M. H. Stenzel, and C. Barner-Kowollik, *J. Am. Chem. Soc.* **2007**, 129, 7145-7154
21. G. Moad, Y. K. Chong, A. Postma, E. Rizzardo, S. H. Thang, *Polymer* **2005**, 46, 8458–8468
22. K. Matyjaszewski, J. Xia, *Chem. Rev.* **2001,** 101*,* 2921-2990

23. M. Yamada, T. Iguchi, A. Hirao, S. Nakahama and J. Watanabe, *Macromolecules* **1995**, 28, 50-58
24. N. Hadjichristidis, S. Pispas and G. Floudas, *Block Copolymers: Synthetic Strategies, Physical Properties, and Applications*, John Wiley & Sons, Inc. **2003**, ISBN: 0-471-39436-X
25. J. A. Opsteen, J. C. M. van Hest, *Chem. Commun.* **2005**, 57–59
26. W. H. Binder, R. Sachsenhofer, *Macromol. Rapid. Commun.* **2008**, Vol. 29, 952-981
27. M. N. Higley, J. M. Pollino, E. Hollembeak and M. Weck, *Chem. Eur. J.* **2005**, 11, 2946 2953
28. M. K. Mahanthappa, F. S. Bates and M. A. Hillmyer, *Macromolecules* **2005**, 38, 7890-7894
29. S. Coca, H.-J. Paik, K. Matyjaszewski, *Macromolecules* **1997,** 30, 6513-6516
30. M. C. Iovu, C. Rockford Craley, M. Jeffries-El, A. B. Krankowski, R. Zhang, T. Kowalewski R. D. McCullough, *Macromolecules* **2007**, Vol. 40, No. 14, 4733-4735
31. K. Matyjaszewski and T. P. Davis, *Handbook of Radical Polymerization*, John Wiley and Sons, Inc., Hoboken, **2002**, ISBN: 0-471-39274-X
32. *Handbook of RAFT polymerization*, edited by C. Barner-Kowollik, WILEY-VCH Verlag GmbH & Co. KGaA, Weinheim, **2008**, ISBN: 978-3-527-31924-4
33. B. Y. K. Chong, T. P. T. Le, G. Moad, E. Rizzardo, S. H. Thang, *Macromolecules* **1999**, 32, 2071-2074
34. G. Moad, R. T. A. Mayadunne, E. Rizzardo, M. Skidmore, S. Thang, *Macromol. Symp.* **2003**, 192, 1-12
35. H.-G. Elias, *Macromolecules*, Bd. **2**, Verlag Wiley VCH, Weinheim, **2001**
36. K. Holmberg, B. Jönsson, B. Kronberg, B. Lindman, *Surfactants and Polymers in Aqueous Solution*, 2nd edition, Verlag WILEY-VCH, Weinheim, **2002**, ISBN: 0-471-49883-1
37. J. Brandrup, E. H. Immergut, *Polymer Handbook*, 3rd edition, Verlag J. Wiley and sons, **1989**
38. S. Dai, P. Ravi, K. C. Tam, *Soft Matter* **2008**, 4, 435-499
39. A. Laschewsky, *Tenside Surf. Det.* **2003**, 40, 246
40. C. J. Hawker, A. W. Bosman and E. Harth, *Chem. Rev.* **2001**, 101, 3661-3688
41. T. Fukuda, T. Terauchi, A. Goto, K. Ohno, Y. Tsujii, and T. Miyamoto, S. Kobatake and B. Yamada, *Macromolecules* **1996,** 29, 6393-6398

42. O. Lagrille, N. R. Cameron, P. A. Lovell, R. Blanchard, A. E. Goeta, R. Koch, *J. Polym. Sci. A,* **2006**, 44, 6, 1926
43. M. K. Georges, R. P. N. Veregin, P. M. Kazmaier, G. K. Hamer, M. Saban, *Macromolecules* **1994**, 27, 7228
44. M. V. Baldovi, N. Mohtat, J. C. Scaiano, *Macromolecules* **1996**, 29, 5497
45. S. Jousset, S. O. Hammouch, J. M. Catala, *Macromol. Rapid Commun.* **1996**, 17, 683
46. S. O. Hammouch, J. M. Catala, *Macromolecules* **1997**, 30, 6685
47. D. Benoit, V. Chaplinski, R. Braslau, C. J. Hawker, *J. Am. Chem. Soc.* **1999,** 121, 3904
48. M. Rodlert, E. Harth, I. Rees, C. J. Hawker, *J. Polym. Sci. Polym. Chem.* **2000**, 38, 4749
49. K. Matyjaszewsky, S. G. Gaynor, D. Greszta, D. Mardare, T. Shigemoto, J. S. Wang, *Macromol. Symp.* **1995**, 95, 217
50. K. Matyjaszewski, *J. Eur. Chem.* **1999**, 5, 11, 3095
51. C. Perruchot, M. A. Khan, A. Kamitsi, S. P. Armes, *Langmuir* **2001**, 17 (15), 4479–4481
52. M. Baum, W. J. Brittain, *Macromolecules* **2002**, 35 (3), 610-615
53. L. Barner, J. F. Quinn, C. Barner-Kowollik, P. Vana, T. P. Davis, *Europ. Polym. J.* ***2003***, 39 (3), 449-459
54. S. Mutukrishnan, E. H. Pan, M. H. Stenzel, C. Barner-Kowollik, T. P. Davis, D. Lewis, L. Barner, *Macromolecules* **2007**, 40 (9), 978–2980
55. M. Laus, R. Papa, K. Sparnacci, A. Alberti, M. Benaglia, D. Macciantelli, *Macromolecules* **2001,** 34*,* 7269-7275
56. L. Nebhani, S. Sinnwell, C. Y. Lin, M. L. Coote, M. H. Stenzel, C. Barner-Kowollik**,** *J. Polym. Sci. A, Polym. Chem.* **2009**, Vol. 47, 6053–6071
57. J. Hong, Q. Wang, Z. Fan, *Macromol. Rapid Commun.* **2006**, 27, 57-62
58. J. Hong, Q. Wang, Y. Lin, Z. Fan, *Macromolecules* **2005**, 38, 2691
59. A. Theis, T. P. Davis, M. H. Stenzel, C. Barner-Kowollik, *Polymer* **2006**, 47, 999–1010
60. M. L. Coote, D. J. Henry, *Macromolecules* **2005**, 38, 5774-5779
61. A. Duréault, D. Taton, M. Destarac, F. Leising and Y. Gnanou, *Macromolecules* **2004,** 37*,* 5513-5519
62. X.-S. Feng and C.-Y. Pan, *Macromolecules* **2002,** 35*,* 4888-4893
63. C. Liu, Y. Zhang and J. Huang, *Macromolecules* **2008,** 41*,* 325-331

64. R. Ranjan, W. J. Brittain, *Macromol. Rapid Commun.* **2008**, 29, 1104–1110
65. M. H. Stenzel, L. Zhang, W. T. S. Huck, *Macromol. Rapid Commun.* **2006**, 27, 1121–1126
66. S. Edmondson, V. L. Osborne and W. T. S. Huck, *Chem. Soc. Rev.* **2004**, 33, 14-21
67. G. Moad, E. Rizzardo, S. H. Thang, *Polymer* **2007**, 1-53
68. G. Moad, E. Rizzardo, S. H. Thang, *Acc. Chem. Res.* **2008**, Vol. 41, No. 9, 1133-1142
69. S. Garnier, *PhD-Thesis*, Universität Potsdam **2005**
70. S. W. Prescott, *PhD-Thesis*, School of Chemistry, University of Sidney, **2003**
71. C. J. Ferguson, R. J. Hughes, D. Nguyen, B. T. T. Pham, R. G. Gilbert, A. K. Serelis, Ch. H. Such, B. S. Hawkett, *Macromolecules* **2005,** 38*,* 2191-2204
72. A. Butté, G. Storti, M. Morbidelli, *Macromolecules* **2001,** 34*,* 5885-5896
73. Y. Luo, R. Wang, L. Yang, B. Yu, B. Li, S. Zhu, *Macromolecules* **2006**, Vol. 39, No. 4, 1328-1337
74. F. M. Calitz, M. P. Tonge and R. D. Sanderson, *Macromolecules* **2003,** 36*,* 5-8
75. M. L. Coote and L. Radom, *J. Am. Chem. Soc.* **2003**, 125, 1490-1491
76. G. Moad, *Aust. J. Chem.* **2006**, 59, 661–662
77. J. Chiefari, Y. K. Chong, F. Ercole, J. Krstina, J. Jeffery, T. P. T. Le, R. T. A. Mayadunne, G. F. Meijs, C. L. Moad, G. Moad, E. Rizzardo, S. H. Thang, *Macromolecules* **1998,** 31*,* 5559-5562
78. S. Perrier, C. Barner-Kowollik, J. F. Quinn, P. Vana and T. P. Davis, *Macromolecules* **2002,** 35*,* 8300-8306
79. M. Drache, G. Schmidt-Naake, *Macromol. Symp.* **2007**, 259, 397–405
80. J. Rosselgong, S. P. Armes, W. Barton, D. Price, *Macromolecules* **2009**, 42, 5919–5924
81. B. Ray, Y. Isobe, K. Morioka, S. Habaue, Y. Okamoto, M. Kamigaito, M. Sawamoto, *Macromolecules* **2003,** 36*,* 543-545
82. H. Lee, E. Terry, M. Zong, N. Arrowsmith, S. Perrier, K. J. Thurecht, S. M. Howdle, *J. Am. Chem. Soc.* **2008**, 130, 12242–12243
83. A. M. Gregory, K. J. Thurecht, S. M. Howdle, *Macromolecules* **2008,** *41,* 1215-1222
84. M. Mertoglu, *PhD Thesis*, Universität Potsdam, **2004**
85. C. L. McCormick and A. B. Lowe, *Acc. Chem. Res.* **2004,** 37, 312-325
86. J.-F. Baussard, J.-L. Habib-Jiwan, A. Laschewsky, M. Mertoglu, J. Storsberg, *Polymer* **2004**, 45, 3615–3626

87. M. Chen, K. P. Ghiggino, A. W. H. Mau, E. Rizzardo, S. H. Thang, G. J. Wilson, *Chem. Commun.* **2002**, 2276-2277

88. S. R. Gondi, A. P. Vogt, B. S. Summerlin, *Macromolecules* **2007**, 40, 474-481

89. D. L. Patton, R. C. Advincula, *Macromolecules* **2006**, 39, 8674-8683

90. P. Lebreton, B. Ameduri, B. Boutevin, J. M. Corpart, *Macromol. Chem. Phys.* **2002**, 23, 522-537

91. J.-F. Baussard, *PhD-Thesis*, Universite Catholique de Louvain, **2005**

92. A. B. Lowe, C. L. McCormick, *Prog. Polym. Sci.* **2007**, 32, 283-351

93. R. T. A Mayadunne, E. Rizzardo, in *Living and Controlled Polymerization: Synthesis, Characterization and Properties of the Respective polymers and Copolymers*, J. Jagur-Grodzinski, Ed., Nova Science Publishers, Hauppauge, NY, **2006**, 65-107

94. M. Bathfield, F. D'Agosto, R. Spitz, M.-T. Charreyre and T. Delair, *J. Am. Chem. Soc.* **2006**, 128, 2546-2547

95. G. Samay, M. Kubín, J. Podešva, *Angew. Makromolek. Chem.* **1978**, 72, 1, 185-198

96. H. Zettl, W. Häfner, A. Böker, H. Schmalz, M. Lanzendörfer, A. H. E. Müller, G. Krausch, *Macromolecules* **2004,** *37,* 1917-1920

97. T. Pellegrino, L. Manna, S. Kudera, T. Liedl, D. Koktysh, A. L. Rogach, S. Keller, J. Radler, G. Natile, W. J. Parak, *Nano Lett.* **2004***,* Vol. 4, No. 4, 703-707

98. G. Z. Zhou, I. I. Harruna, C. W. Ingram, *Polymer* **2005**, 46, 10672-10677

99. S. Garnier, *personal communication*

100. J. P. S. Farinha, P. Relógio, M.-T. Charreyre, T. J. V. Prazeres and J. M. G. Martinho, *Macromolecules* **2007,** 40, 4680-4690

101. A. W. York, C. W. Scales, F. Huang and C. L. McCormick, *Biomacromolecules* **2007**, Vol. 8, No. 8, 2337-2341

102. P. De, S. R. Gondi, R. Debashish and B. S. Sumerlin, *Macromolecules* **2009**, 42, 5614–5621

103. J. M. G. Cowie, *Chemie und Physik der synthetischen Polymeren*, aus dem Englischen übersetzt von H. Mauermann-Düll, F. Vieweg & Sohn Verlagsgesellschaft mbH, Braunschweig/Wiesbaden, **1991**

104. M. S. Montaudo, C. Puglisi, F. Samperi, G. Montaudo, *Rapid Commun. Mass Spectrom.* **1998**, 12, (9), 519-528

105. R. Beckett, Z. Jue, J. C. Giddings, *Environ. Sci. Technol.*, **1987**, 21, (3), 289–295

106. A. T. Jackson, H. T. Yates, C. I. Lindsay, Y. Didier, J. A. Segal, J. H. Scrivens, G. Critchley, *Rapid Commun. Mass Spectrom.* **1997**, 11, (5), 520-526

107. H. Friebolin, *Ein- und zweidimensionale NMR-Spektroskopie, eine Einführung*, dritte Auflage, Verlag WILEY-VCH, Weinheim **1999**, ISBN: 3-527-29514-3

108. M. Hesse, H. Meier, B. Zeeh, *Spektroskopische Methoden in der Organischen Chemie*, 5te überarbeitete Auflage, Verlag Georg Thieme Stuttgart, New York **1995**, ISBN: 3-13-576105-3

109. S. Berger, S. Braun, H.-O. Kalinowski, *NMR-Spektroskopie von Nichtmetallen, Band 4, ^{19}F-NMR-Spektroskopie*, Verlag Georg Thieme, Stuttgart **1994**, ISBN: 3-13-769-301-2

110. P. Lebreton, B. Ameduri, B. Boutevin, J.-M. Corpart, *Macromol. Chem. Phys.* **2002**, 203, 522-537

111. M. Benaglia, E. Rizzardo, A. Alberti and M. Guerra, *Macromolecules* **2005**, 38, 3129-3140

112. P. Takopuckdee, C. A. Mars, S. Perrier, S. J. Archibald, *Macromolecules* **2005**, 38, 1057-1060

113. L. Albertin, M. H. Stenzel, C. Barner-Kowollik, T. P. Davies, *Polymer* **2006**, 47, 1011-1019

114. G. Moad, J. Chiefari, J. Krstina, A. Postma, R. T. A. Mayadunne, E. Rizzardo, S. H. Thang, *Polym. Int.* **2000**, 49, 993-1001

115. J. Chiefari, R. T. A. Mayadunne, C. L. Moad, G. Moad, E. Rizzardo, A. Postma, M. A. Skidmore, S. H. Thang, *Macromolecules* **2003**, 36, 2273-2283

116. M. Destarac, W. Bzducha, D. Taton, I. Gauthier-Gillaizeau, S. Z. Zard, *Macromol. Rapid Commun.* **2002**, 23, 17, 1049-1054

117. A. Postma, T. P. Davies, G. Li, G. Moad, M. O`Shea, *Macromolecules* **2006**, 39, 5307-5318

118. D. C. Wan, K. Satoh, M. Kamigaito, Y. Okamoto, *Macromolecules* **2005**, 38, 10397-10405

119. E. Girard, T. Tassaing, J.-D. Marty, M. Destarac, *Pol. Chem.* **2011**, 2, 2222

120. J. J. L. M. Cornelissen, M. Fischer, N. A. J. M. Sommerdijk, R. J. M. Nolte, *Science* **1998**, Vol. 280, No. 5368, 1427-1430

121. M. E. Cates, S. J. Candau, *J. Phys.: Condens. Matter* **1990**, 2, 6869

122. Z. Gao, S. K. Varshney, S. Wong, A. Eisenberg, *Macromolecules* **1994**, 27, (26), 7923-7927

123. C. Allen, D. Maysinger, A. Eisenberg, *Colloids Surf. B* **1999**, 16, 3-27

124. D. Colombani, *Prog. Polym. Sci.* **1997**, 22, 1649

125. D. Voulgaris, C. Tsitsilianis, *Macromol. Chem. Phys.* **2001**, 202, 3284

126. P. Alexandridis and B. Lindman, B. (Ed.), "*Amphiphilic Block Copolymers: Self Assembly and Applications*", Elsevier Science, Amsterdam, **1997**

127. B. Chu and Z. Zhou, *Surf. Sci. Ser.* **1996**, 60**,** 67

128. P. Alexandridis, *Curr. Opin. Coll. Interface Sci.* **1996**, 1, 490-501

129. Z. Yang, Y. Yang, Z. Zhou, D. Attwood, C. Booth, *J. Chem. Soc. Faraday Trans.* **1996**, 92, 257

130. T. Liu, V. M. Nace, B. Chu, *Langmuir* **1999**,15, 3109

131. Prof. Dr. A. Lendlein, *Vorlesung Hydrogele*, SS **2009**

132. http://de.wikipedia.org/wiki/**Rheologie**

133. C. Gallegos, J. M. Franco, *Curr. Opin. Coll. Interface Sci.* **1999**, 4, 288-293

134. R. P. Borwnkar, *J. Food Eng.* **1992**, 16, 1-16

135. W. B. Russel, *J. of Rheol.* **1980**, 24, 3, 287-317

136. J.-C. Baudez, P. Coussota, *J. Rheol.* **2001**, 45, 5, 1123-1139

137. G. V. Vinogradov and N. V. Prozorovskaya, *Rheol. Acta* **1964**, Band 3, Heft 3

138. F. N. Cogswell, *Trans. Soc. Rheol.* **1972**, 16, 3, 383-403

139. A. V. Bhave, R. C. Armstrong, R. A. Brown, *J. Chem. Phys.* **1991**, 95, 4

140. Y. Cohen, *J. Rheol.* **1985**, 29, l, 67-102

141. B. Jeong, S. Wan Kim, Y. H. Ba, *Adv. Drug Del. Rev.* **2002***,* Vol. 54, 1, 37-51

142. A. M. Bivigou-Koumba, *PhD-thesis*, Universität Potsdam, **2009**

143. P. Glöckner, *PhD-thesis*, Johannes-Gutenberg-Universität Mainz, **2000**

144. *Micelles, Microemulsions and Monolayers, Science and Technology*, edited by Dinesh O. Shah, Marcel Dekker, Inc., New York, Basel, Hong Kong, **1998,** ISBN: 0-8247-9990-9

145. *Fluorinated surfactants, synthesis, properties, applications*, edited by E. Kissa, Marcel Dekker, Inc., New York, Basel, Hong Kong, ISBN: 0-8247-9011-1

146. Y.-Y. Won, H. T. Davis, F. S. Bates, *Macromolecoles* **2003**, 36, 953

147. *Fluorinated surfactants: synthesis, properties, applications*, edited by E. Kissa, Marcel Dekker, Inc., New York, Basel, Hong Kong, ISBN: 0-8247-9011-1

148. A. Laschewsky, *Tenside Surf. Det.* **2003**, 40, 246

149. G. Colafemmina, D. Fiorentino, A. Ceglie, E. Carretti, E. Fratini, L. Dei, P. Baglioni, and G. Palazzo, *J. Phys. Chem. B* **2007**, 111 (25), 7184–7193

150. H. Sawada, Y.-F. Gong, Y. Minoshima, T. Matsumoto, M. Nakayama, M. Kosugi, T. Migata; *J. Chem. Soc., Chem. Commun.* **1992**

151. H. Sawada, M. Umedo, T. Kawase, T. Tomita, M. Baba, *Europ. Polym. J.* **1999**, 35, 1611-1617

152. R. Renner, *Environ. Sci. Technol.* **2001**, 35 (7), 154–160

153. M. M. Schultz, D. F. Barofsky, J. A. Field, *Environ. Eng. Sci.* **2003***,* Vol. 20, No. 5, 2003

154. http://de.wikipedia.org/wiki/**HLB-Wert**

155. http://www.sita-messtechnik.de/theorie/schaum/schaumtesten.html

156. *Vortrag Dr.-Ing. F. Westphal, Siemens A&D SP Prozess-Sicherheit*, Industriepark Höchst, D-65926 Frankfurt, 02.12.2004

157. *Literatur- und Internetrecherche zum Themengebiet* ***Schaum***, Ingenieursbüro für angewandte Strömungsmechanik H.-W. Mindt und W. Ottow GbR, info@a-CFD.de

158. http://de.wikipedia.org/wiki/**Schaum**

159. H. Matsuoka, S. Maeda, P. Kaewsaiha, K. Matsumoto, *Langmuir* **2004**, 20, 7412

160. T. F. Tadros, *Applied surfactants*, Verlag Wiley-VCH Weinheim, Germany, **2005**

161. D. Cochin, A. Laschewsky, F. Nallet, *Macromolecules* **1997**, 30, 2278-2287

162. J. J. Boon, T. Learner, *J. Anal. Appl. Pyrolysis* **2002**, 64, 327–344

163. J. Gabrielsson, N.-O. Lindberg and T. Lundstedt, *J. Chemometrics* **2002**, 16, 141-160

164. D. Miller, E.-M. Wiener, A. Turowski, C. Thunig, H. Hoffmann, *Coll. Surf. A: Physicochem. Eng. Aspects* **1999** ,152, 155–160

165. M. L. Gum, *US Patent 4,801,447*, **1989**

166. D. Myers, *Surfactant Science and Technologie, 3rd edition*, Verlag J. Wiley & Sons, Inc., Hoboken, New Jersey **2006,** ISBN-13 978-0-471-68024-6

167. N. Garti, *Lebensm.-Wiss. u.-Technol.* **1997**, 30, 222–235

168. J. Israelachvili, *Coll. Surf. A: Physicochem. Eng. Aspects* **1994**, 91, 1-8

169. M. Chappat, *Coll. Surf. A: Physicochem. Eng. Aspects* **1994**, 91, 57-77

170. B. Verdonck, E. J. Goethals, F. E. Du Prez, *Macromol. Chem. Phys.* **2003**, 204, 2090–2098

171. M. Klapper, C. G. Clark Jr. and K. Müllen, *Polym. Int.* **2008**, 57, 181–202

172. S. Vass, J. S. Pedersen, M. Klapper and E. Retfalvi , *Physica B: Cond. Matter* **2006** (Amsterdam) 759, 385-386

173. P. Imbert, V. M. Sadtler, E. Dellacherie, *Coll. Surf. A* **2002**, 211, 157

174. M. Kanouni, H. L. Rosano, N. Naouli, *Adv. Coll. Interface Sci.* **2002**, 99, 229–254

175. M. C. Barron et al., *US-Patent 4,916,183* , **1990**

176. F. Robinson, *US-Patent 5,874,495* , **1999**

177. A. Durand, M. Hervé and D. Hourdet, in *Stimuli-Responsive Water Soluble and Amphiphilic Polymers*; C. McCormick, ACS Symposium Series; American Chemical Society: Washington, DC, **2000**

178. A. T. Florence, D. Whitehill, *J. Pharm. Pharmacol.* **1982**, 34, 11, 687-691

179. J. Allouche, E. Tyrode, V. Sadtler, L. Choplin, and J.-L. Salager, *Ind. Eng. Chem. Res.* **2003,** 42*,* 3982-3988

180. *Physics and Chemistry of Interfaces, 2nd revised and enlarged issue*, edited by H.-J. Butt, K. Graf, M. Kappl, WILEY-VCH Verlag GmbH & Co. KGaA, Weinheim, **2006**, ISBN: 3-527-40629-8

181. I. Capek, *Adv. Colloid Interface Sci.* **2004**, 107, 125

182. J. H. Schulman, T. P. Hoar, *Nature* **1943**, 152, 102

183. P. A. Winsor, *Solvent Properties of Amphiphilic Compounds*. Butherworth & Co., London, **1954**

184. *Micelles, Microemulsions and Monolayers, Science and Technology*, edited by Dinesh O. Shah, Marcel Dekker, Inc., New York, Basel, Hong Kong, **1998,** ISBN: 0-8247-9990-9

185. F. Marchal, P. Guenoun, J. Daillant, D. Wade Holley and J. W. Mays, *Soft Matter* **2009**, 5, 4006–4014

186. T. Sottmann and C. Stubenrauch, *Phase Behaviour, Interfacial Tension and Microstructure of Microemulsions, Microemulsions: Background, New Concepts, Applications, Perspectives*, edited by Cosima Stubenrauch, Blackwell Publishing Ltd **2009**. ISBN: 978-1-405-16782

187. B. K. Paul, S. P. Moulik, *Curr. Sci.* **2001***,* Vol. 80*,* No. 8, 25

188. B. Jakobs, T. Sottmann, R. Strey, J. Allgaier, L. Willner, D. Richter, *Langmuir* **1999**, 15, 6707

189. J. Allgaier and H. Frielinghaus, *Microemulsions: Background, New Concepts, Applications, Perspectives*, edited by Cosima Stubenrauch, Blackwell Publishing Ltd **2009**

190. Y. Ishihama, M. Sawamoto, T. Higaehimura, *Polym. Bull.* **1990**, 24, 201-206

191. R. Jordan, A. Ulman, J. F. Kang, M. H. Rafailovich, J. Sokolov, *J. Am. Chem. Soc.* **1999,** 121*,* 1016-1022

192. N. Tomotsu, N. Ishihara, T. H. Newman, M. T. Malanga, *J. Mol. Catal. A* **1998**: Chemical , 128, 167–190

193. W. Kaminsky, S. Lenk, *Macromol. Symp.* **1997**, 118, 45-54

194. C. Schilli, M. G. Lanzendörfer, A. H. E. Müller**,** *Macromolecules* **2002,** 35*,* 6819-6827

195. M. Adamy, A. M. van Herk, M. Destarac, M. J. Monteiro, *Macromolecules* **2003,** 36*,* 2293-2301

196. A. R. Goodall, M. C. Wilkinson and J. Hearn, *J. Polym. Sci.* **1977***, Polym. Chem.*, Vol. 15, 2193-2218

197. M. J. Monteiro and J. de Barbeyrac, *Macromolecules* **2001,** 34*,* 4416-4423

198. K. Matyjaszewski, M. Wei, J. Xia, N. E. McDermott, *Macromolecules* **1997,** 30*,* 8161-8164

199. Y. Tsujii, M. Ejaz, K. Sato, A. Goto, T. Fukuda, *Macromolecules* **2001,** 34*,* 8872-8878

200. K. Matyjaszewski, T. E. Patten, J. Xia, *J. Am. Chem. Soc.* **1997,** 119*,* 674-680

201. V. Percec, H.-J. Kim, B. Barboiu, *Macromolecules* **1997,** 30*,* 6702-6705

202. Y. Kwak, A. Goto, Y. Tsujii, Y. Murata, K. Komatsu, T. Fukuda, *Macromolecules* **2002,** 35*,* 3026-3029

203. G. Moad, D. H. Solomon, Pergamon Press plc, *Comprehensive Polymer Science: the Synthesis, Characterization, Reactions & Applications of Polymers*. *Vol. 3: Chain Polymerization* **1989***,* I, 97-121

204. L. F. Thompson and K. G. Mayhan, *J. Appl. Polym. Sci.* **1972**, Vol. 16**,** 2317-2341

205. A. W. Hui and A. E. Hamielec, *J. Appl. Polym. Sci.* **1972**, Vol. 16**,** 749-769

206. W. A. Pryor and J. H. Coco, *Macromolecules* **1970** ,Vol. 3, No. 5, 500-508

207. D. N. Campbell, US Patent 2,965,685, **1960**

208. G. Moad, D. H. Solomon, *The Chemistry of Free Radical Polymerization*; Pergamon Press, Oxford, U.K., **1995**; p. 92

209. G. Odian, *Principles of Polymerization*, third edition, John Wiley and Sons, **1991**. ISBN: 0-471-61020-8

210. K. S. Khuong, W. H. Jones, W. A. Pryor, K. N. Houk, *J. Am. Chem. Soc.* **2005**, 127, 1265-1277

211. F. R. Mayo, *J. Am. Chem. Soc.* **1968**, 90, 1289

212. Y. K. Chong, E. Rizzardo and D. H. Solomon, *J. Am. Chem. Soc* **1983**, Vol. 105, No. 26, 7761-7762

213. W. C. Buzanowski, J. D. Graham, D. B. Priddy, E. Shero, *Polymer* **1992**, Vol. 33, No. 14, 3055-3059

214. W. Devonport, L. Michalak, E. Malmström, M. Mate, B. Kurdi, C. J. Hawker, G G. Barclay and R. Sinta, *Macromolecules* **1997**, 30, 1929-1934

215. Pryor, W. A.; Lasswell, L. D. *Advances in Free Radical Chemistry*; Academic Press: London, **1975**; chapter 2, p. 27-100.

216. K. Jankova and S. Hvilsted, *Macromolecules* **2003**, 36, 1753-1758

217. H. Tan, H. Hussain, Y. Liu, C. B. He and T. P. Davis, *Langmuir* **2010**, 26, 4, 2361–2368

218. C. Pugh, C. N. Tang, M. Paz-Pazos, O. Samtani and A. H. Dao, *Macromolecules* **2007**, 40, 8178-8188

219. A. M. Nyström, J. W. Bartels, W. Du, K. L. Wooley, *J. Polym. Sci. A: Polym. Chem.* **2009**, Vol. 47, 1023–1037

220. C. Cheng, K. L. Wooley, E. Khoshdel, *J. Polym. Sci. A: Polym. Chem.* **2005**, Vol. 43, 4754–4770

221. S. Suzuki, M. R. Whittaker, E. Wentrup-Byrne, M. J. Monteiro and L. Grøndahl, *Langmuir* **2008**, 24, 13075-13083

222. *Azo Polymerization Initiators*, Wako Pure Chemicals GmbH, Nissanstraße 2, D-41468 Neuss, Germany

223. *Handbook of Fluorous Chemistry*, edited by J. A. Gladysz, D. P. Curran, I. T. Horváth, WILEY-VCH Verlag GmbH & Co. KGaA, Weinheim, **2004**, ISBN: 3-527-30617-X

224. *Nachrichten aus der Chemie* **2005**, 53, 743-746

225. A. Holleman, E. Wiberg, *Lehrbuch der Anorganischen Chemie*, 101. Auflage, Verlag DeGruyter, **1995**, ISBN: 3-11-012641-9

226. J.G. Riess, *Colloids Surf.* **1994**, 84, 33

227. J. G. Riess, *J. Fluorine Chem.* **2002**, 114, 119-126

228. T. M. Reed, in *Fluorine Chemistry, Vol. 5,* J. H. Simmons, Ed. Academic Press, New York, **1964**, p. 133

229. M. P. Krafft, Ed., *Fluorinated Colloids and Interfaces*, *a Section of Curr. Opin. Colloid Interf. Sci.* **2003**, 8, 213

230. S. G. Hatzikiriakos, P. Hong, W. Ho, C. W. Stewart, *J. Appl. Polym. Sci.* **1995**, 55, 4, 595-603

231. F. Hernandez, M. A. Escobar, C. Sanchez, D. Aviles, *Precision Electromagnetic Measurements Digest,* **1998**, pp.414-415

232. K. E. Perepelkin, *Fiber Chemistry* **2004**, Vol. 36, No. 1, 43-58

233. J. Aumann, *European Patent EP0581186*, **1996**

234. F. Yi, S. Zheng, T. Liu, *J. Phys. Chem. B* **2009**, 113, 1857-1868

235. G. Li, H. Zheng, Y. Wang, H. Wang, Q. Dong, R. Bai, *Polymer* **2010***,* 51, 1940-1946

236. B. H. Tan, C. S. Gudipati, H. Hussain, C. He, Y. Liu, T. P. Davis, *Macromol. Rapid Commun.* **2009**, 30, 1002-1008

237. I. Dimitrov, K. Jankova, S. Hilvsted; *J. Polym. Sci. A: Polym. Chem.* **2008**, Vol. 46, 7827-7834

238. Y. W. Chen, L. Ying, W. H. Yu, E. T. Kang, K. G. Neoh, *Macromolecules* **2003**, 36, 25, 9451

239. L. Ying, W. H. Yu, E. T. Kang, K. G. Neoh, *Langmuir* **2004**, 20, 14, 6032

240. Y. W. Chen, W. C. Wang, W. H. Yu, E. T. Kang, K. G. Neoh, R. H. Vora, *J. Mater. Chem.* **2004**, 14, 9, 1406

241. W. H. Yu, E. T. Kang, K. G. Neoh, *Langmuir* **2005,** 21, 1, 450

242. C. S. Gudipati, C. M. Greenlief, J. A. Johnson, P. Prayongpan, K. L. Wooley, *J. Polym. Sci. A: Polym. Chem.* **2004**, Vol. 42, 6193–6208

243. X. Cheng, M. Prehm, M. K. Das, J. Kain, U. Baumeister, S. Diele, D. Leine, A. Blume and C. Tschierske, *J. Am. Chem. Soc.* **2003**, 125, 10977-10996

244. H. Cui, Z. Chen, S. Zhong, K. L. Wooley, D. J. Pochan, *Science* **2007**, Vol. 317, 647-650

245. Y. S. Ko and Y. K. Kwon, *Solid State Phenomena* **2007**, Vol. 124-126, 595-598

246. T. L. Bucholz and Y.-L. Loo, *Macromolecules* **2006,** 39*,* 6075-6080

247. B. Voit, D. Appelhans, *Macromol. Chem. Phys.* **2010**, 211, 727–735

248. C. R. Becer, K. Babiuch, D. Pilz, S. Hornig, T. Heinze, M. Gottschaldt, U. S. Schubert, *Macromolecules* **2009**, 42, 2387.

249. S. Slavin, J. Burns, D. M. Haddleton, C. R. Becer, *Europ. Polym. J.* **2011**, Vol. 47, 4, 435-446

250. C. R. Becer, K. Kokado, C. Weber, A. Can, Y. Chujo, U. S. Schubert, *J. Polym. Sci. A: Polym. Chem.* **2010,** Vol. 48, 1278-1286

251. H. Hussain, B. H. Tan, K. Y. Mya, Y. Liu, C. B. He, T. P. Davis, *J. Polym. Sci. A: Polym. Chem.* **2010**, Vol. 48, 152-163

252. M. L. Becker, E. E. Remsen, K. L. Wooley, *J. Polym. Sci. A, Polym. Chem.* **2001**, Vol. 39, 4152–4166

253. A. W. Stephens, A. W. Levine, J. Fech, JR., T. J. Zrebiec, A. V. Cafiero and A. M. Garofalo, *Thin Sol. Films* **1974***,* 24, 361-379

254. I. A. Rousseau and P. T. Mather, *J. Am. Chem. Soc.* **2003**, 125,15300–15301

255. S. Surgihara, M. Kitagawa, Y. Inagawa, I. M. Zaleska, I. Ikedo, *Polym. Bull.* **2010**, 64, 209-220

256. W. Lehmann, H. Skupin, C. Tolksdorf, E. Gebhard, R. Zentel, P. Kruger, M. Losche and F. Kremer, *Nature* **2001**, 410, 447–450

257. T. Fukushima, K. Asaka, A. Kosaka and T. Aida, *Angew. Chem., Int. Ed.* **2005**, 44, 2410–2413

258. T. Gelbrich, M. Feyen and A. M. Schmidt, *Macromolecules* **2006**, 39, 3469–3472

259. A. Pelah, R. Seemann and T. M. Jovin, *J. Am. Chem. Soc.* **2007**, 129, 468–469

260. Y. Qiu and K. Park, *Adv. Drug Delivery Rev.* **2001**, 53, 321–339

261. O. Tabata, H. Hirasawa, S. Aoki, R. Yoshida and E. Kokufuta, *Sens. Actuators A,* **2002**, 95, 234–238

262. I. Y. Galaev, B. Mattiasson, *Trends Biotech.* **1999**, 17, 8.335-340

263. B. Zhao and J. S. Moore, *Langmuir* **2001**, 17 (16), 4758–4763

264. J. E. Chung, M. Yokoyama, T. Aoyagi, Y. Sakurai, T. Okano, *J. Contr. Rel.* **1998**, 53, 1-3, 119-131

265. C. Petit, P. Lixon, M.-P. Pileni, *J. Phys. Chem.* **1993**, 97, 12974-12983

266. S. J. Holder, G. G. Durand, C.-T. Yeoh, E. Illi, N. J. Hardy, T. H. Richardson, *J. Polym. Sci. A: Polym. Chem.* **2008**, Vol. 46, 7739–7756

267. J.-F. Gohy, *Adv. Polym. Sci.* **2005**, 190, 65–136

268. J.-F. Gohy, N. Willet, S. Varshney, J.-X. Zhang, and R. Jérôme, *Angew. Chem.* **2001**, 113, 17, 3314-3316

269. K. Skrabania, *PhD-thesis*, University of Potsdam, **2009**

270. J.-N. Marsat, *PhD-thesis*, University of Potsdam **2010**

271. F. Franks, D. Eagland, *CRC Crit. Rev. Biochem.* **1985**, 4, 165

272. J. Virtanen, *PhD-thesis*, University of Helsinki, **2002**

273. E. H. Sprecht, A. Neuman, H. T. Neher, *U.S. Pat. 2,773,063*; Rohm & Haas, **1956**

274. CIBA Ltd., *Br. Pat. 746, 747*; **1956**

275. E. H. Sprecht, A. Neuman, H. T. Neher, *Br. Pat. 772,196*; Rohm & Haas, **1956**

276. M. Heskins, J. E. Guillet, *J. Macromol. Sci. Chem.* **1969**, 2, 1441

277. M. A. Cole, N. H. Voelcker, H. Thissen, H. J. Griesser, *Biomaterials* **2009**, 30, 1827–1850

278. M. A. Cole, M. Jasieniak, N. H. Voelcker, H. Thissen, R. Horn, H. J.Griesser, *Proc. SPIE–Int. Soc. Opt. Eng.* **2007**; 6416, 641606/1–641606/10 (Biomedical Applications of Micro- and Nanoengineering III)

279. X. Cheng, H. E. Canavan, D. J. Graham, D. G. Castner, B. D. Ratner, *Biointerphases* **2006**;1(1), 61–72

280. A. Kushida, M.Yamato, C. Konno, A. Kikuchi, Y. Sakurai, T. Okano, *J. Biomed. Mater. Res.* **1999**, 45, 4, 355–62

281. D. L. Huber, R. P. Manginell, M. A. Samara, B. I. Kim, B. C. Bunker. *Science* **2003**, 301, 5631, 352–4

282. X. H. Cheng, Y. B. Wang, Y. Hanein, K. F. Bohringer, B. D. Ratner, *J. Biomed. Mater. Res. A* **2004**, 70A, 2, 159–168

283. M. Kurisawa, M. Yokoyama, T. Okano, *J. Control. Release* **2000**, 69, 1, 127–137

284. A. Zintchenko, M. Ogris, E. Wagner. *Bioconjug. Chem.* **2006**, 17, 3, 766–772

285. M. Y. Arica, H. A. Öktem, Z. Öktem and S. A. Tuncel, *Polym. Int.* **1999**, 48, 879-884

286. I. K. Kwon, T. Matsuda, *Biomaterials* **2006**, 27, 986–995

287. R. Xie, L. Chu, W. Chen, W. Xiao, H. Wang, J. Qu, *Journal of Chemical Industry and Engineering China* **2005**, 11

288. R.-W. Guo, D.-C. Wu, X.-D. Lu, D.-B. Fang, *Journal of Petrochemical Technology* **2003**, 8

289. A. Desponds and R. Freitag, *Langmuir* **2003,** 19*,* 6261-6270

290. J.-P. O`Shea, G. G. Qiao, G. V. Franks, *in: Engineering Our Future: Are We up to the Challenge?* 27.-30. September **2009**, Burswood Entertainment Complex, Barton, ACT. Engineers Australia, **2009**, 1758-1768

291. D. Schmaljohann, *Adv. Drug Del. Rev.* **2006,** 58, 1655–1670

292. T. Oya, T. Enoki, A. Y. Grosberg, S. Masamune, T. Sakiyama, Y. Takeoka, K. Tanaka, G. Wang, Y. Yilmaz, M.S. Feld, R. Dasari, T. Tanaka, *Science* **1999**, 286, 1543

293. K. Yamashita, T. Nishimura, K. Ohashi, H. Ohkouchi, M. Nango, *Polym. J.* **2003**, 35, 545

294. R. Yoshida, *Curr. Org. Chem.* **2005**, *9,* 1617-1641

295. G. Chen, Y. Imanishi, Y. Ito, *Macromolecules* **1998**, 31, 4379

296. E. Kokufuta and Y. Aman, *Polymer Gels and Networks* **1997**, 5, 439-454
297. E. Kokufuta, Y.-Q. Zhang, T. Tanaka. *J. Biomater. Sci., Polym. Edn.* **1994**, 35
298. Y. Osada, A. Matsuda, *Nature* **1995**, 376, 219
299. J. H. Holtz, S.A. Asher, *Nature* **1997**, 389, 829
300. Y. Okumura, K. Ito, K. *Adv. Mater.* **2001**, 13, 485
301. K. Haraguchi, T. Takehisa, S. Fan, *Macromolecules* **2002**, 35, 10162
302. Y. Kaneko, K. Sakai, A. Kikuchi, R. Yoshida, Y. Sakurai, T. Okano *Macromolecules* **1995**, 28, 7717
303. Y. Takeoka, M. Watanabe, *Langmuir* **2002**, 18, 5977
304. A. M. Bivigou-Koumba, *PhD-thesis*, Universität Potsdam, **2009**
305. S. Ito, O. Hirasa, A. Yamauchi, *Kobunshi Robunshu* **1989**, 46, 427
306. S. Ito, K. Mizoguchi, *IUPAC MACRO88 preprint*, **1988**, 767
307. H. G. Schild, *Prog. Pol. Sci.* **1992**, 17, 163-249
308. X. Wang, X. Qiu, C. Wu, *Macromolecules* **1998**, 31, 2972-2976
309. J.-F. Lutz, Ö. Akdemir, and A. Hoth, *J. Am. Chem. Soc.* **2006**, 128, 13046-13047
310. J. Storsberg, *Labbook*
311. *Japan Patent 58-103348*, U.S.A. patent pending
312. S. W. Kim, J. H. Bae, T. Okano, *Pharm. Res.* **1992**, 9, 3
313. N. Kuramoto, Y. Shishido, K. Nagai, *Macromol. Rapid Commun.* **1994**, 15, 441-444
314. S. Garnier, A. Laschewsky, *Langmuir* **2006**, 22, 4044–53
315. A. B. Lowe, C. L. McCormick, *Prog. Polym. Sci.* **2007**, 32, 283–351
316. M. Mertoglu, S. Garnier, A. Laschewsky, K. Skrabania, J. Storsberg, *Polymer* **2005**, 46, 7726–7740
317. M. Kobayashi, S. Okuyama, T. Ishizone, and S. Nakahama, *Macromolecules* **1999**, 32, 6466-6477
318. K. Fujimoto, Y. Nakajima, M. Kashiwabara, H. Kawaguchi, *Polym. Internat.* **1993**, 30, 237-241
319. I. Prigogine, R. DeFay, *Chemical Thermodynamics*; *2nd French edition,* translated by D. H. Everett, Longmans, Green and Co, London **1954**, p. 229
320. L. D. Taylor, L. D. Ceranowski, *J. Polym. Sci.* **1975**, 13, 2551
321. J. A. Walker, C. A. Vause, *Sci. Am.* **1987**, 253, 98
322. C. Tanford, *Hydrophobic Effect*, *2nd edition*, J. Wiley and Sons, New York **1973**
323. A. Ben-Naim, *Hydrophobic Interactions*, Plenum Press, New York, **1980**
324. S. Förster, M. Schmidt, M. Antonietti, *Polymer* **1990**,31,(5), 781-792

325. W. Burchard, *Adv. Polym. Sci.* **1998**, 143, 173

326. F. Hua, X. Jiang, D. Li, B. Zhao, *J. Polym. Sci. A: Polym. Chem.* **2006**, 44, 2454-2467

327. C. Petit, P. Lixon, M.-P. Pileni, *J. Phys. Chem.* ***1993***, 97, 12974-12983

328. S. Kawaguchi, G. Imai, J. Suzuki, A. Miyahara, T. Kitano, K. Ito, *Polymer* ***1997***, 38, 12

329. Q. Duan, Y. Miura, A. Narumi, X. Shen, S.-I. Sato, T. Kakuchi, *J. Polym. Sci. A: Polym. Chem.* **2006**, 44, 1117-1124

330. Y. Xia, N. A. D. Burke, and H. D. H. Stöver, *Macromolecules* **2006,** 39*,* 2275-2283

331. H. Schild, D. A. Tirrell, *J. Phys. Chem.* **1990**, 94, 4352-4356

332. K. Van Durme, S. Verbrugghe, F. E. Du Prez, and B. Van Mele, *Macromolecules* **2004,** 37*,* 1054-1061

333. A. B. Faust, P. S. Sremcich, and J. W. Gilmer, J. W. Mays, *Macromolecules* **1989**, 22, 1250-1254

334. S. Huber, N. Hutter, R. Jordan, *Colloid Polym. Sci.* **2008**, 286, 1653–1661

335. J. H. Laurer, S. A. Khan, R. J. Spontak, M. M. Satkowski, J. T. Grothaus, S. D. Smith, J. S. Lin, *Langmuir* **1999**, 7947-7955

336. T. Ishizone, A. Seki, M. Hagiwara, S. Han, H. Yokoyama, A. Oyane, A. Deffieux and Stéphane Carlotti, *Macromolecules* **2008**, 41, 2963-2967

337. T. I. Mana-Ito, *J. Polym. Sci. A: Polym. Chem.* **2006**, 44, 4832-4845

338. B. Ray, Y. Isobe, K. Matsumoto, S. Habaue, Y. Okamoto, M. Kamigaito and M. Sawamoto, *Macromolecules* **2004**, 37, 1702-1710

339. H. Feil, Y. H. Bae, J. Feijen, S. W. Kim, *Macromolecules* **1993**, 26, 2496-2500

340. S. Beltran, J. P. Baker, H. H. Hooper, H. W. Blanch, J. M. Prausnitz, *Macromolecules* **1991**, 24, 549-551

341. G. Bokias, D. Hourdet, I. Iliopoulos, *Macromolecules* **2000**, 33, 2929-2935

342. X. Yin and H. D. H. Stöver, *Macromolecules* **2005,** 38*,* 2109-2115

343. O. R. Costa Ricardo, F. S. Freitas Roberto, *Polymer* **2002**, 43, 5879-5885

344. K. Skrabania, J. Kristen, A. Laschewsky, Ö. Akdemir, A. Hoth, J.-F. Lutz: *Langmuir* **2007**, 23, 84

345. J. Virtanen, M. Arotçarèna, B. Heise, S. Ishaya, A. Laschewsky and H. Tenhu, *Langmuir* **2002**, 18, 5360-5365

346. H. Schott, A. E. Royce and S. K. Han, *J. Coll. Interface Sci.* **1984***,* Vol. 98, No. 1, 196-201

347. H. Faes, F. C. D. Schryver, A. Sein, K. Bijma, J. Kevelam, J. B. F. N. Engberts, *Macromolecules* **1996,** 29, 3875

348. B. M. Hasch, S.-H. Lee, M. A. McHugh, *Fluid Phase Equilibria* **1993**, Vol. 83, 341-348

349. M. R. Aguilar, C. Elvira, A. Gallardo, B. Vázquez and J.S. Román, Smart Polymers and Their Applications as Biomaterials, *Topics in Tissue Engineering* **2007**, Vol. 3, Eds. N. Ashammakhi, R. Reis & E. Chiellini © 2007

350. Q. Duan, Y. Miura, A. Narumi, X. Shen, S.-I. Sato, T, Satoh, T. Kakuchi, *J. Polym. Sci. A: Polym. Chem*. **2006**, 44, 1117-1124

351. F. M. Winnik, A. Adronov, H. Kitano, *Can. J. Chem.* **1995**, 73, 2030-2040

352. T. Baltes, F. Garret-Flaudy, R. Freitag, *J. Polym. Sci. A: Polym. Chem.* **1999**, 37, 2977

353. R. Freitag, T. Baltes, M. Eggert, K. Schuegerl, B. Ute, *Bioseparation* **1994**, 4, 353

354. U. Rauwald, J. del Barrio, X. J. Loh and O. A. Scherman, *Chem. Commun.* **2011**, 47, 6000–6002

355. S. W. Choi, H. Ritter, *Macromol. Rapid. Commun.* **2007**, 28, 101-108

356. P. A. Schacht, J. T. Koberstein, *Polymer* **2002**, 43, 6527–6534

357. H. G. Schild, D. A. Tirell, *Langmuir* **1990**, 6, 1676-1679

358. Z. Tong, F. Zeng, X. Zheng, T. Sato, *Macromolecules* **1999**, 32, 4488-4490

359. Z. Ding, G. Chen, A. S. Hoffman, *Bioconjugate Chem.* **1996**, 7, 121-125

360. F. Afroze, E. Nies, H. Berghmans, *J. Mol. Struct.* **2000**, 554, 55

361. S. Fujushige, K. Kubota, I. Ando, *J. Phys. Chem.* **1989**, 93, 3311-3313

362. C. Chaibundit, P. Sumanatrakool, S. Chinchew, P. Kanatharana, C. E. Tattershall, C. Booth, X.-F. Yuan, *Coll. Interf. Sci.* **2005**, 283, 544

363. G. Riess, *Prog. Polym. Sci.* **2003**, 28, 1107

364. Y. Jiang, T. Chen, F. Ye, H. Liang, A.-C. Shi, *Macromolecules* **2005**, 38, 6710

365. M. Mertoglu, *PhD-thesis*, University of Potsdam, **2004**

366. H. Schott, *J. Pharm. Sci.* **1995,** Vol. 84, No. 10, 1215-1222

367. H. Schott, *J. Pharm. Sci.* **1971,** Vol. 60, No. 4, 648-649

368. R. C. Pasquali, M. P. Taurozzi, C. Bregni, *Int. J. Pharm.* **2008**, 356, 44–51

369. H. Kunieda and K. Shinoda, *J. Coll. Interface Sci.* **1985***,* Vol. 107, No. 1, 107-121

370. M. Buzier and J.-C. Ravey, *J. Coll. Interface Sci.* **1983***,* Vol. 91, No. 1, 20-3

371. J. Szymanowski, *Fette, Seifen, Anstrichmittel* **1982,** 84, 6, 245-248

372. M.Y. Kozlow, N.S. Melik-Nubarov, E.V. Batrakova, A.V. Kabanov, *Macromolecules* **2000**, 33 (9), 3305–3313

373. A. D. Bedells, R. M. Arafeh, Z. Yang, D. Attwood, F. Heatley, J. C. Padget, C. Price and C. Booth, *J. Chem. Soc., Faraday Trans.* **1993**, 89, 1235-1242

374. K. Troll, A. Kulkarni, W. Wang, C. Darko, A. M. Bivigou-Koumba, A. Laschewsky, P. Müller-Buschbaum, C. Papadakis, *Colloid Polym. Sci.* **2008**, 286, 1079-1092

375. Z. Tuzar and P. Kratochvil, *Adv. Colloid Interface Sci.* **1976**, 6, 201

376. L. Maibaum, A. R. Dinner and D. Chandler, *J. Phys. Chem. B* **2004,** 108*,* 6778-6781

377. W. Blokzijl and J. B. F. N. Engberts, *Angew. Chem. Int. Ed. Engl.* **1993,** 32, 1545-1579

378. L. R. Pratt, D. Chandler, *J. Chem. Phys.* **1977**, Vol. 67, No.8, 3683-3704

379. B. Jeong, A. Gutowska, *Trends Biotechnol.* **2002**, 20, 305-311

380. P. Dimitrov, S. Rangelov, A. Dvorak, C. B. Tsvetanov, *Macromolecules* **2004**, 37, 1000-1008

381. L. Qiao, C. Leibig, S. F. Hahn and K. I. Winey, *Ind. Eng. Chem. Res* **2006**, Vol. 45, No. 16

382. G. He, L. L. Ma, J. Pan, S. Venkatraman, *Int. J. Pharm.* **2007**, 334, 48–55

383. X. Zhao, W. Liu, D. Chen, X. Lin, W. W. Lu, *Macromol. Chem. Phys.* **2007**, 208, 1773–1781

384. Y. He, T. R. Lutz, M. D. Ediger, *Macromolecules* **2003,** 36*,* 8040-8048

385. V. Darcos, D. M. Haddleton, *Europ. Polym. J.* **2003**, 39, 855–862

386. J. Mohammadi-Rovsandeh, S. M. F. Farnia, M. N. Sarbouluki, *J. Appl. Polym. Sci.* **1999**, Vol. 74, 2004–2009

387. Y. Z. Luo, C. V. Nicholas, D. Attwood, J. H. Collett, C. Price, C. Booth, *Colloid Polym. Sci.* **1992**, 270, 1094-1105

388. Z. Yang, R. Sharma, *Langmuir* **2001**, 17, 6254-6261

389. R. J. Spontak, E. A. Wilder and S. D. Smith, *Langmuir* **2001,** 17*,* 2294-2297

390. A. Keralakis, V. Havredaki, C. Booth, *Macromol. Chem. Phys.* **2003**, 204, 15-21

391. K. Mortensen, J. S. Pedersen, *Macromolecules* **1993**, 26, 805-812

392. L. Qiao, C. Leibig, S. F. Hahn and K. I. Winey, *Ind. Eng. Chem. Res* **2006**, Vol. 45, No. 16

393. A. Avgeropoulos, V. Z.-H. Chan, V. Y. Lee, D. Ngo, R. D. Miller, Nikos Hadjichristidis and E. L. Thomas, *Chem. Mater.* **1998**, Vol. 10, No. 8, 2109-2115

394. J. Heller, E. Schacht, V. Toncheva, *US 2006/023508 4A1,* **2006**, Heller Ehrman LLP, 275 Middlefield Road, Menlo Park CA, 94025-3506 US

395. X. Zhao, W. Liu, D. Chen, X. Lin, W. W. Lu, *Macromol. Chem. Phys.* **2007**, 208, 1773–1781

396. C. B. Packhaeuser, J. Schnieders, C. G. Oster, T. Kissel, *Eur. J. Pharm. Biopharm.* **2004**, 58, 445–455

397. M. S. Shim, H. T. Lee, W. S. Shim, I. Park, H. Lee, T. Chang, *Wiley Periodicals, Inc., **2002***

398. J. R. Quintana, E. Hernáez, and I. Katime, *J. Phys. Chem. B* **2001**, 105, 2966-2970

399. H. T. Lee and D. S. Lee, *Macromol. Res.* **2002**, Vol. 10, No. 6, 359-364

400. S. J. Bae, J. M. Suh, Y. S. Sohn, Y. H. Bae, S. W. Kim and B. Jeong, *Macromolecules* **2005**, 38, 5260-5265

401. Y. H. Bae, S. W. Kim, *J. contr. Rel.* **2000**, 63, 155-163

402. C. L. McCormick, B. S. Sumerlin, B. S. Lokitz and J. E. Stempka, *Soft Matter* **2008**, 4, 1760–1773

403. L. Yu and J. Ding, *Chem. Soc. Rev.* **2008**, 37, 1473–1481

404. O. Ortona, G. D' Errico, L. Paduano, V. Vitagliano, *J. Coll. Interface Sci.* **2006**, 301, 63–77

405. M. Bohorquez, C. Koch, T. Trygstad, and N. Pandit, *J. Coll. Interface Sci.* **1999**, 216, 34–40

406. P. Alexandridis, J. F. Holzwarth and T. A. Hatton, *Macromolecules* **1994,** 27, 2414-2425

407. H.-W. Tsui, Y.-H. Hsu, J.-H. Wang and L.-J. Chen, *Langmuir* **2008,** 24*,* 13858-13862

408. Y.-L. Su, X.-F. Wei, and H.-Z. Liu, *Langmuir* **2003**, 19*,* 2995-3000

409. M. Desai, N. J. Jain, R. Sharma, and P. Bahadur, *J. Surf. Det.* **2000**, Vol. 3, No. 2, 193-199

410. Y. H. Bae, S. W. Kim, *J. contr. Rel.* **2000**, 63, 155-163

411. Z. Zhou and B. Chu, *J. Coll. Interface Sci.* **1988**, Vol. 126, No. 1, 171-180

412. X. Zhao, W. Liu, D. Chen, X. Lin, W. W. Lu, *Macromol. Chem. Phys.* **2007**, 208, 1773–1781

413. K. Mortensen, *Curr. Opin. Coll. Interface Sci.* **1998**, 3, 12-19

414. K. Mortensen, K. Almda, R. Kleppinger, N. Mischenko, H. Reynaers, *Physica B* **1998**, 241-243, 1025-1028

415. R. Saito, S. Yoshida, K. Ishizu, *J. of Appl. Polym. Sci.* **1997**, 63, 849–854

416. M. Nguyen-Misra and W. L. Mattice, *Macromolecules* **1996,** 28, 1444-1457

417. M. S. Donovan, A. B. Lowe, T. A. Sanford, C. L. Mc Cormick, *J. Polym. Sci. A, Polym. Chem.* **2003**, Vol. 41, 1262–1281

418. C. Chassenieux, T. Nicolai, L. Benyahia, *Curr. Opin. Coll. Interface Sci.* **2010***,* Vol. 16, 1, 18-26

419. S. H. Kim and W. H. Jo, *J. Chem. Phys.* **2002**, Vol. 117, No. 18, 8565-8572

420. J. Yuan, Z. Xu, S. Cheng, L. Feng, *Europ. Polym. J.* **2002**, 38, 1537–1546

421. J. Yuan, Y. Li, X. Li, S. Cheng, L. Jiang, L. Feng, Z. Fan, *Europ. Polym. J.* **2003**, 39, 767–776

422. K. Yu, A. Eisenberg, *Macromolecules* **1998**, 31, 3509–3518

423. K. Mortensen, W. Brown, E. Joergensen, *Macromolecules* **1994**, 27, 5654-5666

424. R. Kleppinger, N. Mischenko, E. Theunissen, H. L. Reynaers, M. H. J. Koch, K. Almdal and K. Mortensen, *Macromolecules* **1997**, 30, 7012-7014

425. D. S. Lee, M. S. Shim, S. W. Kim, H. Lee, I. Park, T. Chang, *Macromol. Rapid Comm.* **2001***,* 22, 587-592

426. T. Annable, R. Buscall, R. Ettelaie, D. Whittlestone, *J. Rheol.* **1993***,* 37, 695-726

427. S. J. Bae, J. M. Suh, Y. S. Sohn, Y. H. Bae, S. W. Kim, B. Jeong, *Macromolecules* **2005**, 38, 5260-5265

428. N. Kumar, M. N. V. Ravikumar, A. J. Domb, *Adv. Drug Del. Rev.* **2001**, 53, 23–44

429. L. Yu, G. T. Chang, H. Zhang, J. D. Ding, *Int. J. Pharm.* **2008,** 348, 95-106

430. G. M. Zentner, R. Rathi, C. Shih, J. C. McRea, M.-H. Seo, H. Oh , B.G. Rhee , J. Mestecky , Z. Moldoveanu , M. Morgan , S. Weitman, *J. Control. Rel.* **2001**, 72, 203–215

431. R. T. A. Mayadunne, E. Rizzardo, J. Chiefari, J. Kristina, G. Moad, A. Postma and S. H. Thang, *Macromolecules* **2000**, Vol. 33, No. 2, 243-245

432. M. Drew, E. Orton, P. Krolikowski, J. M. Salvino, N. V. Kumar, *J. Comb. Chem.* **2000**, 2, 8-9

433. E. Amado, J. Kressler, *Macromol. Chem. Phys.* **2005**, 206, 850–859

434. L. He, J. P. Hinestrosa, J. M. Pickel, S. Zhang, D. G. Bucknall, S. M. Kilbey, J. W. Mays, K. Hong, *J. Polym. Sci. A: Polym. Chem.* **2011**, Vol. 49, 414–422

435. P. Miles and H. Suschizky, *Tetrahedron* **1963**, Vol. 19, 385-390

436. Prof. A. Laschewsky, *personal message*

437. R. Wang, C. L. McCormick, A. B. Lowe, *Macromolecules* **2005**, 38, 9518-9525

438. R. A. Mayadunne, G. Moad, E. Rizzardo, *Tetrahedron Lett.* **2002**, 43, 6811-6814

439. G. Moad, Y. K. Chong, E. Rizzardo, A. Postma, S. H. Thang, *Polymer* **2005**, 46, 8458-8468

440. E. Rizzardo, S. H. Thang, G. Moad, *WO9905099*, **1999**, Commonwealth Scientific and Industrial Research Organization, Australia, E. I. Du Pont de Nemours & Co.

441. J. Bang, S. H. Kim, E. Drockenmuller, M. J. Misner, T. P. Russell, C. J. Hawker, *J. Am. Chem. Soc.* **2006**, 128, 7622-7629

442. J. T. Lai, D. Filla, R. Shea, *Macromolecules* **2002,** *35*, 6754-6756

443. R. A. Mayadunne, G. Moad, E. Rizzardo, *Tetrahedron Lett.* **2002**, 43, 6811-6814

444. W. M. Lee , W. H. Chan and H. C. Wong, *Synth. Commun.* **1988**, 18:13, 1531-1536

445. C. Barner-Kowollik, H. Dalton, T. P. Davis and M. H. Stenzel, *Angew. Chem.* **2003**, 115, 3792 –3796

446. H. Zhang, J. Deng, L. Lu, and Y. Cai, *Macromolecules* **2007,** 40*,* 9252-9261

447. G. Zhou and I. I. Harruna, *Macromolecules* **2005,** 38*,* 4114-4123

448. T. Gruendling, R. Pickford, M. Guilhaus, C. Barner-Kowollik, *J. Polym. Sci. A: Polym. Chem.* **2008**, 46, 7447-7461

449. W. Jiang, S. Khan and Y. Wang, *Macromolecules* **2005**, 38, 7514-7520

450. K. Kubota, S. Fujishige, I. Ando, *J. Phys. Chem.* **1990**, 94, 5154-5158

451. C. Wu, S. Zhou, *Macromolecules* **1995**, 28, 5388-5390

452. H. Ringsdorf, J. Venzmer, F. M. Winnik, *Macromolecules* **1991**, 24, 1678-1686

453. K. Skrabania, W. Li, A. Laschewsky, *Macromol. Chem. Phys.* **2008**, 209, 1389–1403

454. C. Y. Gong, Z. Y. Qian, C. B. Liu, M. J. Huang, Y. C. Gu, Y. J. Wen, B. Kan, K. Wang, M. Dai, X. Y. Li, M. L. Gou, M. J. Tu and Y. Q. Wei, *Smart Mater. Struct.* **2007**, 16, 927–933

455. V. V. Vasilevskaya, P. G. Khalatur, A. R. Khokhlov, *Macromolecules* **2003**, 36, 10103-10111

456. C. Wu, W. Li, X. X. Zhu, *Macromolecules* **2004**, 37, 4989-4992

457. P. Kujawa, F. Tanaka, F. M. Winnik, *Macromolecules* **2006**, 39 (8), 3048–3055

458. M.-C. Jones, J.-C. Leroux, *Europ. J. Pharm. Biopharm.* **1999**, 48, 101-111

459. V. S. Trubetskoy, V. P. Torchilin, *Adv. Drug Del. Rev.* **1995**, 16, 311-320

460. J. Storsberg, A. Laschewsky, *SÖFW-Journal* **2004**, 14, 130

461. *Nanoelectronics and Information Technology, Advanced Electronic Materials and Novel devices*, 2nd corrected edition, edited by R. Waser, Verlag Wiley-VCH **2005**, ISBN: 3-527-40542-9

462. G. ten Brinke and G. Hadziioannou, *Macromolecules* **1987**, 20, 486-489

463. I. W. Hamley, *Phil. Trans. R. Soc. Lond. A* **2001**, 359, 1017-1044

464. C. Booth, D. Attwood, *Macromol. Rapid Commun.* **2000**, 21, 501-527

465. R. K. Prud'homme, G. Wu and D. K. Schneider, *Langmuir* **1996**, 12, 4651-4659

466. V. Castelletto, I. W. Hamley, X. F. Yuan, A. Kelarakis, C. Booth, *Soft Matter* **2005**, 1, 138–145

467. A. Kelarakis, V. Havredaki, X.-F. Yuan, C. Chaibundit, C. Booth, *Macromol. Chem. Phys.* **2006**, 207, 903–909

468. X. Zhao, W. Liu, D. Chen, X. Lin, W. W. Lu, *Macromol. Chem. Phys.* **2007**, 208, 1773–1781

469. S. E. Kirkland, R. M. Hensarling, S. D. McConaughy, Y. Guo, W. L. Jarrett and C. L. McCormick, *Biomacromolecules* **2008,** 9*,* 481–486

470. Dr. E. Görnitz, *personal communication*

471. H. Huang, T. Kowalewski, E. E. Remsen, R. Gertzmann and K. L. Wooley, *J. Am. Chem. Soc.* **1997,** 119*,* 11653-11659

472. D. J. Enscore, H. B. Hopfenberg, V. T. Stannett, *Polymer* **1977**, Vol.18, 793-800

473. Y. Ma, T. Cao, S. E. Webber, *Macromolecules* **1998,** 31*,* 1773-1778

474. A. Lavasanifar, J. Samuel, G. S. Kwon, *Coll. Surf. B* **2001***: Bioint.*, 22, 115–126

475. S. E. Webber, *J. Phys. Chem. B* **1998,** 102*,* 2618-2626

476. A. Matsuda, J. Sato, H. Yasunaga, Y. Osada, *Macromolecules* **1994,** 27**,** 7695-7698

477. M. Uchida, M. Kurosawa, Y. Osada, *Macromolecules* **1995**, 28**,** 4583-4586

478. J. Ruokolainen, M. Torkkeli, R. Serimaa, B. E. Komanschek, O. Ikkala and G. ten Brinke, *Phys. Rev. E* **1996**, Vol. 54, 6, 6646-6649

479. A. R. Katritzky, S. Sild, V. Lobanov and M. Karelson, *J. Chem. Inf. Comput. Sci.* **1998,** 38*,* 300-304

480. C. Cao and Y. Lin, *J. Chem. Inf. Comput. Sci.* **2003,** 43*,* 643-650

481. X. Yu, X. Wang, X. Li, J. Gao, H. Wang, *Macromol. Theory Simul.* **2006**, 15, 94–99

482. R. García-Domenech, J. V. de Julián-Ortiz, *J. Phys. Chem. B* **2002,** 106*,* 1501-1507

483. P. Camelio, V. Lazzeri, B. Waegell, C. Cypcar and L. J. Mathias, *Macromolecules* **1998,** 31*,* 2305-2311

484. P. J. Willcox, D. W. Howie jr., K. Schmidt-Rohr, D. A. Hoagland, S. P. Gido, S. Pudjijanto, L. W. Kleiner, S. Venkatraman, *J. Polym. Sci., Part B: Polym. Phys.* **1999**, 37, 3438–3454

485. R. Ricciardi, F. Auriemma, C. De Rosa and Françoise Lauprêtre, *Macromolecules* **2004,** 37*,* 1921-1927

486. H. S. Mansur, R. L. Oréfice, A. A. P. Mansur, *Polymer* **2004**, 45, 7193–7202

487. F. X. Quinn, T. Hatakeyama, M. Takahashi, Hyoe Hatakeyama, *Polymer* **1994**, Vol. 35 No. 6, 1248-1252

488. S. K. Bajpai, S. Singh, *React. Funct. Polym.* **2006**, 66, 431–440

489. R. Ricciardi, F. Auriemma, C. Gaillet, C. De Rosa and Françoise Lauprêtre, *Macromolecules* **2004,** 37*,* 9510-9516

490. R. Barbieri, M. Quaglia, M. Delfini, E. Brosio**,** *Polymer* **1998**, 39, 5, 1059-1066

491. M. Knörgen, K.-F. Arndt, S. Richter, D. Kuckling, H. Schneider, *J. Mol. Struct.* **2000**, 554, 69–79

492. C. A. Fyfe and A. I. Blazek, *Macromolecules* **1997,** 30, 6230-6237

493. A. W. Watkins and K. S. Anseth, *Macromolecules* **2005,** 38*,* 1326-1334

494. T. Gunnlaugsson, C. P. McCoy, R. J. Morrow, C. Phelan, F. Stomeo, *ARKIVOC* **2003**, vii, 216-228, https://www.arkat-usa.org/get-file/18982/

495. http://www.sigmaaldrich.com/life-science/life-science catalog/products

496. http://sigmaaldrich.com/engineeringpolymers

497. Technical information of *Zonyl® fluorosurfactants*, DuPont **2010**

498. Technical Information BASF, supersedes edition dated November **2002** on *Pluronic®PE* types

499. R. P. Mason, W. Rodbumrung, P. P. Antich, *NMR in Biomedicine* **1996**, Vol. 9**,** 125-134

500. Y. Marcus, *Chem. Soc. Rev.* **1993**, 409-416

501. H. Meinert, *US Patent 5,397,805*, **1995**

502. A. Robert, C. Tondre, *J. Coll. Interface Sci.* **1994***,* Vol. 98, 2, 515-522

503. M. C. Papadakis, *US- Patent 5,567,427A*, **1996**

504. I. Marzi, K. Cowper, Y. Takei, K. Lindert, J. J. Lemasters, R. G. Thurman, *Transplant International* **1991***,* Vol. 4, 1, 215-220

505. N. R. Di Luzio, W. R. Wooles, *Am. J. Physiol.* **1964***,* Vol. 206, 5, 939-943

506. A. Rižner Hraš, M. Hadolin, Žknez, D. Bauman, *Food Chem.* **2000**, 71, 229-233

507. A. E. Abdalla, J. P. Roozen, *Food Chem.* **1999**, 64, 323-329

508. K. P. Mc Donnell, S. M. Ward, P. B. Mc Nulty, R. Howard-Hildige, *Transactions of the ASABE* **2000**, 43, 6, 1309-1316

509. M. Guderjan, P. Elez-Martínez, D. Knorr, *Innov. Food Sci. Emerg. Tech.* **2007**, 8, 55–62

510. M. H. Gordon, L. Kourimská, *Food Chem.* **1995**, 52, 175-177

511. http://de.wikipedia.org/wiki/**Sonnenblumenoel**

512. http://de.wikipedia.org/wiki/**Rapsoel**

513. S. G. Honavar, M. Goyal, A. B. Majji, P. K. Sen, T. Naduvilath, L. Dandona, *Opthalmology* **1999**, 106, 169-177

514. Y. Sawada, *Brit. J. Plast. Surg.* **1990**, 43, 6, 683-688

515. E. Speeleveld, J. M. Fossépré, B. Gordts and H. W Van Landuyt, *J. Clin. Microbiol.* **1994** , 32, 5, 1362-1363

516. C. Erlanson, B. Borgström, *Scand. J. Gastroenterol.* **1970**, 5, 4, 293-295

517. H. Endo, J. Allgaier, G. Gompper, B. Jakobs, M. Monkenbusch, D. Richter, T. Sottmann, R. Strey, *Phys. Rev. Lett.* **2000**, 85, 102

518. T. Sottmann, *Curr. Opin. Coll. Interface Sci*. **2002**, 7, 57-65

519. H. Frielinghaus, D. Byelov, J. Allgaier, G. Gompper, D. Richter, *Physica B* **2004**, 350, 186–192

520. D. Byelov, H. Frielinghaus, O. Holderer, J. Allgaier, D. Richter, *Langmuir* **2004,** 20, 10433-10443

521. C. Frank, T. Sottmann, C. Stubenrauch, J. Allgaier, R. Strey, *Langmuir* **2005**, 21, 9058-9067

522. S. Creutz, J. van Stam, F. C. De Schryver, R. Jérôme, *Macromolecules* **1998**, 31, 681

523. S. Förster, Ber. Bunsenges., *Phys. Chem*. **1997**, 101, 1671

524. G. Riess, C. Labbe, *Macromol. Rapid Commun.* **2004**, 25, 401

525. J.-F. Gohy, S. Antoun, R. Jérôme, *Polymer* **2001**, 42, 8637-8645

526. Y. Chang, J. D. Bender, M. V. B. Phelps, H. R. Allcock, *Biomacromolecules* **2002**, 3, 1364

527. T. Rager, W. H. Meyer, G. Wegner, *Macromolecules* **1997**, 30, 4911

528. D. G. Oakenfull and L. R. Fisher, *J. Phys. Chem.* **1977**, Vol. 81, No. 19, 1838-1841

529. B. D. Flockhart, *J. Coll. Sci.* **1961**, 16, 484-492

530. T. Nakashima, T. Anno, H. Kanda, Y. Sato, T. Kuroi, H. Fujii, S. Nagadome, G. Sugihara, *Coll. Surf. B: Bioint.* **2002**, 24, 103–110

531. V. Sovilj, *Colloid. Polym. Sci.* **1998**, 276, 328-334

532. A. Dominguez, A. Fernandez, N. Gonzalez, E. Iglesias and L. Montenegro, *J. Chem. Educ.* **1997**, 74, 10, 1227-1232

533. A. Beyaz, W. S. Oh, V. P. Reddy, *Coll. Surf. B: Bioint.* **2004**, 35, 119–124

534. M. H. Gehlen and F. C. De Schryver, *Chem. Rev.* **1993**, 93, 199-221

535. R. G. Alargova, I. I. Kochijashky, M. L. Sierra, and R. Zana, *Langmuir* **1998,** 14*,* 5412-5418

536. J. R. Lopes and W. Loh, *Langmuir* **1998,** 14*,* 750-756

537. P. Venkatesan, Y. Cheng and D. Kahne, *J. Am. Chem. Soc.* **1994**, 116, 6955-6956

538. R. M. M. Brito and W. L. C. Vaz, *Analyt. Biochem.* **1986**, 152, 250-255

539. Krüss GmbH, *technical information on ring tensiometers*, **2001**

540. P. L. Du Nouy, *J. Gen. Physiol.,* **1925**

541. N. A. Bulychev, I. A. Arutunov, V. P. Zubov, B. Verdonck, T. Zhang, E. J. Goethals, F. E. Du Prez, *Macromol. Chem. Phys.* **2004**, 205, 2457–2463

542. X. L. Chen, S. A. Jenekhe, *Macromolecules* **2000**, 33, 4610-4612

543. T. K. Sievers, D.G. Kurth, *Curr. Opin. Coll. Interface Sci.* **2008**, 13, 86-95

544. Dr. T. K. Sievers, *personal correspondence*

545. J. Mata, T. Joshi, D. Varade, G. Ghosh, P. Bahadur, *Colloids Surf. A: Physicochem. Eng. Asp.* **2004**, 247, 1-7

546. J. Dong, B. Z. Chowdhry, S. A. Lehane, *Colloids Surf. A: Physicochem. Eng. Asp.* **2003**, 212, 9-17

547. I. F. Paterson, B. Z. Chowdhry, S. A. Lehane, *Chemosphere* **2000**, 40, 1399

548. K. Matsumoto, R. Nishimura, H. Mazaki, H. Matsuoka, H. Yamaoka, *J. Polym. Sci. A: Polym. Chem.* **2001**, Vol. 39, 3751–3760

549. A. Ertekin, Y. Kim, C. M. Kausch, R. R. Thomas, *J. Coll. Interface Sci.* **2009**, 40-45

550. Image J® , *picture analyzing software*: http:/ /rsb.info.nih.gov/ij/

551. http:/ /imagejdocu.tudor.lu/doku.Php

552. A. P. Narrainen, S. Pascual, D. M. Haddleton, *J. Polym. Sci.* **2002**, 40, 439

553. E. Szajdzinska-Pietek, M. Pinteala, S. Schlick, *Polymer* **2004***,* 45, 4113

List of figures

List of tables

Annex

1. Kinetics applying newly synthesized, fluorinated CTAs

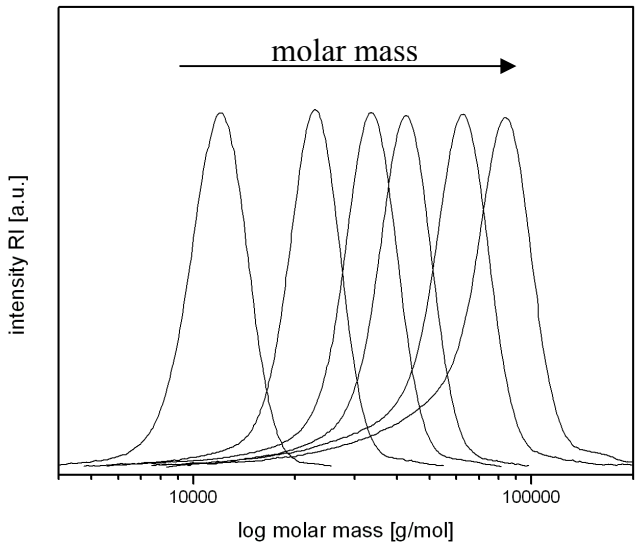

Figure 1: Evolution of GPC elugram with polymerization time (eluent: THF, internal standard: BHT) showing the thermally initiated polymerization of styrene (**M3)** in bulk applying non-symmetric **CTA XXXV** at 110 °C after (from left to right). The molar mass of the polymer is increasing with time (~ 10000 to ~ 100000 g/mol). Polymerizations up to high conversions ~ 100000 g/mol are possible.

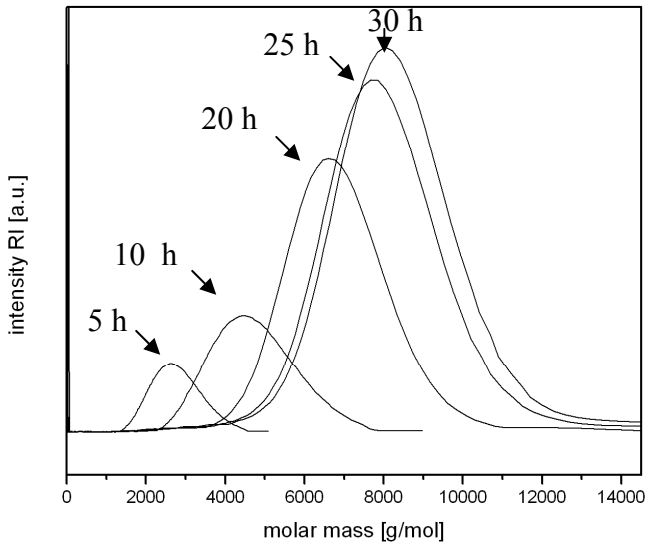

Figure 2: Evolution of GPC elugram with polymerization time (eluent: THF, internal standard: BHT) displaying the thermally initiated polymerization of styrene (**M3**) in bulk applying non-symmetric, monofunctional **CTA XXXVII** at 110 °C after 5, 10, 20, 25 and 30 h (from left to right). The molar mass of the polymer is increasing with time.

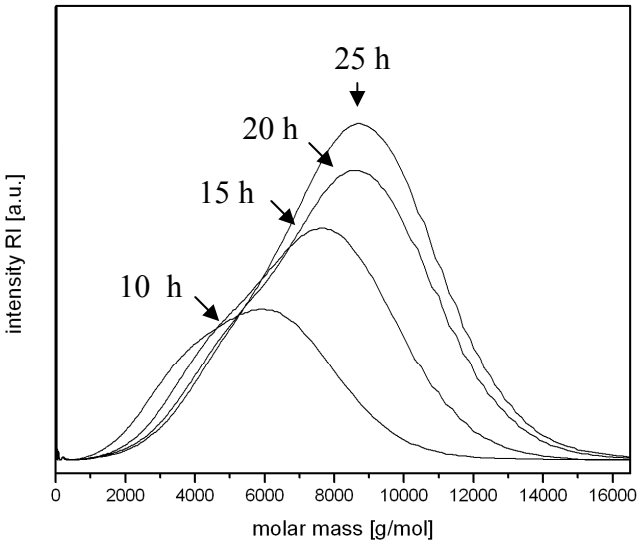

Figure 3: Evolution of GPC elugram with polymerization time (eluent: THF, internal standard: BHT) displaying the thermally initiated polymerization of styrene (**M3**) in bulk applying symmetric **CTA XXXXII** at 110 °C after 10, 15, 20, 25 h (from left to right). The molar mass of the polymer is increasing with time.

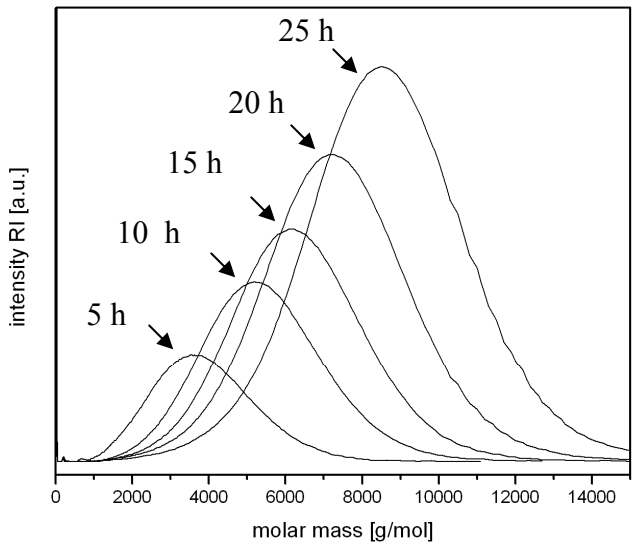

Figure 4: Evolution of GPC elugram with polymerization time (eluent: THF, internal standard: BHT) showing the thermally initiated polymerization of styrene (**M3**) in bulk applying non-symmetric **CTA XXXVI** at 110 °C after 5, 10, 15, 20 and 25 h (from left to right). The molar mass of the polymer is increasing with time.

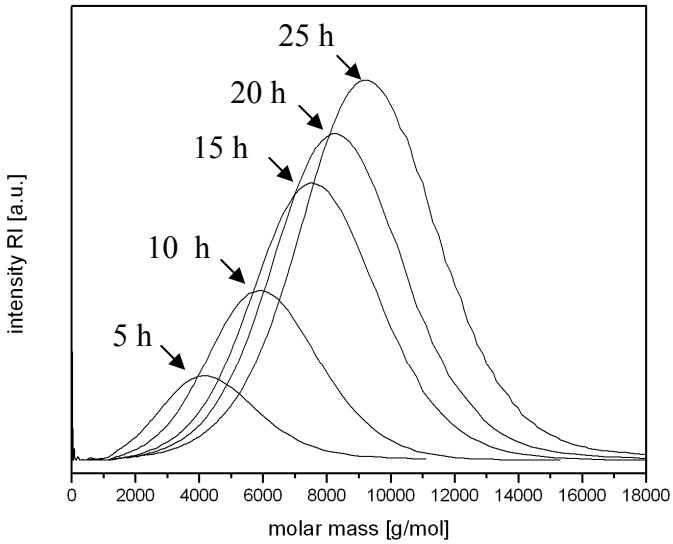

Figure 5: Evolution of GPC elugram with polymerization time (eluent: THF, internal standard: BHT) displaying the thermally initiated polymerization of styrene (**M3**) in bulk applying non- symmetric **CTA XXXIV** at 110 °C after 5, 10, 15, 20 and 25h (in right direction). The molar mass of the polymer is increasing with time.

2. Synthesis of BAB-triblock copolymers from PS, FS and PFS precursors

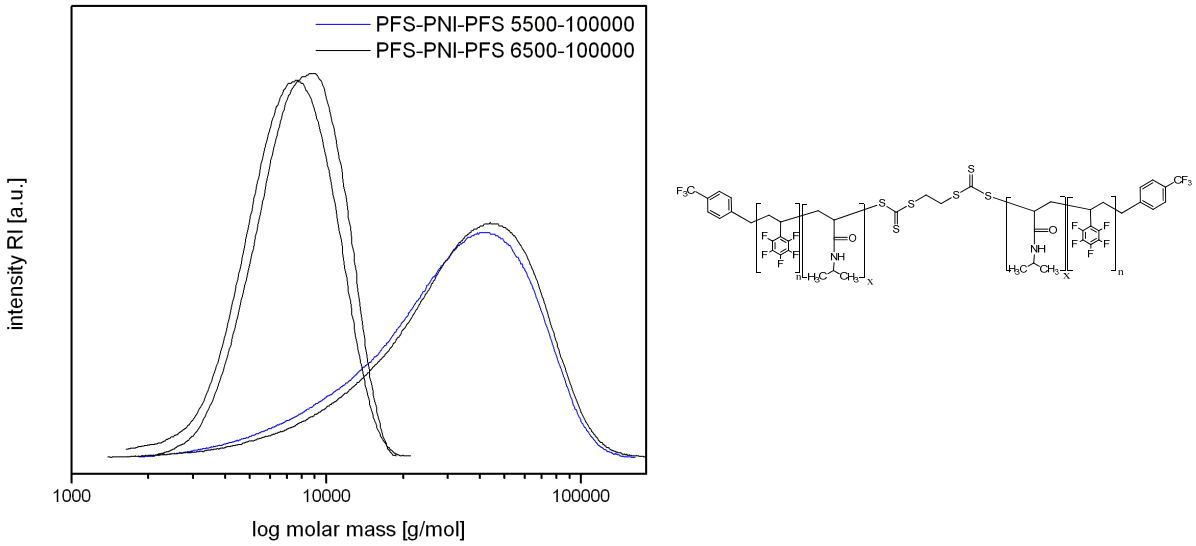

Figure 6: Elugram of **PFS-PNI-PFS 100000** series: **PFS-PNI-PFS 5500-100000, 6500-100000**. PFS 60 to PFS 100 (shifted to lower molecular weight, molecular weight of homopolymer increasing from left to right) are the PFS-macro-RAFT precursors for the synthesis of these BAB-systems.

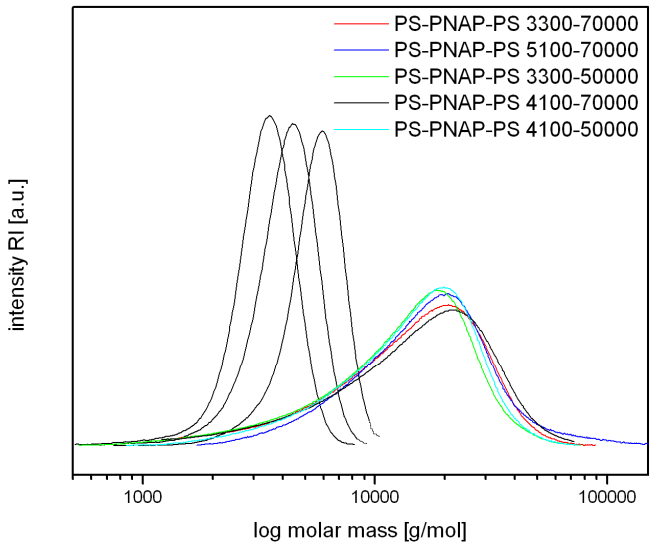

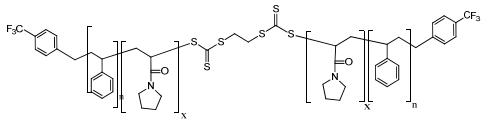

Figure 7: Elugram of **PS-PNAP-PS 50000 and 70000** series: **PS-PNAP-PS 3300-50000, 3300-70000, 4100-50000, 4100-70000** and **5100-70000**. PS 3300 to PS 5500 (shifted to lower molecular weight, molecular weight of homopolymer increasing from left to right) are the PS-macro-RAFT precursors for the synthesis of these BAB-systems.

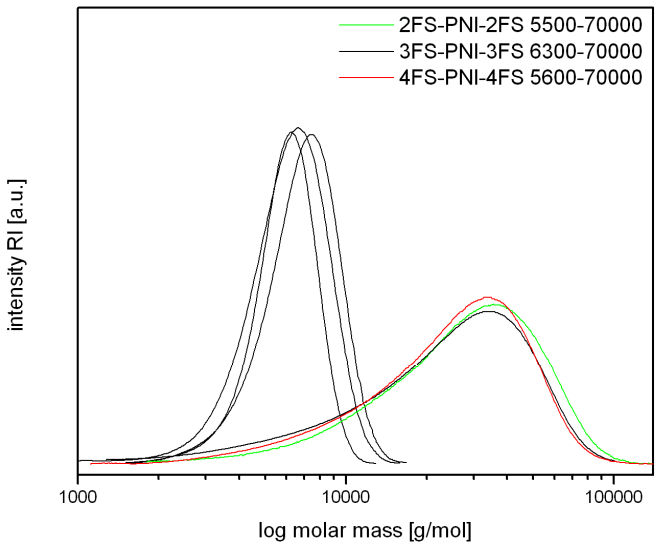

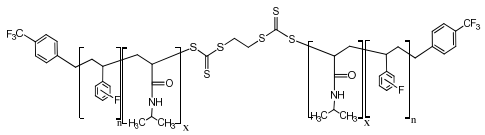

Figure 8: Elugram of **PFS-PNI-FS 70000** samples **2FS-PNI-2FS 5500-70000**, **3FS-PNI-3FS 6300-70000** and **4FS-PNI-4FS 5600-70000**. PS samples around 5000 g/mol (shifted to lower molecular weight, molecular weight of homopolymer increasing from left to right) are the FS-macro-RAFT precursors for the synthesis of these BAB-systems.

3. Turbidimetry measurements applying BAB-triblock copolymers

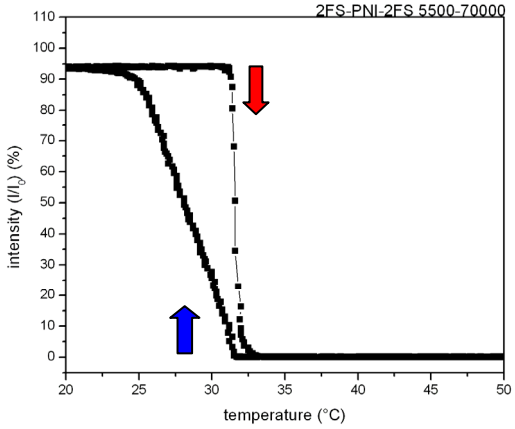

Figure 9: Transmission of aqueous solutions of **FS-PNI-FS series 70000**, example **2FS-PNI-2FS 5500-70000** as a function of temperature. (Cooling/heating rate of 1 °C per minute; sample concentration 1 g/L). The red arrow represents the heating, the blue arrow the cooling curve. All investigated transmissions are reversible.

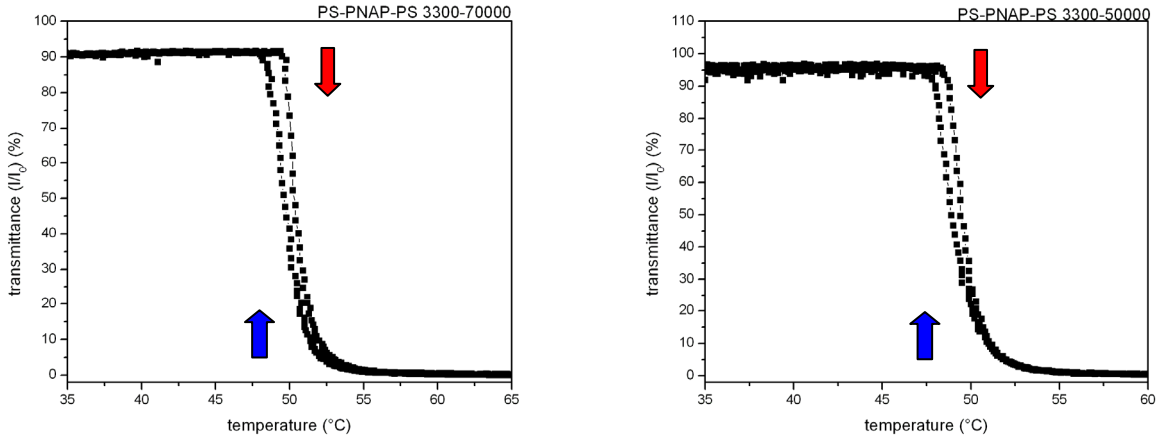

Figure 10: Transmission of aqueous solutions of **PS-PNAP-PS 3300-70000** and **3300-50000** as a function of temperature. (Cooling/heating rate of 1 °C per minute; sample concentration 1 g/L). The red arrow resembles the heating, the blue arrow the cooling curve. All investigated transmissions are reversible.

4. Stability of BAB-triblock copolymer micelles against dilution

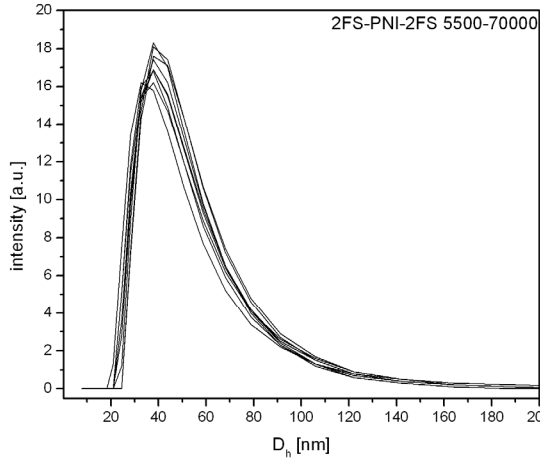

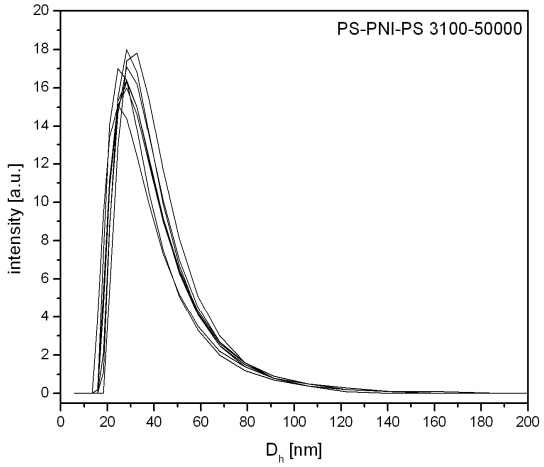

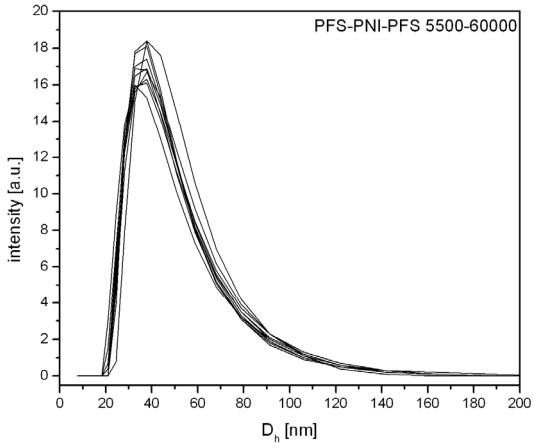

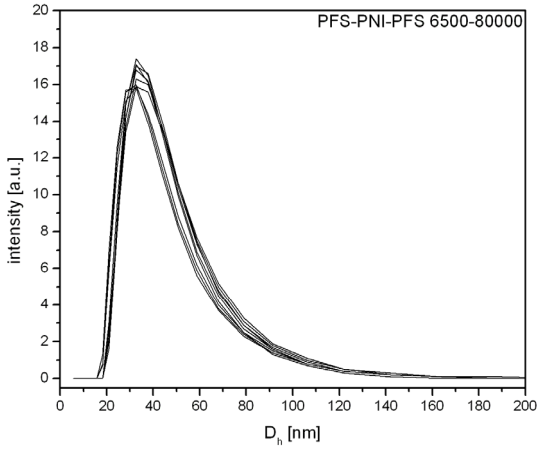

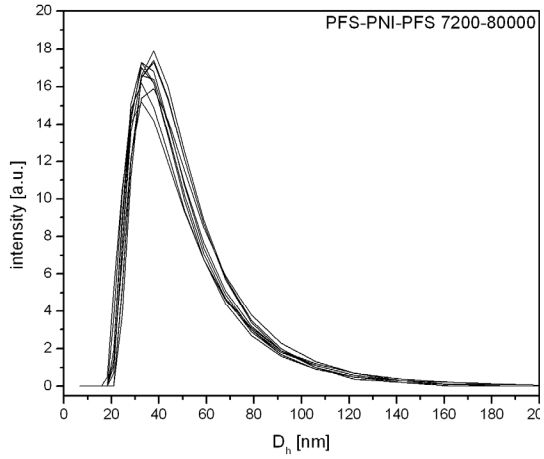

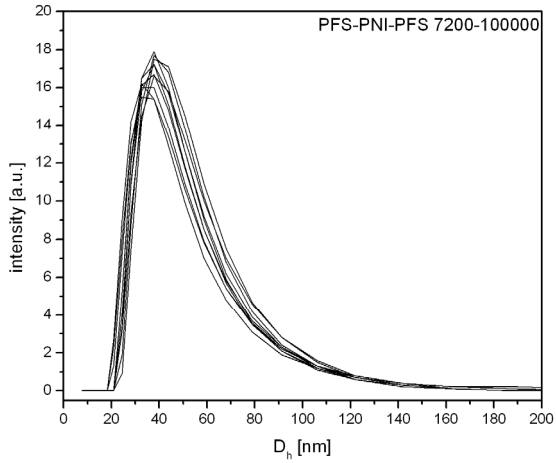

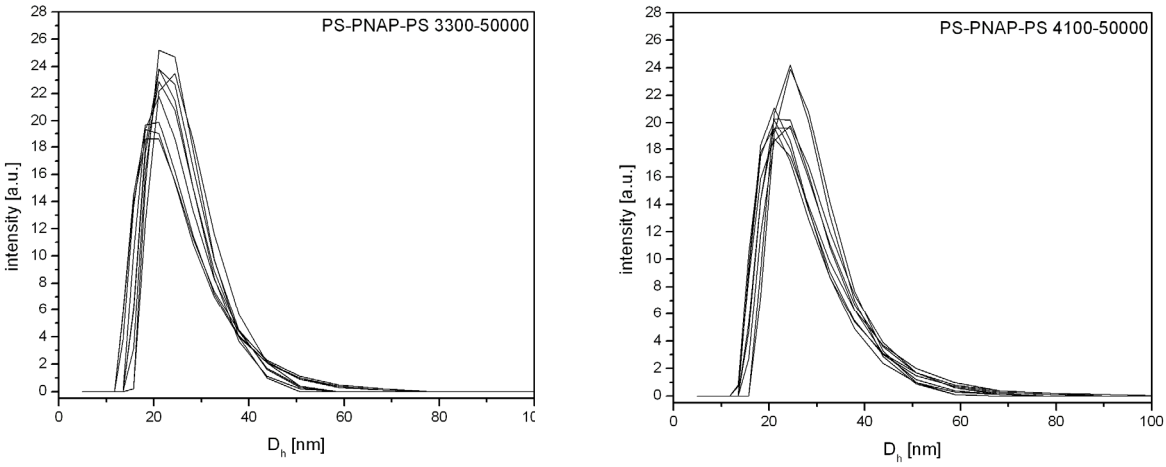

Figure 11: DLS studies obtained from diluted aqueous solutions of **PS-PNI-PS**, **PFS-PNI-PFS, FS-PNI-FS** and **PS-PNAP-PS**-triblock copolymers. The solutions were diluted from 10- to 0.1 g/L.

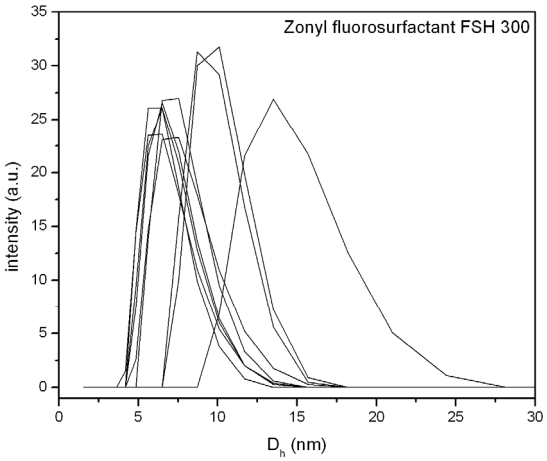

Figure 12: DLS studies obtained from diluted aqueous solutions of Zonyl®-FSH fluorosurfactant. The solutions were diluted from 10- to 1 g/L. The surfactant is not stable against dilution.

5. Temperature dependent change of the hydrodynamic diameter of micelles

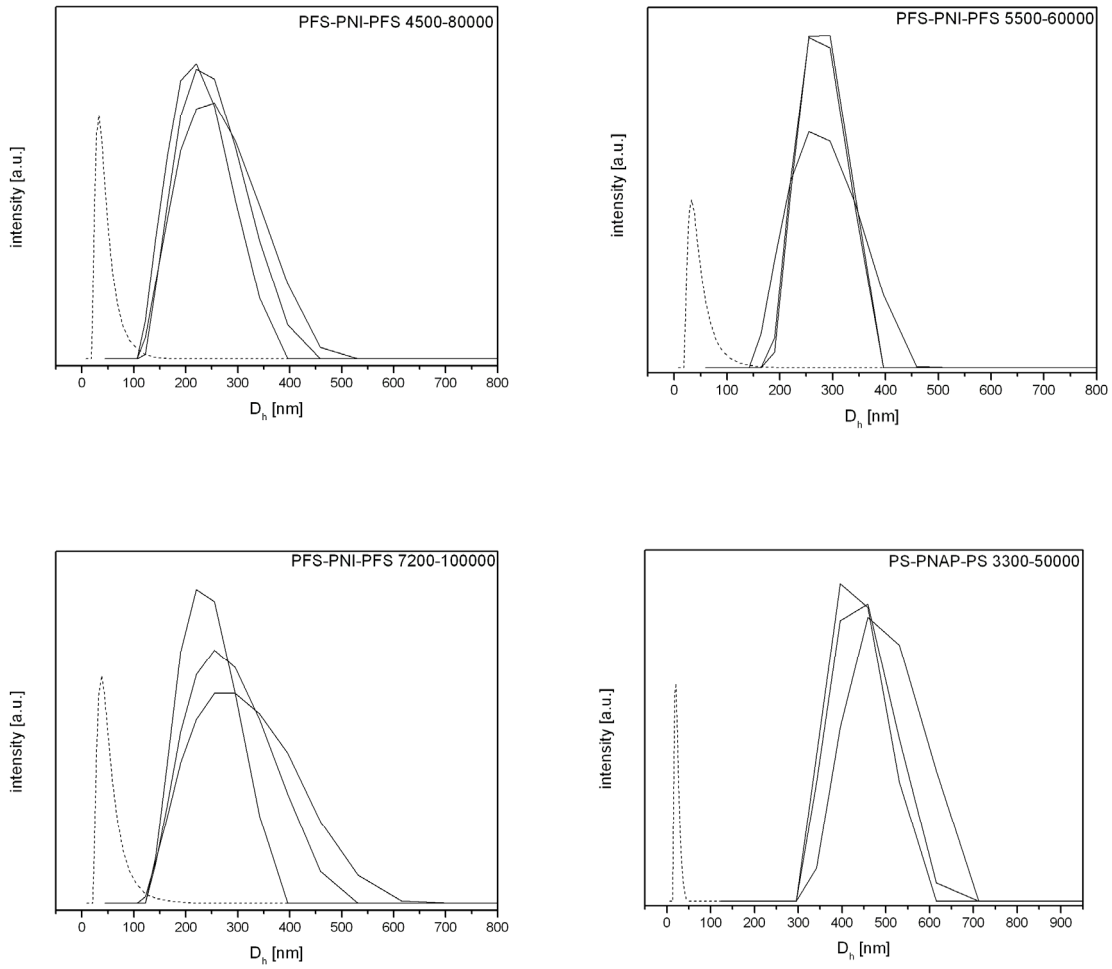

Figure 13: Temperature dependent change of the hydrodynamic diameter of aqueous solutions of micelles of **PS-PNI-PS**, **PFS-PNI-PFS**, **FS-PNI-FS** and **PS-PNAP-PS** samples.

The aggregation behaviour seems to be different for the different BAB-types. Especially the **PNAP** containing systems undergo a tremendous change in the particle size. The dotted graph resembles the micellar size at room temperature 25 °C, the straight line the aggregates above the cloud point.

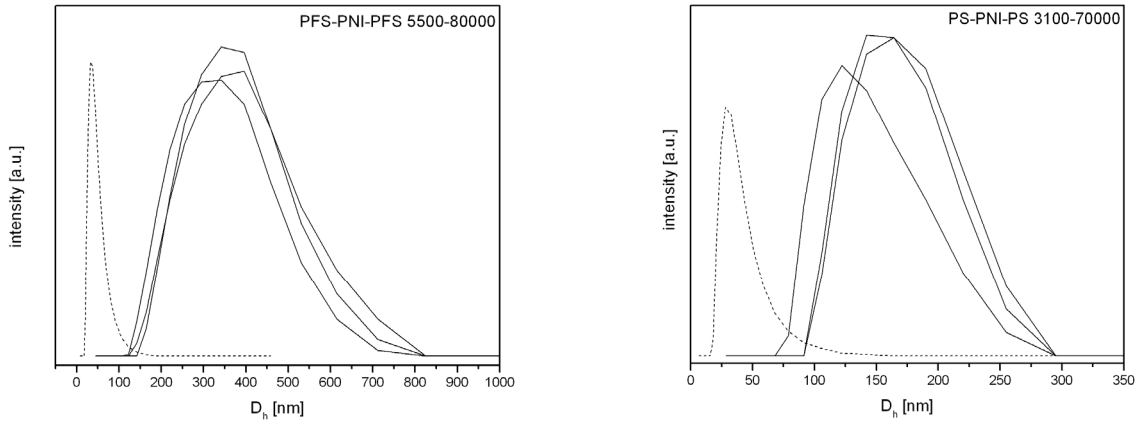

Figure 14: Temperature dependent change of the hydrodynamic diameter of aqueous solutions of **PS-PNI-PS** and **PFS-PNI-PFS** samples and **PS-PNAP-PS** sample applying DLS measurements.

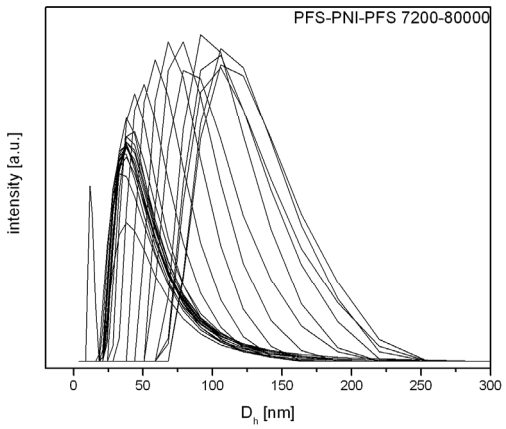

Figure 15: Temperature dependent change of the hydrodynamic diameter in aqueous solution of sample **PS-PNI-PS 7200-80000** applying DLS measurements with a heating rate of 0.1 °C per minute.

Changing the temperature by 0.1 °C per minute, the cloud point can be also determined exactly applying DLS (small peak in the left part of figure 15). At the same time, the stepwise growth of the micelles can be envisaged.

6. SEM-measurements of aqueous solutions of BAB-triblock copolymers

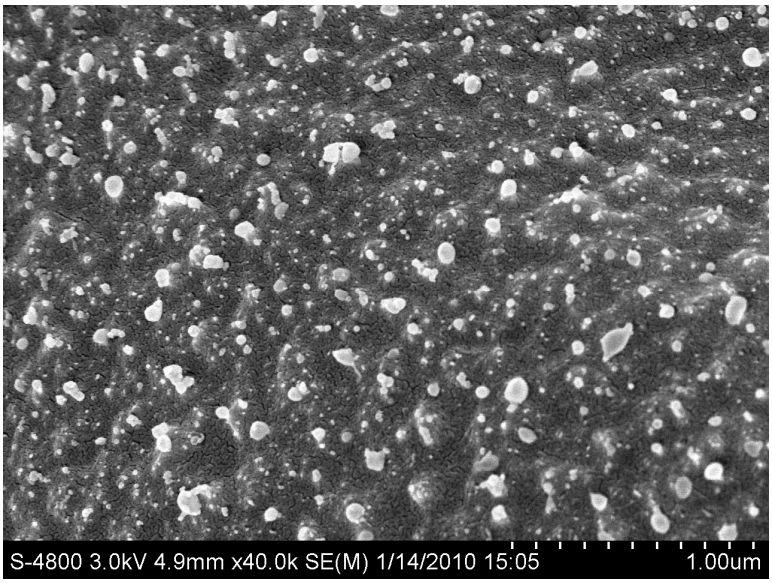

Figure 16: Globular structures of dried micellar solutions of sample **PS-PNI-PS 5700-70000** investigated using SEM.

7. Emulsions prepared from BAB-triblock copolymers and oils of different polarity

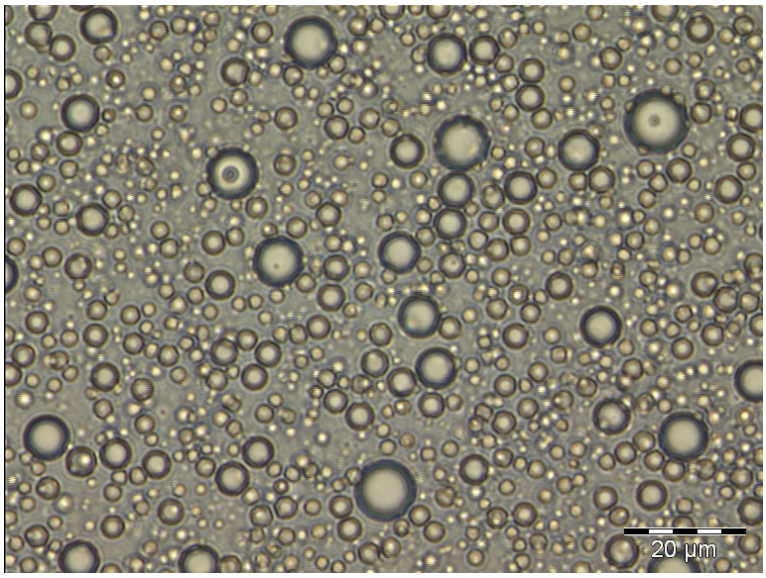

Figure 17: Optical micrograph of emulsions made using **PS-PNI-PS 3100-70000**, 1 g rapeseed as oil (oil-in-water emulsion).

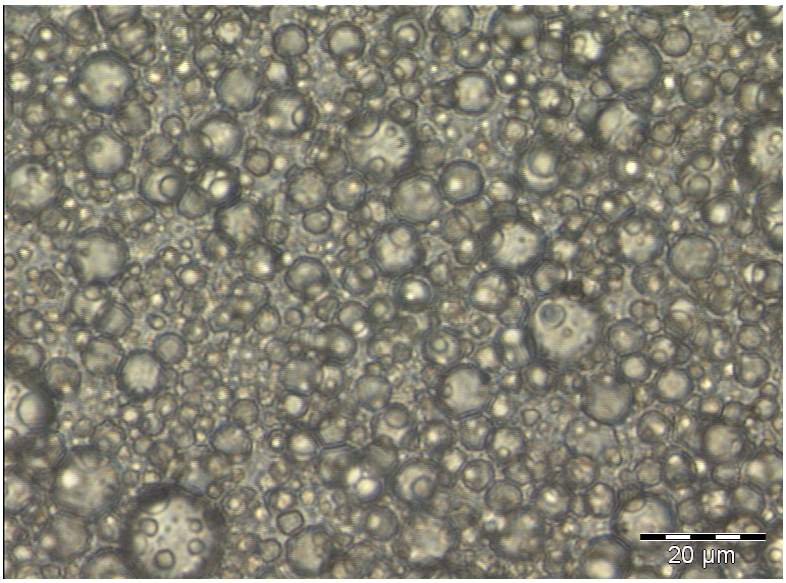

Figure 18: Optical micrograph of emulsions made using **PS-PNI-PS 3100-70000**, 4 g rapeseed as oil (water-in-oil emulsion).

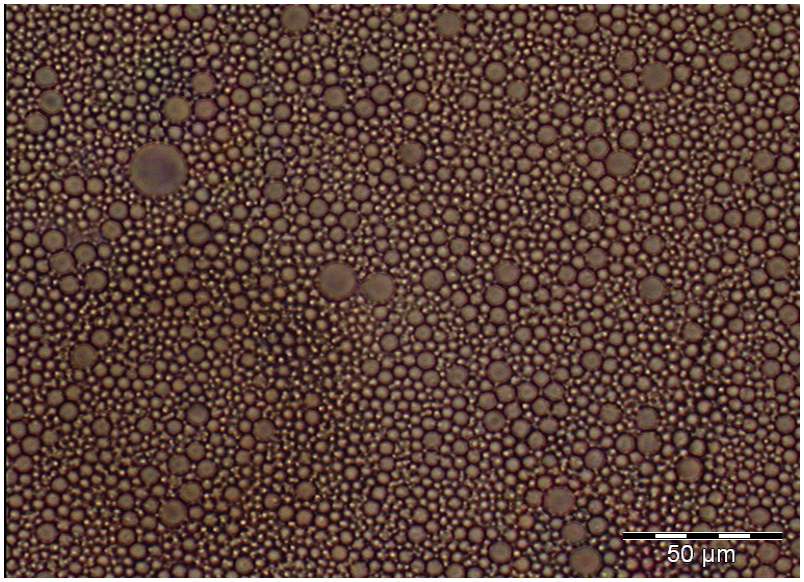

Figure 19: Optical micrograph of emulsions made using **PS-PNI-PS 3100-70000**, 1 g hexafluorobenzene as oil (oil-in-water emulsion).

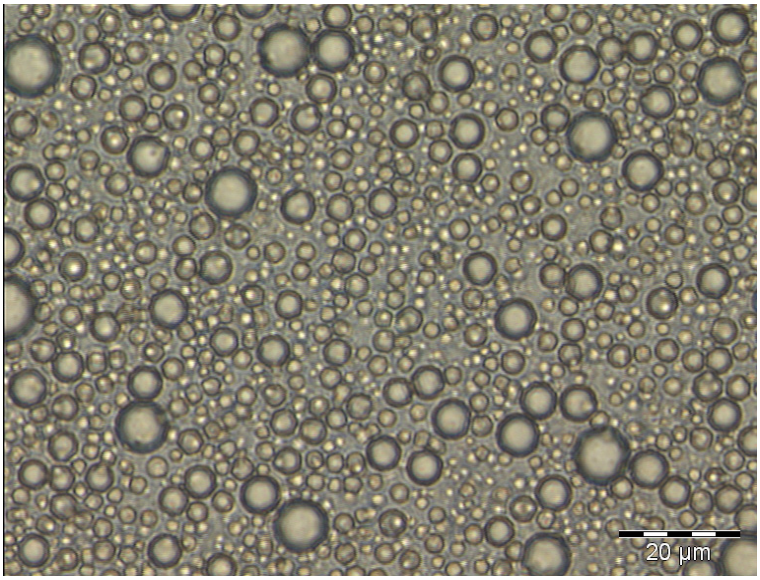

Figure 20: Optical micrograph of emulsions made using **PFS-PNI-PFS 4200-80000**, 1 g rapeseed as oil (oil-in-water emulsion).

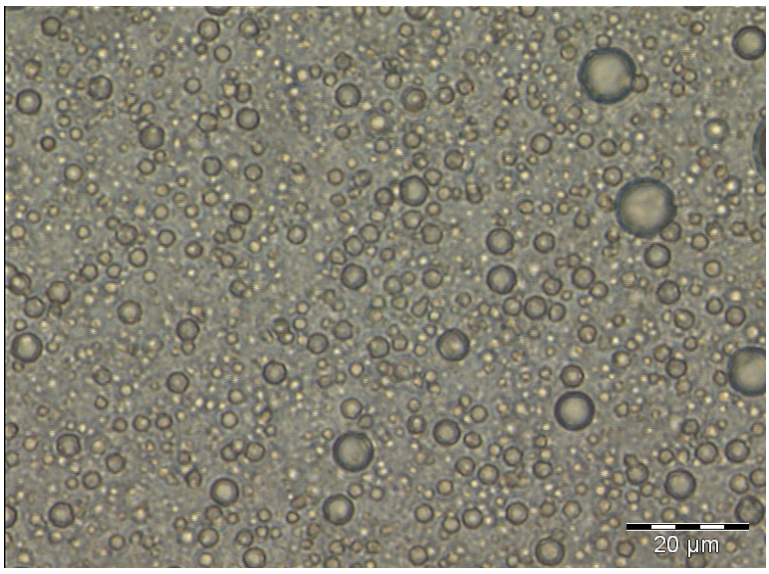

Figure 21: Optical micrograph of emulsions made using **PFS-PNI-PFS 4200-80000**, 4 g rapeseed as oil (water-in-oil emulsion).

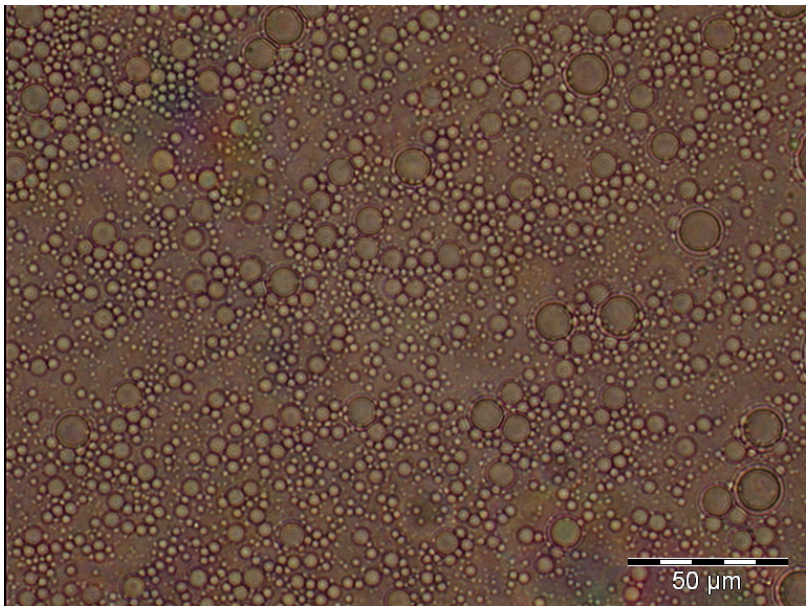

Figure 22: Optical micrograph of emulsions made using **PFS-PNI-PFS 4200-80000**, 1 g fluorobenzene as oil (water-in-oil emulsion).

Preparation of emulsions applying BAB-triblock copolymers offer the possibility to destroy the emulsion on demand by just heating it above the cloud point of PNIPAM changing the HLB of the triblock copolymers with temperature. Passing the cloud point the molecule becomes completely hydrophobic and is no longer capable of stabilizing the interface between oil and water droplets or water and oil droplets leading to a breakdown of the emulsion.

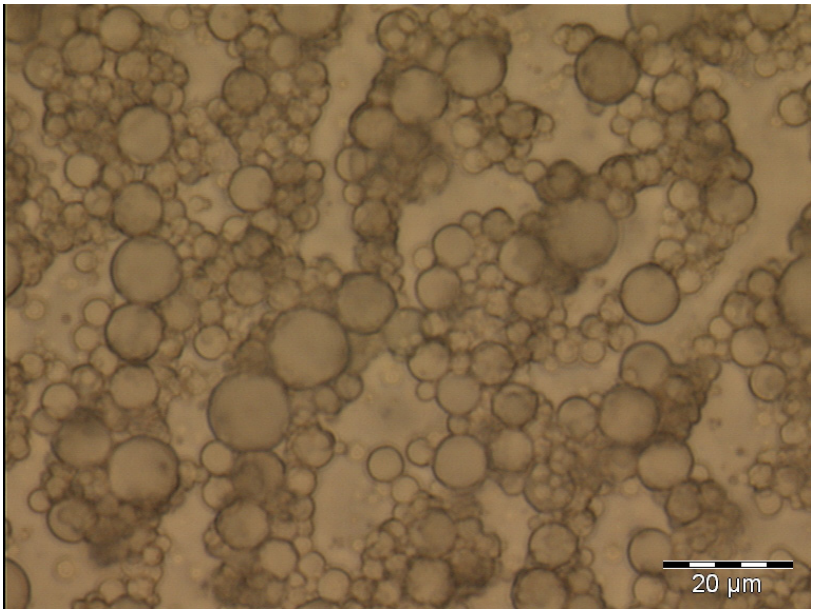

Figure 23: Optical micrograph of emulsions made using **PS-PNI-PS 3100-70000**, 4 g oil (water-in-oil emulsion), after 1 minute at 50 °C.

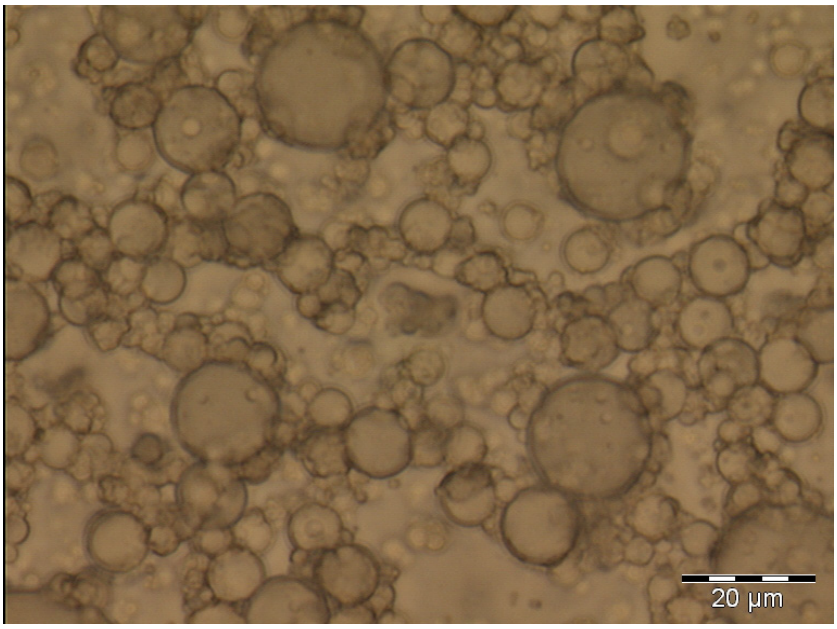

Figure 24: Optical micrograph of emulsions made using **PS-PNI-PS 3100-70000**, 4 g oil (water-in-oil emulsion), after 2 minutes at 50 °C.

Figure 24 shows the breakdown of emulsion after heating sample from room temperature (25 °C) to 40 °C, a temperature well above the cloud point of PNIPAM (32 °C).

8. Foams prepared from aqueous solutions of BAB-triblock copolymers

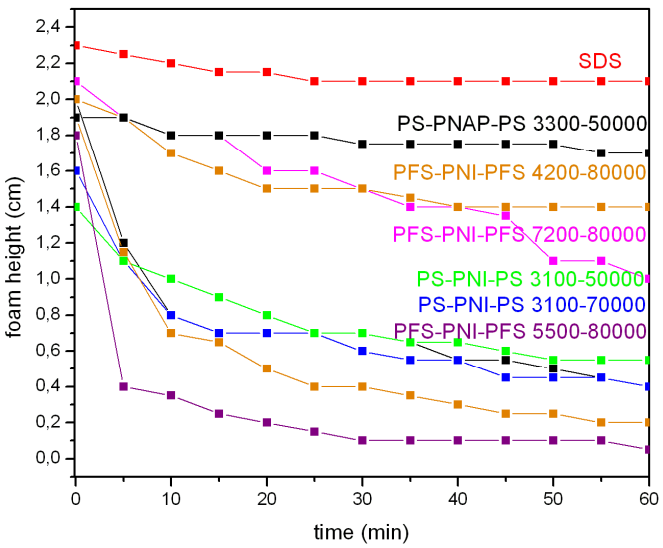

Figure 25: Foam decay of aqueous polymer solutions including **SDS** as a low molecular weight surfactant as a function of time (comparison). Lines are meant as guides for the eye.

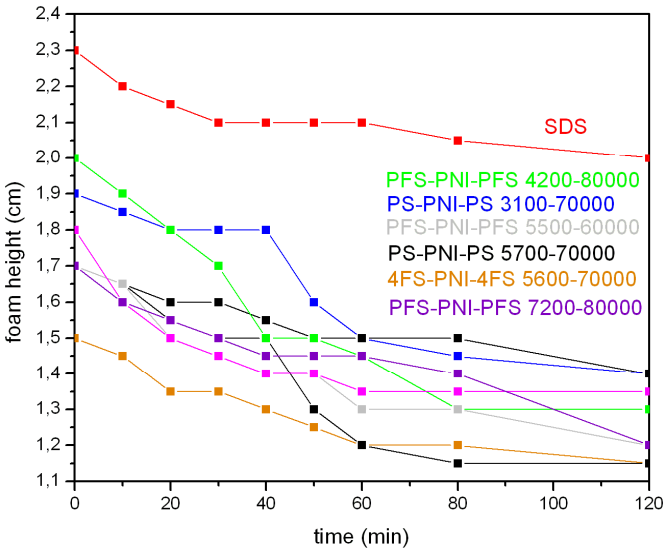

Figure 26: Foam decay of aqueous BAB-polymer solutions -fluorinated and non fluorinated- as a function of time. Lines are meant as guides for the eye.

9. CMC-measurements of aqueous solutions of BAB-triblock copolymers

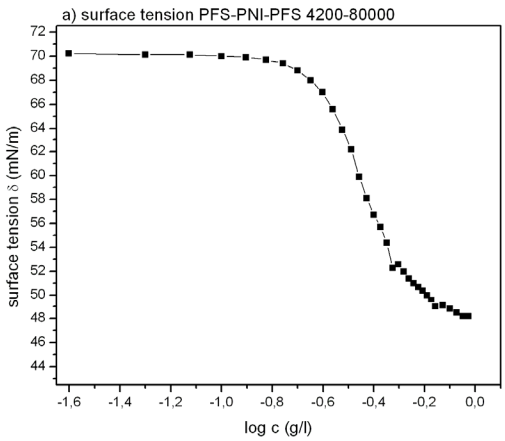

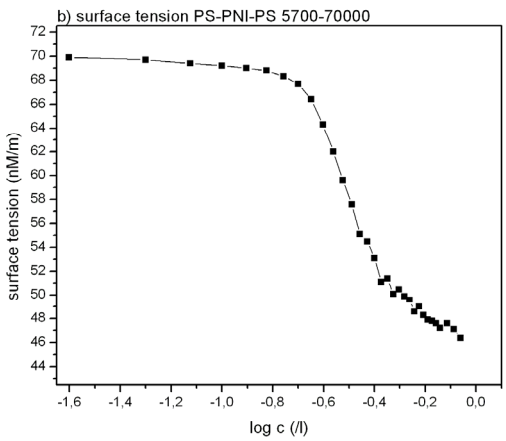

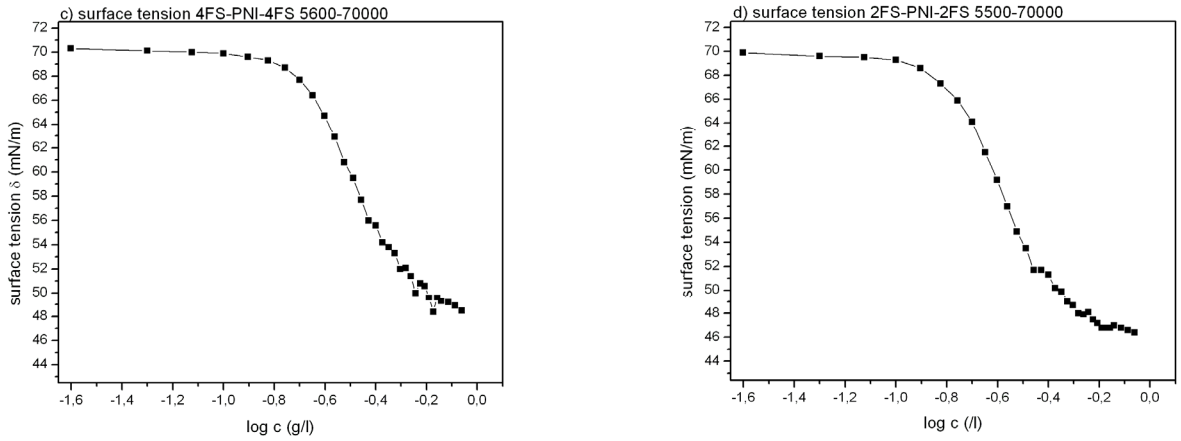

Figure 27: CMC-measurements of aqueous solutions of polymer a) **PFS-PNI-PFS 4200-80000**, b) **PFS-PNI-PFS 5500-70000**, c) **4FS-PNI-4FS 5600-70000**, d) **2FS-PNI-2FS 5500-70000.**

List of figures Annex

symmetric CTAs

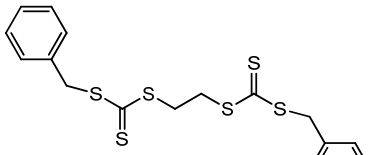

XXXIX

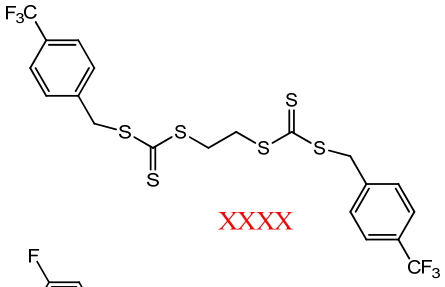

XXXX

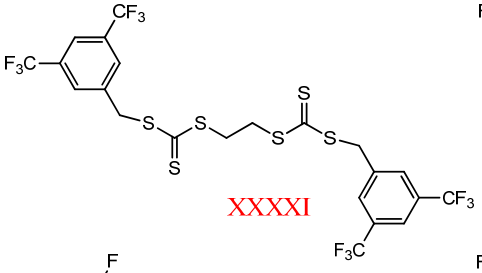

XXXXI

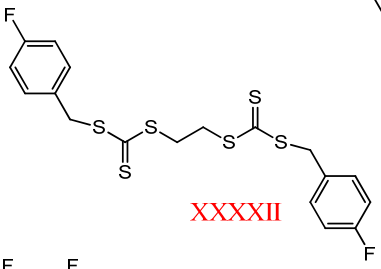

XXXXII

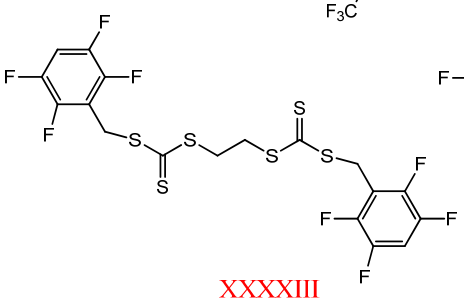

XXXXIII

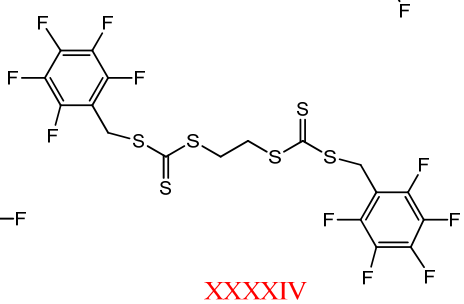

XXXXIV

non-symmetric CTAs

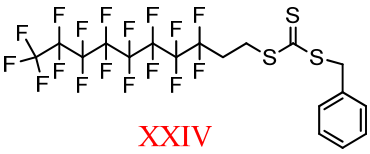

XXIV

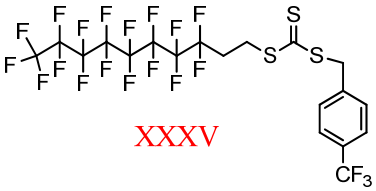

XXXV

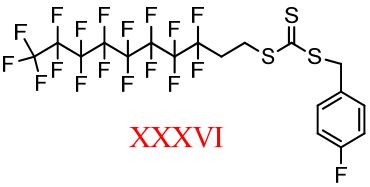

XXXVI

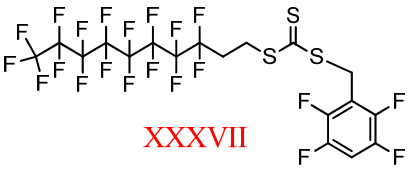

XXXVII

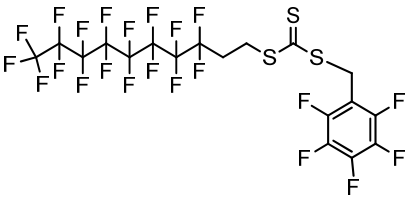

XXXVIII

hydrophobic styrene monomers

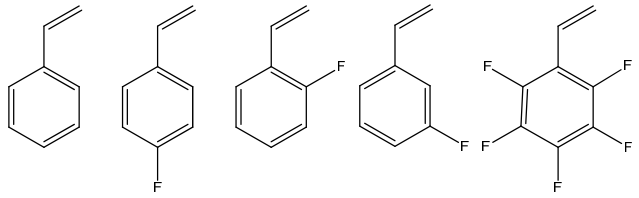

M3 M6 M5 M4 M7

hydrophilic monomers

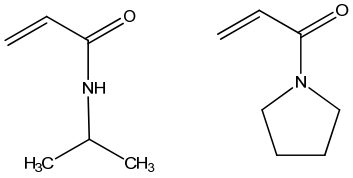

M1 M2

initiators used for polymerizations

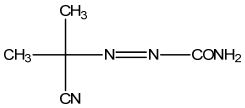

V30

M.W.= 140,14 g/mol

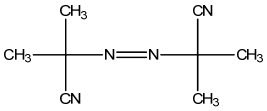

AIBN

M.W.= 164,21 g/mol

Synthesized BAB-triblock copolymers

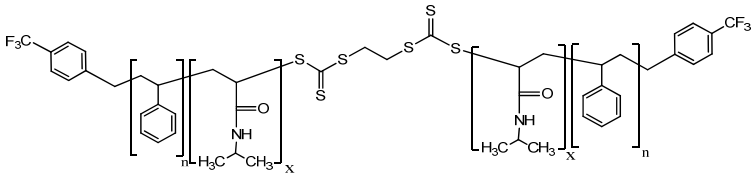

PS-PNI-PS

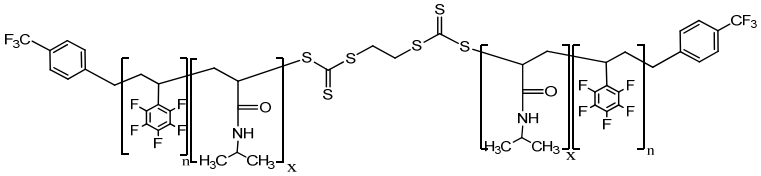

PFS-PNI-PFS

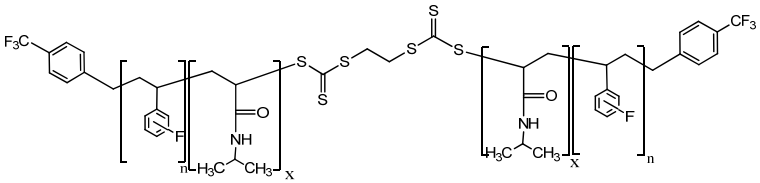

FS-PNI-FS

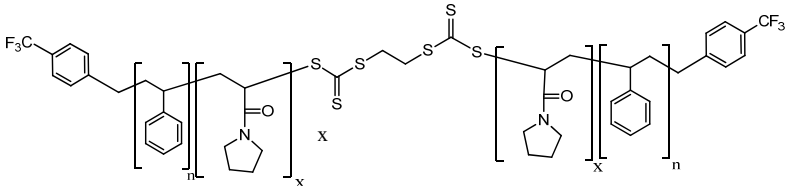

PS-PNAP-PS

oils used for emulsification studies

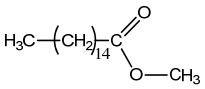

methyl palmitate

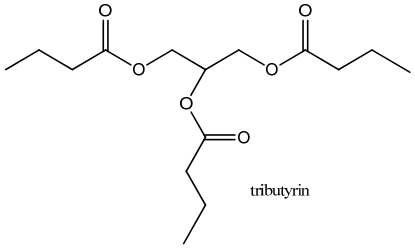

tributyrin

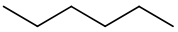

n-hexane

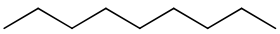

n-nonane

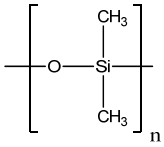

silicon oil

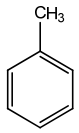

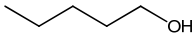

toluene and pentanol for microemulsions

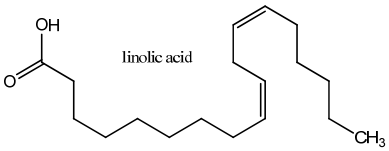

linolic acid

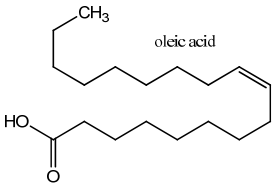

oleic acid

fluorinated oils for emulsification studies

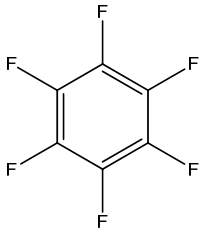

hexafluorobenzene

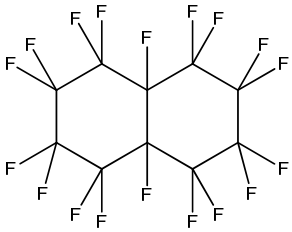

perfluorodecaline

Fluorinated and non-fluorinated surfactants

Brij 56
n= 10

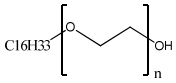

Triton X 100
n= 9-10

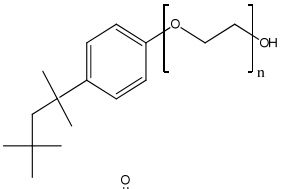

SDS

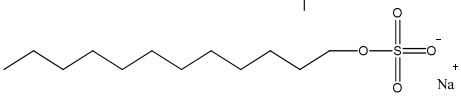

TWEEN 56

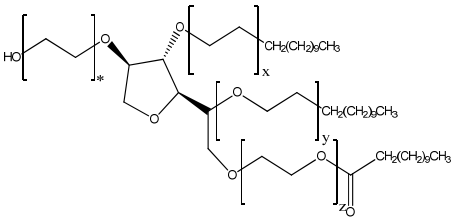

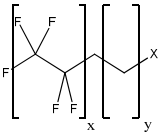

Zonyl
fluorosurfactants

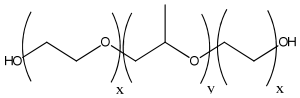

Pluronics
PEO-PPO-PEO

Pluronics 6400
x~14, y~15